ORNL-3650

Full Release

Oak Ridge National Laboratory 1963

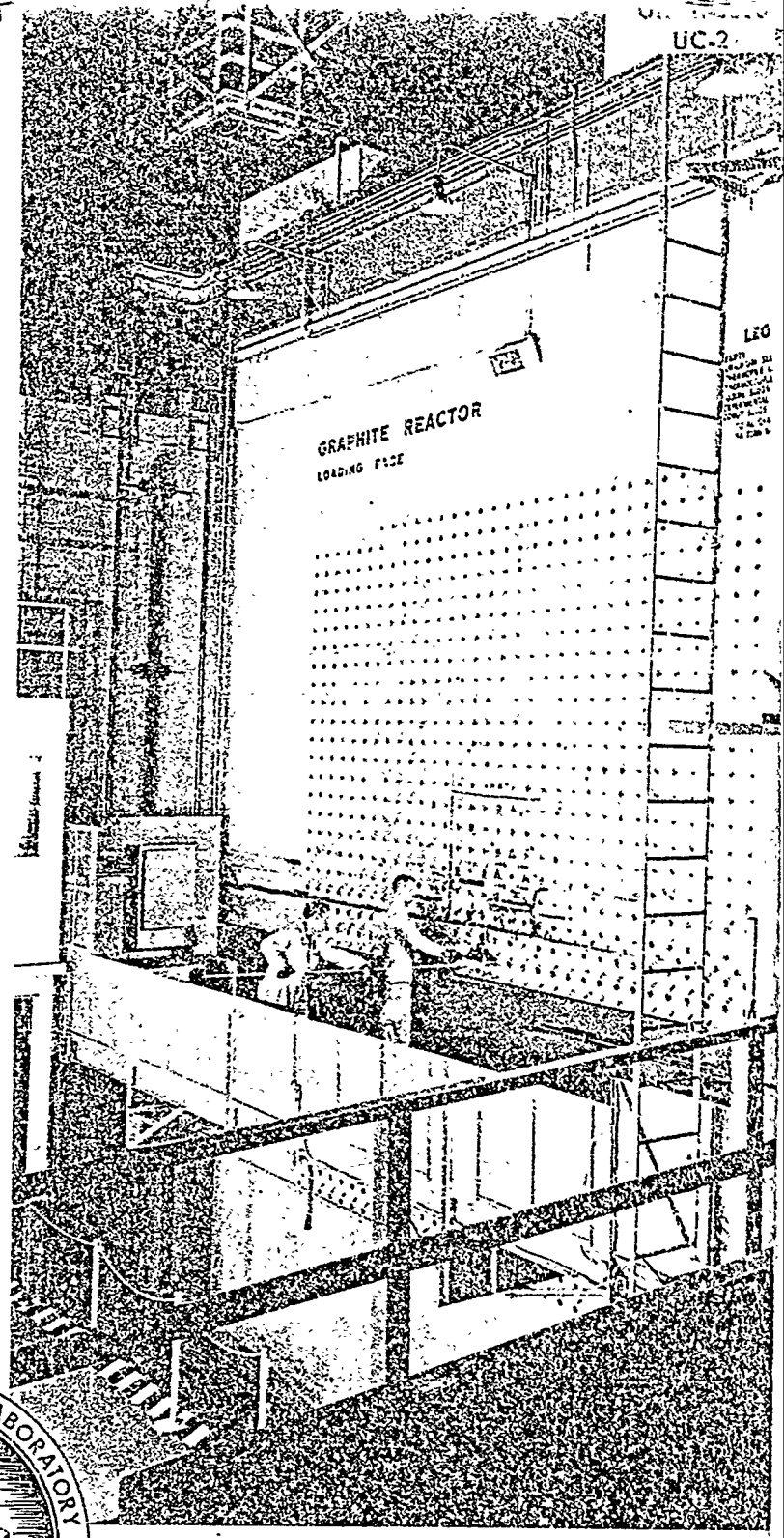

pages missing around pg 187-190
also ~ p 237

OAK RIDGE NATIONAL LABORATORY
U.S. ATOMIC ENERGY COMMISSION

OAK RIDGE NATIONAL LABORATORY
OPERATED BY UNION CARBIDE CORPORATION • FOR THE U.S. ATOMIC ENERGY COMMISSION
CONTRACT NO. W-7405-ENG-26

ChemRisk Document No. 613

ORNL-3650

95

ORNL-3650
UC-2

Oak Ridge National Laboratory 1963

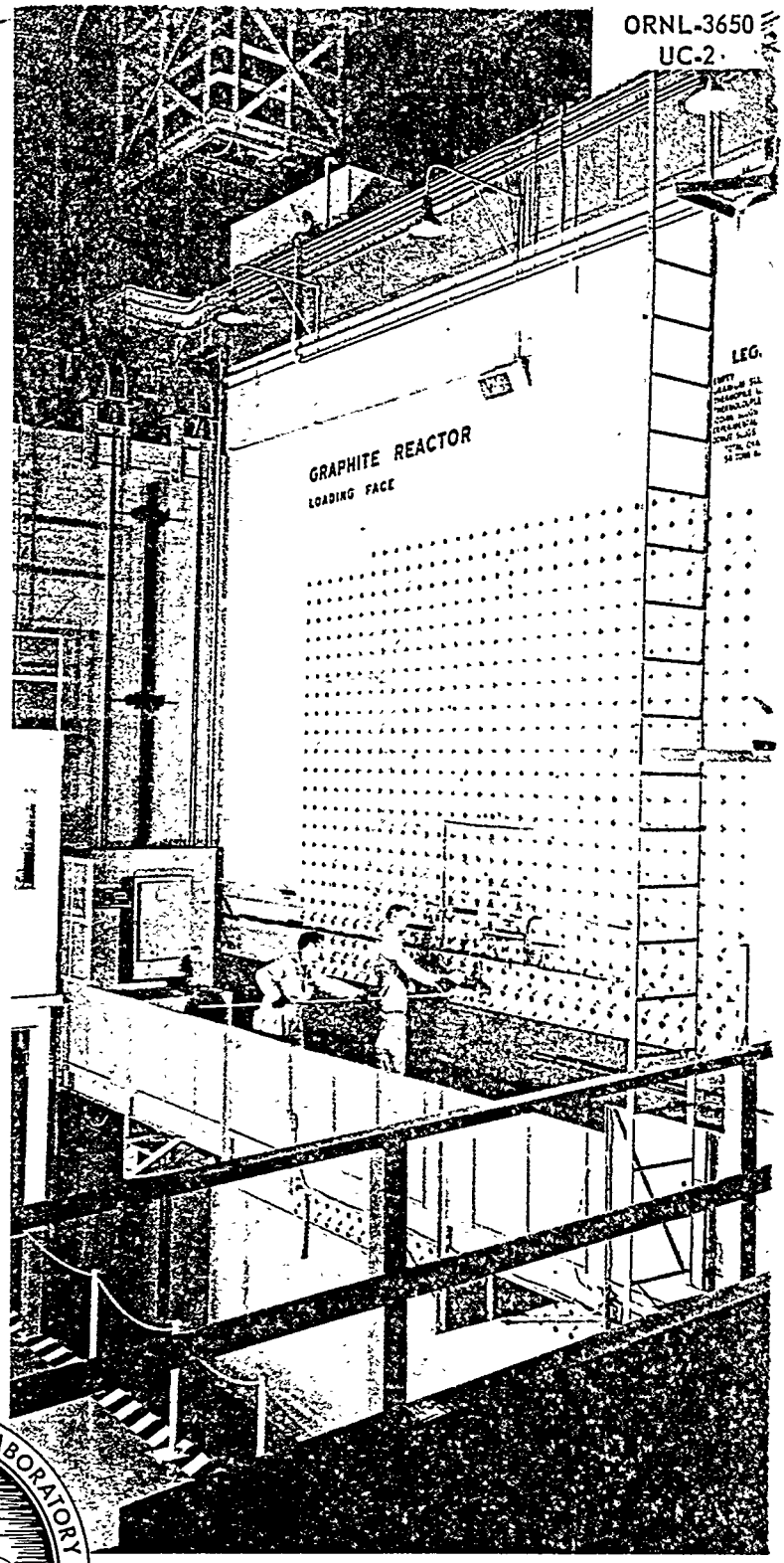

OAK RIDGE NATIONAL LABORATORY

OPERATED BY UNION CARBIDE CORPORATION • FOR THE U.S. ATOMIC ENERGY COMMISSION

CONTRACT NO. W-7405-ENG-26

ABOUT THE COVER

The world's oldest operating nuclear reactor, the Graphite Reactor at Oak Ridge National Laboratory, was initially used to fulfill its primary purpose, the production of gram quantities of plutonium-239. After the war it was used in the training of reactor technicians; later it became the world's leading source of radioisotopes. In recent years it has been a valuable research tool. The Graphite Reactor went into operation November 4, 1943, and was shut down November 4, 1963, a victim of advancing technology in atomic energy.

Some of the reactors that have superseded the ORNL Graphite Reactor are shown on these two pages. The Health Physics Research Reactor, designed to produce short bursts of very intense radiation for biomedical and health physics research, has no moderator and is shielded only by its location in a depression among several heavily wooded hills. Its control building is about 800 feet away, shielded by a ridge. The glow of Cerenkov radiation surrounds the core of the Oak Ridge Research Reactor, one of the most powerful at ORNL. The ORR is used in research and in the production of isotopes. The Tower Shielding Reactor is designed to emit radiation of equal intensity in all directions. It can be suspended at any height up to 200 feet from its 325-foot towers. The controls are in an underground building. The TSR is used in studies of the effects of air, structures, and ground on radiation scattering. The Experimental Gas-Cooled Reactor, which will produce 22 megawatts of electrical power, is the first civilian gas-cooled power reactor in the United States. Much of the research, design, and development work for the EGCR was done at ORNL.

HPRR

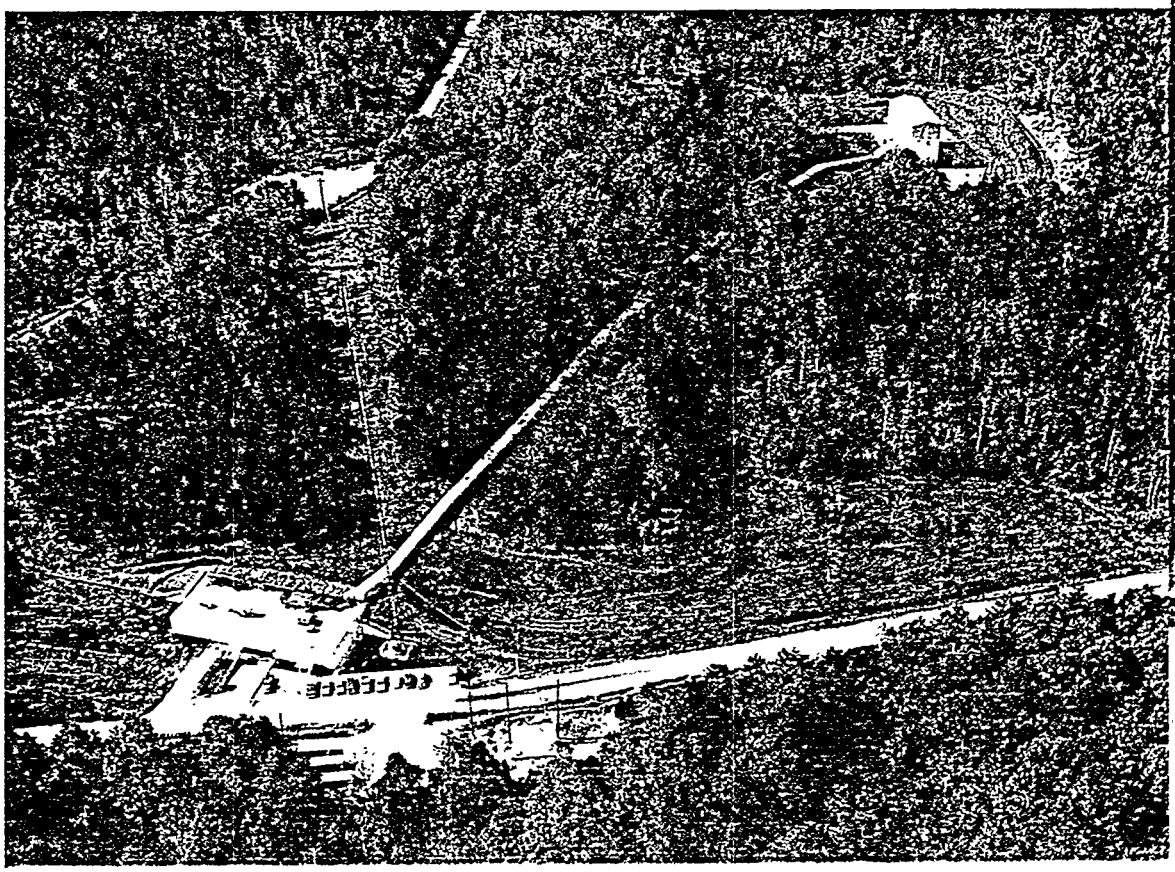

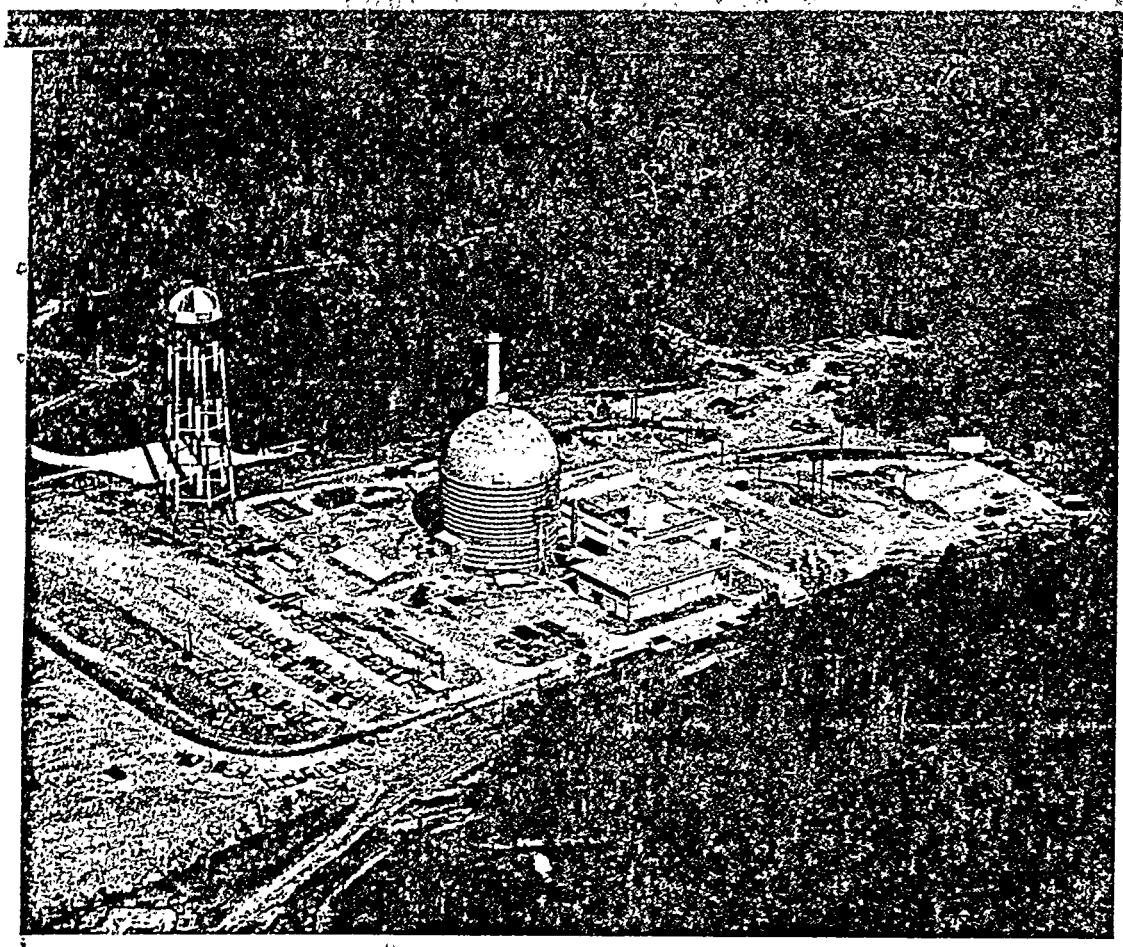

EGCR

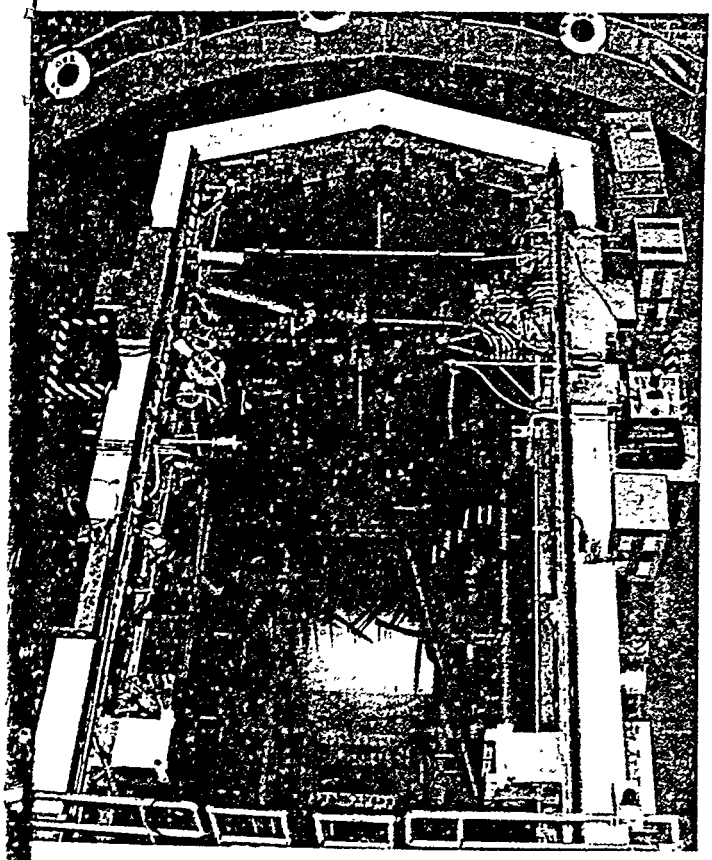

ORR

TSF

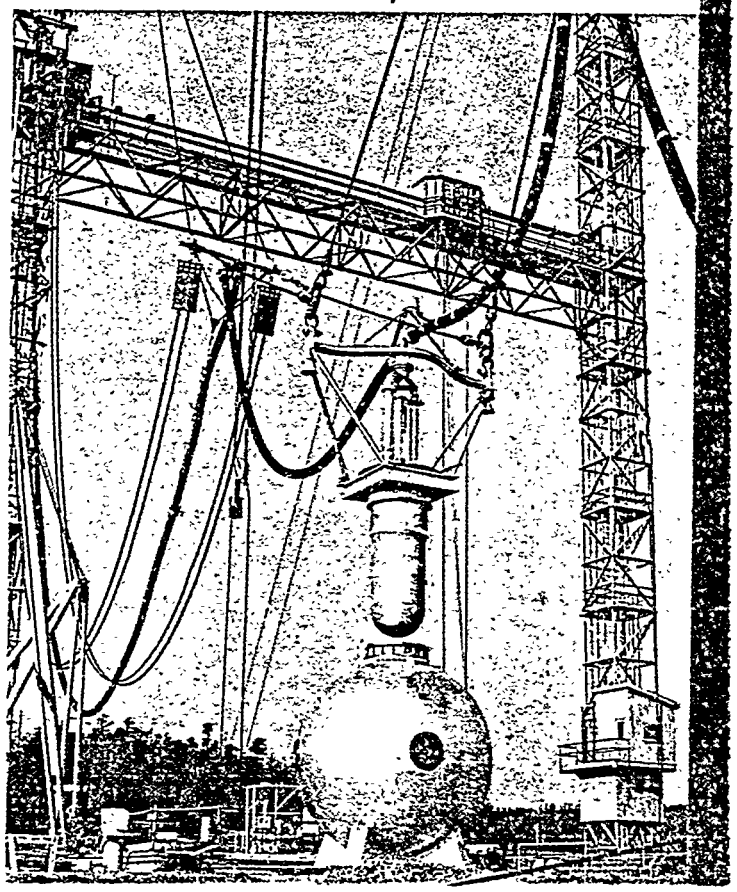

About this Report

This report is a summary of important goals and the progress toward them at Oak Ridge National Laboratory during calendar year 1963. These activities touch on most areas of interest to the Atomic Energy Commission. They include reactor development, reactor fuel processing, radioactive waste disposal, physics, mathematics, chemistry, metallurgy, solid-state physics, controlled thermonuclear research, biology, medicine, health physics, training and education, and radioisotope and stable isotope research, development, and production.

Details of the work are not included here but may be obtained from the progress and topical reports issued by ORNL.

A. M. Weinberg, Laboratory Director

J. A. Swartout, Deputy Director

F. R. Bruce, Assistant Deputy Director

ASSISTANT DIRECTORS

G. E. Boyd
R. W. Johnson
W. H. Jordan
H. G. MacPherson
M. E. Ramsey
A. H. Snell
Gale Young

Contents

About This Report .....

REACTOR DEVELOPMENT

Gas-Cooled Reactor Program 3
Experimental Gas-Cooled Reactor 3
Physics Analysis 3
Procurement of the EGCR Fuel Assemblies 4
Irradiation Testing of the EGCR Fuel Element Concept 4
Instrumented Fuel Assemblies 5
Fuel Rod Spacing Measurements 5
Steam-Graphite Reaction Experiments 5
In-Pile Creep Testing of Graphite 6
Materials Studies 6
Fission-Gas Release from Uranium Dioxide 6
Thermal Conductivity of Uranium Dioxide 8
Reactivity of Graphite with Water Vapor and Carbon Dioxide in Helium 8
Fission Product Transport and Deposition 9
Radiological Decontamination of Metal Surfaces 10
Compatibility of Graphite and Metal in Hydrogen 10
Irradiation Tests and Facilities 11
Fuel Capsule Irradiations in LITR, ETR, and ORR 11
GCR-ORR Loop No. 2 Irradiation Tests 12
Fuel Element Irradiations in the ORR In-Pile Loop No. 1 13
German Pebble-Bed Reactor 13
AVR Reactor Physics 14
Design and Analysis 14
Fuel Element Development 15
Fueled Graphite Program 15
Coated-Particle Development 15
Reactivity of Fueled Graphite with Steam 15
Fission-Gas Release from Coated Particles 16
Irradiation Effects on Fueled Graphite 17
Diffusion of Actinides in Pyrolytic Carbon and Porous Graphite 18

Design Analysis 19
Design of Graphite Structures for Use in a Nuclear Reactor 19
Analyses of Single-Nozzle to Spherical-Shell Attachments 19

Fast Gas-Cooled Reactors 20
Fast Gas-Cooled Reactors with Indirect Power Cycles 20
Fast Gas-Cooled Reactor with Direct Power Cycle 20
Concrete Pressure Vessels 21

Molten-Salt Reactor Program 22
Introduction 22
Development and Construction 22
Chemical Development for the MSRE 27

High Flux Isotope Reactor 29
Introduction 29
Project Status 30
Instrumentation 31
Reactor Physics 33
Control Plates 33
Fuel Elements 33
HFIR Development 35
Control-Plate Pressure-Equalization Test Facility 35
Control-Plate Drive 36
Bearing Tests 36
Remote Refueling Tools 37
Miscellaneous Investigations 38

Army Reactors Program 39
Europium Oxide Studies 39
Pressurized-Water Reactor Chemistry 40

Space Reactor Program 41
Forced-Circulation Boiling-Potassium Corrosion Loops 42
Type 316 Stainless Steel Loops 42
Columbium—1% Zirconium Loop 43

Thorium Utilization Program 46
Sol-Gel Process for Remote Preparation and Fabrication of Recycle Fuels 46

Reactor Shielding 49
A Shielded-Diode Fast-Neutron Spectrometer 49
Energy Spectra of Fast Neutrons in BSR-I Water Shield 50
Energy Spectra of Gamma Rays Emitted by BSR-II 51
Time-of-Flight Measurements of the Spectra of Fast Neutrons Leaking from Water and LiH Slabs 54
A Method for Analyzing Neutron and Gamma-Ray Spectra 55
Shielding Studies for SNAP Systems 56
Studies of Shielding Against Nuclear Weapons Radiation 57
Radiation Shielding Information Center 59

Basic Reactor Physics 61
Neutron Cross-Section Studies 61
Measurement of α as a Function of Energy 63

Prompt-Neutron Lifetimes in Critical Assemblies of 93.2 Percent Uranium-235-Enriched Uranium Metal in Cylindrical Geometry 64
Application of Monte Carlo Calculational Techniques to the Study of Fast Critical Assemblies 65

Reactor Fuels and Materials 66
Radiation Effects in Structural Materials 66
In-Reactor Internal Friction Measurements of Precipitation in Alloys 66
Radiation-Enhanced Diffusion in Copper-Base Alloys 67
Tensile Properties of Irradiated Nickel 68
Nondestructive Test Development 69
Low-Voltage Microradiography 69
Ultrasonic Detection of Nonbond 70
Use of Eddy Currents for Nondestructive Testing 70
Nondestructive Determination of Fuel Homogeneity 73
Mechanical Properties 74
Effect of Hydrogen on the High-Temperature Properties of Metals and Alloys 74
Radiation Effects in Fuel Cladding Materials 75
Radiation Creep of Graphite 76
Behavior of Stainless Steels in Carbon Dioxide 77
Zirconium Alloy Development 77
Diffusion in High-Temperature Metals 78
Corrosion in Liquid-Alkali-Metal Systems 80
Fuel Element Development 80
Pyrolytic Fabrication of Refractory Carbides 80
Fabrication of Aluminum-Base Fuel Plates 81
Aided Sintering of Uranium Monocarbide 81
Stress-Induced Release of Fission Gases from Reactor Fuels 81
Radiation Damage to Beryllium Oxide 82

Reactor Components 83
Reactor Controls Development 83
Measurement of Shutdown Reactivity 83
Electrically Adjustable Compensated Ion Chamber 83
Use of Gamma Radiation as a Reactor Control and Safety Parameter 84
Modular Electronic Instruments 84

Power Reactor Fuel Processing 86
Chemical Analysis of Advanced Reactor Fuels 86
Studies on the Dissolution of Ceramic Fuels for Breeder Reactors 87
Chemical Process Development: Carbide Fuels 87
Selective Removal of the Fuel from Tubular Fuel Elements by the Chop-Leach Process 88
Oxidation of Spent Graphite-Matrix Fuel Elements Prior to Recovering the Uranium 90
Recovery of Fissile and Fertile Fuel from Thorium Breeder Reactors 91

Fused-Salt Fluoride-Volatility Process for Recovering Uranium from Certain Alloyed Fuels 91

Nuclear Safety 93
Release of Fission Products on In-Pile Melting of Reactor Fuels Under Transient Reactor Conditions 94
Fission Product Release from Meltdown of a Cluster of Center-Heated UO_2 Fuel Pins 95
Iodine Control on the Nuclear Ship "Savannah" 96

Criticality Safety 97
Critical Three-Dimensional Arrays of Neutron-Interacting Uranium Enriched Uranium Metal Units 98
Effects of Borosilicate Glass Raschig Rings on the Criticality of Aqueous Uranyl Nitrate Solutions 98

Waste Disposal 99
Clinch River Studies 99
Sediment Studies 99
Safety 99
Mineral Exchange Studies 100
Studies of Cesium Selective Minerals 100
Disposal of Radioactive Waste in Geologic Formations 102
Disposal in Natural Salt Formations 102
Disposal in Permeable Formations by Well Injection 103
Hydrofracturing Pilot Plant 104
Foam Separation Studies 106
Removal of Strontium from Process Waste Water Low in Radioactivity 106
High-Activity-Waste Calcination 106
Engineering, Economic, and Safety Evaluation 107
Evaluations of Waste-Management Methods 107

Studies and Evaluations 109
Studies Relating to Shipping Containers for Spent Reactor Fuel 109

PHYSICAL RESEARCH

Physics and Mathematics 113
Neutron Capture and Cosmology 113
Accelerator Terminal Pulsing and Klystron Bunching 114
Free Neutrons and Gravity 116
Gamma Rays from Resonance Neutron Capture 116
Nuclear Reaction Theory 117
Nuclear Recoils Following Radioactive Decay 118
Data Information and Evaluation Center 118
Shielding Against High-Energy Radiations 118
Mass Spectrometry 120
Thermal Diffusion Isotope Separations 120
Mathematics and Programming Research 120

Electronuclear Research and Development 121
Accelerator Development 121
Introduction 121
The Oak Ridge Isochronous Cyclotron 121
Proposed High-Intensity Proton Accelerator 123
Cyclotron Analogue II 127
Residual Radiation Studies 128
Separated-Orbit Cyclotron 129
Superconducting Magnet Studies 130
Nuclear Physics 130
Introduction 130
Elastic Scattering of Helium-3 Ions 131
Fluctuations in Nuclear Cross Sections 132
Fine Details of the Shell Model in the Mass Region $90 < A \lesssim 100$ 132
Useful Diagrams for Representing Nuclear States 133

Chemistry 135
Analytical Chemistry Research 135
Gas-Chromatographic Determination of Trace Contaminants in Helium 135
Effects of Radiation on Analytical Methods 136
Radiolysis of Chloride Solutions 136
Effect of Gamma Radiation on Arsenazo III Solutions 136
Effect of Gamma Radiation on the Nickel-Dimethylglyoxime Reaction 137
Analytical Instrumentation 137
Voltammetric Studies in Molten Fluoride Salt Systems 138
Molten-Salt Spectrophotometry 139
Advances in Apparatus 139
Reactions of Active Metals with Molten LiF-NaF-KF 139
Coordination of Dissolved Ionic Species in Fluoride Melts 140
Chemical Engineering Research 140
High-Performance Solvent-Extraction Equipment 140
Systems and Materials Chemistry 141
Recovery and Separation of Fission Product Elements 141
Recovery and Separation of Alkali Metals 141
Purification of Transplutonium Elements 141
Acid Recovery 142
Fundamental Extraction Chemistry 142
Recovery of Thorium from Granitic Rock 142
Radiolysis of Metallic Fluorides 142
Pyrolysis of Biphenyl 143
Nuclear Methods of Chemical Analysis 143
Neutron Energy Distribution from ^{241}Am-Be Neutron Sources 143
Chemical Effects of Isomeric Transitions in Tellurium 143
Activation Analysis of High-Purity Materials 144
14-Mev Neutron Reactions 144
Nuclear Methods 145
X-Ray and Spectrochemical Analysis 145

Aqueous Solution Chemistry 145
Nuclear Chemistry 146
Radiation Chemistry 147
Formation of Ozone in the Radiolysis of Liquid Oxygen and in Oxygen-Nitrogen Solutions 147
"Thermal Spikes" in Radiation Chemistry 148
Carbon Dioxide Sensitized Radiolysis of Hydrogen and Oxygen 148
Organic Chemistry 148
Recent Studies on Molecular Rearrangements 148
Isotope Effect Studies 149
New Organic Solvents for the Extraction of Source and Fissionable Materials 150
Grafting Polymers onto Cellulose Membranes 150
Purification of Organic Compounds 151
Solutions of Metals in Molten Salts 151
Development of an Electrochemical pH Stat 151
Electrochemical Study of the Mechanism of Corrosion Inhibition on Iron 152
The Crystal Structures of Some Xenon Fluorides 152
Determination of Molecular and Crystal Structure of Sucrose by Neutron Diffraction Analysis 153
Molecular-Beam Studies in Physical Chemistry 154
Radio-Frequency and Microwave Spectroscopy 154
Physical Chemistry of Gaseous Thermodynamic Working Fluids 155
Physical Chemistry of Molten Salts 156
Chemical Studies in Support of the Fluoride Volatility Process 156
Chemical Behavior in Molten Fluoride Solutions 156
Complex Compounds Between Fluorides 157
High-Temperature Aqueous Solution Chemistry 157
Electrical Conductance of Aqueous Solutions at Very High Temperatures and Pressures 157
High-Temperature Acidity Measurements: Thorium(IV) and Iron(II) Hydrolysis 157
High-Temperature Isopiestic Studies 158
Phase Equilibria in High-Temperature Systems 158
Isotope Chemistry 159
Oxygen Isotope Enrichment 160
Target Preparation 160
Transuranium Processing Plant 161
Metallurgy and Materials 163
Preparation of Pure Materials 163
Purification of Beryllium by Solvent Extraction and Preparation of Pure Beryllium Hydroxide 163
Research and Development on Pure Materials 163
Information for Materials Research 163
Reactions at Metal Surfaces 164
Mechanism of Metal Oxidation 164
Deformation of Crystalline Solids 165

Fundamentals of Metal Deformation 165
Deformation of Refractory Metals 165

Structure of Metals 166
Grain Growth During Recrystallization of Aluminum 166
Structure of Molten Salts 166

Fundamental Research in X-Ray Diffraction 166
Structure of Irradiated Beryllium Oxide 166

Physical Properties Studies 167
Fundamental Properties of Metals and Alloys 167
Thermal Conductivity of Uranium Dioxide and Iron 168

Crystal Physics 169
Growth and Study of High-Temperature Crystals 169

Fundamental Investigation of Radiation Damage in Solids 169
Interactions Between Color Centers in Alkali Halides 169
The Theory of Atom Ejection Patterns 170
The Pseudo-Potential and Liquid Metals 171
Theoretical Studies of the Electronic Structure of Lattice Defects in Ionic Crystals 171
Diffusionless Self-Anneal in Vacancy-Interstitial Clusters 171
Nonlinear Ultrasonic Effects in Metals 172
Chemical Reactivity of Metal Surfaces 172
Anomalous X-Ray Transmission in Copper Crystals 172
Phonon Scattering by the *F*-Center Electron 174
Electron Microscope Studies of Fission Fragment Damage in Molybdenum Trioxide 174
Electron Spin Resonance of Defects in Diamagnetic Insulating Materials 175
Resistive Transitions and Critical Fields in Pb-Tl Superconducting Alloys 175

Controlled Thermonuclear Research 176
DCX-1 176
DCX-2 177
Electron-Cyclotron Heating 178
Plasma Physics 179
Vacuum Arc Research 179
Cross-Section Measurements 180
Production, Acceleration, and Injection of Ionic and Atomic Beams 181
Vacuum 181
Magnetics and Superconductivity 181
Plasma Theory and Computation 182
Chemical Studies of High-Vacuum Technology for Thermonuclear Fusion Experiments 183

Reactor and Hot-Cell Operations 184
Reactor Operations 184
Radioactive Waste Disposal 185
Hot-Cell Operations 186

BIOLOGY AND MEDICINE

Statistical Services and Research 189

Radiation Effects 191
- Identification and Isolation of Bone-Marrow Stem Cells 191
- A Specific Chromosomal Abnormality in Mice with Myeloid Leukemia 191

Radiation Genetics 193
- Effects of Radiation on Plants and Seeds 193
- Studies on the Nature of Initially Reparable Premutational Lesions 194
- Genetic Analysis of Radiation Behavior in *Escherichia coli* 194
- Mammalian Genetics 195
  - Radiation Mutagenesis in Mice 195
  - Mouse Cytogenetics 200
  - Radiation-Induced Death in Different Mammalian Germ-Cell Stages 201

Molecular- and Cellular-Level Studies 202
- Molecular Changes that Lead to Recovery from Radiation Damage 202
- Studying Plant Development Using Irradiation to Prevent Cell Division 203
- Localization and Progressive Appearance of Lens Antigens in Transformation of the Iris into the Lens 204
- Photosynthesis 205
- Hormonal Control 205

Terrestrial and Fresh-Water Ecology 207
- Radiation Ecology 207
  - Glass-Rod Dosimetry in Environmental Studies 207
  - Biological Half-Life of Strontium in White Crappie 208
  - Biological Movement of Strontium-90 by Emergent Aquatic Insects 209
  - Transport of Radioactive Mud by Mud-Dauber Wasps 209
- Evaluation of Fission Product Distribution and Movement in White Oak Drainage System 210
  - Accumulation and Movement of Radionuclides in White Oak Creek Basin 210

Radiological Physics, Health Physics, and Radiation Instrumentation 211
- Health Physics Research Reactor Studies 211
- Radiation Physics and Dosimetry 211
  - Interaction of Low-Energy Electrons 211
  - Electron Spectra in Irradiated Matter 212
  - Studies of Plasma Effects in Solids 213
  - Energy-Loss Processes from Low-Energy Heavy Particles 213
  - Calculation of Radiation Dose from Protons of Energy up to 400 Mev 214
  - Cross Sections for Emission of Light from Electron-Irradiated Metals 214
- Estimation of Internal Dose 214

Basic Instrumentation 216
Lithium-Drifted Germanium Detectors 216
Charge-Sensitive Preamplifier 216
Instrumentation for Photosynthesis Studies 217

Nuclear Energy Civil Effects 218
Ichiban Dosimetry Program 218

ISOTOPE DEVELOPMENT

Nuclear Analysis Research and Development 223
Determination of the Origin of Opium 223
Neutron Activation Analysis of Wool 223
Neutron Activation Analysis Studies on Hair 223
Guide to Activation Analysis 224

Application of Radioisotopes in Analytical Chemistry 224
Radioisotope Studies of Determinations of the Alkaline-Earth Elements 224
Extraction and Determination of Cesium and Rubidium with 4-*sec*-Butyl-2(α-methylbenzyl)phenol (BAMBP) 224
Liquid Scintillation Counting of Carbon-14 Using a "Balanced Quenching" Technique 225
Wear Rates in Automotive Engines by Liquid Scintillation Counting of Iron-55 225
A New Liquid Scintillator for Neutron Detection 225
Selective Determination of Mercury by Isotope Exchange 225

Analysis of Gamma-Ray Nuclides by Electronic Spectra Resolution 226
Electronic Resolution of Gamma-Ray Spectra 226
Gamma-Ray Branching Determinations 226

Isotopic Power and Heat Sources Development (Curium Program) 226

Radioisotope Production and Separations Technology Development 227
Fission Products Development 227
Neutron Products Development 230
Cyclotron Products Development 231
Advanced Technology 231
Safety Testing 231
Isotopes Information and Quarterly Review 232

Electromagnetic Stable-Isotope Separations 232
Special Separations 234

EDUCATION AND TRAINING

Oak Ridge School of Reactor Technology 237

He cooled
graphite moderated
2.46% enriched UO_2 in
stainless steel tubing

Gas-Cooled Reactor Program

EXPERIMENTAL GAS-COOLED REACTOR

The Experimental Gas-Cooled Reactor (EGCR) is a dual-purpose test facility being constructed by the Atomic Energy Commission at Oak Ridge, Tennessee. The plant will demonstrate the generation of electricity by a gas-cooled nuclear reactor and permit experimental testing of large-scale gas-cooled reactor components for advanced applications. The reactor will have a thermal power output of 85,000 kilowatts and a net electrical output of about 22,000 kilowatts. The reactor will be cooled by an inert gas, helium, and moderated by nuclear-grade graphite. The fuel is slightly enriched uranium dioxide clad in stainless steel tubes.

An extensive research and development program has been carried out in support of the EGCR concurrently with construction activities. Most of the research activities have been completed, and the reactor itself is approximately 70 percent complete.

As a part of the Commission's overall program for the development of civilian power reactors, the Oak Ridge National Laboratory (ORNL) has performed a large amount of design analysis and experimental investigations applicable to the EGCR. In addition, the Laboratory designed, developed, and procured the fuel and control-rod assemblies. Assistance has been provided to the construction contractor, the H. K. Ferguson Company, and the reactor operator, the Tennessee Valley Authority, in the preparation of procedures and specifications, investigation of specific problems associated with major components, and development of startup and operational manuals. The principal areas of these activities and the accomplishments during the year are described in the following paragraphs.

Physics Analysis

The increasingly widespread use of pulsed-neutron techniques has emphasized the absence of a general theoretical treatment of transient flux distributions in pulse-reflected reactors. The importance of pulsed-source experiments during the startup of the EGCR has prompted a study of this problem, and analytical techniques have been developed for calculating the neutron flux distributions during the transients.

Expansions in terms of orthogonal functions are used to express the diffusion equations in a form which allows analytical integration of the space dependence and casts the equations into matrix form. An eigenvalue problem is then identified, whose solution provides eigenvectors corresponding to the spatial modes in the reactor and eigenvalues corresponding to the decay constants of the modes. Three classes of modes have been identified. Two of these have time constants related to the reactivity of the system through the well-known inhour equation, and the third has time constants related to the reactivity with nonthermal fissions only. The method has been programmed for the IBM 7090 computer, and a number of practical applications have been made to the planning of experiments.

Procurement of the EGCR Fuel Assemblies

The 1404 fuel assemblies for the first core of the Experimental Gas-Cooled Reactor, plus an additional 300 spares, were delivered by the Atomic Fuel Department of the Westinghouse Electric Company. Accurate production records were maintained so that fuel assembly performance characteristics may be evaluated with respect to fuel assembly quality. Such comparisons will be useful in determining the quality requirements for subsequent core loadings. The fuel assemblies are now stored at the Oak Ridge Gaseous Diffusion Plant.

Each fuel assembly is composed of seven 29-inch-long rods of 2.46 percent enriched uranium dioxide bushings clad with 0.020-inch-thick type 304 stainless steel tubing 0.750 inch in outside diameter. The seven rods are supported in a cluster within a 5-inch-diameter, 1-inch-thick graphite sleeve by cast stainless steel "spiders." The UO_2 bushings are cored (0.323 inch in inner diameter) to permit lower fuel central temperatures and facilitate fission product gas storage.

The fuel assemblies cost $55 per kilogram of contained uranium metal — a fabrication price lower than comparable metal-clad ceramic fuel assemblies for other concepts.

UNCLASSIFIED
R-12142

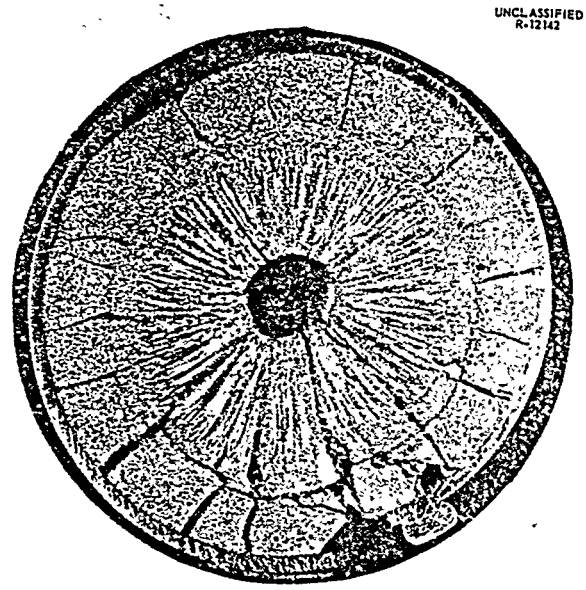

Transverse section through a failed capsule. Note void in center of originally solid UO_2 pellet, columnar grains radiating from central void, and large fracture in the stainless steel cladding. 6X. Reduced 41%.

Irradiation Testing of the EGCR Fuel Element Concept

The program for proof testing the EGCR fuel element concept, which is sintered UO_2 fuel pellets contained in type 304 stainless steel, is near completion. Thirty-six prototype fuel capsules, each simulating the EGCR fuel elements except for length, have been irradiated and examined. These capsules were irradiated at cladding temperatures of 1300 to 1600°F to fuel burnups as high as 10,000 megawatt-days per metric ton of uranium. Most of the capsules performed satisfactorily and displayed no adverse effects as a result of the irradiation. Dimensional changes (diameter, length, and bowing) were small; the cladding tended to collapse against the fuel, as expected, and bowing was usually less than 0.010 inch. Although it was somewhat variable, fission-gas release was low, generally 0.1 to 1.0 percent of the ^{85}Kr. The fuel pellets usually fractured into several pieces, but remained in place. There were no significant reactions between the fuel and cladding.

by what?

Eight of the capsules suffered some type of failure which allowed fission products to escape from the container. Detailed examination showed that each of these failures had been associated with, and in most cases was a result of, conditions outside those of the EGCR design. Severe cladding fractures occurred as a result of high stresses, which were caused by the expansion of overheated UO_2, imposed on nitride embrittled cladding. The nitride, which had originated as an impurity in the UO_2, had decomposed and migrated to the cladding during the irradiation. Minor fractures occurred in other capsules at cladding depressions, which resulted from a lack of support for the cladding. In addition, voids formed in the cladding in areas which had been subjected to severe and repetitive stress, caused by thermal cycling. Several other capsules did not fail under similar extreme conditions.

These studies have revealed some of the potential weaknesses in EGCR fuel elements. However, the results indicate that adherence to the design operating conditions for the reactor should result in satisfactory operation of the fuel elements.

8/36 failed (leaked)

Instrumented Fuel Assemblies

Four instrumented fuel stringers have been fabricated. Each stringer is composed of four standard EGCR fuel assemblies and top and bottom dummy assemblies. The standard assemblies were instrumented with thermocouples, which will measure the fuel central temperature, the metal cladding temperature, and the helium coolant temperature. Such instrumented stringers are required to monitor the performance of the EGCR fuel assemblies at steady state and transient reactor conditions, and to supply data for postirradiation evaluation.

Fuel Rod Spacing Measurements

The spacing of fuel rods is an important consideration in nuclear fuel element operation. Excessive variations in rod-to-rod spacing may cause overheating of the rods through constriction of the coolant flow. A nondestructive testing device was developed, which determines the rod spacing through changes in the impedance of a coil passed between the fuel rods. The changes in impedance were calibrated so that the instrument's accuracy is ±0.002 inch. This device will be invaluable in postirradiation remote evaluation of rod spacings in a "hot cell."

Steam-Graphite Reaction Experiments

The leakage of high-pressure steam into the EGCR coolant circuit presents an important safety consideration since graphite is the moderator material. Chemical reactions between the steam and graphite under certain conditions may produce large quantities of hydrogen. In order to investigate the consequence of such reactions, an experimental test facility was constructed in which hydrogen generation rates are studied. The facility permits exposure of graphite specimens to steam at temperatures ranging from 1000 to 1800°F and to pressures up to 450 pounds per square inch. Initial shakedown operation of the loop has been completed and preliminary data are being obtained.

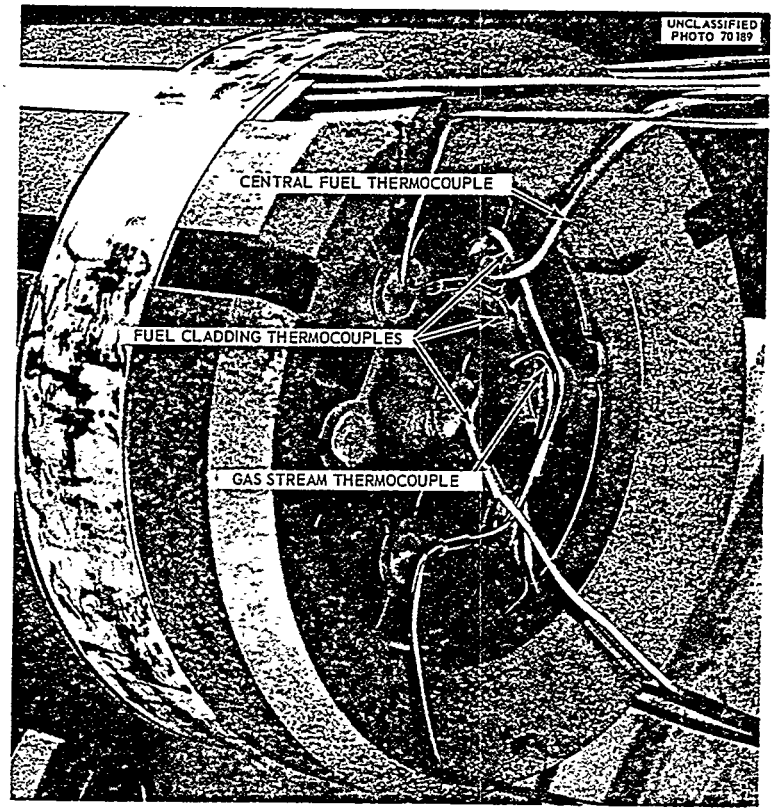

Top view of one assembly of an EGCR instrumented fuel stringer, showing thermocouples which measure the clad, coolant, and fuel central temperatures.

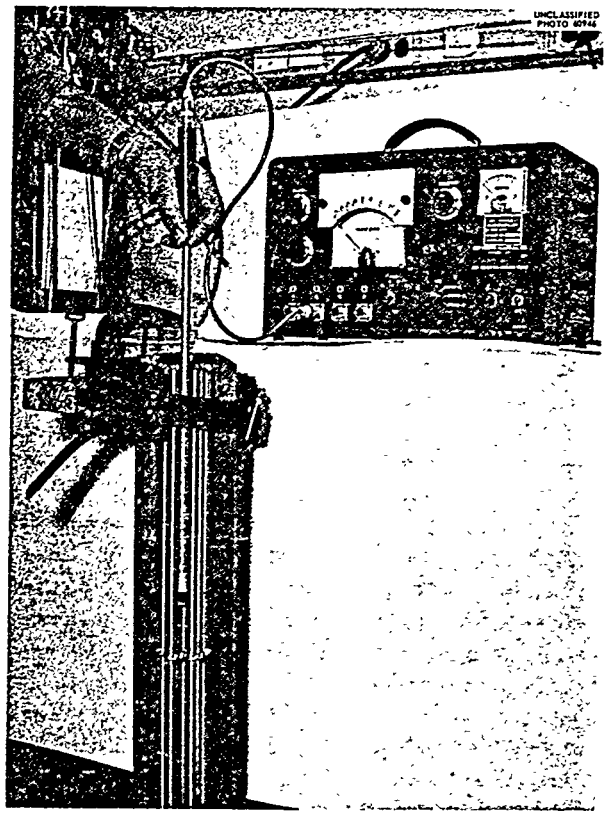

Measurement of interrod spacing of an EGCR fuel assembly with an impedance coil probe.

In-Pile Creep Testing of Graphite

A series of in-pile creep tests are being carried out on EGCR nuclear-grade AGOT-type graphite as means of determining if radiation-induced creep will allow the material to sustain greater strains than those observed when graphite is tested in the absence of irradiation. The strains expected in the EGCR graphite core due to differential shrinkages produced by neutron flux gradients are sufficiently large, on the basis of out-of-pile tests, to cause fracturing. However, recent in-pile creep test results have shown that irradiated graphite can withstand strains as much as twice that of unirradiated graphite without fracturing.

MATERIALS STUDIES

Fission-Gas Release from Uranium Dioxide

The mechanism of the release of fission gas from ceramic fuels is being studied by measuring the fission gas released from carefully characterized UO_2 specimens during irradiation at controlled temperatures. The nuclear power is regulated by moving the specimen into or out of the neutron flux of the Oak Ridge Research Reactor. The specimen is heated by its own nuclear power, and the temperature is controlled by air cooling the capsule which contains the fuel specimen. Fission gases are entrained in a continuously flowing stream of sweep gas, and the sweep gas is sampled to determine the steady-state escape rate of fission gas for a given set of conditions.

We have concluded that the fission-gas release from UO_2 during irradiation is a combination of two processes:

1. A recoil process, in which fissions near the surface of the specimen release fission gas in a manner directly proportional to fission rate and independent of temperature.
2. A temperature-dependent process, which is a combination of trapping and diffusion. The trapping process is the rate controlling factor for the high-temperature release of fission gas.

The concept that a trapping process controls the high-temperature fission-gas release is consistent with recent evidence that fission products are trapped and concentrated at defects in the UO_2 crystal structure. We postulate that the fission gases are trapped at defects and that the release of fission gas from the UO_2 is controlled by its escape from traps rather than by diffusion.

We propose that three categories of defect traps are in operation during irradiation:

1. Intrinsic traps; closed pores, grain boundaries, and impurities. These traps are constant and do not change location during irradiation at the temperatures considered here.
2. Point defects; created by fission. These traps can anneal and vanish, combine with another defect, or trap a fission product. The point defect can also migrate.
3. Clusters of point defects. These traps are semipermanent traps which are formed by the combination of point defects.

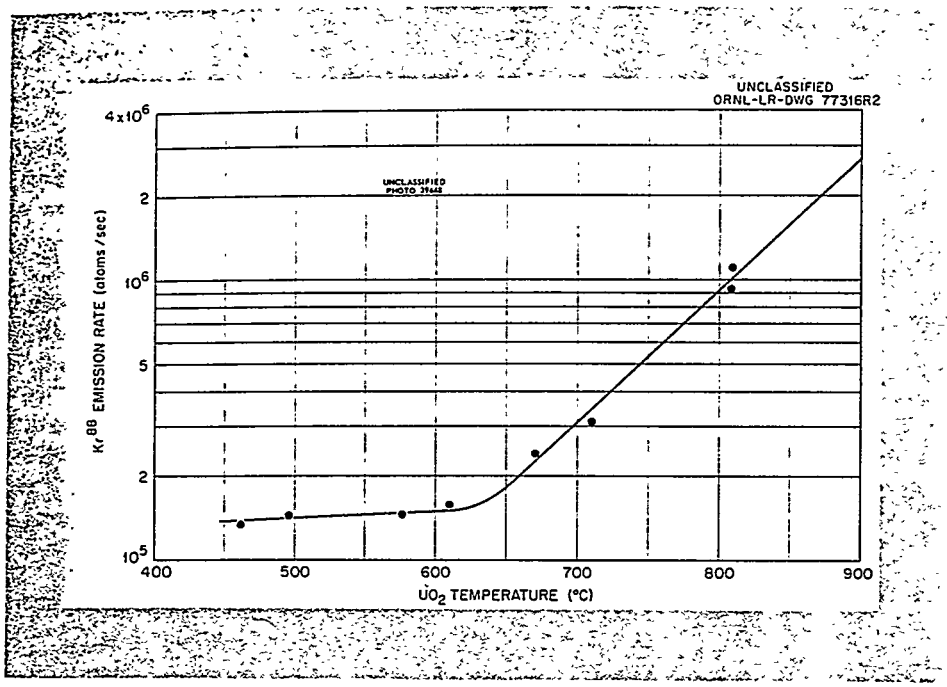

Steady-state release rate of krypton-88 from single-crystal UO_2 during irradiation ($\phi = 2.0 \times 10^{13}$).

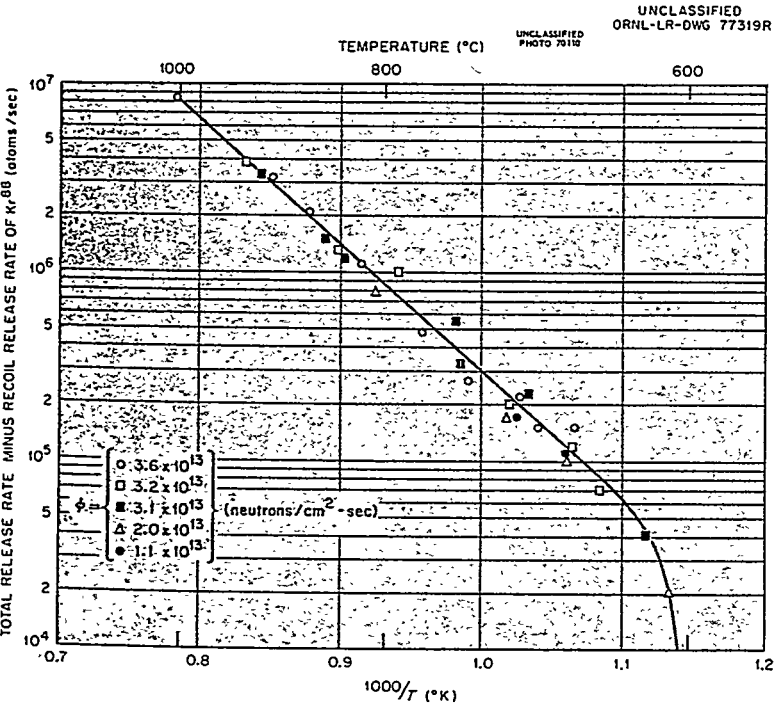

Steady-state, temperature-dependent release of krypton-88 from single-crystal UO_2 during irradiation (non-temperature-dependent contribution subtracted).

By the defect-trap theory, the trapping probability will increase when the fission density increases, and therefore the fractional release rate will decrease with increased fission rate. The high-temperature fission-gas release from single crystal UO_2 at several fission rates behaves as predicted.

Currently, we are attempting to evaluate the relative importance of the various factors influencing the fission-gas release. The fission-gas release from fine-grain specimens of UO_2 (10-micron grain size and identical in shape and density to the single-crystal specimens) was as predicted by our theory.

Thermal Conductivity of Uranium Dioxide

The thermal conductivity of nuclear fuels must be accurately known in order to predict the thermal performance of reactor fuel element concepts. In a recent series of experiments, the thermal conductivity of UO_2 was measured in a radial heat-flow apparatus from –65°C (–85°F) to 1100°C (2012°F). The thermal resistance of UO_2 (the reciprocal of its conductivity) was found to be a minimum near 0°C (32°F).

Reactivity of Graphite with Water Vapor and Carbon Dioxide in Helium

Advanced designs of gas-cooled reactors utilize an inert coolant (helium), but corrosion of graphite components may occur upon prolonged circulation of the coolant after it has become contaminated by oxidizing gases such as water vapor and carbon dioxide. Rate data which show the effects of reactant concentration, temperature, and buildup of reaction products on the gas-graphite reactions find application in the design of high-temperature gas-cooled reactors. The amount of graphite that will be lost during the lifetime of such a reactor may be estimated from the experimentally determined weight losses.

Nuclear-grade graphite was exposed at elevated temperatures to helium containing low concentrations of water vapor or carbon dioxide. The rate at which the gas mixtures reacted with the graphite was determined by following the loss in weight of the specimen continuously by means of the semimicro vacuum balance as well as from analyses of the effluent gases by a sensitive gas chromatograph. The graphite was reacted with helium–water vapor mixtures containing 20 to 760 parts per million by volume of water vapor in the temperature range of 825 to 1025°C. The same graphite specimen was reacted with helium–carbon dioxide mixtures containing 60 to 1600 parts per million by volume of carbon dioxide in a similar temperature range.

Rates of 0.025 and 0.003 mg g^{-1} hr^{-1} were found for the graphite–water vapor and graphite–carbon dioxide reactions, respectively, at 975°C and water vapor or carbon dioxide concentrations of 300 parts per million by volume. Water vapor, therefore, is about eight times more reactive than carbon dioxide under comparable conditions. The rate of the graphite–water vapor and the graphite–carbon dioxide reaction increases with increasing concentrations of oxidants. The increase, however, is not directly proportional to the increase

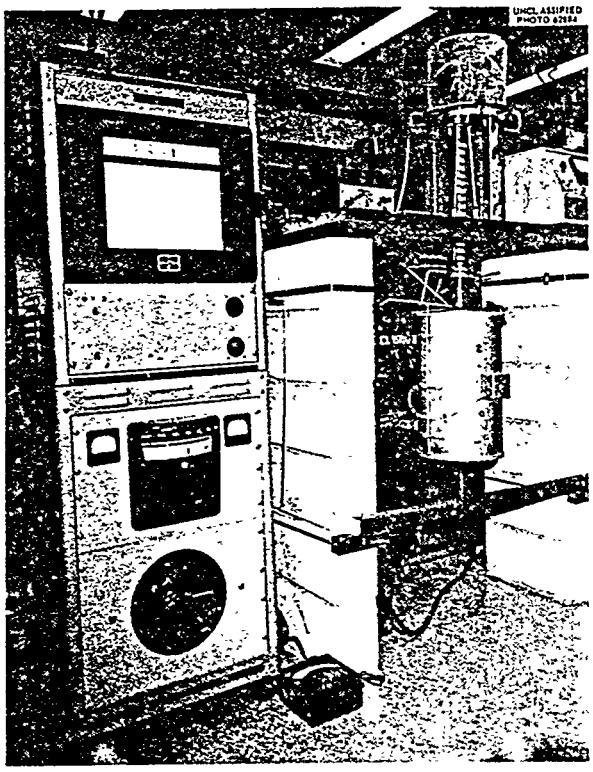

Continuously recording semimicro vacuum balance for use in following weight changes resulting from reactions such as the graphite–water vapor reaction.

in the reactant concentration but varies as the concentration raised to the 0.7 power over most of the range of concentrations examined. Hydrogen retards the graphite–water vapor reaction while carbon monoxide retards the graphite–carbon dioxide reaction. The reaction rates, therefore, may decrease with time if the reaction products are allowed to accumulate in the system or, alternatively, the corrosion of graphite may be inhibited by a deliberate addition of reaction products.

In order to more nearly simulate the conditions expected to exist in a reactor coolant system, a low-pressure loop was built in which temperature gradients can be controlled. Graphite specimens are placed in the high-temperature zone, and metal samples are placed in the cooler zone. A series of tests designed to produce data on reactions of trace amounts of carbon dioxide and carbon monoxide in helium with the graphite and the subsequent reaction and/or deposition of the products with the metal specimens are in progress.

The initial experiments in this loop operated for 833 hours with a maximum graphite temperature of 1825°F. The carbon monoxide and carbon dioxide levels were controlled at 125 and 225 parts per million respectively. On termination of the test, the graphite showed a weight loss of 0.747 gram from an initial weight of 698 grams.

Fission Product Transport and Deposition

An understanding of the mechanism for the transport and deposition of fission products throughout the primary circuit of gas-cooled reactors is important to the reactor designer in establishing shielding and remote maintenance equipment requirements.

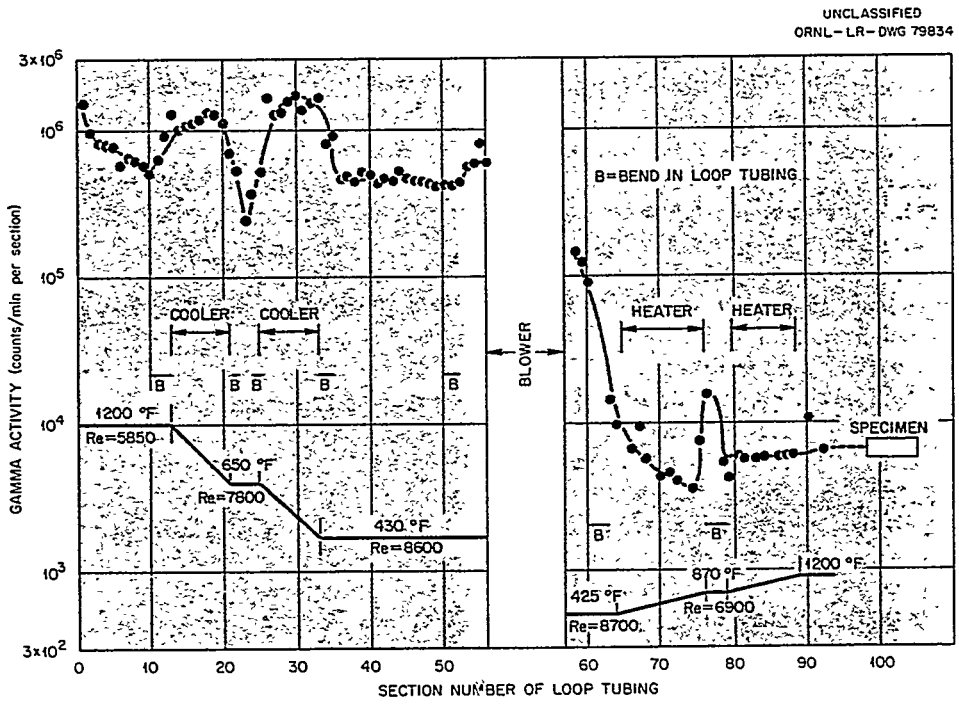

Distribution of gross gamma activity in fission product deposition facility as a function of distance from the source.

An experimental loop facility for determining fission product deposition behavior in which reactor temperatures and flow conditions can be simulated was built and operated. A radioactive specimen representative of typical unclad fuel elements is heated to cause release of fission gases to the flowing helium and subsequent deposition in the cooler regions of the loop. At the termination of each experiment, the loop piping is sectioned and the amount of deposited fission products in each section is determined.

Radiological Decontamination of Metal Surfaces

The direct maintenance of gas-cooled reactor components contaminated with gas-borne fission products would be restricted or impossible without effective noncorrosive decontamination methods. Promising new reagents have been developed and laboratory tested for the decontamination of carbon steel and stainless steel after exposure to contaminated high-temperature helium.

An effective reagent for use with carbon steel, a type of steel corroded by weak acids, is a slightly acidic solution of ammonium oxalate, ammonium citrate, and hydrogen peroxide used at or near the boiling point. The hydrogen peroxide acts as a corrosion inhibitor, metal brightener, and oxidizer. The oxalate and citrate components dissolve metal oxides and hold fission products in complexed forms. This reagent is superior to most acidic decontaminants which are much more corrosive. Room-temperature decontamination of carbon steel has also been demonstrated with modified oxalate-peroxide mixtures when about 0.0001 inch of corrosion penetration can be tolerated.

Stainless steels exposed to gas-borne fission products at about 1000°F have been much more difficult to decontaminate. Oxalic acid–hydrogen peroxide solutions with added fluoride have been satisfactory, however. No stress-corrosion cracking was observed on U-bends of stainless steels after 22 hours in 0.5 molar oxalic acid with 0.1 molar fluoride and 0.2 molar hydrogen peroxide at 95°C. The acid and peroxide concentrations were restored every hour to compensate for the slow mutual destruction of oxalic acid and hydrogen peroxide in the hot solution.

A very desirable feature of oxalate-peroxide decontamination solutions is that most of the components are volatile as gases when strongly heated, so that waste disposal in a very sma volume of solids is possible.

Photomicrograph of type 304 stainless steel surface o U-bend stressed specimen, immersed 22 hours in a oxalic acid–fluoride–peroxide solution. No stress corrosion cracks are seen. 200X. Reduced 39%.

Compatibility of Graphite and Metal in Hydrogen

Proposals to use hydrogen as a coolant in hig temperature gas-cooled reactor systems prese two potential problems involving the moderator ar structural material. First, if hydrogen is used combination with graphite, the reaction wi graphite will tend to establish a highly ca burizing gas mixture through the formation methane and subsequent mass transfer of carbo Second, in systems that do not contain graphit an opposite effect will occur; namely, there wi be hydrogen embrittlement and decarburization structural steels.

In order to study the gas-metal and gas-graphi reactions, a test program utilizing a high-temper ture autoclave was initiated. In the initial e periment, metallographic examination of type 304L and 310 stainless steel, Inconel, and 19 DL metal indicated the rate of carburization to strongly dependent on the methane concentrati

in the hydrogen and the carbon concentration in the metal. Specimens located in the gas stream were less carburized than the specimens in contact with the graphite.

IRRADIATION TESTS AND FACILITIES

Fuel Capsule Irradiations in LITR, ETR, and ORR

A new facility, the ORR Eight-Ball, for the simultaneous irradiation of several fuel elements, up to eight $1\frac{1}{2}$-inch spheres, has been installed in the core of the ORR. Four experiments were irradiated to assess the effects of fabrication variables and internal distribution of the fuel on the mechanical and chemical stability of spherical fuel elements typical of pebble-bed reactor application. The results of these irradiations will be applied to the determination of optimum specifications for fuel element design. The fuels tested to date consist of pyrolytic-carbon-coated uranium carbide and uranium-thorium carbide fuels uniformly dispersed in a graphite matrix. The fuel matrix may constitute the entire sphere or in other cases form a central fueled core surrounded by a protective spherical graphite shell of different internal configuration and formed by different processes. Tests have operated with a fuel power density of 45 watts per cubic centimeter of sphere and at sphere surface temperatures to 1725°F.

Other irradiation tests were performed in capsule irradiation facilities in the LITR, ETR, and ORR test reactors for evaluating graphite-matrix coated-particle fuels and for proof-testing vendor-made fuel in vendor-made stainless steel tubing for EGCR fuel elements. In addition, one stainless-steel-clad UO_2 fueled element was irradiated at a heat rating of 50,000 Btu hr^{-1} ft^{-1} and another fueled with UO_2 in a BeO matrix was tested.

Irradiation tests of coated-particle fuels included pyrolytic-carbon-coated uranium carbide particles both in graphite-matrix spherical elements and as loose, unsupported beds. Some fueled particles also contained thorium carbide. Sweep capsules, each containing either four $1\frac{1}{2}$-inch-diameter or three 6-centimeter-diameter fueled-graphite balls, were irradiated in the ORR poolside facility.

Test conditions and performance for the sphere irradiation tests are monitored with thermocouples and by analysis of fission gases released from certain of the fueled balls. The fuel center temperature is measured in the capsules, and development of suitable high-temperature thermocouples is

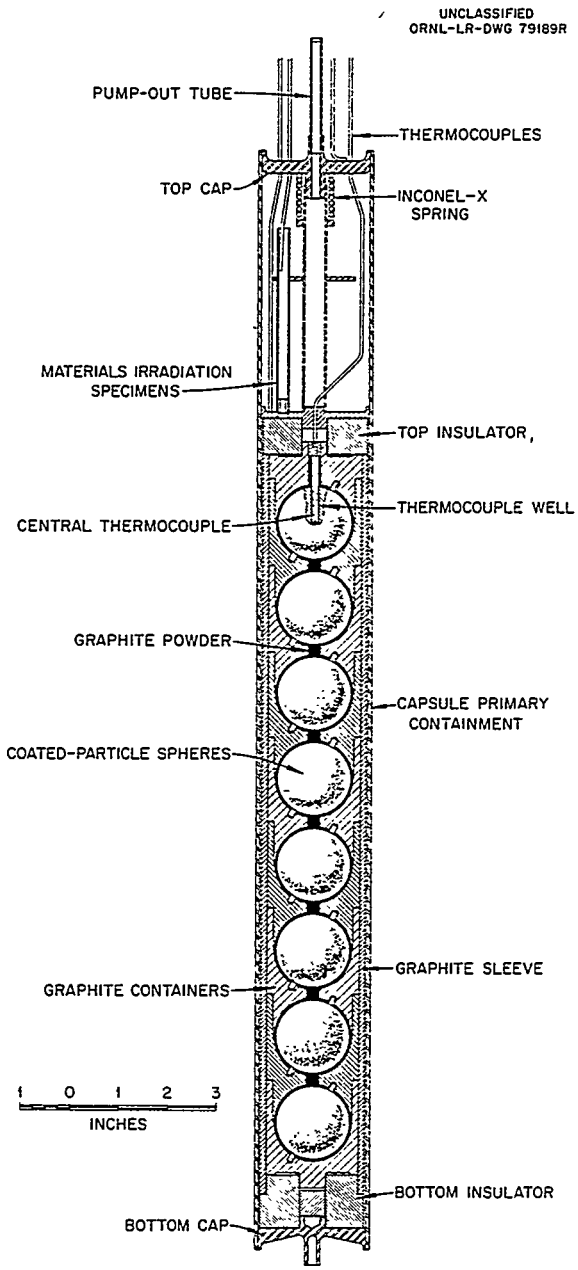

Cross section of ORR Eight-Ball primary containment capsule.

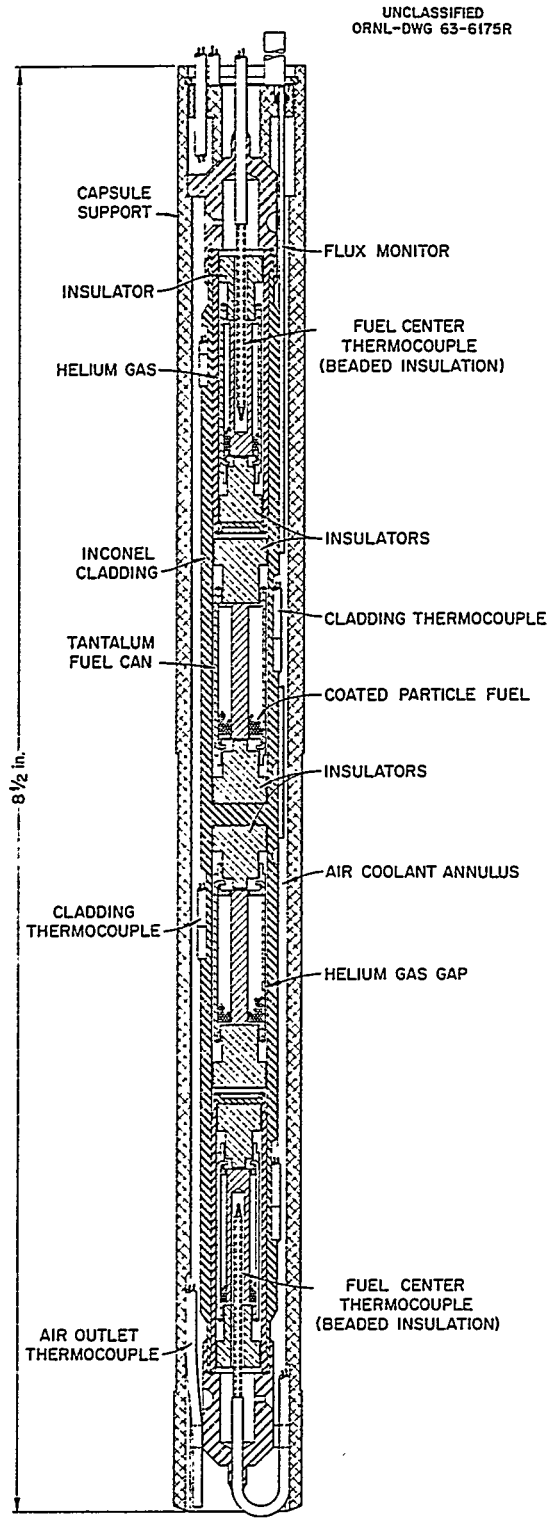

LITR capsule design for irradiation of loose or unsupported pyrolytic-carbon-coated fuel particles.

included as part of the experimental program. Or thermocouple system employs a tungsten sleeve a tantalum-sheathed beryllium-oxide-insulate tungsten–5 percent rhenium alloy vs tungsten–2 percent rhenium alloy thermocouple.

A new capsule design for irradiation of loos or unsupported coated fuel particles in the LIT increases the fuel-holder capacity from two is lated specimens to four. Fuel center temperature are measured in the top and bottom compartmen of the tandem-type vertical capsules. Upon cor pletion of an irradiated test, the released fissic gases are measured, thus determining the fissio gas retention characteristics of the coated pa ticles.

GCR-ORR Loop No. 2 Irradiation Tests

Construction and shakedown of the loop facili were completed, and three irradiation tests we conducted. The first test assembly was design to measure the perturbed thermal-neutron fl profile both within the test section and for sever positions relative to the reactor core. The fl was determined by measuring the activation argon flowing through the test assembly. The te assembly also contained a cylindrical surface which natural UO_2 was coated to provide a sour of fission products which would be transferr around the loop by the flowing stream of heli coolant. Operation of this experiment demo strated operability of the loop and its sampli equipment for fission product analysis and show that gaseous impurities such as water, hydroge oxygen, carbon monoxide, and carbon dioxide we maintained at very low levels.

The first full-scale fuel irradiation experime was run to determine the effects of irradiation four graphite-matrix spheres containing pyrolyti carbon-coated particles of uranium dicarbide fu at conditions which simulate operation in a pebbl bed reactor. Fission-gas release from the fuel spheres was very low, indicating no coati failures. The loop operated satisfactorily exce for high heat losses in the test region, whi limited the fuel temperatures.

A second fueled experiment assembly consist of three coated-particle, fueled graphite spher 6 centimeters in diameter. Each sphere contain

10 grams of 93 percent enriched uranium in the form of pyrolytic-carbon-coated particles of uranium dicarbide dispersed in a graphite matrix and was coated with an outer layer of unfueled graphite. This experiment, irradiated for 15 weeks, included study of fission-product-deposition behavior. Plans are in progress for more detailed studies of fission product behavior in circulating gas systems.

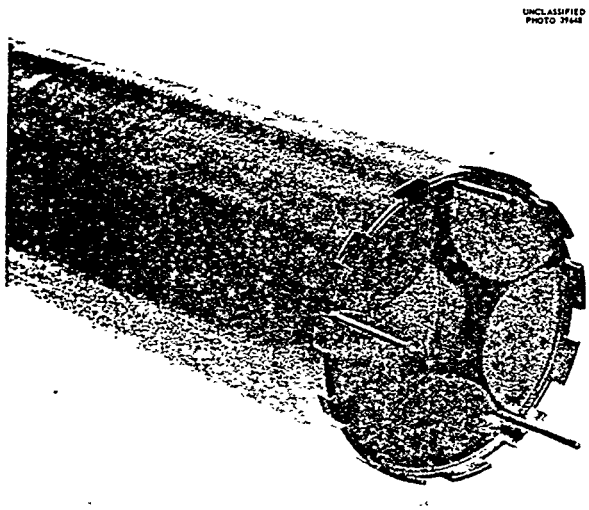

GCR-ORR loop No. 2 experiment No. 1, fuel sphere and unfueled supports which simulate pebble-bed reactor core passages.

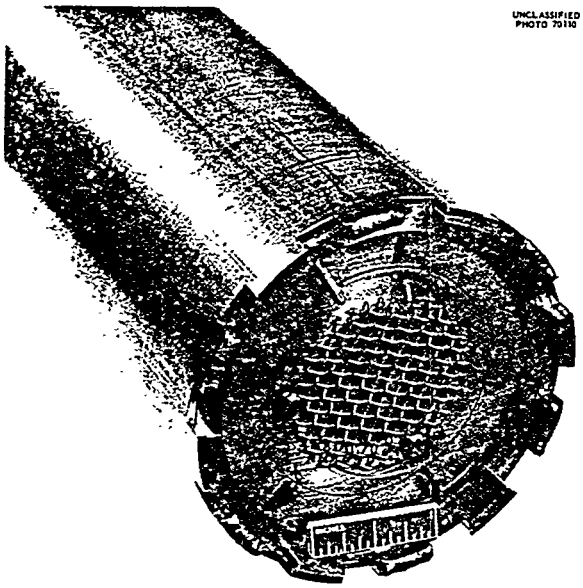

GCR-ORR loop No. 2 experiment No. 2, showing thermocouples and coolant entrance to fueled end of test assembly.

Fuel Element Irradiations in the ORR In-Pile Loop No. 1

A vented stainless-steel-clad UO_2 fuel element was operated in the loop for seven weeks to evaluate the consequences of fuel rupture in a recirculating helium system and to explore the feasibility of employing vented elements in fast and thermal gas-cooled reactors. The fuel was an EGCR-type element generating 23,600 British thermal units per foot and vented by a $\frac{1}{16}$-inch-diameter hole through the cladding near the top. The fission-product-retention characteristics of the particular fuel used was, purposely, rather poor. Nonetheless, the residual activity in the loop after operation of the element was small, permitting routine maintenance, including replacement of the compressors. Because the residual activity was small and the steady-state activity levels in the helium coolant during operation were about as predicted, the results of this test were interpreted as favorable for vented fuel elements, particularly if highly retentive fuels are used.

Several tests were run for the evaluation of clad uranium dioxide fuels for advanced gas-cooled reactors. One element operated for eight weeks with a heat generation rate of 70,000 Btu hr^{-1} ft^{-1}, about five times the average of the EGCR fuel. The higher power elements employed surfaces roughened by wrapping with fine wires or by machining grooves in the cladding to promote turbulence and thereby increase heat transfer. Test results indicate an approximate 50 percent reduction in temperature difference between the fuel element surface and the helium coolant.

GERMAN PEBBLE-BED REACTOR

Research and development was undertaken in support of the German Pebble-Bed Reactor (AVR) in view of the possibility that the first core loading for this reactor would be supplied by the

United States. The effort included reactor physics studies, design and analysis, and fuel element development.

The AVR is a 15,000 electrical kilowatt helium-cooled system having proposed inlet- and exit-gas temperatures of 350 and 1560°F respectively. The cylindrical reactor core (approximately 10 feet × 10 feet) will accommodate about 100,000 graphite spheres, 2.36 inches in diameter, and about one-third of these spheres will initially contain nuclear fuel. The research and development effort in support of this program has been guided by the long-range reactor goals of the United States with respect to thorium-uranium fuel cycles, power density, and fuel burnup.

AVR Reactor Physics

Calculations were made to select the fuel composition which would provide the most meaningful test for the fueled graphite concept in the AVR. Previous studies had shown low power costs for these fuels when the fissile material is highly enriched uranium and the fertile material is thorium; the optimum loading of the fuel spheres is about 5 percent by weight of thorium plus uranium. By having fuel in only one-third of the graphite spheres in the AVR reactor, the power density in the fueled spheres can be made as high as that anticipated in a larger power reactor.

Design and Analysis

The primary requirements for the AVR fuel elements are that they exhibit a high level of fission product retention and maintain their integrity under the thermal and mechanical effects (impact and abrasion) experienced in the reactor over two full-power years. It was demonstrated that the first major requirement can be met by incorporating the fuel in the graphite spheres as small, spherical particles (average diameter, 0.008 inch) of thorium-uranium carbide, each with a coating of carbon (average thickness, 0.004 inch) deposited from pyrolytically decomposed methane gas in a fluidized bed at high temperatures (2550 to 3650°F). The second requirement introduces the need for an unfueled graphite shell – either molded integrally or machined separately – of such a thickness that the center temperature will not exceed that demonstrated for satisfactory performance of the coated fuel particles (first requirement).

The molded-shell concept was considered initially but discarded in favor of the machined-shell concept. A detailed thermal analysis of the

UNCLASSIFIED
ORNL-LR-DWG 70105R

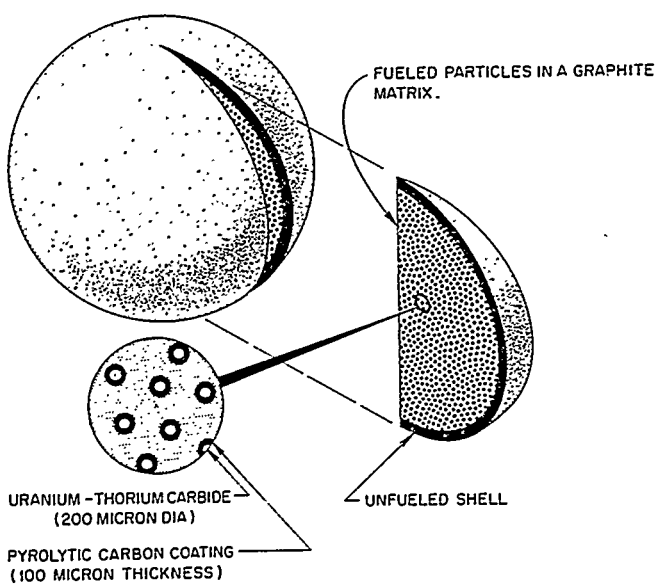

Schematic drawing of molded-shell design for AVR reactor fuel elements.

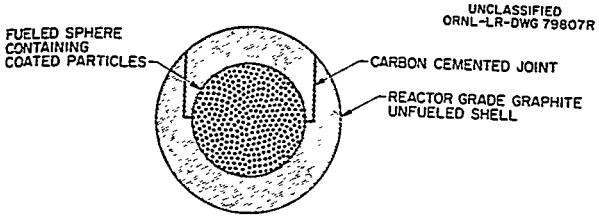

Schematic drawing of machined-shell design for AVR reactor fuel element.

reactor and fuel elements with shell thicknesses of 0.3 to 0.4 inch indicated a maximum fuel temperature of 2500°F. The resulting thermal stress for these conditions is well within the strength range of high-quality, commercially available graphite.

Fuel Element Development

Techniques for fabricating machined-shell fuel elements were developed and tested along with a variety of U.S. vendor-supplied products. A relation between forming pressure and coated-particle damage in graphite matrices was determined for guidance in design and fabrication of fuel inserts for the AVR element.

Extensive mechanical property studies on graphite and fueled-graphite spheres were performed. The results led to (1) the selection of the type of material required for the graphite shell and (2) the fuel-sphere configuration described above. Fuel spheres of the configuration adopted exhibited excellent attrition resistance and mechanical strength.

A process was developed for removal of exposed uranium and thorium from the surfaces and within the matrices of molded fueled graphite spheres of the AVR type by exposure to flowing chlorine gas at 1850°F.

Guidance in the selection of the AVR fuel element design was provided by irradiation tests on fueled graphite spheres. The facilities are described in the preceding section of the report. The in-reactor performance and postirradiation examination of these spheres and of unsupported coated particles are described in a subsequent section.

FUELED GRAPHITE PROGRAM

Coated-Particle Development

Coated-particle development work included particle preparation coating studies, out-of-reactor evaluation of coated-particle materials, and fueled graphite fabrication studies.

Carbon-coating capability was established for a range of conditions of pressure, temperature (up to 3650°F), and flow rate to produce a variety of coating structures and properties for systematic optimization studies. Carbon coatings were successfully applied to both uranium carbide and sol-gel produced oxide particles. Chemical stability of the latter was demonstrated at 3200°F, suggesting that a more extensive evaluation of carbon-coated oxide particles, including irradiation testing, is warranted.

Phase studies in the ThC_2-UC_2 systems were undertaken and a crystal-structure transformation was found in thorium-rich compositions by high-temperature x-ray diffraction and differential thermal analysis. For thorium dicarbide, the transformation from monoclinic (low-temperature form) to face-centered cubic structures was established at 2580 ± 20°F. The effect of uranium additions is to lower this transformation temperature.

Reactivity of Fueled Graphite with Steam

Fueled graphite spheres are being considered for use as fuel bodies in advanced gas-cooled reactor designs. One type of such fuel body consists of coated fuel particles dispersed in a spherical graphite matrix. The coated fuel particles contain a spherical core of uranium-thorium dicarbide protected by a pyrolytic-carbon coating. The reactivity of the fueled graphite spheres with steam at elevated temperatures is of interest because a failure in the steam generator could result in steam contacting the hot fuel bodies in an operating reactor. The hydrogen formed by the graphite-steam reaction could form an explosive mixture with air, while a failure of the fueled graphite spheres could lead to a rapid release of the contained fission products.

Fueled graphite spheres (1.5 inches in diameter), prepared by various manufacturers, were exposed to a steam pressure of approximately 1 atmosphere

at temperatures of 800 to 1000°C. The rate of reaction of the fueled graphite spheres with steam was determined from weight changes. The rate of production of hydrogen and the carbon monoxide to carbon dioxide ratio in the effluent gases were determined by gas analyses. Similar studies were made using unfueled graphite spheres for comparison with the data obtained for the fueled spheres.

Reaction rates ranging from 1 to 5 mg g^{-1} hr^{-1} were found at 900°C for the various fueled graphite spheres. Reaction rates for the unfueled graphite spheres averaged only slightly lower. The effect of temperature (800 to 1000°C) on the reaction rates was comparable for the fueled and unfueled graphite spheres. The rate of hydrogen production and the carbon monoxide to carbon dioxide ratio in the effluent gases varied widely from lot to lot of the fueled graphite spheres. The incidence of failure of the graphite matrices also varied considerably. The coated fuel particles were damaged very slightly in those cases where the matrices failed, indicating that retention of the bulk of the fission products is likely even though the matrices fail.

Fission-Gas Release from Coated Particles

In the graphite matrix fuel material concept, the fuel element is made by dispersing fuel particles in a graphite body. To reduce the amount of fission products that will be released, the fuel particles may be coated with pyrolytic carbon before being dispersed in the graphite. Four different types of pyrolytic-carbon coatings applied to either uranium carbide or uranium-thorium carbide cores are being studied to determine the fission-gas retention properties of these coatings. In these studies, the release rates of two isotopes of xenon and three isotopes of krypton are being measured during irradiation at temperatures from 1700 to 2500°F to establish the best coating specifications and to determine the fission-gas release mechanisms. The fission-gas release from uncoated uranium carbide cores was measured for comparison.

The type of coatings that have been studied are: (1) laminar, which consists of multi-layers of pyrolytic carbon; (2) columnar, which has a columnar structure and exhibits an oolitic outer surface; (3) duplex, which has a laminar inner and a columnar outer coating; and (4) triplex, which consists of a porous carbon inner coating, a laminar intermediate coating, and a columnar outer coating.

It was found that the duplex and triplex coatings were superior to the other types. The triplex-coated uranium carbide particles, which were irradiated at 2500°F to 20 atomic percent uranium burnup, showed no evidence of ruptured coatings. Triplex-coated uranium-thorium carbide particles were irradiated at 2050°F to 15 atomic percent heavy metal burnup and were cycled through the transformation temperature (from 2000 to 24,000°F) without breaking any of the coatings. Duplex-coated particles were irradiated at 2500°F to 10 atomic percent uranium burnup with equally good results.

Particles having uranium-thorium cores showed no difference in fission-gas release characteristics from particles having uranium carbide cores. Reaction zones at the core-coating interface are caused by irradiation, but after 10 percent burnup, these zones do not seem to increase with additional burnup. The isotopic proportions of fission gases from coated particles irradiated at temperatures from 2000 to 2500°F indicate that the escape is by diffusion through the coatings rather than through cracked coatings. The release rate, however, is so low that the gas may be coming from

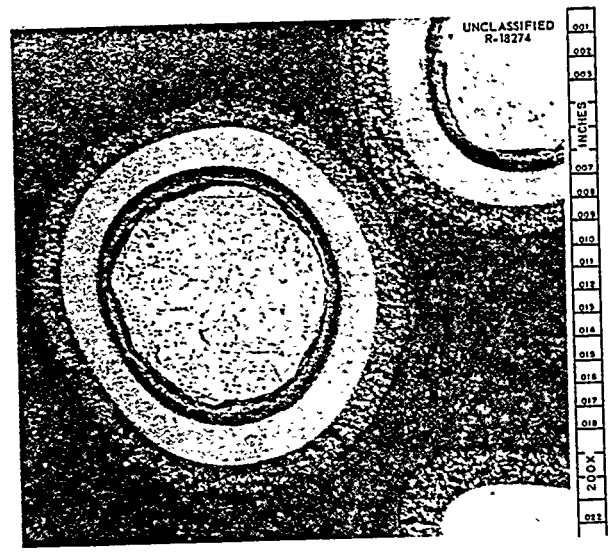

Sectional view of triplex pyrolytic-carbon-coated uranium carbide particles irradiated to 20 atomic percent uranium burnup at 2500°F. Reduced 39%.

uranium contamination in the coating rather than from the fuel cores. The diffusion of krypton is favored over xenon.

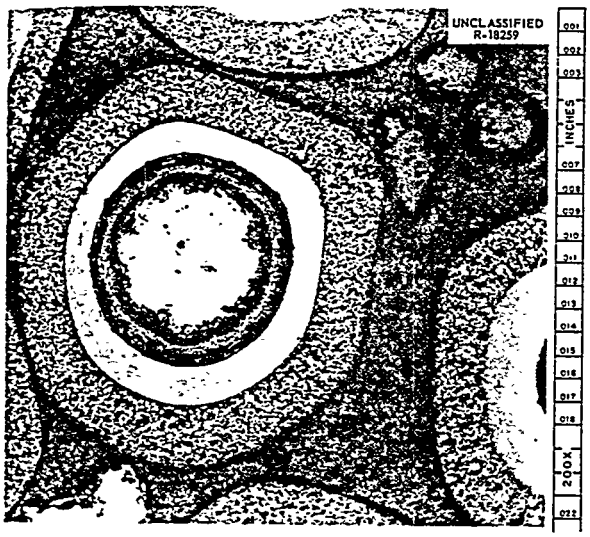

Sectional view of triplex pyrolytic-carbon-coated uranium-thorium carbide particle irradiated to 15 atomic percent heavy metal burnup at 2050° F. Reduced 39%.

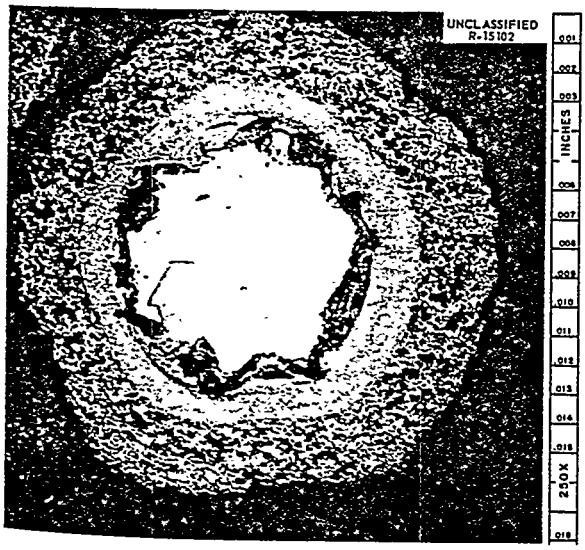

Sectional view of duplex pyrolytic-carbon-coated uranium-thorium carbide particle irradiated to 10 atomic percent heavy metal burnup at 2050° F. Reduced 39%.

Irradiation Effects on Fueled Graphite

Fuel elements in the form of either 1½-inch- or 2.36-inch-diameter graphite spheres have been irradiated in the ORR at surface temperatures ranging from 535 to 1975°F. Measured central temperatures ranged from 940 to 2650°F. These spheres were fueled with pyrolytic-carbon-coated uranium carbide or uranium-thorium carbide particles dispersed in a graphite matrix, and were of several types of construction. Burnup of the heavy metal ranged from 0.7 to 19.5 atomic percent, and fission-power densities were 14 to 167 watts per cubic centimeter.

Following irradiation, the spheres were examined in the hot cells. Only two spheres, of about 50 examined, showed any outward signs of physical deterioration. These were 1½-inch-diameter spheres fueled with uncoated uranium carbide particles. Weight and dimensional changes were generally not significant.

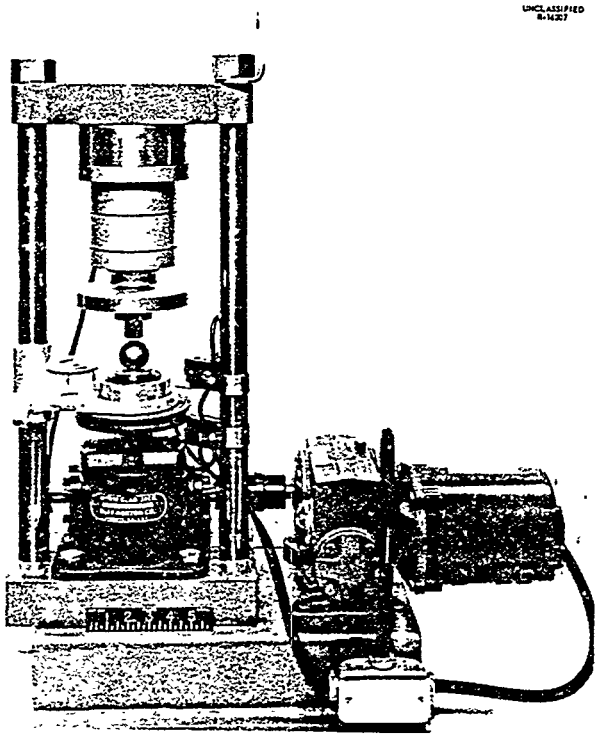

Compression test apparatus for testing fueled spheres in the hot cell. A sphere, shown in place, is loaded by a motorized worm-gear jack.

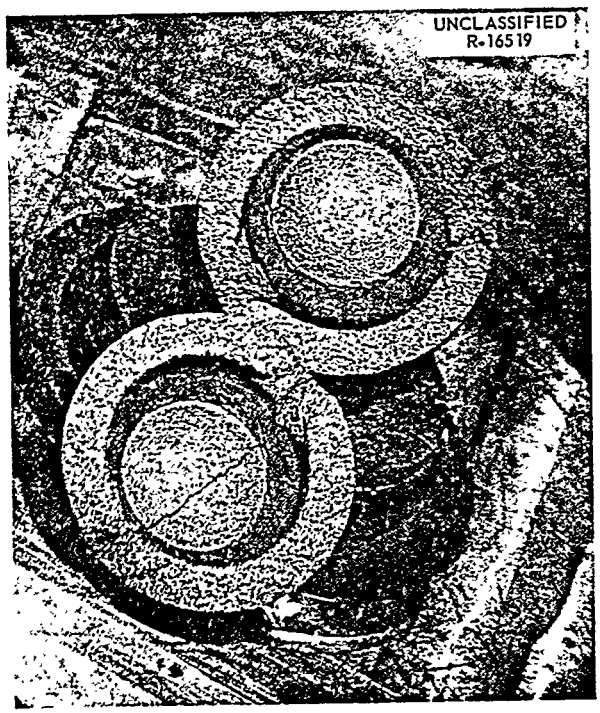

An irradiated fueled graphite sphere after compression test. The sphere contained a molded ¼-inch unfueled shell and broke into two halves with the fueled core intact.

The compression test apparatus used in the hot cell is shown in the figure. The force applied and the movement of the cross-head are recorded by instruments in front of the hot cell. In the next figure, a sphere is shown after the compression test. This sphere had a molded ¼-inch unfueled shell, which broke into two halves leaving the fueled core intact. Neither compressive strength nor impact resistance was found to change measurably because of irradiation.

The escape of fission products from the spheres during irradiation was determined. The fractional fission product releases were very small (of the order of 10^{-6}) for the spheres with unfueled shells.

Diffusion of Actinides in Pyrolytic Carbon and Porous Graphite

Rates of migration of heavy metals (actinides) in carbons and graphites are of practical importance though accurate determinations and interpretations of this behavior present difficult problems both in experiment and theory. Such information is of importance in the development of gas-cooled reactors containing ceramic core components. We are concerned with the immobilization of fuel materials and the degree to which they might remain localized within assigned regions of graphite fuel elements at high (but uniform) temperatures.

The diffusion coefficient is one of the parameters indicative of the migration rate. Coefficients for uranium in porous graphites have been available for several years. We have recently obtained diffusion coefficients for uranium, thorium, and protactinium at several temperatures in a porous graphite and in a columnar pyrolytic carbon as well. Thus, all major components of an operating graphite fuel element (fission products excluded) have been covered in this investigation.

The porous graphite used was prepared by impregnating a fine-grained graphite with an organic compound that was subsequently carbonized. This treatment, typical for fuel element graphites, is carried out to close pore openings and reduce permeation rates of volatile fission products. The pyrolytic carbon was prepared by the thermal decomposition of methane – presumably in the temperature range 1800 to 2000°C. Since carbons so formed are highly anisotropic, a complete study requires the determination of two sets of coefficients; one set for diffusion across basal surfaces (D_c) and another set for diffusion along basal surfaces (D_a). We are primarily interested in values of D_c for reactor applications.

The materials were machined into appropriate rectangular specimens that were degassed and placed on a rotating assembly in an electromagnetic separator wherein the exposed surfaces were bombarded with singly charged thorium or uranium ions to ensure a uniform distribution of isotopically pure actinide on the specimen surfaces. The specimens were then annealed for predetermined periods at controlled high temperatures to allow diffusion to take place. Distributions of diffused actinide within the specimens were determined with the aid of neutron activation, gamma counting, and precision grinding techniques. Coefficients indicative of the actinide migration were computed on the basis of the distribution data.

We have tentatively concluded that fuel migration in isothermal pyrolytic carbon is negligible at temperatures envisaged for advanced gas-cooled reactors. One may speculate that the only conditions at which migration in pyrolytic carbon could cause concern are those associated with fuel element fabrication and possibly those associated with large temperature gradients. The relatively good fuel retention properties of pyrolytic carbon, as compared with those of porous graphites, have been demonstrated via experiments.

DESIGN ANALYSIS

Design of Graphite Structures for Use in a Nuclear Reactor

Graphite bodies undergo dimensional changes when subject to fast-neutron irradiation. These changes depend upon both the amount of fast-neutron exposure and the temperature and are affected by variations within the body. The elements in a continuous body cannot expand or contract freely and stresses and strains are set up. In designing graphite components for use in the core of a nuclear reactor, careful attention must be given to these stresses and strains. Therefore, one of the important objectives in designing graphite components for use in nuclear reactors is to provide structures for which the effects of nuclear irradiation (shrinkage, distortion, and internal stresses) are minimized without compromising the objectives of the design. A generalized study applicable to all reactors cannot be made because the individual nuclear characteristics differ. However, an understanding of the importance of geometry, based on current reactor designs, will be of great value in the design of future graphite-moderated reactors.

The stresses and displacements induced by nuclear radiation have been calculated for thick-walled and nested thin-walled circular cylinders and cylindrical sectors; for various single-channel cylinders with square, hexagonal, and circular cross sections; for rectangular elements with one, two, and four channels; and for bodies infinite in extent with many channels.

The stresses and displacements were calculated using a computer program which allows exact representation of the geometry without resort to approximation, as has often been necessary in the past. The studies are valuable for selecting the best geometry for a given application and for comparing alternate arrangements.

Analyses of Single-Nozzle to Spherical-Shell Attachments

One of the most basic problems associated with pressure vessel design is the design of nozzle attachments. For each case, the stresses caused by the applied loads must be held within allowable limits. Thus, accurate methods for determining these stresses are required. In the case of spherical shells, the theoretical analysis of single radially attached nozzles (the longitudinal axis of the nozzle coincides with a line drawn from the center of the sphere through the center point of the nozzle opening) is in the development stage. Theoretical methods for examining nozzles that are not radially attached (hillside nozzles) do not exist, however, and definite experimental results are needed before methods now being considered can be evaluated.

In order to obtain the required data, an experimental program is being conducted to examine the stress distributions around both radially and nonradially attached nozzles in test models made of steel and instrumented with strain gages. Attachment angles of 0 (radial nozzles), 15, 30, and 45 degrees are being investigated. Other parameters are nozzle diameter and thickness and the influence of internal nozzle stubs, or nozzle extensions, inside the vessel. The models are being subjected to axial, overturning movement, and transverse (perpendicular to the nozzle) loads on the nozzles and to internal pressures. The results will be used for making design correlations and for comparison with stresses calculated from existing theories for radially attached nozzles.

The first radial nozzle configuration was fabricated, instrumented, and tested. The experimentally determined stresses were compared with calculated values, and differences are now under study. In the cases of axial and moment loads on the nozzle, good agreement exists between experimental and calculated results.

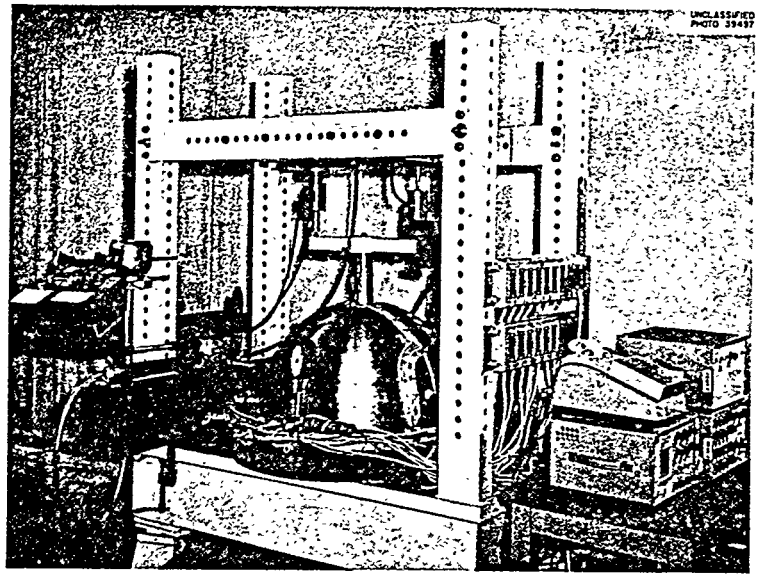

Photograph showing instrumentation and strain-gaged steel hemisphere with a nozzle mounted at the apex. This model configuration is the first in a series to be tested in an experimental stress analysis program, being conducted under subcontract by the University of Tennessee, for examining the stress distributions around both radially and nonradially attached nozzles. The program will provide information essential to the design and analysis of nozzle-to-spherical-shell attachments for reactor vessels.

FAST GAS-COOLED REACTORS

Fast Gas-Cooled Reactors with Indirect Power Cycles

Work was initiated at Oak Ridge National Laboratory to examine the potential value in using gaseous coolant to remove heat from a fast reactor system. The early studies showed that fast reactor breeding margin could be improved appreciably by using helium or carbon dioxide gases instead of sodium as the reactor coolant since the neutron energy level would not be degraded by the coolant and could be maintained at values where fast fission is most effective in terms of neutron economy. This early work also shows that two of the safety problems associated with sodium-cooled fast reactors can be materially reduced by use of helium or carbon dioxide coolants. First, core nuclear reactivity cannot be altered appreciably by accidental local displacement of the coolant, and second, neither of the two gases is subject to secondary chemical reactions with water or air which might violate containment provisions under accident conditions. The use of gaseous coolants would necessitate high coolant working pressures (1000 to 1500 pounds per square inch, depending upon the selected operating conditions) at some capital cost penalty which should be materially offset by the elimination of intermediate coolant circuitry and by less difficult containment requirements. Gas-cooled systems can use uranium dioxide fuels similar to those proposed for sodium-cooled systems.

Fast Gas-Cooled Reactor with Direct Power Cycle

A direct cycle system, using sulfur dioxide at supercritical pressures as the coolant and working fluid, was also investigated and showed that thermal efficiencies above 30 percent can be realized by coupling a sulfur dioxide condensing turbine to an electric generator. The system has the advantage of eliminating secondary power recovery equipment associated with steam systems as well as intermediate coolant circuitry. Furthermore, compact liquid-coolant circulation equipment is used to pump the coolant through the core. All heat transfer equipment is operated at low pressure (less than 100 pounds per square inch) and is thus inexpensive. Construction can be from conventional carbon steels or comparable low-cost materials. Gas-temperature conditions are modest (915°F maximum coolant temperature), and boiling of sulfur dioxide can provide built-in emergency heat removal capability. This system, in common with sodium-cooled systems, has the disadvantage

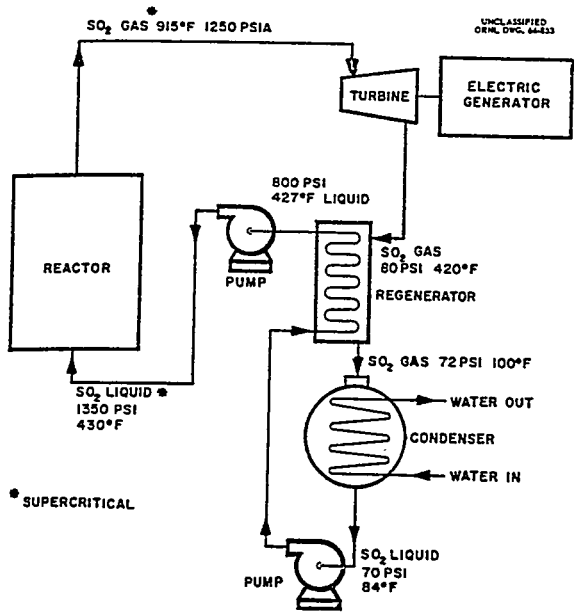

Direct Rankine cycle sulfur dioxide cooled fast reactor.

that core reactivity effects associated with complete coolant displacement can be large, although local void problems are not a major consideration.

Concrete Pressure Vessels

Work carried out in conjunction with the Franklin Institute has shown that prestressed concrete has great merit as a means for reducing the capital cost of primary coolant containers in high-pressure reactor systems. Working pressures up to the range of boiling-water reactors (1200 to 1500 pounds per square inch) appear to be immediately feasible. The value of prestressed concrete stems from the fact that low-cost concrete can be combined with high-strength prestressed steel, permitting reduction in the bulk requirement of steel by a factor of 2 to 3 over conventional steel vessels and, because welded fabrication is largely eliminated, permitting steel installation costs in the range of $0.50 per pound compared to $3.00 to $6.50 per pound for conventional steel vessels.

Molten-Salt Reactor Program

INTRODUCTION

The goal of the Molten-Salt Reactor Program – to exploit the unique properties of molten-salt fuels in developing thermal breeder reactors for producing cheap nuclear power – was discussed in the first annual progress report (ORNL-3350, p. 40). We described the design of the Molten-Salt Reactor Experiment, the major tool for the Program, and told about some of the research and development that was being done in support of the design and construction of the reactor.

At that time our plans called for essential parts of the MSRE to be completed so that prenuclear testing could begin in the summer of 1963. However, difficulties, both technical and budgetary, slowed the progress of the work, and the prenuclear testing is now expected to begin in the summer of 1964. At present most of our effort is going into developing, building, and testing components for the reactor, and installing the components, piping, instruments, and auxiliaries in the reactor building.

Since the liquid fuel in the MSRE circulates through the reactor and some auxiliary equipment, the success of the Experiment depends in a large measure on complete compatibility of the fuel with the structural metals, graphite, and helium, all of which will contain some contaminants. Chemical studies of the fuel and materials in and out of radiation are a major effort in support of the Experiment.

In this report we will discuss some of the progress made in building the MSRE and some of the chemistry studies.

DEVELOPMENT AND CONSTRUCTION

The molten fluoride fuel forms a critical mass in the reactor vessel, where it heats from 1175 to 1225°F. The fuel pump circulates the heated fuel through the heat exchanger and back to the reactor vessel. In the heat exchanger, heat transfers from the fuel salt on the shell side to a similar but unfueled molten fluoride coolant salt in the tubes. The coolant salt is pumped through tubes in the radiator, where the heat is dissipated to the atmosphere. Salt in the fuel and coolant systems can be drained to tanks to shut the reactor down completely. Because the fuel and coolant salts freeze at about 840°F, all the salt-containing equipment is provided with electrical heaters and insulation to keep the salts molten at all times.

In the coolant and drain tank cells, all the equipment has been installed and the piping has been completed. Heaters and insulation are now being installed in those cells. In the reactor cell, much of the work has been done, but the pump, heat exchanger, and reactor vessel must be finished and set in place; heaters and insulation must be applied, and some instrumentation must be installed to complete the essential work there.

The graphite core for the reactor consists of graphite bars 2 inches square and about 5½ feet long. The grooves in the sides form passages to direct the flow of salt through the core.

Rough bars of ordinary grades of reactor graphite are made by mixing graphite particles with a binder, extruding the plastic mixture to rough

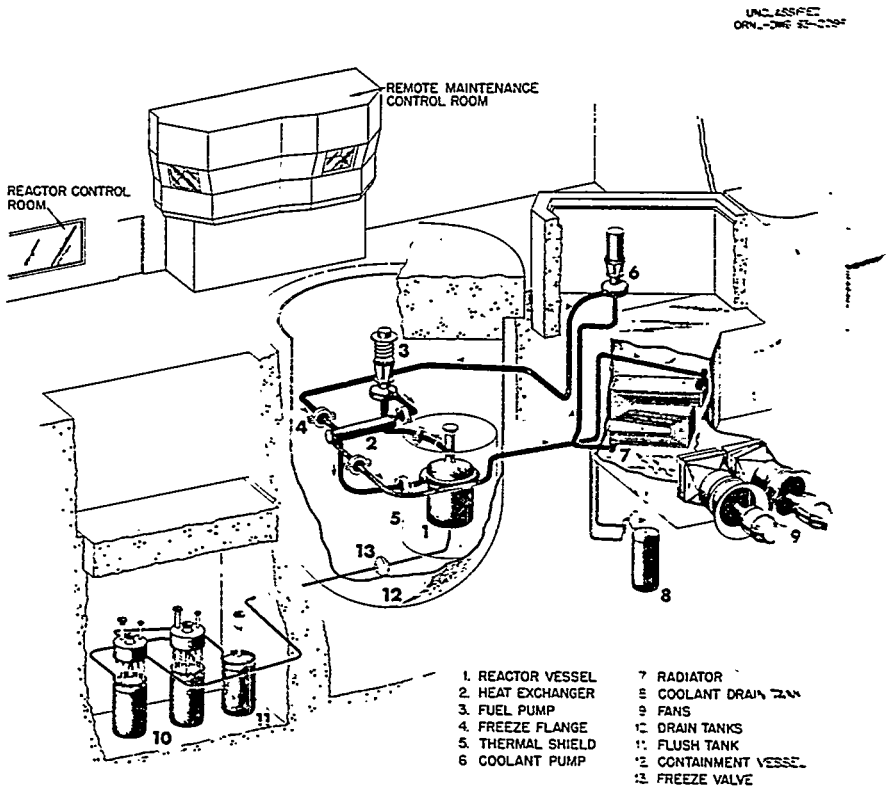

Schematic of reactor plant.

shape, and heating to 2800°C to graphitize the binder. The resulting material has a density near 1.6 grams per cubic centimeter and contains about 27 volume percent of voids in the form of small pores. We want to circulate the salt in contact with the graphite but will permit only 0.5 volume percent of the graphite or less than 2 percent of the pores to be filled with salt. The MSRE fuel salt does not wet graphite and will not enter pores of given diameter until the surface tension forces are overcome by the pressure on the salt. Standard grades of reactor graphite have the pore openings large enough for the salt to be forced into them at pressures less than 50 pounds per square inch, the design pressure of the MSRE, so a special material had to be produced for the MSRE. By proper selection of starting materials and repeated impregnation and graphitizing treatments, a material was produced with a density of 1.86 grams per cubic centimeter – only 16 percent voids – and with most of the pore openings less than about 0.2 micron in diameter. The fuel salt will not enter such small pores at pressures below several hundred pounds per square inch.

Manufacture of this material was an experiment, and there were problems in producing bars of sufficiently high quality for use in the MSRE and in examining them to be certain of the quality. These problems delayed the delivery about a year; but the assembly has been completed, and the core was installed in the reactor vessel on April 1, 1964.

The heat exchanger was assembled and then tested under full flow conditions with water. Those tests showed that the tubes vibrated excessively in the baffles; so the shell was removed, and spacers are being inserted between the tubes at the baffles to eliminate the vibrations. This should be completed soon, and the unit will be ready for installation in the reactor cell.

The fuel and coolant pumps were finished, and the rotary elements are being tested in the prototype pump test facility. In this facility the pump is run at full flow and temperature for about 200 hours before it is delivered to the reactor.

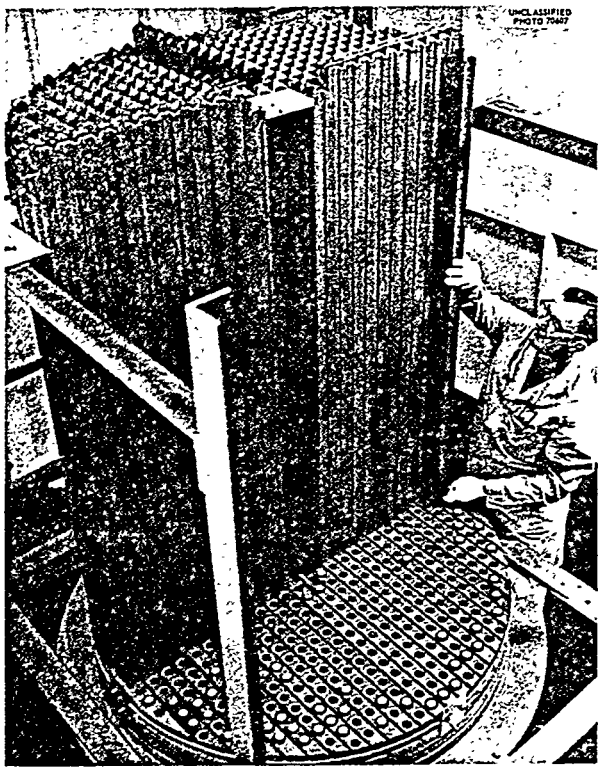

The graphite core for the MSRE. The graphite core is shown partially assembled on the support grid. The graphite bars are 2 inches square and about 5½ feet long, with grooves in the sides to direct the flow of salt through the core. The graphite material, which is highly impermeable to penetration by the fuel salt at pressures below several hundred pounds per square inch, was manufactured especially for use in the MSRE.

The completed radiator contains 120 tubes; each is 30 feet long, is bent into a serpentine shape, and is welded into a header at each end. Doors and heaters are provided on the enclosure so that the coils can be completely enclosed and heated to keep the salt molten when the reactor is not producing heat. This unit is now installed in the radiator duct and ready for testing with full air flow.

Each of the two drain tanks has a volume of about 80 cubic feet and will contain 75 cubic feet of salt. When the fuel is drained from the reactor after several weeks of operation at high power, the decay of fission products will produce heat at a rate above 50 kilowatts. Water for cooling will be admitted into a tank from which tubes are suspended, extending into vertical thimbles projecting downward into the drain tank. The water will circulate into the tubes, where it will boil. The steam will be separated in the tank and condensed in a condenser outside the drain tank cell, and the condensate will be returned. The drain tanks have been installed in their furnaces in the drain tank cell, and one of the tanks has been heated to 1200°F in a test to show that the furnace will operate satisfactorily.

In preparing the reactor for operation, much work is being done in testing control rods, heaters and insulation, remote maintenance tools, and other important components and systems. By February 28, 1964, the plant was 91 percent complete. The draft of the safety analysis report had been sent to

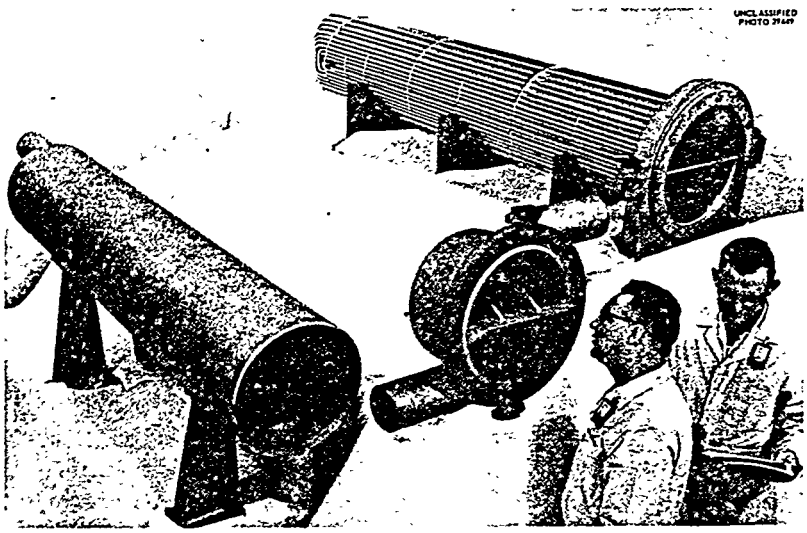

MSRE heat exchanger. The shell and tube bundle for the MSRE heat exchanger are shown in an exploded view. The exchanger has been assembled and tested and will be installed in the reactor after minor modifications.

Characteristics of MSRE

Heat output: 10 Mw

MSRE Design Data

Reactor vessel

Over-all ht; i.d.:	100¾ in.; 58 in.
Wall:	9/16 in.
—material:	INOR-8
Design pressure, temp.:	50 psi, 1,300°F

Core

Container:	INOR-8 wall ¼ in. thick
—size:	56 in. o.d. × 68 in. high
Moderator:	Graphite
—total dia:	54¼ in.
—block size:	~2 × 2 × 67 in. high
Fuel-channel size:	1.2 × 0.4 in.
—number:	1,140

Fuel salt

Composition:	65 mole % Li^7F–29.1% BeF_2–5% ZrF_4–0.9% UF_4
Liquidus:	842°F
Density:	141 lb/ft³ at 1,200°F
Heat capacity:	0.455 Btu/lb/°F at 1,200°F
Heat of fusion:	139 Btu/lb
Viscosity:	7.64 centipoises at 1,200°F
Σ_a:	7.0×10^{-3} cm^{-1}
Σ_f:	5.4×10^{-3} cm^{-1}
Fuel into reactor; out:	1,175°F; 1,225°F
—flow in fuel channel:	0.75 ft/sec

Coolant salt

Composition:	66 mole % LiF–34% BeF_2
Liquidus:	851°F
Density:	120 lb/ft³ at 1,062°F
Specific heat:	0.526 Btu/lb/°F at 1,062°F
Thermal conductivity:	3.5 Btu/ft/ft²/hr/°F at 1,062°F
Viscosity:	8.3 centipoises at 1,062°F
Coolant into ht. exch.; out:	1,025°F; 1,100°F

Control rods

Number; shape:	3; hollow cylinder
Material:	Gd_2O_3-Al_2O_3
—Gd_2O_3 o.d.; i.d.:	1.10 in.; 0.83 in.
—Gd_2O_3 weight:	1.1 kg/rod
—cladding (inner and outer):	0.02-in. 304Lss
Rod worth, one rod:	2.8% $\Delta k/k$
—two rods:	5.0% $\Delta k/k$
—three rods:	6.7% $\Delta k/k$
Drive rate:	0.5 in./sec max
—motor:	Instantly reversible; single-phase, 60-cycle
—attachment:	Flexible cable, magnetic release
Scram time:	0.85 sec max
Max withdrawal (1 at a time):	0.04% $\Delta k/k$/sec
Insertion (3 at a time):	0.09% $\Delta k/k$/sec
Power gen. in rod:	2,725 watts/rod max
Cooling:	Cell air, forced convection

Nuclear Design Data

Eff. core size:	59 in. dia × 78 in. high
Moderator:	69 ft³ graphite
Fuel volume:	25 ft³ in core; 70.5 ft³ system total
Delayed neut. fraction:	0.0067 static, 0.0036 circulating
Initial critical conc.:	0.291 mol % U^{235}; 0.83 mol % U
Temp. coef., total:	-6.96×10^{-5} $\Delta k/k$/°F
—fuel:	-3.28×10^{-5} $\Delta k/k$/°F
—graphite:	-3.68×10^{-5} $\Delta k/k$/°F
Prompt-neut. life:	2.40×10^{-4} sec
Th.-neut. ϕ, avg:	1.5×10^{13} n/cm²/sec
—peak:	3.4×10^{13} n/cm²/sec
Power density, avg:	14 w/cm³ in fuel; 0.34 in graphite
—peak:	31 in fuel; 0.98 in graphite

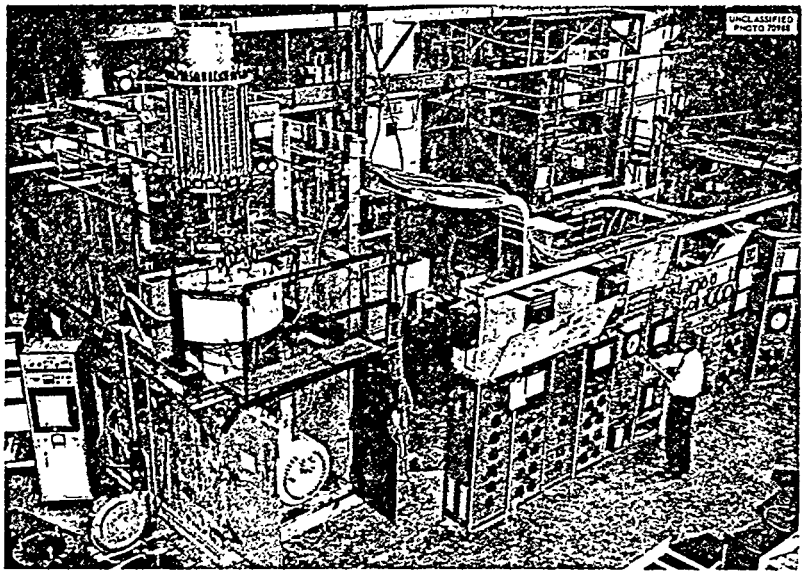

MSRE prototype pump test facility. This facility is used to develop and proof test the circulation pumps for the MSRE. The fuel salt pump and drive motor are shown in the upper left; some of the controls and instrumentation may be seen at the lower right. The lubrication system located to right of the support structure at floor level provides lubrication for the pump shaft bearings and cooling for the nuclear shield plug.

Radiator.

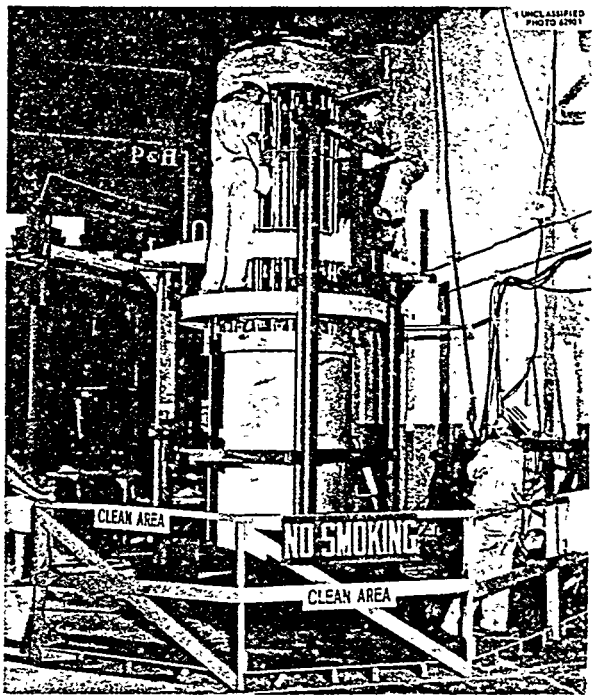

Drain tank assembly.

the AEC for review and the design report for the plant was well along. Operating procedures were being written in preparation for assembling and training the operations staff and for beginning the operation of the reactor with unfueled salt.

CHEMICAL DEVELOPMENT FOR THE MSRE

Reactors with circulating liquid fuels have the advantage that fuel can be added easily to compensate for fuel burned while the reactor is operating. Additions to the fuel in the MSRE will be made in the form of a concentrate ($LiF-UF_4$ eutectic, melting point 490°C) containing 27 mole percent of fully enriched UF_4. To ensure that no possible combinations of concentrate and fuel could give a mixture that deposited high-melting compounds, a traverse involving all pertinent compositions was examined in the Reactor Chemistry Division; as predicted from previous phase diagram studies, only melting points grading intermediately between that of the concentrate and the fuel were found.

Further studies of the freezing behavior of the fuel were made also. The first crystals to appear (at 434°C) are Li_2BeF_4; these crystals have virtually the same composition as the coolant but appear at a lower temperature than the coolant freezing point because the fuel freezing point is depressed by the additional solutes in the fuel. At 431°C, $2LiF{\cdot}ZrF_4$ begins to crystallize out of the fuel, and $7LiF{\cdot}6UF_4$ joins both the earlier phases at 416°C. The last liquid to freeze disappears as the temperature drops to 350°C, provided that equilibrium freezing is maintained.

Impurities in the fuel components tend to be corrosive and must be removed by thorough treatments with HF, and with H_2 and other reducing agents. Improved facilities for blending and purifying the fluorides were placed in use as production was started on the 11,260 pounds of fuel, 9500 pounds of flush salt, and 5800 pounds of coolant required for the operation of the reactor experiment. The fuel circuit is maintained in a chemically clean condition by the use of a flush salt that is nominally the same composition as the coolant salt.

When oxide, as from reaction with moisture or air, makes its way into a fluoride fuel, a precipitation of insoluble oxides generally ensues, and there is a tendency for UF_4 to precipitate as insoluble UO_2. To protect against loss of UF_4, ZrF_4 has been included in the fuel to serve as a getter for oxide. Extensive experiments have shown that precipitation of UO_2 can be avoided, at the expense of precipitation of ZrO_2, as long as the fuel contains about three times as much ZrF_4 as UF_4. Further insurance that the ample excess of ZrF_4 in the fuel is effective has come from experiments that show that precipitating ZrO_2 does not carry any UO_2 by occlusion or in solid solution; some of the phase diagrams in the literature, which implied that such might occur, were shown to be wrong.

Another matter of interest is the possibility of permeation of moderator graphite pores as a consequence of wetting by the fuel. Recent experiments with sessile drops have confirmed that neither the fuel nor any other high-melting fluoride (surface tension ~200 dynes per centimeter or higher) wets either graphite or clean metal. Thus, under MSRE operating conditions no difficulties from permeation are anticipated; however, the presence of oxide or moisture does cause the melts to spread on solids. With clean surfaces, a fluoride melt with a surface tension (as measured at the melting point) that is greater than 180 dynes per centimeter will not wet graphite; a melt with a surface tension greater than about 210 dynes per centimeter will not wet metals. The surface tension of the MSRE fuel, as measured from the shape of sessile drops, is about 230 dynes per centimeter at the melting point.

Moisture removal from "as-received" MSRE graphite has been measured under conditions simulating those planned for the MSRE prior to startup. Very little water was released from the graphite. The relatively impermeable nature of the graphite was attested by the fact that exposure to moist environments did not cause an appreciable amount of adsorption of water; indeed, even immersion in water led to the release of only a small amount of chemisorbed water. Such results indicate that contamination by water from the MSRE graphite will be within easily tolerable limits.

As the fuel comes to equilibrium with the containing metal (INOR-8, a nickel alloy containing molybdenum and chromium), a small amount of UF_3 will be formed as a steady state is reached. Studies of the solubility and stability of UF_3 showed that while the solubility is lower than

anticipated, there is no cause for concern about adequate solubility (~0.4 mole percent) at operating temperatures.

For arriving at the fuel composition, an important guide was to use as much LiF as is consistent with a suitable melting point; this gave a minimized viscosity. The melting point behavior was explored through an extensive program of preparation of phase diagrams for multicomponent systems. The viscosities of fuel-type mixtures were measured with a rotating spindle viscometer at 475 to 830°C. The fuel and coolant viscosities ranged from 9 to 25 centipoises between 475 and 600°C. The effect of additions of LiF (up to 6.7 mole percent) on the viscosity of LiF-BeF_2 mixtures was determined in the temperature range 525 to 840°C and found to be quite large; decreases in viscosity of up to two orders of magnitude were noted at 700°C in BeF_2-rich mixtures.

When fissioned fuel is allowed to freeze and cool to room temperature, as it must in order to be examined in detail, the decay energy from fission products causes radiation damage to the crystals and leads to the evolution of F_2 gas. Such effects were found to be absent in the molten fuel, presumably because the fluorine is recombined as fast as it is formed. This result has been confirmed in experiments covering several thousands of hours in in-pile operation with fuels that underwent greater than 10 percent burnup.

The generation of fluorine was of sufficient interest to stimulate studies of this phenomenon in out-of-pile experiments using x rays, gamma rays, and electron bombardment. All these high-energy radiations sooner or later caused enough damage to fuels or fluoride crystals at room temperature to release fluorine. But an annealing of the salt crystals at temperatures not far above the boiling point of water made them immune to the effects of irradiation at the annealing temperature.

High Flux Isotope Reactor

INTRODUCTION

The primary purpose of the High Flux Isotope Reactor (HFIR) is to produce research quantities of transplutonium isotopes.

The reactor design employs a central, light-water region for irradiation of the target material. The maximum unperturbed thermal neutron flux in this target region is expected to be about 5×10^{15} neutrons sec^{-1} cm^{-2} when the reactor is operating at the design power level of 100 megawatts. This target region is the center of a concentric cylindrical arrangement of target, fuel, control, and reflector regions respectively. The fuel element is composed of aluminum-clad, 93 percent enriched-uranium, 50-mil-thick plates with 50-mil-thick coolant channels. A thin annular control region separates the fuel from the beryllium reflector.

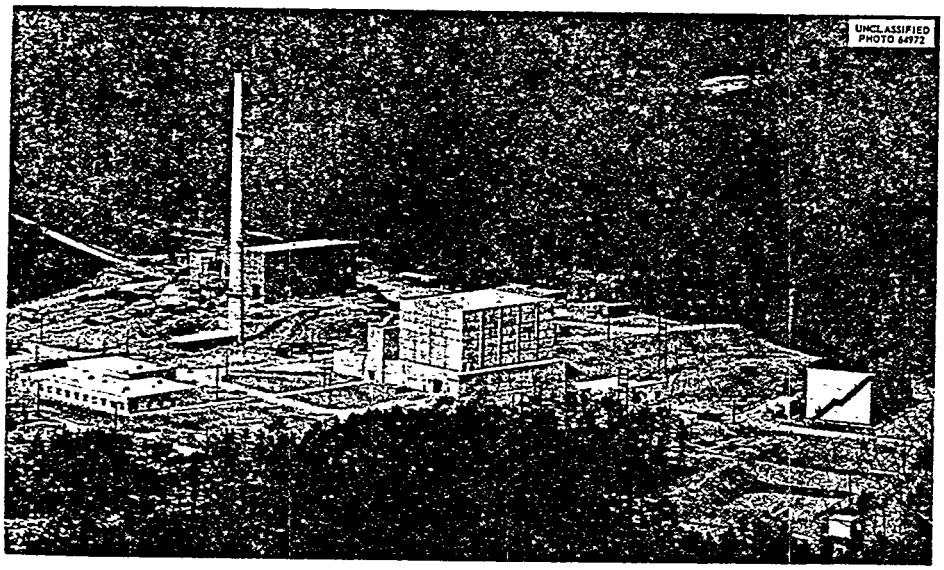

HFIR reactor site (April 1964). The concrete structure shown in the center is the reactor building. At the right of the reactor building are the electrical distribution building and the cooling tower. At the left are the office and maintenance building and the fan shed and exhaust stack. The concrete block building behind the stack is the Transuranium Processing Plant.

PROJECT STATUS

Specifications and drawings for the reactor building, reactor pressure vessel, reactor primary and secondary cooling systems, and the auxiliary equipment are complete. Delivery of all the long-lead critical items such as the reactor vessel, heat exchangers, and main circulating pumps was completed in 1963 and procurement of all other equipment, except some minor valves, is essentially complete. Design of most of the core components is finished and many of these are in fabrication. As of December 1963, construction was about 75 percent complete and is scheduled for completion by mid-1964.

The HFIR is scheduled to reach criticality in May 1965 and to achieve full power several months later.

Further analytical studies, based on new experimental information, were conducted on the HFIR fuel elements. These results indicated the steady-state burnout power level will be approximately 150 megawatts; however, this provides adequate margin above the nominal full power design power level of 100 megawatts.

Procurement of the rough machined beryllium for the reflector was completed. As a result of new radiation damage data, modifications in the beryllium final machining details were made to reduce the structural requirements on the beryllium and provisions were made to accommodate the expected dimensional changes caused by radiation.

The design of the core structural components was completed and drawings were issued for procurement. Fabrication of these components was initiated.

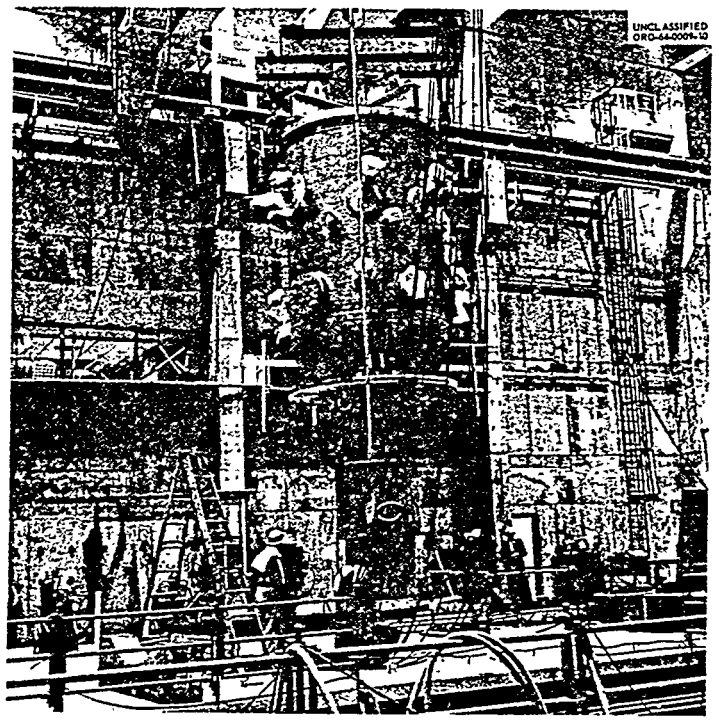

HFIR reactor vessel. This photograph shows the reactor vessel as preparations are made for lowering it into the reactor pool. The vessel is made of $2\frac{7}{8}$-inch-thick carbon steel with a minimum of 0.1-inch stainless steel cladding on both sides. The weight of the vessel, including its 14-inch-thick top head which is not shown in this picture, is approximately 50 tons. The vessel is designed for operating pressures up to 1000 pounds per square inch at 200°F.

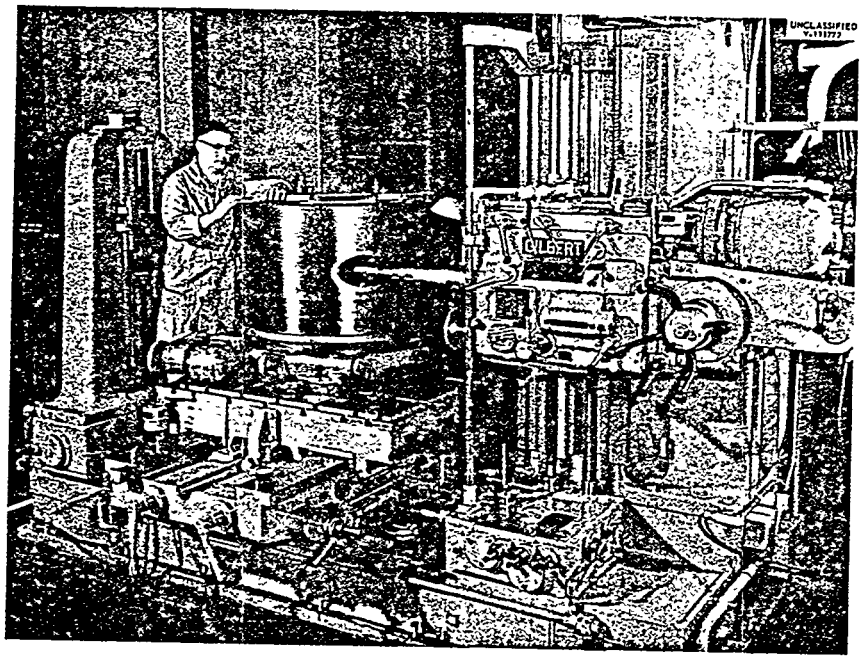

Machining of the HFIR beryllium reflector. Shown in this photograph is the machining of the 4-inch through beam hole in the HFIR permanent beryllium reflector. In addition to the through beam hole there are two other tangential holes and one radial to the core. The permanent beryllium is 43 inches in outside diameter and 24 inches high. Cooling for the beryllium is provided by axially drilled $\frac{1}{8}$-inch-diameter holes.

Design and development work are in progress on the control plates, the control plate guidance system, the control plate drives, and the assembly installation, and alignment tools associated with the core structural components.

Instrumentation

The design of the overall control and instrumentation system is nearing completion. Procurement of the major items of the process instrumentation is 90 percent complete and these items are presently being installed at the site.

Work is proceeding on the fabrication and procurement of the components of the nuclear instrumentation systems, and approximately 70 percent of the components are on hand. Prototypes of these systems are being assembled for testing. The wide range counting rate system prototype has been assembled in the laboratory. The laboratory tests indicated that minor changes were necessary. These changes have been made and the equipment is now ready for field testing in the Bulk Shielding Facility. Functional assemblies of the servo systems are under construction.

A test model of the coincidence magnet has been constructed. Test stand data indicates that acceptable holding force and release time performance has been obtained. Work is in progress to reduce the release time to the shortest practical value.

The preliminary design of a fuel element cladding failure detector was completed.

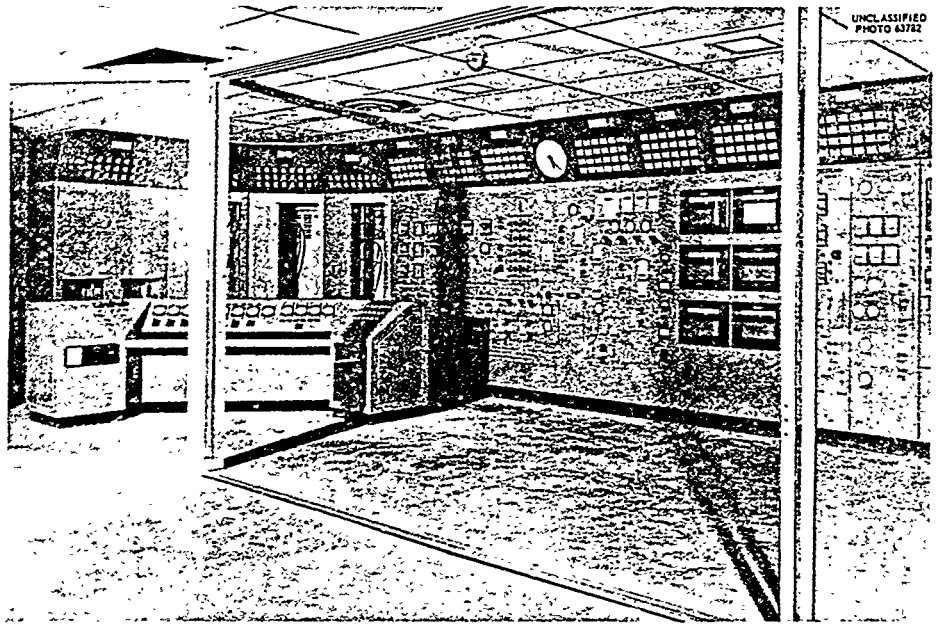

HFIR control room. The HFIR control room is located on the third floor of the reactor building. The corridor side of the control room is enclosed by glass panels through which visitors can view the control room. The reactor console, graphic and annunciator panels, and process instruments have been installed. The nuclear instrumentation will be mounted in the space provided in panels "B," "C," and "D."

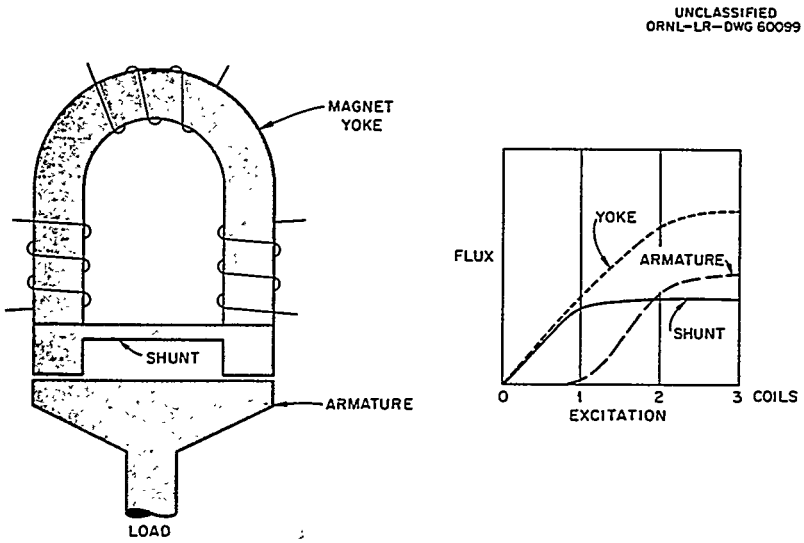

HFIR magnet with saturating shunt. The HFIR safety instrumentation is based on a triple-channel coincidence system. The output from each safety channel controls the current in one of the three electrically independent coils in each scram-latch magnet, as indicated. Magnetic fluxes in the various portions of the magnetic circuit as a function of the exciting ampere-turns are shown in the graph. The first increment of excitation produces flux only in the yoke and shunt. Increased excitation saturates the magnetic material in the shunt and armature.

Reactor Physics

Results from the second HFIR critical experiment and further analytical studies indicated that the weight of uranium-235 in the HFIR core should be increased from 8.0 to 9.4 kilograms to achieve the desired average fuel cycle time of 14 days. The weight of boron burnable poison was also increased so that the reactivity shutdown margin would be acceptable with the heavier fuel loading.

Improved analytical techniques were used to study the fuel cycle characteristics of the above core. It was found that the thermal neutron flux in the plutonium target and the peak power density in the fuel region were essentially constant throughout the cycle.

Additional HFIR critical experiments were planned. They will be used primarily for determining power distributions associated with the 9.4 kilogram fuel loading and for studying the characteristics of the new Eu_2O_3-Ta-Al control plates. These experiments will be conducted during 1964.

Control Plates

The Metals and Ceramics Division has successfully fabricated plates for the HFIR control system. The control system consists of two concentric cylinders approximately 18 inches in diameter and over 5 feet long. The inner cylinder is a single plate while the outer contains four 90 degree segments. Each plate contains three discrete aluminum-clad longitudinal regions, a dispersion of europium oxide in aluminum, a dispersion of tantalum in aluminum, and an aluminum region. Aluminum dispersion plates of this size or with these materials have not been fabricated previously. Plates for the outer cylinder have been formed to very close radial tolerances using explosive forming. Forming studies for the inner cylinder are now under way.

Fuel Elements

Metals and Ceramics groups have shown that it is practical to fabricate HFIR fuel assemblies

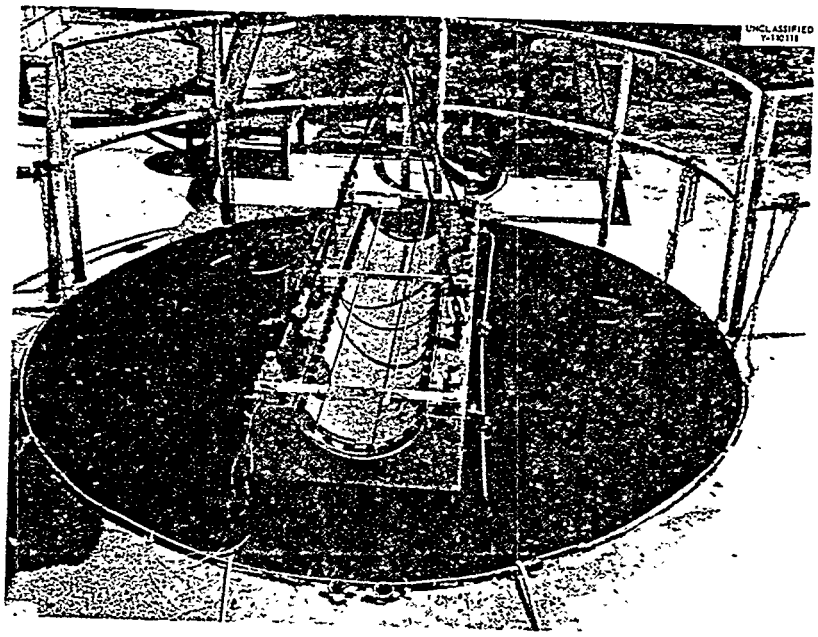

HFIR control-plate sizing die. The HFIR control plates are sized by explosive forming. Shown here is a control plate sizing die as it is lowered into the water tank in which the explosive forming takes place. The liner is under vacuum and the end of the plate can be seen under the rubber. Two ropelike explosives are carefully positioned above the die where they are detonated.

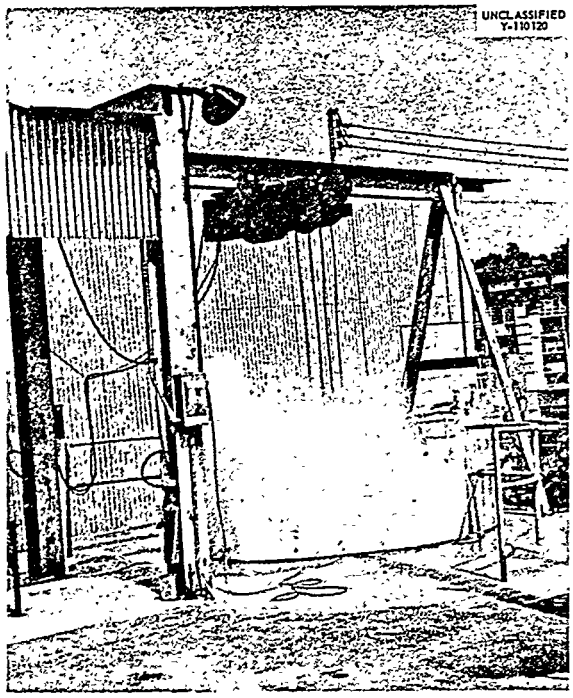

Explosive forming of HFIR control plate. Shown in this photograph is the water tank at the moment the explosive was detonated. Two explosives were carefully placed above the die so as to produce directional shockwaves that meet at the center of the die. This was a relatively small shot fired locally. Larger shots are fired from a remote control station.

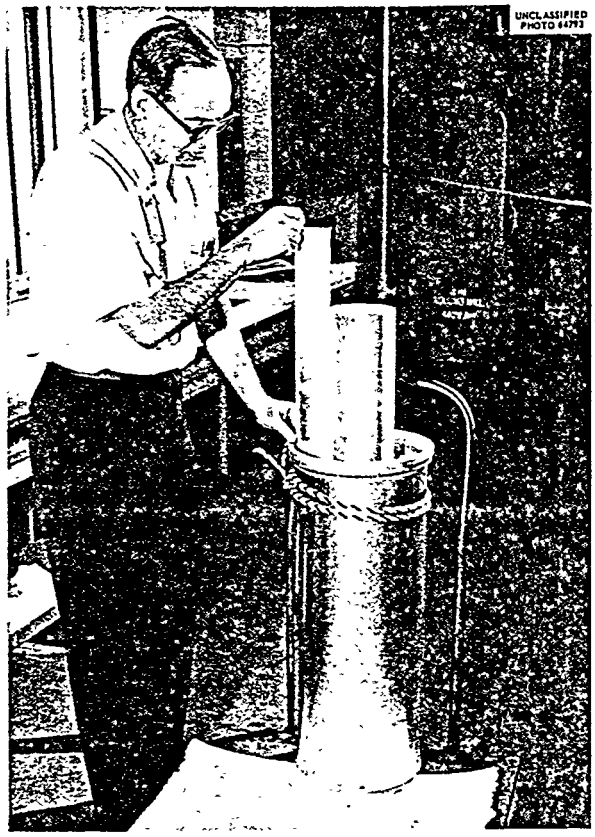

HFIR critical experiment fuel element. A special fuel element with removable fuel plates was fabricated for HFIR critical experiment number 3. The removable plates provide a method of taking punchings from the plate for analysis to determine the flux and power distribution. Shown above is a removable plate being inserted into the outer annulus element.

to the extremely tight tolerances required. Each assembly consists of only two elements, an inner- and an outer-annular ring, each ring being made up of fuel plates curved to an involute configuration and welded to the tubular side plates. Several elements have been fabricated by the Metals and Ceramics Division, and now a commercial contract has been placed for the procurement of the elements.

To minimize the ratio of maximum to average power density, the fuel must be distributed closely within the manner specified. No devices were available which could nondestructively measure the fuel to the required accuracy. Such a device which measures x-ray attenuation of the fuel plate was developed in a joint program of the Metals and Ceramics and Instrumentation and Controls Divisions. This device will measure the fuel concentration in the volume through a plate corresponding to a $^5/_{64}$-inch-diameter surface area. Plates which show variations greater than ±10 percent from a theoretical value are automatically marked. The entire plate is inspected at speeds up to 150 inches per minute. When required, average fuel concentrations over a given length may also be determined.

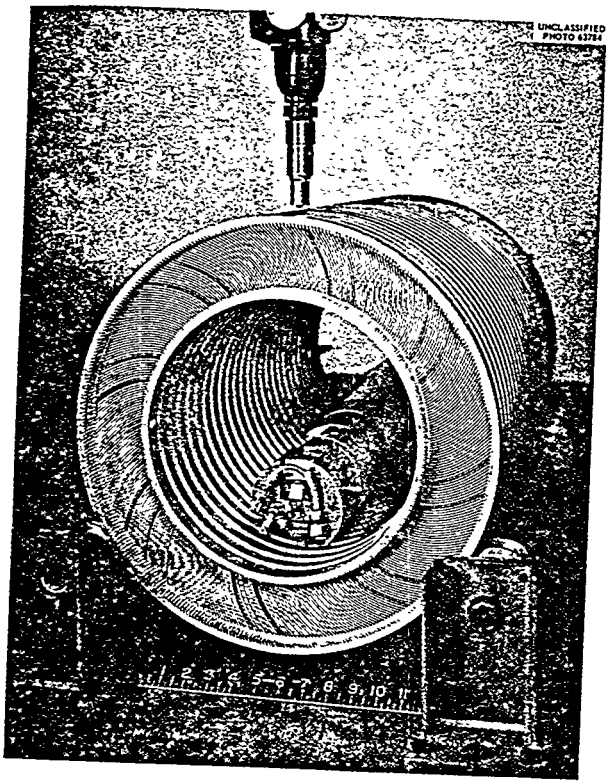

Welding HFIR fuel element. An automatic welding procedure has been developed which is capable of reproducibly attaching the large number of fuel plates to both the inner and outer tubes while maintaining the required, very narrow dimensional tolerances. Shown above is the welding of fuel plates of an outer element to its inner tube.

HFIR Development

Development work supporting various phases of the HFIR design was continued throughout the year. Facilities ranging from small bench tests to a full-scale mockup of the reactor were operated and tested as a part of this program.

Control-Plate Pressure-Equalization Test Facility

This facility is a full-scale mockup of one outer control plate with its related coolant channels. A straight (middle) coolant channel, a simulated (flat) control plate, and a stepped (outer) channel which simulates the flow restriction at the core are incorporated in the test unit. Tests were conducted at flow rates up to 125 percent of the design value. Pressure drop data down the length of the plate and from channel to channel were obtained from the 47 pressure taps located in each coolant channel. Thirty-nine places were provided for measuring channel thicknesses.

This facility was originally used to determine the optimum number and size of holes to be drilled in the control plate to minimize the effect of hydraulic loading. Later tests were conducted to determine the magnitude of the hydraulic loads at various flow rates, control plate positions, and step configurations. Deformed control plates and nonuniform channels were also studied.

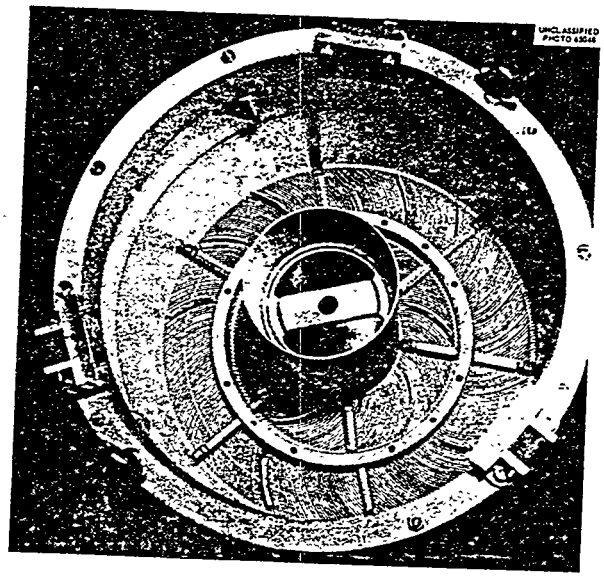

HFIR critical experiment. A series of critical experiments were conducted in support of the design of the HFIR. These experiments included measurements of coefficients of reactivity for the fuel, voids, and temperature, power and flux distributions, and control plate calibrations. Shown above is a fuel element in the critical facility tank as preparations are being made for conducting an experiment.

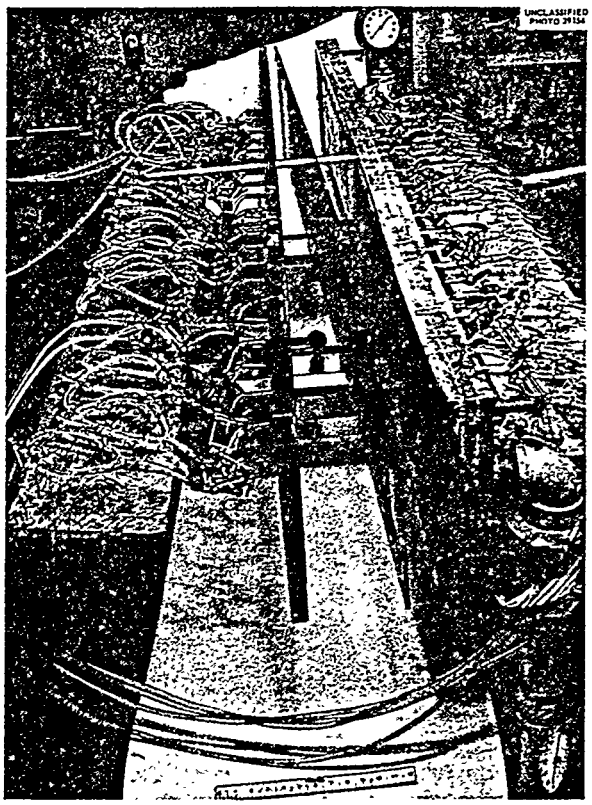

Control-plate pressure-equalization flow testing rig. Tests were conducted to determine the hydraulic pressure loads on the HFIR control plates at various positions. Shown above is the rig used in conducting these tests. Ninety-four pressure taps are provided for collecting the pressure data. This rig is also used in studying the effects of nonuniform channel width between the plates.

Control-Plate Drive

The four quadrants of the outer control plate are each coupled to a drive mechanism which incorporates shim and safety modes of operation. The drive is a lead screw and nut type unit, and the safety or "scram" mechanism consists of a magnet which releases the control plate through a mechanical ball latch. A full size prototype of this assembly has been fabricated and tested at conditions of pressure, flow, and temperature equivalent to reactor operation. Results obtained thus far indicate that the "scram" response criteria of 10 milliseconds can be met and that the overall drive performance is satisfactory.

The inner control plate drive mechanism has both shim and regulating modes of operation. An electromechanical servo mechanism controls the ball nut and screw regulating drive. The lead screw and nut type shim drive is mounted "piggy back" on the regulating drive. The entire drive assembly is currently being life tested under load conditions typical of reactor operation. Results to date indicate satisfactory performance.

Bearing Tests

This program was designed to test and develop bearings for use in the reactor. Various types of bearings including ball, roller, and sleeve type have been tested under conditions anticipated in the reactor.

A test assembly consists of a pot into which two test bearings can be mounted on a pair of lever arms. Dead weights suspended from the arms load the bearings on opposite sides of a plate which simulates the bearing mating surface in the reactor. The plate is attached to the rod of a pneumatic cylinder with an 8-inch stroke and a continuous cycling air motor. Water of the same quality and pH as that specified for the reactor is circulated through the pot; tests are conducted at atmospheric pressure and at a temperature of about 190°F. Three test assemblies are utilized.

By mounting a load cell between the plate and the cylinder rod, coefficients of friction were determined. First the rolling coefficient was determined and then the bearing was locked to prevent rotation and the skidding or sliding coefficient determined. Bearing performances were evaluated at various loads, the highest load being 100 pounds. In some cases, the bearings were deliberately misaligned and the performance tests repeated. Life tests were conducted under ideal water conditions and with water containing 5 to 10 parts per million of aluminum oxide.

Results of the test program have enabled the selection of bearings and bearing materials that should provide excellent service in the reactor, excluding possible damage due to radiation. The effect of the bearing on the mating surface has

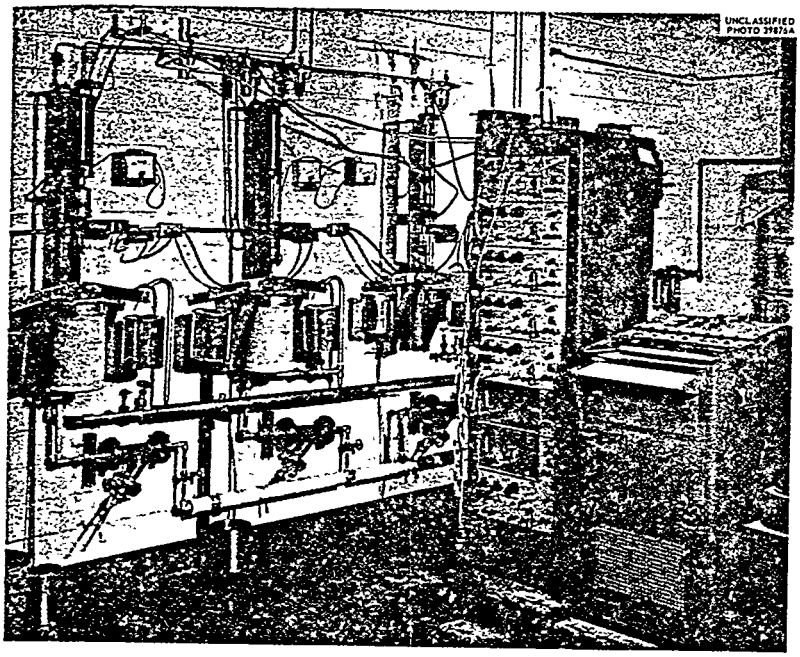

HFIR bearing test rig. Shown above are the pots, load devices, interconnecting piping, and the instrumentation composing the bearing test rig. This is used to measure the rolling coefficients of friction of the HFIR control plate bearings. The tests were conducted in water of comparable quality expected in the HFIR.

also been noted. In one case, pitting type corrosion was observed on the simulated outer control plate surface at the point of contact with the bearings. Consequently, a study is under way to determine the most suitable bearing outer face material for use in contact with the control plates.

HFIR remote fuel handling tools. Prototype remote fuel handling tools for handling the HFIR fuel elements have already been fabricated. Shown in the picture above from left to right are the inner element tool, the outer element tool guide post inserted into the fuel grid which supports a dummy outer fuel element, and the outer element tool. The three fin-like appendages on the inner tool serve as a guide while the element is being engaged.

Remote Refueling Tools

The tooling necessary for refueling the reactor was designed, developed, and partially fabricated by December 31, 1963. In the design of the tools, special consideration was given to the requirements for accurate alignment of reactor components, reliability, and prevention of inadvertent exposure of personnel to radiation through misuse of the tools. In addition, special attention was given to the simplicity of design, frequency of usage, and durability. Preliminary testing of prototype tools indicates the design objectives have been accomplished.

Miscellaneous Investigations

An important phase of HFIR bench testing has been the empirical sizing of inlet orifices for the parallel flow regions of the reactor. In these tests the inlet region or a representative segment is mocked up full size. Flow versus pressure drop data are taken for orifice sizes which bracket the design point, and the data plotted. The points from each of these curves which give the design flow rate are then plotted on pressure drop versus orifice size coordinates. Since all points on the resulting curve represent the design flow rate, the exact orifice size to give the design pressure drop can be selected. This method was used to size orifices for a dummy target and the vertical engineering facility plugs.

A test was run to determine the effect of thermal cycling on the rivets utilized in the spacer strips between the outer control rods in the core section. Aluminum rivets fasten together the spacer strips, a $\frac{1}{16}$-inch-thick aluminum liner, and the inner removable reflector cylinder. This configuration was mocked up full size substituting mild steel for the beryllium cylinder, the two having about the same thermal expansion coefficient. The assembly was submerged in a tank of water and thermal cycled over a range of 120°F. Longitudinal differential expansion of the components caused no significant damage to the rivets during the 100 cycles of operation. In the original assembly, peripheral expansion of the liner resulted in closure of the $\frac{1}{10}$-inch liner gap and damage to the adjacent rivets. This problem was alleviated by eliminating the gap and spacing the liner 0.005 inch from the cylinder. This allowed for the greater thermal expansion of the liner, which contacted the cylinder at the higher temperatures.

Army Reactors Program

The Laboratory's participation in the Army Nuclear Power Program dates from 1953, just shortly after the joint program was established by the Army and the Atomic Energy Commission. At this time ORNL was requested to design a practical nuclear reactor power plant that could furnish electric power in certain isolated localities. The first Army Package Power Reactor (now known as the SM-1) was built at Fort Belvoir, Virginia, based on the ORNL conceptual design. During construction, the Laboratory assisted the project by reviewing the detailed design, performing critical experiments, developing and testing fuel and control materials, and fabricating the first core. Since completion of the SM-1, the Laboratory has continued to assist the AEC-Army joint group by making studies and evaluations, by providing specialized services, and by a continuing program of research and development activities concerned principally with improving fuel and neutron absorber materials. A major activity during the past year was the operation of a pressurized-water in-pile loop for the testing of proposed fuel systems and for water chemistry studies.

EUROPIUM OXIDE STUDIES

Control of the SM-1 and other Army reactors is provided by movable neutron absorber sections consisting of stainless-steel-clad plates containing 37 weight percent europium oxide (Eu_2O_3) dispersed in stainless steel. The favorable neutron absorption cross sections of the europium isotopes and the chemical stability of europium oxide were major factors that led to the selection of this control material. Operating experience to date has been satisfactory, but presently available fabrication techniques are costly. It has also been noted in laboratory tests that under some conditions the europium oxide may react with the constituents of stainless steel, and that the dispersions are susceptible to swelling when specimens containing defects are exposed to 570°F water.

The Metals and Ceramics Division is investigating a stabilized form of europium oxide, $Eu_{5.3}MoO_{11}$, which is obtained by a comparatively small addition of molybdenum oxide. The stabilized oxide resists hydration attack by high temperature water, but its chemical compatibility with other constituents of the dispersion was not known. To investigate this property, small powder metallurgy compacts of $Eu_{5.3}MoO_{11}$ dispersed in various metal matrices of interest were heat-treated in the temperature range 1100 to 1200°F in atmospheres of hydrogen, argon, and vacuum and then examined for evidence of reactions. These studies indicate that it is feasible to fabricate chemically stable dispersions containing europium molybdate, but irradiation testing of such dispersions is needed before $Eu_{5.3}MoO_{11}$ can be considered for reactivity control in operating reactors.

Europium oxide, as received from the supplier, is generally in the form of a light fluffy powder which is not suitable for dispersing in a metal matrix. A conditioning treatment is required and has usually consisted of pelletizing the as-received oxides, high firing in a hydrogen atmosphere at 1600 to 1700°F, and crushing to the desired particle size. A shortcoming of this procedure

has been its tendency to yield a nonuniform product. The Metals and Ceramics Division has used arc melting techniques to improve the reproducibility of the oxide particle density and other characteristics and to reduce processing costs. Rare-earth oxide powders were successfully consolidated by melting in an inert-arc furnace, and this procedure was also shown to be applicable to the production of the molybdenum-stabilized europium oxide ($Eu_{5.3}MoO_{11}$).

PRESSURIZED-WATER REACTOR CHEMISTRY

Water chemistry studies of the ORR pressurized-water in-pile loop (presently being used to test advanced fuel elements for Army Power Reactors) have continued during the past year. An improved water sampling procedure, developed by Sweeton of the Reactor Chemistry Division, is now being used in which particulate and dissolved material are removed by filtration and ion exchange of a cooled side stream of the loop over extended periods. Sufficiently large samples of water-borne material have thus been obtained to permit direct estimates of their very low concentrations in the loop water (see data in following table).

The water circulating in the ORR loop is seen to have a chemical purity which exceeds normal distilled water and is similar to "conductivity" water. This is also typical of large pressurized-water reactor systems operated at neutral pH. Yet the minute amounts of dissolved and suspended corrosion products and the small amount of radioactivity they contain are of significance since they are continuously produced in the reactor flux, and are continuously deposited about the circulating system resulting in a buildup of radioactivity throughout such systems and a preferential deposition of the corrosion product solids, "crud," on the fuel element surfaces. It is believed that the study of the chemistry of these trace quantities of corrosion products and the mechanisms by which they and their associated activity are liberated to and removed from the water will suggest the means with which to deal with the problems they cause in the operation of PWR systems. This is the goal of the present program.

To improve upon the water purification method presently in use (resin ion exchange of cooled water), tests of inorganic ion exchangers which may be used at the high operating temperatures of PWR systems (up to 260°F) are continuing. Magnetite, Fe_3O_4, which is the principal constituent of the particulate corrosion products, has been found to remove the most important corrosion product activities from the water (1) by mechanical filtration, (2) by surface adsorption, and (3) presumably, by an "ion-exchange" process in which radioactive atoms in solution change places with normal iron atoms in the oxide crystal. This latter process is normally very slow, but at the elevated temperatures of PWR coolants it may be rapid enough to effectively reduce radioactive contamination of PWR coolants with a capacity much greater than would be offered by materials which allow surface adsorption alone.

Typical Water Analysis from ORR In-Pile Pressurized-Water Loop

[Insoluble solids, 6 ppb; conductivity at 25°C, 0.14 μmho/cm; pH at 25°C, 7.8]

Fraction	Concentration (10^{-9} mole/liter)				Activity (dis sec^{-1} $liter^{-1}$)		
	Fe	Cr	Ni	Mn	^{59}Fe	^{60}Co	^{54}Mn
Soluble fraction	200	1	100	12	100	3000	700
Insoluble fraction	40	7	1	<0.1	90	200	20

Space Reactor Program

There are strong indications that nuclear reactors might be the best sources of large amounts of power for long periods of time for space vehicles and stations. A few kilowatts of electrical power for a year in an orbiting space laboratory or a hundred kilowatts for a powerful communications satellite might best be provided by nuclear reactors. These space electrical plants powered by nuclear reactors are known as Systems for Nuclear Auxiliary Power or SNAP power plants. Nuclear rocket systems are also being considered. It is conceivable that nuclear rocket systems can be useful on lunar missions and that nuclear-electric propulsion systems could make corrections to the attitude or to the orbit of a satellite. On the other hand, very large payloads can be transported on long-range missions only by nuclear rocket systems, nuclear-electric propulsion, or some other very advanced system.

The space reactor research and development program at ORNL has been concentrated on the SNAP-type electrical power supplies. Low weight, long life, and high reliability are the prime requisites; they lead toward the development of small reactors which contain large amounts of nuclear fuel, operate at high temperatures to provide good thermal efficiency, and have small high-temperature radiators for disposal of waste heat.

The ORNL effort has centered about the Medium Power Reactor Experiment (MPRE), which was conceived about five years ago by A. P. Fraas of the Reactor Division and has been under development by a project group from several divisions. In the MPRE type of power plant, potassium boiled from the core of the reactor serves both as the reactor coolant and as the thermodynamic working fluid for the turbine of a Rankine cycle plant. The single-loop simplicity leads to a system with few components and, consequently, high potential reliability. The potassium reaches the turbine at the same temperature at which it leaves the reactor; therefore a reactor of adequate performance can be developed from conventional high-temperature materials such as stainless steel. It is expected that an MPRE power plant producing 140 kilowatts of electricity, and shielded to protect an instrument payload rather than to human tolerance, would weigh about 4000 pounds. Problems of materials stability, reactor physics, heat transfer in boiling potassium, and overall system stability have been under study. Operation of the ground-based MPRE experiment is planned to take place in 1968. An MPRE of higher temperature and lower specific weight could be constructed of refractory alloys. The MPRE concept also might have application in the civilian power field.

A large program of study on refractory alloys is carried out at ORNL, mainly in conjunction with the liquid-lithium and boiling-potassium circuits of the SNAP-50/SPUR system of Pratt and Whitney Aircraft and AiResearch. Materials compatibility studies are conducted on the SNAP-8 liquid-NaK primary circuit for the National Aeronautics and Space Administration on the basis of an interagency agreement with the Atomic Energy Commission. The properties and stress analysis of high-temperature graphite are studied for the KIWI type of nuclear rocket, while other studies are in progress on the aqueous moderator and aqueous poison control systems of an advanced version of the nuclear

rocket being investigated by NASA. Also in connection with the nuclear rocket, materials research and consultation are provided to NASA on the fabrication of rocket nozzles for the NERVA engines. The shielding of radiations from nuclear reactors is another field in which ORNL has been active, and an intensive study, both theoretical and experimental, has been made on the shielding of SNAP reactors. These programs involve teams from many areas of the Laboratory, such as the Reactor, Metals and Ceramics, Reactor Chemistry, Neutron Physics, and Instrumentation and Controls Divisions.

FORCED-CIRCULATION BOILING-POTASSIUM CORROSION LOOPS

Boiling potassium is a promising working fluid in Rankine cycle turboelectric systems for space power applications. Accordingly, experiments have been and are now in progress to evaluate the corrosion-erosion mass transfer effects of potassium vapor on potential power plant structural materials and potential turbine nozzle and blade materials.

Type 316 Stainless Steel Loops

A series of type 316 stainless steel forced-circulation boiling-potassium corrosion loops have been run or are running. These loops are operated at 1600°F for conducting screening tests to determine the effects of high-velocity potassium vapor of varying quality and temperature on potential power-plant structural materials and potential turbine nozzle and blade materials.

In a loop of this type, potassium vapor is generated in the boiler and passes through a drying section. The dry vapor enters the test section and flows through a series of three nozzles, each of which discharges its vapor jet against an inclined blade specimen. After leaving the test section, the vapor is desuperheated, condensed, and subcooled prior to entering the inlet of a rotating magnetic-field (electrodynamic) pump. A control valve is included downstream of the pump to provide a stabilizing pressure drop.

While the loop material for all these tests has been type 316 stainless steel, nozzles and blade specimens in various tests have been constructed of molybdenum alloy TZM, Haynes alloy No. 25, and type 316 stainless steel for purposes of comparison.

Before the evolution of the loop design, operations were hampered by boiling instabilities. Slugs of liquid carried from the boiler over to the test section. The addition of a long drying section, replacement of a sodium-jacketed 2-inch-diameter boiler with a 4-inch-diameter boiler without jacket, addition of a control valve, and use of large amounts of preheat upstream of (and flashing across) the control valve resulted in greatly improved boiling

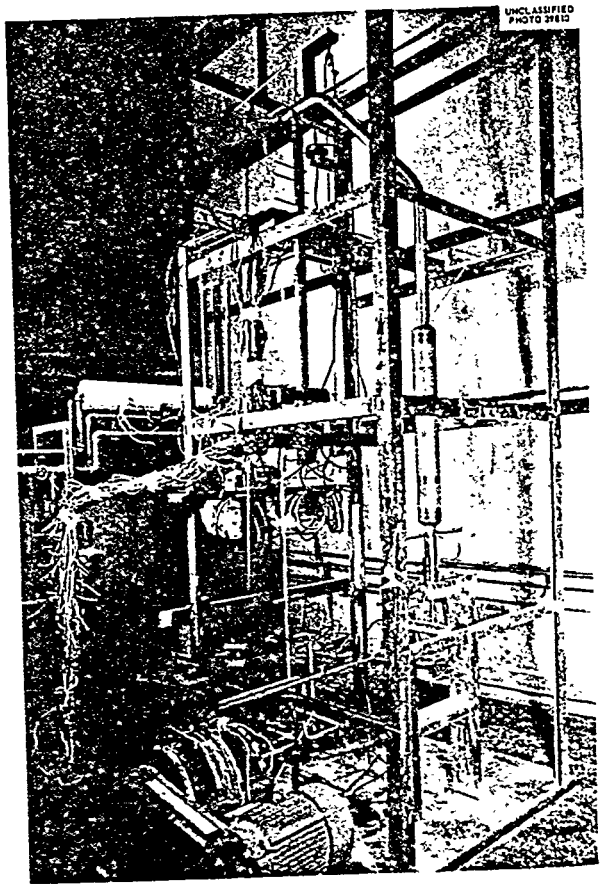

This forced-circulation boiling-potassium corrosion loop is typical of a series of loops operated at 1600°F to determine the corrosion, erosion, and mass transfer effects of potassium vapor. The loops were constructed of type 316 stainless steel, and the turbine nozzle and blade specimens were fabricated from Haynes alloy No. 25, molybdenum TZM alloy, and type 316 stainless steel.

stability. However, excellent boiling stability was achieved only after the installation of two boiling "hot fingers." The hot fingers are ¾-inch Haynes alloy No. 25 rods mounted horizontally and 180 degrees apart in the loop wall at the preheater outlet (boiler inlet). They are heated well above loop temperature by individual clam-shell heaters with Kanthal heater elements. At the end of each hot finger exposed to the potassium pool, a bubble nucleation cavity is provided. One cavity is a ⅜-inch-diameter hole, ½ inch deep, at the base of which is a 0.052-inch hole, ½ inch deep. The other cavity is a 0.032-inch hole, ½ inch deep, inclined downward toward the open end at an angle of 45 degrees. Tests have shown that either configuration will promote and maintain stable boiling.

Columbium–1% Zirconium Loop

The loop for operation at 2000°F, with its associated vacuum system, was completed and was run for an extended period of time. This loop was constructed and run to determine the effects of high-velocity potassium vapor of varying quality and temperature on columbium–1% zirconium.

The forced-circulation boiling-potassium corrosion loops for 1600°F operation are composed of a preheater and boiler, a drying section between the boiler and test section, the tandem nozzle and turbine blade specimens, the air-cooled condenser, and the electrodynamic pump which returns condensed liquid to the boiler. Boiling stabilizers are used between the preheater and boiler to ensure smooth, continuous boiling of the potassium pool and to improve the operating stability of the loop.

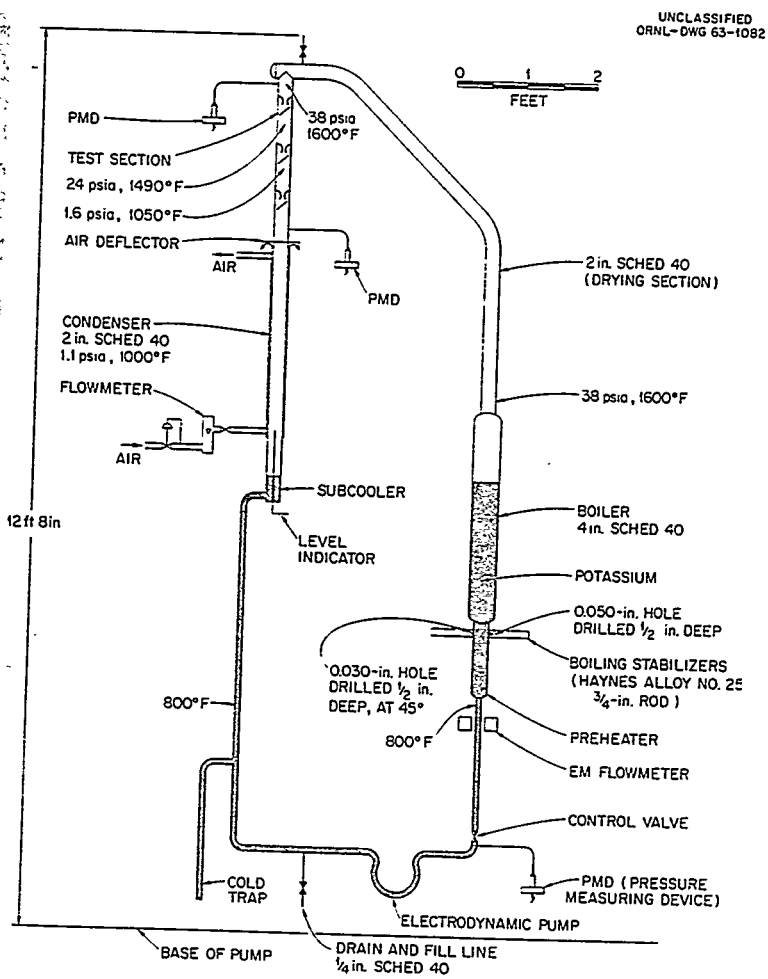

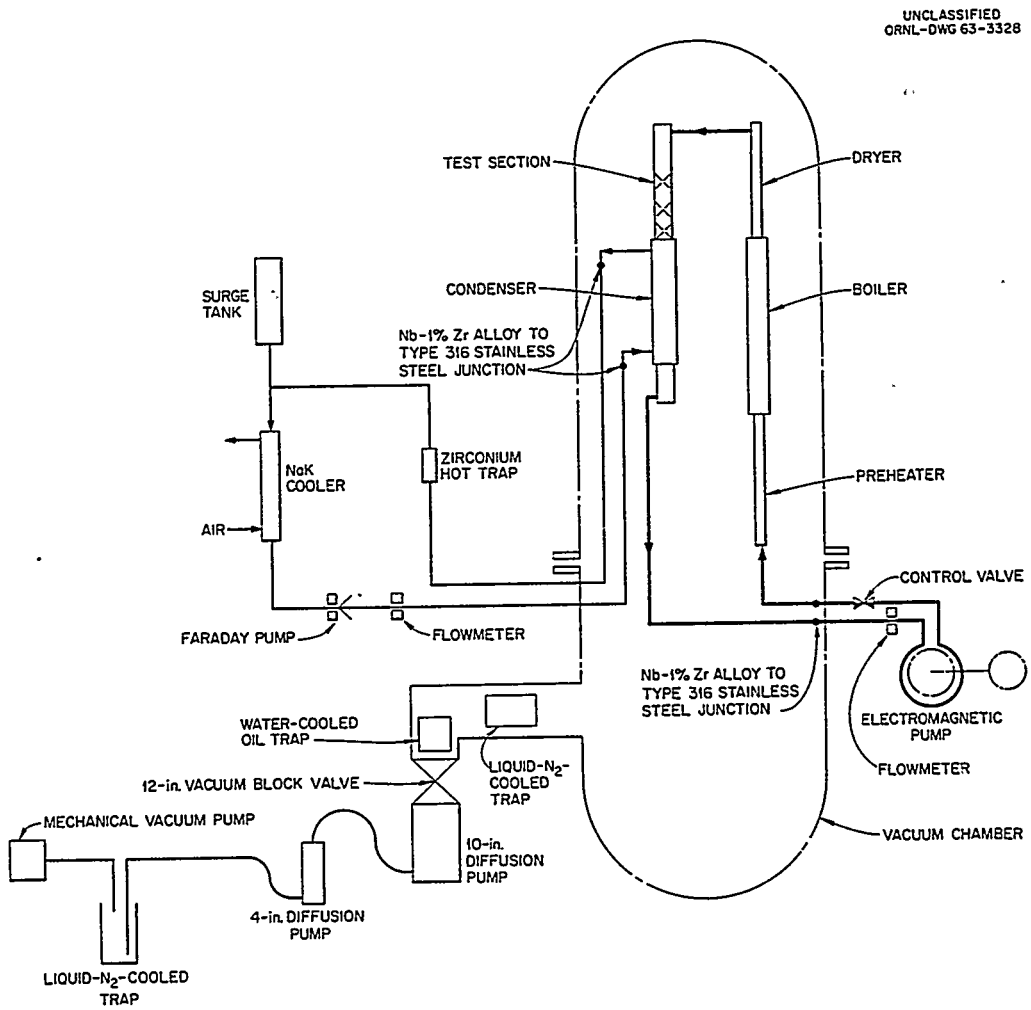

The forced-circulation boiling-potassium corrosion loop for operation at 2000°F was constructed primarily from columbium–1% zirconium alloy. The turbine nozzle and blade specimens were also of this material. Because of the deleterious effects of atmospheric gases on this alloy, the loop was installed in a vacuum chamber during operation. Heat was removed from the loop by a secondary NaK system, located outside the vacuum chamber, which delivered coolant to the primary system condenser. The chamber was evacuated by oil diffusion pumps to a pressure level of 5×10^{-8} to 5×10^{-9} mm Hg during testing.

The primary loop consists of a preheater, a boiler with a sodium-filled jacket, a dryer, a test section containing columbium–1% zirconium nozzle and blade specimens, a NaK-cooled condenser, a rotating magnetic-field (electrodynamic) pump, and a control valve. The preheater, lower boiler, upper boiler, and dryer are surrounded by separately controlled tantalum tube resistance heaters. Reflective insulation composed of tantalum, columbium–1% zirconium, and zirconium foil was used exclusively within the vacuum chamber. As many as ten individual layers of insulation were used at various locations. Temperature measurements within the tank were made by using both tantalum-sheathed, BeO-insulated W–5% Re vs W–26% Re thermocouples and columbium-sheathed, MgO-insulated Pt–10% Rh vs Pt thermocouples.

A secondary NaK loop provides cooling for the potassium condenser. This loop consists of the shell side of the potassium condenser, a hot trap

packed with zirconium foil for oxygen removal, a counterflow NaK-to-air cooler, an electromagnetic pump (Faraday type), and an electromagnetic flowmeter.

In both the primary boiling potassium and secondary NaK circuits of this columbium–1% zirconium loop, a transition was required between the columbium–1% zirconium tubing and the type 316 stainless steel tubing. Coextruded tubular transition joints were used in the construction of the loops.

All portions of both primary and secondary loops external to the vacuum chamber are of type 316 stainless steel. The bimetallic transition is made inside the vacuum chamber in each case. In order to protect the columbium–1% zirconium from contamination by gaseous impurities, portions of the primary and secondary loops were contained within the vacuum chamber, which was held approximately in a range of 5×10^{-8} to 5×10^{-9} mm Hg during full-power operation.

Loop operation was characterized by periods of both moderately stable boiling and violently unstable boiling. Severe temperature and pressure fluctuations accompanied sudden boiling instabilities. Operation of the type 316 stainless steel loops indicated that an effective bubble nucleating site in the boiler would have produced consistently stable operation.

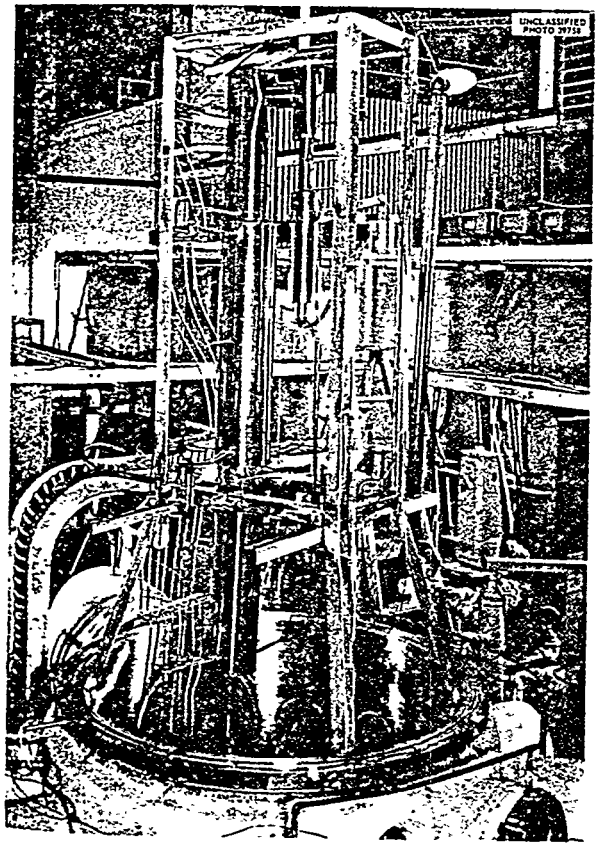

Completed columbium–1% zirconium forced-convection boiling-potassium corrosion loop prior to installation of the top half of the vacuum enclosure. The loop is supported in a stainless steel framework, which also supports the insulated leads to the resistance heaters. The long leg to the left is the preheater, boiler, and dryer encased in reflective foil insulation. The short leg to the right is the test section and condenser, appropriately insulated to give desired heat losses.

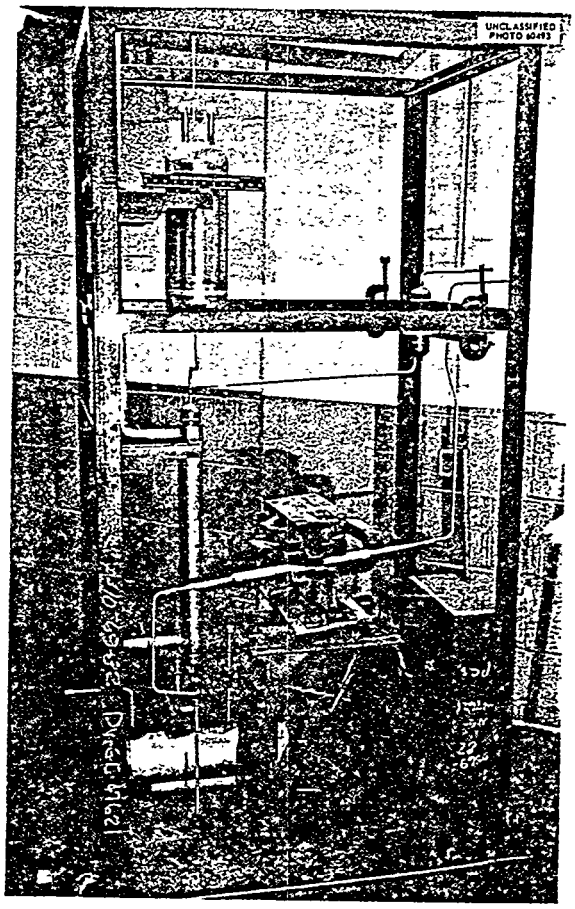

The secondary NaK circuit for removing heat from the primary potassium loop of the columbium–1% zirconium boiling-potassium corrosion test facility was located outside the vacuum chamber and NaK was fed through penetrations in the vacuum chamber walls to the potassium condenser. The secondary system consisted of an electromagnetic pump (lower center), a sump tank (lower left), an air-cooled heat exchanger (center left), a surge tank (top left), and a small hot trap (top right).

Thorium Utilization Program

SOL-GEL PROCESS FOR REMOTE PREPARATION AND FABRICATION OF RECYCLE FUELS

The sol-gel process is being developed by the Chemical Technology Division as a simple, economical process for the remote preparation and fabrication of recycle power-reactor fuels. In four simple steps, the process as applied to recycle thorium-bearing fuels converts the nitrate-solution products from the solvent extraction processing of spent reactor fuels to fuel materials suitable for use in remote fuel fabrication. These steps are: denitration to obtain a reactive oxide, dispersion of this oxide in dilute nitric acid to form a hydrosol, gelation by evaporation or extraction of water from the sol, and calcination to obtain the final ceramic form desired. The process can produce the oxides or the carbides of thorium, uranium, or plutonium. It can produce powder suitable for vibratory packing into metal tubes, or microspheres for subsequent coating and use in high-temperature gas-cooled reactors. Differences in the process steps for preparing oxides of the above fuel materials are relatively minor and are related primarily to the fact that care must be taken to retain both uranium and plutonium in the proper chemical state. Because of its extraordinary flexibility, the sol-gel process promises to become an almost universal method for preparing ceramic reactor fuel materials.

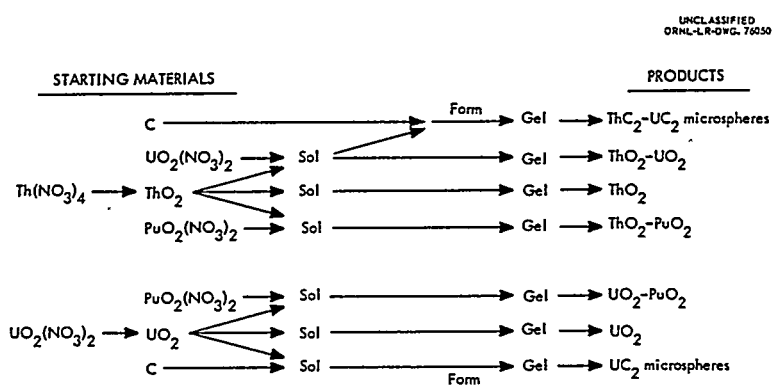

Examples of the versatility of the sol-gel process as applied to the preparation of ceramic reactor fuels. The nitrate solutions produced in conventional fuel-purification processes are the starting point for all the variations shown.

The most advanced application in the development program is the preparation of mixed oxides of thorium and uranium-233 for loading into fuel tubes by vibratory compaction. A ton of this fuel has been prepared and loaded into 1000 Zircaloy tubes, 40 inches long and ½ inch in diameter, in the Kilorod Facility at ORNL. This facility includes shielded and remotely operable equipment for the preparation of dense particles of mixed thorium-uranium oxides by the sol-gel process, conditioning of the powder by grinding and sizing, loading of the Zircaloy tubes by vibratory compaction, and welding and inspection of the completed element. Operation at 90 percent of the design capacity was routinely attained, with less than 3 percent of the elements requiring recycle because of density defects. This facility is the forerunner of the Thorium-Uranium Fuel Cycle Development Facility now being designed for future development of integrated fuel recycle processes.

From analysis of the radiation levels observed in the Kilorod Facility operations, it is concluded that on a 10-kilogram-batch scale, reactor fuel rods containing uranium-233 contaminated with about 500 ppm of uranium-232 can be safely fabricated by use of the shadow shielding provided by about a 2-inch thickness of lead. However, final assembly of the fuel bundle, larger-scale operation, or higher levels of uranium-232 contamination will require complete shielding and remote operation.

An irradiation testing program is being conducted on vibratorily packed, sol-gel-derived thorium oxide fuels. Our findings indicate that this is a suitable form of fuel for power reactors. Irradiations to 35,000 Mwd per ton at peak heat ratings of $\int k\, d\theta = 40$ watts per centimeter have produced insignificant changes in the oxide. (The parameter $\int k\, d\theta$ is a measure of the severity of thermal treatment. Uranium dioxide fuel elements typically are subject to $\int k\, d\theta = 30$ to 50 watts per centimeter.) In capsules now being irradiated, burnups have reached 75,000 Mwd per ton. At a heat rating of $\int k\, d\theta = 60$ watts per centimeter, recrystallization and sintering of the oxide are observed, but with no noticeable deleterious effects. Fission-gas release from the sol-gel oxide is comparable to that from fused oxide.

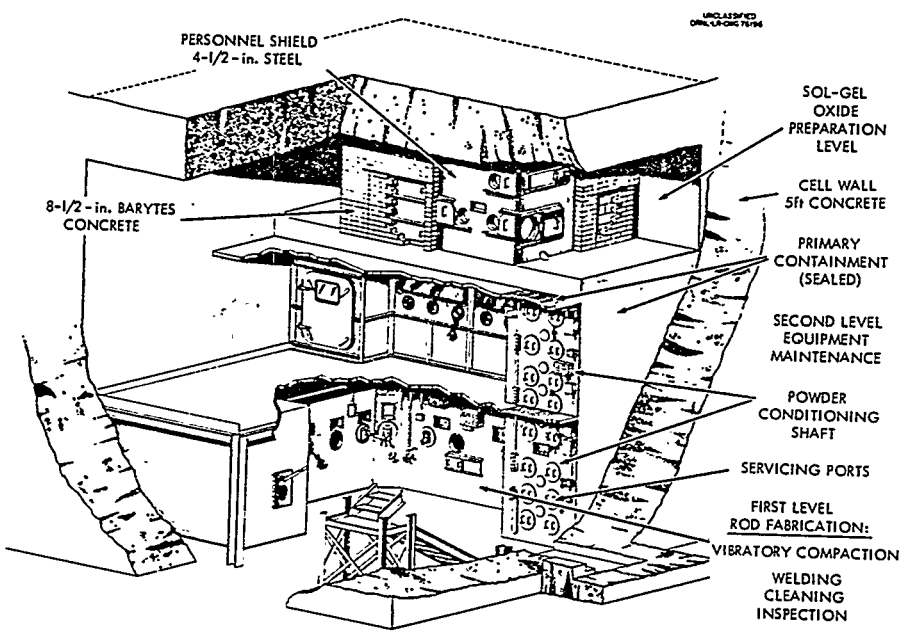

The Kilorod Facility is a shielded, remotely operable pilot plant for the demonstration of the sol-gel process. In it, 1000 Zircaloy rods containing mixed oxides of thorium and uranium-233 have been successfully prepared by the sol-gel process and vibratory compaction of the fuel into the tubes.

By introducing carbon of fine particle size into the oxide sol, a mixed oxide-carbon gel can be prepared. After drying, the constituent gels react (in an argon atmosphere) at about 1750°C to give high-purity carbide. Mixed thorium-uranium dicarbide has been prepared in this manner; the density was 8.9 grams per cubic centimeter, and the product was sufficiently pure for use as a reactor fuel.

Microspheres of oxide or carbide can be prepared by dispersing the sol in an immiscible liquid and then gelling the suspended spherical droplets. An organic compound, such as 2-ethylhexanol, in which water is moderately soluble, has proved most successful for the dispersing medium. By this method, the sol is "set" to the gel by the extraction of water into the organic phase. After this forming process, the microspheres are converted to dense oxide or carbide by calcination. Microspheres of both oxide and carbide prepared by this procedure were successfully coated with pyrolytic graphite, and they appear suitable for use as fuels in high-temperature gas-cooled reactors.

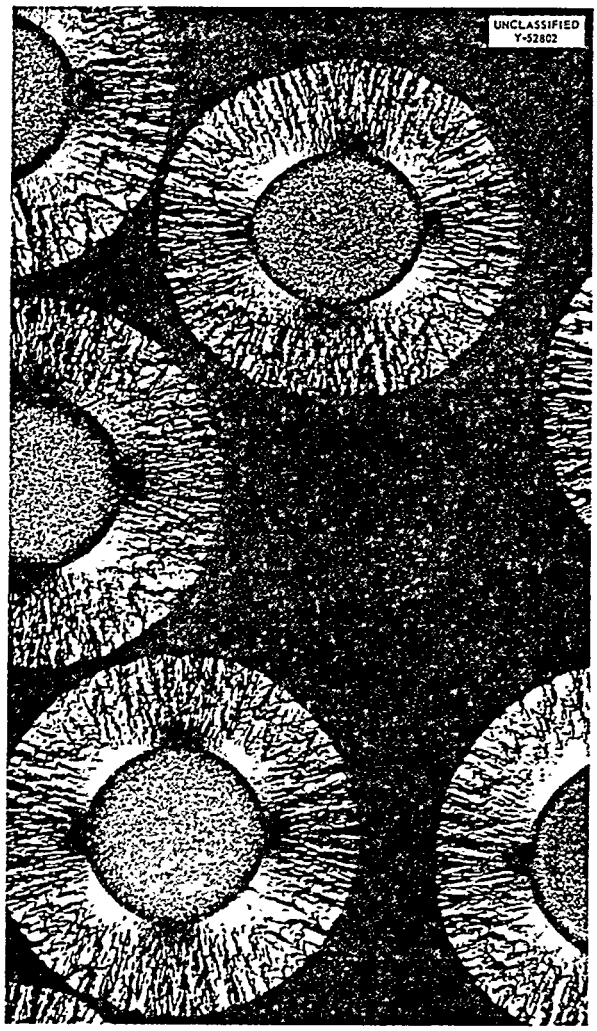

Thorium oxide microspheres prepared by the sol-gel process have been coated with pyrolytic graphite for testing purposes. The photomicrograph shows not only the sphericity of the particles, but also the high crystallinity and good coating obtained when carbon is deposited as pyrolytic graphite on thoria produced by the sol-gel process.

Reactor Shielding

The 1963 reactor shielding program at the Laboratory consisted both of studies designed to provide data applicable to a wide spectrum of reactor types and of studies performed specifically to aid the design of shields for reactors used on spacecraft. In addition, investigations of the effectiveness of structures against radiation from nuclear weapons were continued, with the Tower Shielding Reactor II simulating a source of prompt weapons radiation.

In the basic shielding studies, emphasis was placed on measurements of the energy spectra of neutrons and gamma rays emitted from reactors and on the transmission of neutrons through water and LiH shields. A primary purpose of the experiments was to provide measured spectra which could be used to test neutron transport calculations by various methods. In conjunction with the experiments, development of a fast-neutron spectrometer was continued, and a method for analyzing observed neutron and gamma-ray spectra was devised.

The shielding studies for spacecraft reactors were sufficiently general to be applicable to the Commission's SNAP (Space Nuclear Auxiliary Power) reactor development programs at Atomics International, Pratt and Whitney, and ORNL. For all systems it is proposed that highly asymmetrical shields be used, but since it is important to minimize the weight of the shield for a particular system, very accurate design methods which can be applied to each system are required. The aim of the ORNL shielding program is the development of suitable design methods.

While the studies of shielding against nuclear weapons radiation are not properly categorized as reactor shielding studies, the problems are quite similar and are treated with the same experimental and theoretical techniques. For this reason, they are included in this section.

A SHIELDED-DIODE FAST-NEUTRON SPECTROMETER

An important phase of the basic reactor shielding program is the development of techniques for measuring the radiations of interest. An instrument which has long been needed for such measurements is a neutron spectrometer that can be used in a reactor environment. One of the most promising devices developed for this purpose was a neutron-sensitive detector consisting of an ^{6}LiF layer sandwiched between two silicon surface-barrier diodes [T. A. Love and R. B. Murray, *IRE Trans. Nucl. Sci.* 8(1), 91 (1961)]. The alpha particle and the triton emitted in approximately opposite directions in the ^{6}Li(n,α)T reaction were separately detected in the diodes, and the sum of their energies gave the energy of the incident neutron plus the Q value (4.78 Mev) of the reaction. The detector was satisfactory for neutrons having energies less than 5 Mev, but above this energy the determination of the background due to neutron interactions in the silicon of the diodes became difficult.

Recently this device was further developed by V. V. Verbinski and M. S. Bokhari into a spectrometer of a "shielded-diode" design that has been used successfully to measure the energy spectra of directed fast-neutron fluxes from the

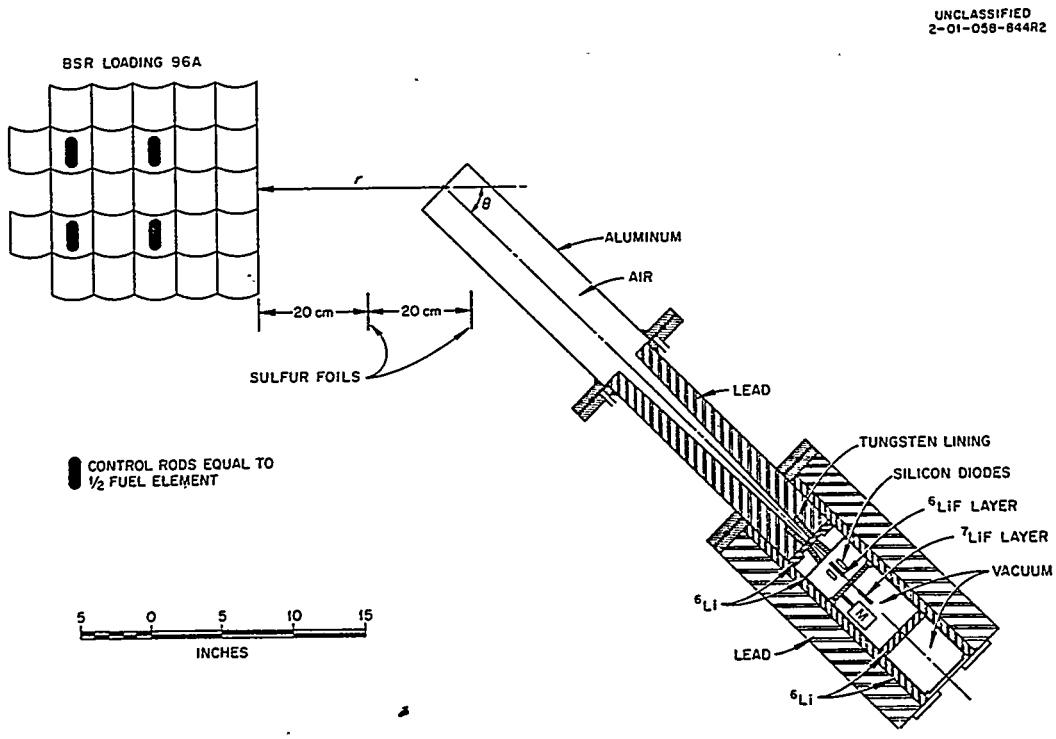

The shielded-diode fast-neutron spectrometer. The spectrometer has been used to measure the energy spectra of directed fast-neutron fluxes in the Bulk Shielding Facility pool at various distances r from the reactor face and at various angles θ from the reactor center line. The incoming neutron strikes the ^{6}LiF layer, and an alpha particle and a triton are emitted in approximately opposite directions. The emitted particles are detected separately by the silicon diodes on either side of the ^{6}LiF layer, and the sum of their energies less the Q value of the reaction (4.78 Mev) equals the energy of the incident neutron.

Bulk Shielding Reactor. The new design differs from the earlier version in that the ^{6}LiF layer and the diodes are spaced apart so that the diodes can be shielded from direct radiations, which would give spurious pulses. As a result of adding the shield, neutrons from only one direction can be observed, since they must traverse the shield collimator to interact with the lithium-6. Thus, the spectrum obtained is one of angular flux rather than scalar flux. Attenuation of the alpha particle and the triton by air spaces between the ^{6}LiF layer and a diode is avoided by evacuating the region between the diodes. Another modification allows the background to be accurately determined by substitution of an ^{7}LiF layer for the ^{6}LiF; both layers are mounted on a thin aluminum wheel that can be rotated.

The response of the spectrometer is linear over the neutron energy range from 0 to 14.7 Mev, and its detection efficiency is $\sim 3.5 \times 10^{-3}$ for thermal neutrons and 5.2×10^{-7} for 3-Mev neutrons.

ENERGY SPECTRA OF FAST NEUTRONS IN BSR-I WATER SHIELD

The accurate calculation of the attenuation of neutrons in a reactor shield, as well as the production of secondary gamma rays within and outside of the shield, requires a knowledge of the spectral and spatial distributions of the neutrons throughout the shield and those leaking from it. Since water is the standard material used to shield against neutrons, studies that yield information on the energy and angular distributions of neutrons in water are of considerable interest to shield designers, but experimental measurements of such

details have always been hampered by the lack of suitable spectrometers. The availability of the shielded-diode fast-neutron spectrometer discussed in the preceding section prompted a series of measurements of the energy spectra of fast neutrons in the water shield around the Bulk Shielding Reactor I and a comparison of the results with spectra obtained from calculations with the NIOBE code (Numerical Integration of the Boltzmann Equation) of Preiser *et al.* (*ARL Technical Report* 60-314).

In these measurements the spectrometer was positioned in the horizontal midplane of the reactor, and the energy spectra were measured as a function of θ and r. Sulfur foils were used to monitor the relative power of the reactor for various runs; the relative power level from one run to the other was thereby determined to an accuracy of about 2 percent.

The energy spectra of neutrons in the forward direction show a hardening of the spectrum, that is, a shift toward higher energies, and the emergence of some structure (broad peaks) with increased distance in water. In the measurements at 51 and 40.5 degrees this structure essentially disappears, and the spectra become softer.

The overall agreement between these measurements and the calculated values obtained from NIOBE calculations in which the source distribution was taken to be the same as that measured at the face of the reactor is reasonably good, except that the calculations predict more pronounced dips in the spectrum. This disagreement is attributed at least in part to the difference in the experimental and calculational geometries (the calculations were for a spherically symmetric geometry with a source region 20 centimeters in diameter) and to the finite spectrometer resolution.

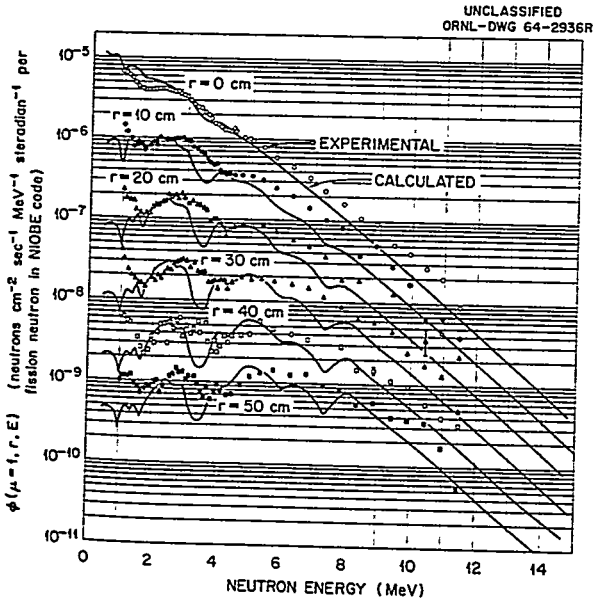

Measured and calculated energy spectra of fast neutrons in the Bulk Shielding Facility pool. The distance from the reactor face is r. Outward-directed neutrons ($\mu = 1$, where $\mu = \cos\theta$).

ENERGY SPECTRA OF GAMMA RAYS EMITTED BY BSR-II

Just as a knowledge of neutron energy and angular distributions is required to calculate neutron attenuation through a reactor shield, a knowledge of gamma-ray energy and angular distributions is needed to calculate gamma-ray attenuation through a shield. But while the spectrum of neutrons emerging from a reactor is essentially independent of the materials of the reactor core – except for their attenuating effects – the spectrum of gamma rays is greatly affected by the core constituents. This is because the gamma rays originate not only from the uranium-235 fission and from fission products but also from the capture and inelastic scattering of neutrons by the core materials, and the number and energy of capture and inelastic-scattering gamma rays are wholly dependent on the type of materials used in the core. Thus, the designer of a gamma-ray shield for a reactor must consider the effects of the materials in the core on the gamma-ray spectrum emitted from the core.

Stainless steel is a material which from an engineering viewpoint offers many advantages as a reactor structural component. It has been particularly recommended for fuel element cladding in pool-type reactors, since elements then would no longer have to be replaced because of corrosion. In order that the safety and physics characteristics of such reactors could be studied, a

stainless-steel-clad core loading was fabricated for the Bulk Shielding Reactor several years ago. The most recent measurements with the reactor (called the BSR-II) have been of the spectra of gamma rays at the core surface and at various positions in the reactor water shield.

These measurements were made with the model IV gamma-ray spectrometer, a total-absorption

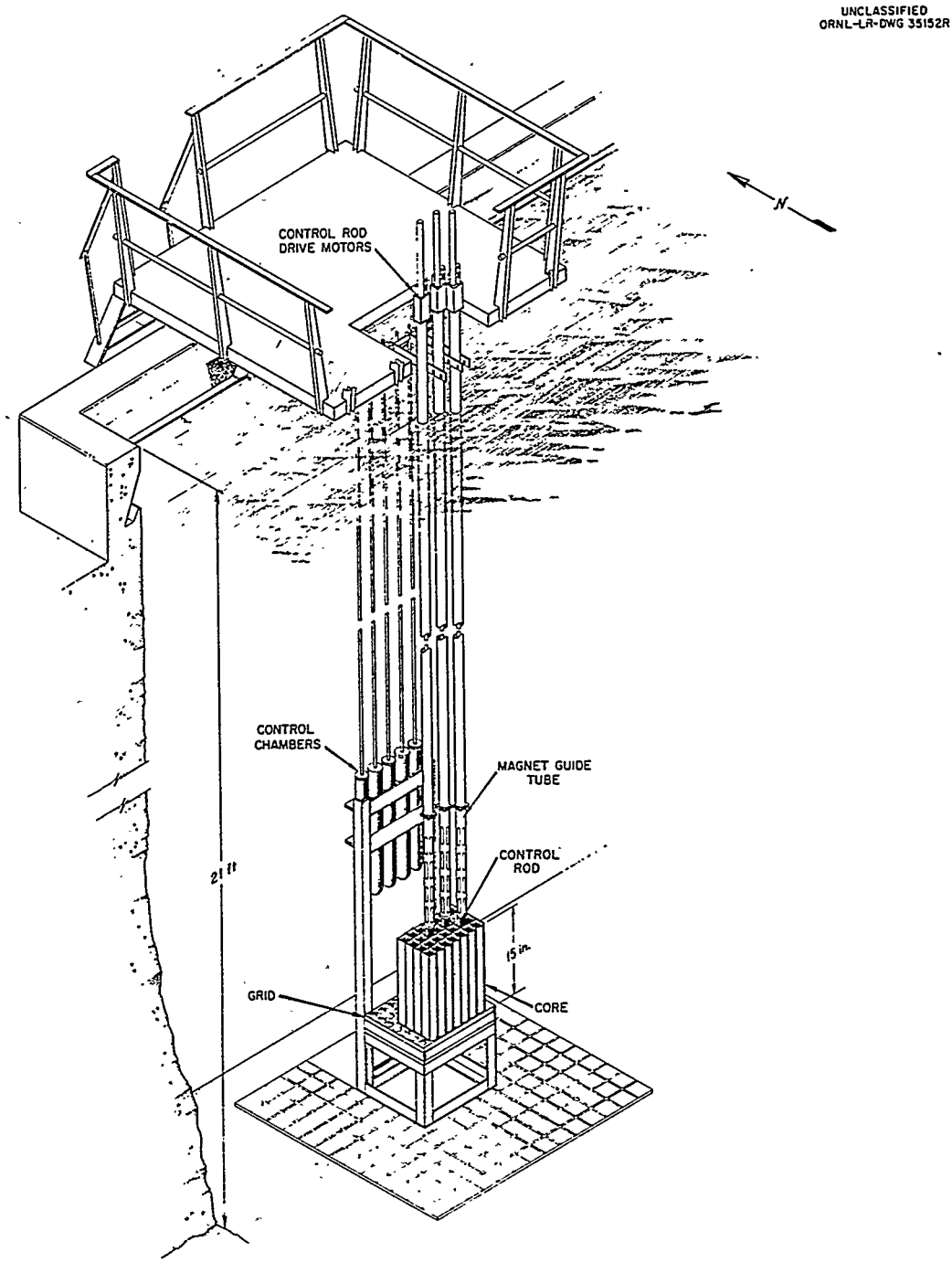

Loading of BSR-II fuel elements in the reactor pool.

NaI(Tl) spectrometer especially developed for gamma-ray spectral measurements at the Bulk Shielding Facility. The NaI(Tl) crystal, 9 inches in diameter and 12 inches long, was encased in a 15-ton lithiated-lead housing which had an air-filled conical collimator extending from one end.

For these particular measurements the BSR-II elements were loaded in the stationary grid in the

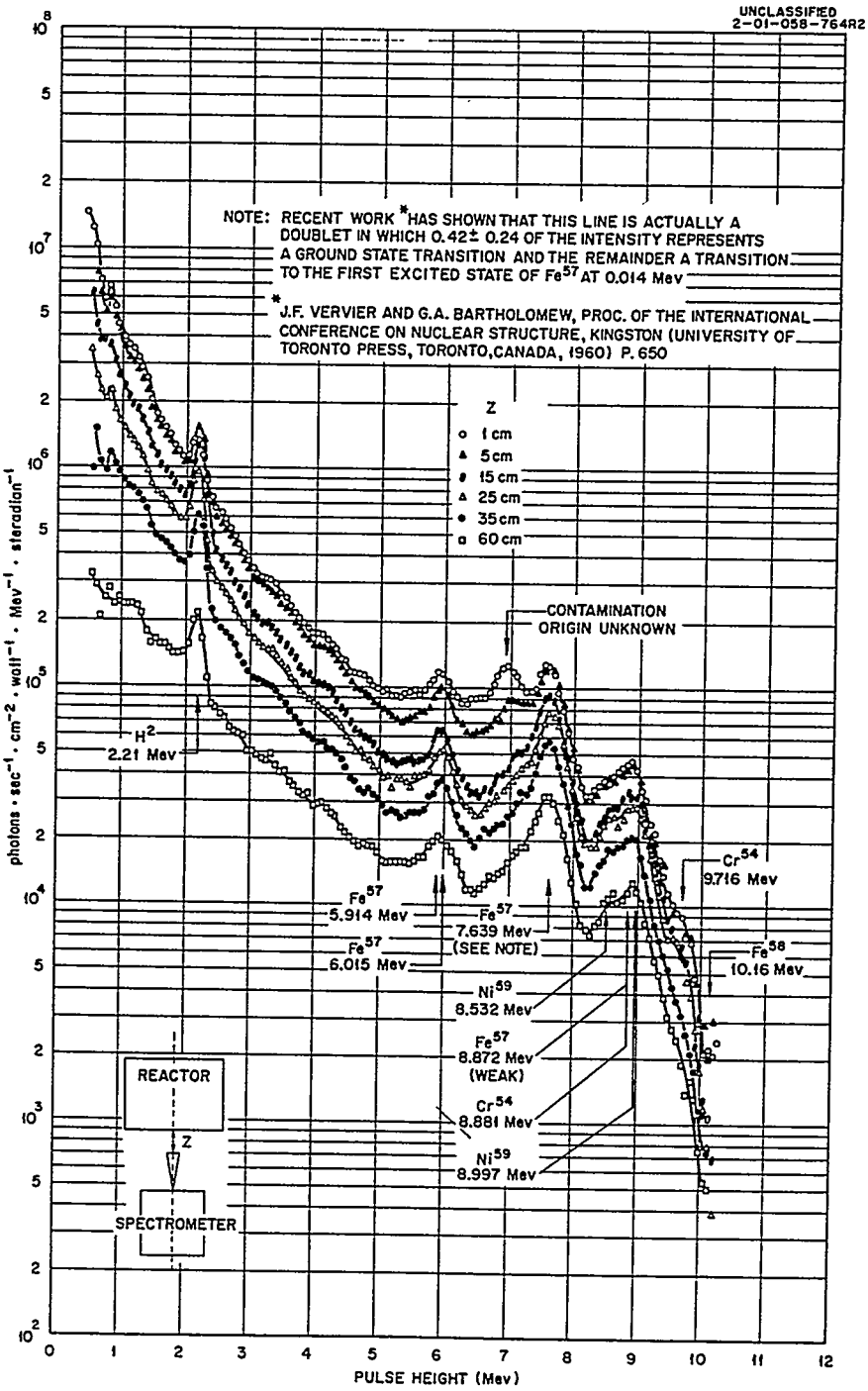

Pulse-height distribution of gamma rays emitted from the BSR-II.

BSF pool, rather than in its regular portable grid. None of the elements had been used during reactor operations at power levels greater than about 2 watts and thus had not suffered much fission product buildup.

The examination of the gamma-ray spectra for various distances from the reactor reveals that the gamma rays above 5 Mev are predominantly those arising from the capture of thermal neutrons in the stainless steel. Although many energies in the spectra are too close together to be completely resolved by the NaI(Tl) crystal, some peaks are recognizable. The most distinct peak is the iron-57 peak found at 7.639 Mev. Below 5 Mev the spectrum is apparently composed of the expected continua of prompt-fission and fission product gamma rays plus a large contribution from thermal-neutron captures in the hydrogen of the water. Spectra obtained at various angles from the core center line show the same structural shape, although, unlike all other peaks, the hydrogen-capture peak at 2.21 Mev shows no increased attenuation as the angle is increased. This implies that the origin of these gamma rays is largely in the water external to the core rather than in the water between the fuel plates.

The data presented here are preliminary, since corrections for the imperfect instrument response have not yet been made. The final analysis will be performed with the SLOP code, which is discussed in a later section of this report (see "A Method for Analyzing Neutron and Gamma-Ray Spectra").

TIME-OF-FLIGHT MEASUREMENTS OF THE SPECTRA OF FAST NEUTRONS LEAKING FROM WATER AND LiH SLABS

The importance of measuring the energy spectra of both those neutrons within the reactor shield and those leaking from it was pointed out in a preceding section, along with the difficulties encountered when such measurements are attempted. In an effort to circumvent these difficulties, some experiments utilize the time-of-flight technique, in which the energy of a neutron emerging from a shield is deduced from the length of time required for the neutron to travel through the shield and down a relatively long flight tube to a detector some distance away. For this system to be workable, however, the time of birth of the neutron must be known. This information obviously cannot be ascertained from a steadily operating reactor such as the BSR, but can be obtained when a source of pulsed neutrons, such as that which can be produced by a linear accelerator, is used. However, for the resulting data to be of maximum usefulness to reactor shield designers, the pulsed-neutron source must have an energy spectrum similar to that of fission neutrons.

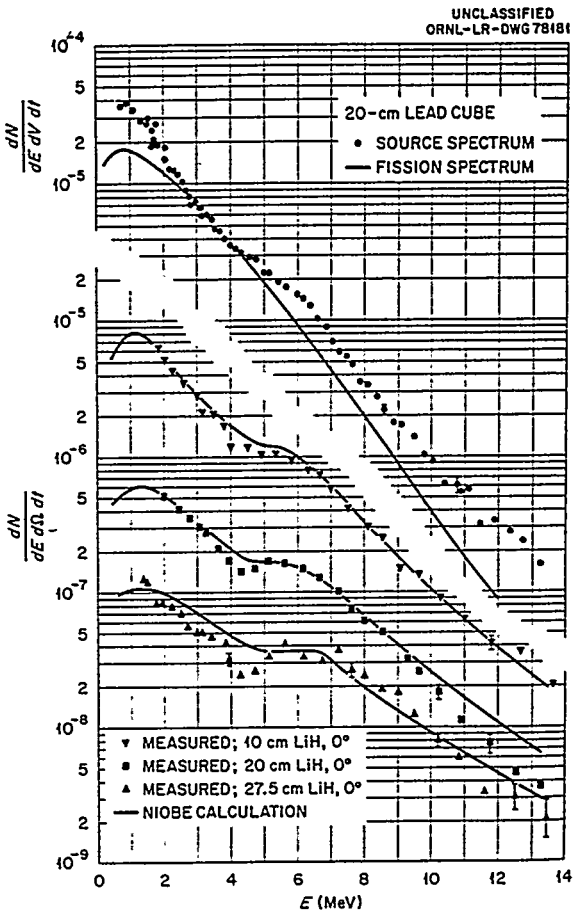

Energy spectra of neutrons leaking normally from various thicknesses of LiH. The spectrum of incident neutrons is shown in upper portion of figure. The source neutrons were obtained by placing a lead cube in the beam from an electron accelerator. The calculated points were obtained from a NIOBE code calculation in which the measured source spectrum was used.

For a recent series of experiments in which the spectra of neutrons emerging from water and LiH slabs were measured, a near-fission neutron source was obtained by placing a 20-centimeter cube of lead in the beam of the General Atomic Linear Accelerator. The resulting spectrum does indeed approximate a fission spectrum. As a result of the large size of the source – which was necessary to reduce the bremsstrahlung flash that would otherwise overload the scintillator detector – the low-energy end of the spectrum was somewhat enriched by neutrons inelastically scattered in lead, and the spectrum above about 4 Mev was hardened because of the drop-off of the lead cross section with increasing energy.

The measured spectra of neutrons leaking normally from three different thicknesses of LiH are compared with spectra calculated with the NIOBE code of Preiser *et al.* (*ARL Technical Report* 60-314). The measured source spectrum was used in the calculations, and the source was assumed to be a sphere 20 centimeters in diameter; the LiH was taken to be a concentric spherical shell with an inner radius of 37 centimeters. The calculations do not reflect the spectral detail of the measurements around the 4½-Mev peak in the lithium cross section. This is understandable on the basis of the difference between the experimental and calculational geometries. The experiment is essentially a good-geometry measurement, emphasizing uncollided flux, whereas in the calculation, scattered neutrons are more likely to be counted. Since scattering implies energy reduction, the calculations mostly count neutrons that have traveled at more than one energy, with a resultant smearing in sensitivity to the cross-section structure.

Although the data obtained with water slabs have not yet been converted to energy spectra, the detail noticeable in the pulse-height spectrum for normal leakage from a slab that is 40 centimeters thick is interesting because (1) it shows the expected spectrum hardening, and (2) the resonance structure in the oxygen cross section is much exaggerated because the observations are made on the beam axis, so that the uncollided flux is principally what is measured. Measurements at an angle of 30 degrees from a normal to the slab show much less structure in the spectra, as is to be expected for scattered radiation.

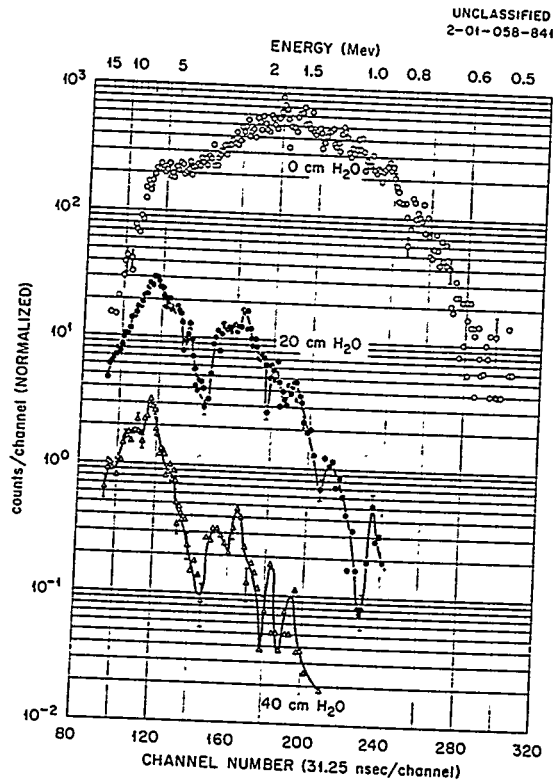

Pulse-height spectra of neutrons leaking normally from 20- and 40-centimeter-thick water slabs. The source neutrons (top curve) were obtained by placing a 20-centimeter cube of lead in the beam from an electron accelerator.

A METHOD FOR ANALYZING NEUTRON AND GAMMA-RAY SPECTRA

Scintillation counters and many other instruments commonly used to detect nuclear radiations in shielding experiments produce such a large amount of data that it is not feasible to examine the results of a given experiment directly. Instead, the data are customarily plotted automatically or displayed on a television-type screen, with each different energy of the incident radiation producing a characteristic response curve. If there are several different energies present, however, the curves become scrambled, or folded together, and only the mixture is seen. In order to determine the intensities of the different components, the scrambled

curve must be unscrambled. This problem is a common one, and many methods and computer programs exist for its solution. All the methods, however, have the serious limitation that if there are too many components scrambled together, very large uncertainties remain after the unfolding.

A new code has been developed at the Laboratory which greatly reduces the errors associated with other methods and makes possible the routine unfolding of energy spectra of neutrons and gamma rays from reactors and accelerators, even though the spectra contain an unlimited number of components. The new code is unique in that information usually ignored in other codes is used advantageously to obtain much smaller errors. It utilizes the relatively new technique of quadratic programming (a mathematical technique which was developed to aid in optimum economic scheduling) to make the best use of certain known properties of the radiation – such as continuity, decrease in pulse size with radiation energy, nonnegativity of response, etc.

The new code consists of a main program, known as SLOP, and four special programs which must be written for each different application. The first of these special programs describes the shapes of the curves resulting from single-energy radiations; the second defines the shapes of the unfolded curves; the third reads the experimental data into the computer; and the fourth specifies the restrictions that are to be placed upon the radiation.

Work is continuing in the application of the basic method to different problems in spectroscopy, dosimetry, medical scanning, and cross-section measurements. A parallel effort is being directed toward improvement of the code to obtain faster running times and smaller errors.

SHIELDING STUDIES FOR SNAP SYSTEMS

One of the significant technical problems in developing reactors to be used on spacecraft is that of designing a shield which will adequately protect the sensitive components of the payload against reactor radiation and at the same time will be of minimum weight. Most shields proposed for reactors on SNAP systems are shadow shields, so-called because the shield is interposed between the reactor and the payload and casts a "shadow" which protects the payload from direct radiation from the reactor. Such shields are usually in the shape of a truncated cone; the smaller end is nearest the reactor, and its diameter is at least as large as that of the reactor. Because the flight path of the spacecraft will be beyond the atmosphere, there is no danger that the radiation leaving the sides of the reactor will be scattered back toward the payload by air. There is a danger, however, that radiation, particularly neutrons, scattered in structural components protruding from the sides of the spacecraft will increase the dose at the payload. Thus to design an optimum shield for a particular SNAP system, we must have information not only on the attenuation characteristics of a shadow shield as a function of its composition and shape but also on the scattering characteristics of the various materials that might be used in protruding components.

The neutron-scattering characteristics of beryllium, carbon, aluminum, and iron have been studied in experiments performed at the Tower Shielding Facility (TSF), and the results have been compared with Monte Carlo calculations performed both at ORNL and at Atomics International. The Tower Shielding Reactor II (TSR-II) was placed inside a spherical lead-water shield from which a neutron beam emerged through an air-filled collimator which had a diameter of 6 inches. Cylindrical samples of the scattering material, all 6 inches long and having diameters of 1, 2, 4, and 6 inches, were suspended in the beam, and neutrons scattered at the angle θ were detected by a Hurst-type dosimeter.

The energy spectrum of the direct beam was measured both with nuclear emulsions and with the shielded-diode spectrometer described in a preceding section, and the measured spectrum was used as the source spectrum in the calculations. In general, the calculated and measured data were in good agreement, which indicates that methods can be developed for calculating the scattering effects of any material in a number of geometries.

Other phases of the SNAP shielding program have been devoted to studies of the attenuation characteristics of lithium hydride, a high-performance neutron shielding material proposed for use in the shadow shield. Because we were required to demonstrate that meaningful experiments could be performed within the atmosphere, the first

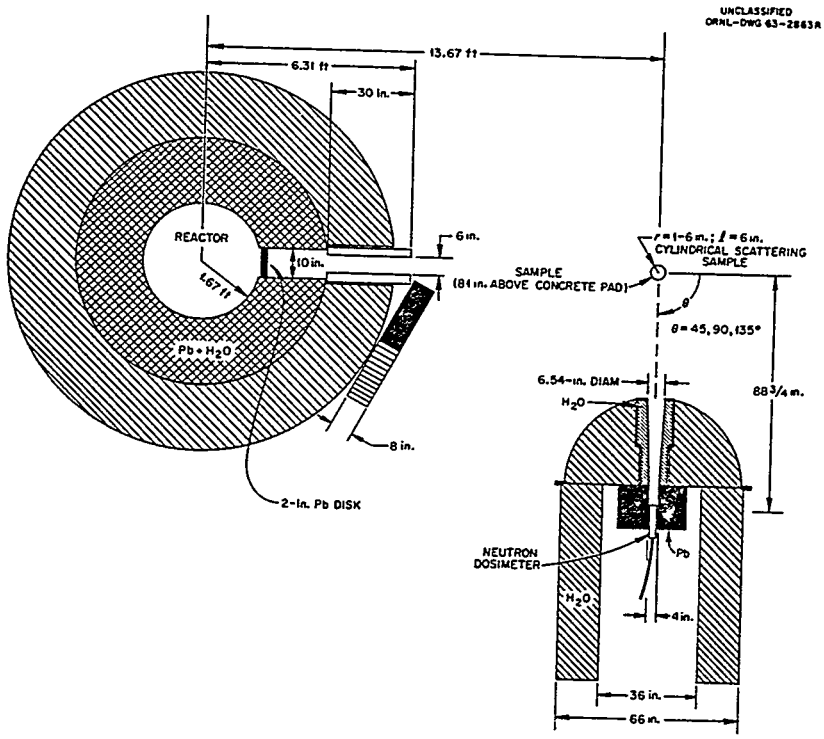

Experimental arrangement for measuring scattered neutron doses from cylindrical samples of Be, C, Al, and Fe in the Tower Shielding Reactor II beam. The experiment yielded information on the contribution to the dose at the payload of a SNAP-type space vehicle by neutrons scattered by protruding structural components.

calculations for lithium hydride were for a truncated cone surrounded by a lithium hydride collar such as might be used in experiments to intercept air-scattered radiation. The calculations indicated that the collar itself would not scatter an intolerable background to the detector and that meaningful experiments could indeed be performed.

Additional calculations for lithium hydride resulted in an apparent relaxation length of 4.8 grams per square centimeter for the final increment of an infinite slab 50 grams per square centimeter thick and an isotropic disk source. This number agreed with the results of an experiment by Atomics International, but experiments at the TSF and accompanying calculations, both of which are in a preliminary stage, indicate that this so-called relaxation length is strongly dependent on the source, the shield, and the detector.

The scattering of neutrons by small cylinders of lithium hydride has also been studied experimentally. For these measurements, which were performed at the General Atomic accelerator, a time-of-flight technique was used in conjunction with a pulsed-neutron source (see description of technique in preceding section).

A principal effort in the SNAP theoretical shielding program has been the development of the ORNL O5R Monte Carlo system as a generalized neutron transport program. All the ORNL calculations discussed above used O5R programs.

STUDIES OF SHIELDING AGAINST NUCLEAR WEAPONS RADIATION

Shielding studies for civil and military defense programs continued with an experimental and calculational investigation of the effectiveness of two cubical bunkers and a connecting three-legged tunnel against prompt weapons radiation. The two bunkers were 12-foot concrete-lined cubicles, one having an open front face and the other having an open top face. The interconnecting tunnel, also concrete lined, had a 3- by 8-foot cross section; an entranceway 3 feet in diameter covered

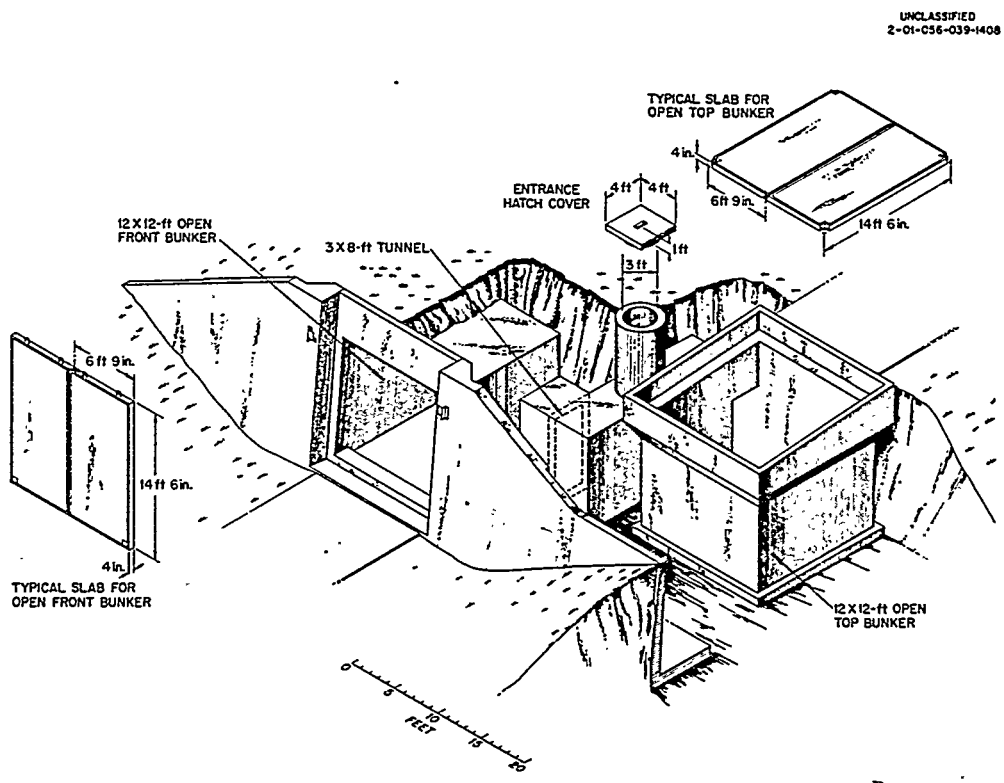

Two cubical bunkers and interconnecting tunnel used in experiment at Tower Shielding Facility to study the effectiveness of concrete structures against prompt nuclear weapons radiation.

by a concrete hatch one foot thick extended upward from its middle leg. The entire structure was covered by earth so that radiation could enter through the openings only.

The prompt weapons radiation source was simulated by the spherically shaped TSR-II, which was operated at a distance of approximately 700 feet from the bunkers and 100 feet above the ground. For this experiment the reactor was encased in a shield that modified the radiation leakage spectrum to more closely resemble that of a weapon's spectrum.

During the experiment, fast-neutron and gamma-ray dose rate and thermal-neutron flux measurements were made at several positions inside the bunkers and the tunnel, both with and without concrete slab shields in position over the open faces. The immediate objectives of the experiment were to study the attenuation of radiations by various thicknesses of the concrete shields (4 to 20 inches), to investigate the buildup of radiation intensities within the cavities by the scattering or capture of radiation in the walls, and to study the transmission of radiation down a tunnel with two right-angle bends. The long-range goal was to develop simplified calculational methods for estimating the effectiveness of structures of this type in shielding against weapons radiation.

In analyzing the bunker measurements the premise was made that the radiation entering the openings could be predicted in terms of the external radiation environment, provided that the radiation environment was specified in sufficient detail. Thus it was necessary to develop a detailed set of data on the spatial and angular distributions of the radiations incident on the openings. These included not only those radiations that traveled directly from the reactor to the bunker openings, but also those radiations that were scattered by

air toward the openings and those radiations that were born as a result of neutron interactions with air (air-capture gamma rays).

The analysis performed thus far has been for the unshielded bunkers only (no covers over the openings). The steps consisted in calculating the portions of the incident radiations that could reach certain positions within the structure without interacting with it and then separately calculating the dose contributions at the same positions that were due to interactions in the concrete wall (for example, neutrons or gamma rays scattered from the walls or gamma rays emitted when neutrons were captured in the walls). The sums of the various contributions were compared with the measured dose rates for the same points. With few exceptions the calculated dose rates agreed with the measured dose rates within 25 percent; hence, it seems likely that the techniques used in the analysis can be used to predict dose rates in similar underground structures due to a nuclear weapon detonation, provided that the radiation incident on the structures is known in suitable detail.

A significant result of the tunnel measurements was that the dominant radiation component in the tunnel was the gamma-ray dose rate resulting from the capture of low-energy neutrons in the walls of the tunnel. This is of particular interest, since civil defense structures may be penetrated by ducts of similar geometry. Thus it is important that a method be available for calculating capture gamma-ray doses in such configurations. Any such method must include the determination of the spatial distribution of the low-energy neutrons, which, in turn, involves calculations of the slowing down of the higher-energy neutrons and the transport of the low-energy neutrons themselves. A method was developed for calculating the low-energy neutron distribution within three-legged rectangular ducts which is based on an albedo model and a Monte Carlo technique. When an albedo similar to that to be expected for a pure thermal-neutron source was used, the results agreed closely with the TSF measurements along the tunnel center line.

In calculating the capture gamma-ray dose rate in the tunnel it was assumed that the thermal-neutron flux incident upon the tunnel wall was simply related to the measured flux at the corresponding position on the tunnel center line. The resulting capture gamma-ray dose rates were considerably lower than the measured dose rates; therefore it is presently assumed that a more accurate calculational model must be developed.

RADIATION SHIELDING INFORMATION CENTER

The Radiation Shielding Information Center (RSIC) has been established at the Laboratory for collecting, evaluating, and disseminating information on radiation shielding. During 1963, only reactor shielding was considered, but in future years the coverage will be expanded to include shielding against weapons radiation and the shielding of space vehicle payloads from the natural radiations in space.

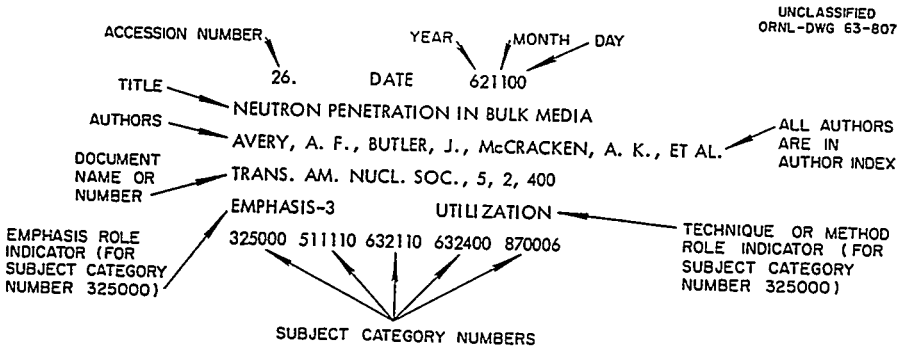

Example of an entry in the RSIC bibliography by subject category.

The activities of the center thus far have included the development of an information retrieval system for storing bibliographic and indexing information on magnetic tapes and for producing literature searches and shielding bibliographies. In preparing information for the system, each literature specimen is identified by an accession number and is indexed under as many subject categories as are applicable. The subjects cover 9 main shielding categories, which at present are divided into a total of 118 subcategories.

For each subject category number assigned to a literature specimen, an emphasis role indicator number is also assigned which gives a semiquantitative evaluation of the emphasis or relevance placed upon the category by the specimen. When applicable, another role indicator is assigned which indicates whether the specimen describes or merely uses a given technique, theory, or device.

The shielding bibliographies produced by the information retrieval system differ from the usual bibliography by being in readily searchable form. The bibliographies list the documents covered by the 118 subject categories and include an author index. Since the subject matter of most documents rarely falls into only one category, multiple categorical listing is used to ensure complete coverage. The author index gives all relevant document accession numbers and subject category numbers for each author's publications.

The Center has also organized a computer code section to accumulate experience with various computer codes; to examine the codes as to operability, ease of dissemination, and production of the desired results; and to intercompare codes. Code packages are prepared for distribution.

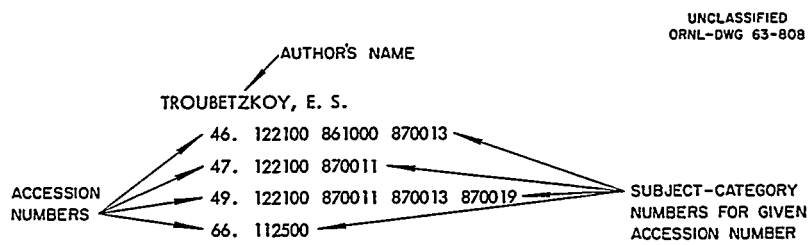

Example of an entry in the author index of the RSIC bibliography.

Basic Reactor Physics

The aim of the basic reactor physics program is to generate information that will facilitate the design and use of many types of reactors. The work performed during 1963 can be broadly classified as that which added to the knowledge of cross sections for reactions of neutrons with various nuclei and that which yielded information on the behavior of neutrons in critical uranium assemblies. Included in the former category was a series of experiments designed to measure neutron capture cross sections and fission cross sections for the three principal reactor fuels and calculational and experimental studies of the scattering of neutrons with various nuclei. The latter category included several critical experiments – and corresponding calculations – with assemblies of uranium metal enriched to 93.2 percent in uranium-235. These studies are summarized in the following subsections.

NEUTRON CROSS-SECTION STUDIES

It has long been recognized that until the cross sections for the reactions of neutrons with the various nuclei of interest are known over a wide energy range, the accuracy desired in reactor calculations will not be achieved. Since there are practically an infinite number of cross sections, it is obviously impractical to measure them, and we have turned therefore to the development of calculational methods for rapidly computing cross-section data. The methods must be proved experimentally, however, and the scarcity of available data necessitates that experiments be an integral part of the cross-section studies. But neutron reaction experiments are difficult to perform, much more so than charged-particle reaction experiments, and since the latter can often be interpreted so that they apply to neutron reactions as well, many experiments in the current studies use protons and deuterons as the incident particles. To summarize, then, the reactor cross-section program at the Laboratory consists in developing methods with which both neutron and charged-particle cross sections can be calculated and in performing a sufficient number of experiments to verify the methods.

The development of a nonlocal optical model that can be used to predict total neutron cross sections and differential neutron elastic-scattering cross sections in the 4- to 50-Mev energy range for all the elements heavier than magnesium was described previously (ORNL-3350, p. 91). The validity of the method was established by the agreement of the calculated total cross sections, within 5 percent, and of the calculated differential cross sections, within 15 percent, with the experimental data. The effort has since been concentrated on increasing the speed of the calculation and thereby reducing the cost of computing the cross sections. A very good approximation to the nonlocal potential was found which decreased the amount of computer time required by a factor of 20. Also, the insight that the approximation provides enables some of the approximations in existing nuclear reaction theories to be removed.

This work was extended with the development of a local optical model for calculations of 9- to 22-Mev protons and 7- to 27-Mev deuterons, also for elements heavier than magnesium. Some specific details of the model were studied in proton elastic-scattering experiments with nuclei between titanium-48 and germanium-76. Again the differential cross sections agreed with experimental data within 15 percent, but the quantity of data available on total cross sections is insufficient to validate the method.

In developing methods for calculating nonelastic scattering of particles with nuclei, we are taking two approaches, one using the distorted-wave Born approximation (DWBA) and the other using a coupled-channel principle. The current endeavor in this area is aimed at performing experiments that are specifically designed to test the hypotheses used in the calculations. Thus far, these experiments have included studies of proton inelastic scattering for nuclei between titanium-48 and germanium-76 and studies of proton stripping from nickel-60 and zirconium-90 by deuteron bombardment. Insofar as proton inelastic scattering is concerned, coupled-channel calculations of the absolute differential cross sections for the first 2^+ excited states of even-even nuclei agree with experimental data within 20 percent. With regard to the (d,p) reactions, it seems apparent that when the DWBA model is used in its most general form, that is, with as few approximations as possible, the differential cross sections can be reproduced fairly well.

The experiments in this program are performed at the various Laboratory accelerators.

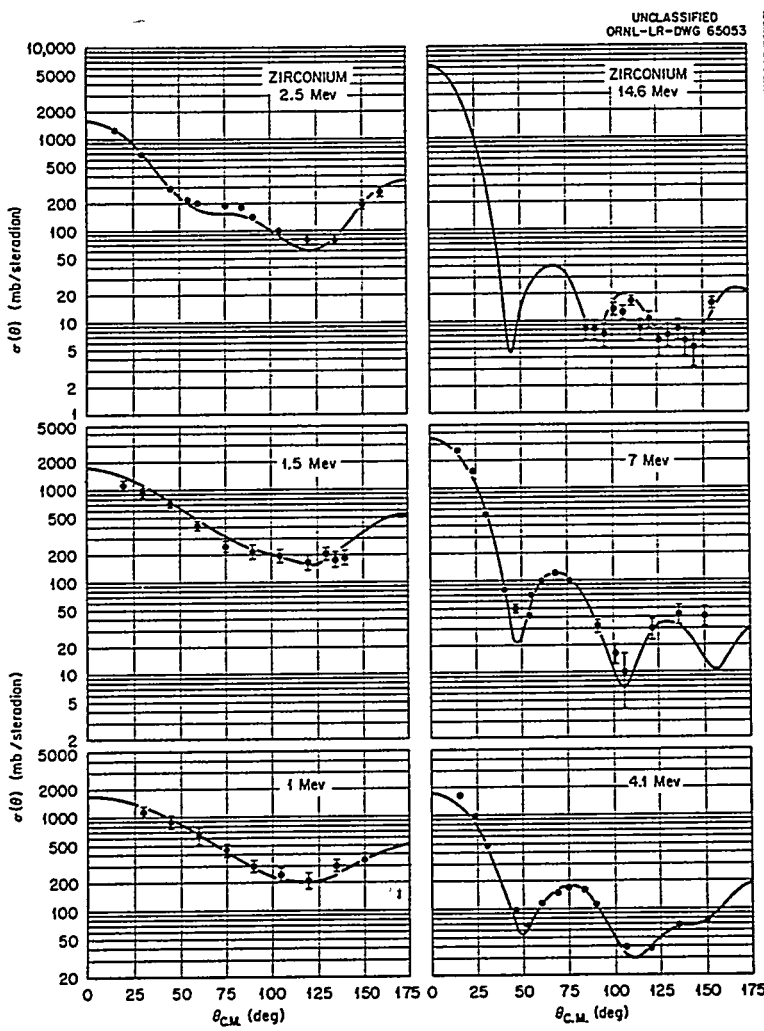

Comparison of predictions of differential elastic cross sections by the nonlocal optical model with experimental values for 1- to 14.6-Mev neutrons incident on zirconium. The solid lines represent calculations; the data are from BNL-400, *Angular Distributions in Neutron-Induced Reactions*, by M. D. Goldberg, V. N. May, and J. R. Stehn (1962).

MEASUREMENT OF α AS A FUNCTION OF ENERGY

The design of breeder reactors – those which produce more fuel than they burn – continues to be hampered by the lack of accurate values of the fission parameter α, the ratio of the neutron capture cross section to the fission cross section, for the three principal reactor fuels uranium-233, uranium-235, and plutonium-239. The series of α experiments being performed at the Laboratory, which are designed to yield values over a wide neutron energy range (ORNL-3350, p. 90), have progressed to the extent that results can be quoted for uranium-235 in the energy ranges from 4 ev to 2 kev and from 10 to 700 kev. The technique used for the lower range consisted in directing pulsed neutrons at a multiplate uranium-235 fission chamber placed in the center of a large liquid scintillator. Gamma rays from both capture events and fission events in the uranium-235 of the fission chamber were detected with high efficiency by the scintillator, while fission alone was detected by the fission chamber. The value of α was then the ratio of the scintillator counts in anticoincidence with the fission chamber counts to those in coincidence with the fission chamber counts. The incident neutrons were produced in a target bombarded by electron bursts from the Rensselaer Polytechnic Institute linear accelerator, and their energies were measured by time-of-flight methods.

The same technique was used for measurements at 30 and 64 kev, except that the source neutrons were produced by protons from the ORNL Van de Graaff accelerator incident on lithium-7 and tritium targets respectively. Other measurements at the Van de Graaff in the 10- to 700-kev range also used the $^{7}Li(p,n)$ reaction, but the fission chamber was replaced with a uranium-235 sample, and the liquid scintillator was loaded with gadolinium. In this case a capture event in the sample was characterized by a scintillator pulse due to a single fast cascade of gamma rays in coincidence with the beam pulse, while a fission event was characterized by a pulse due to prompt fission gamma rays followed by additional pulses a few microseconds later due to gamma rays produced by the capture of thermalized fission neutrons in the gadolinium-loaded solution.

The values of α obtained for energies above 10 kev can be approximately described by a linear decrease from 0.374 at 10 kev to 0.177 at 210 kev followed by a less rapid linear decrease to 0.095 at 700 kev. For the energy range from 4 ev to 2

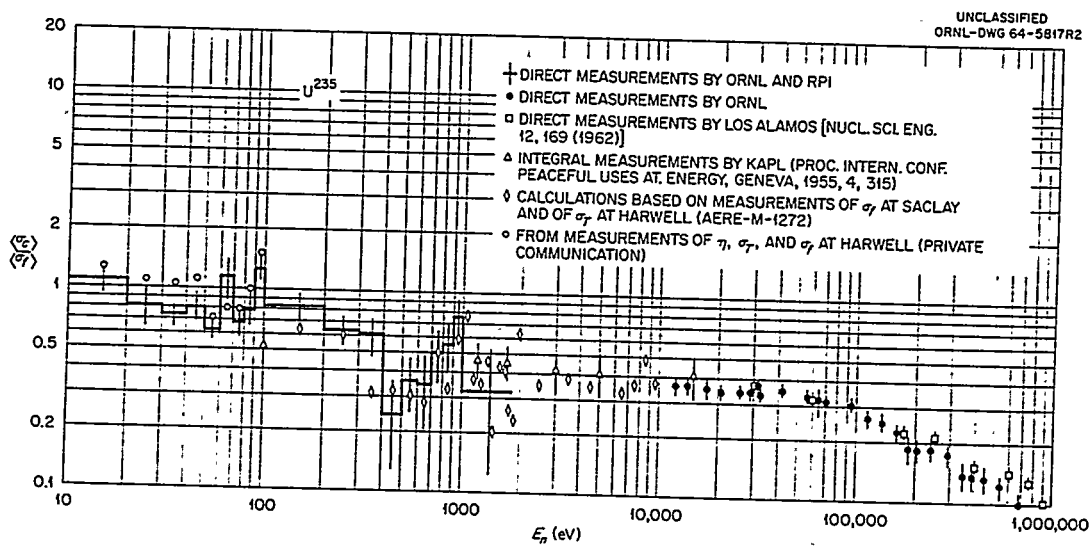

Ratio of the average value of the ^{235}U neutron-capture cross section to the average value of the fission cross section as a function of neutron energy. The vertical lines are error bars for the energy intervals in which they appear. Similar ratios (called α values) are needed over a wide energy range for the three principal reactor fuels, ^{235}U, ^{233}U, and ^{239}Pu, in order to determine the feasibility of breeder reactors.

kev, large fluctuations in the data were observed; the value of α for many energies was greater than 1.

The α experiments will be continued at the Rensselaer linear accelerator by a method which will also utilize a pulsed beam of neutrons striking a sample positioned at the center of a large liquid scintillator, but fission and capture events will be distinguished by the difference in the pulse-height distributions of the fission gamma rays and capture gamma rays. The feasibility of the method was demonstrated by a preliminary run at General Atomic for uranium-235 in the energy range from 10 to 20 ev. In preparation for these measurements, which hopefully will cover all three of the fissionable isotopes in the energy range from thermal to 20 kev, a time-of-flight (or multidimensional) analyzer is being assembled that uses a general-purpose digital computer as an integral part of its system. The analyzer will not only increase the accuracy of the measurements but will also reduce the total LINAC time required.

PROMPT-NEUTRON LIFETIMES IN CRITICAL ASSEMBLIES OF 93.2 PERCENT URANIUM-235-ENRICHED URANIUM METAL IN CYLINDRICAL GEOMETRY

Since the speed with which a reactor responds to a change in its reactivity varies inversely with the length of time that fission neutrons "live" in the

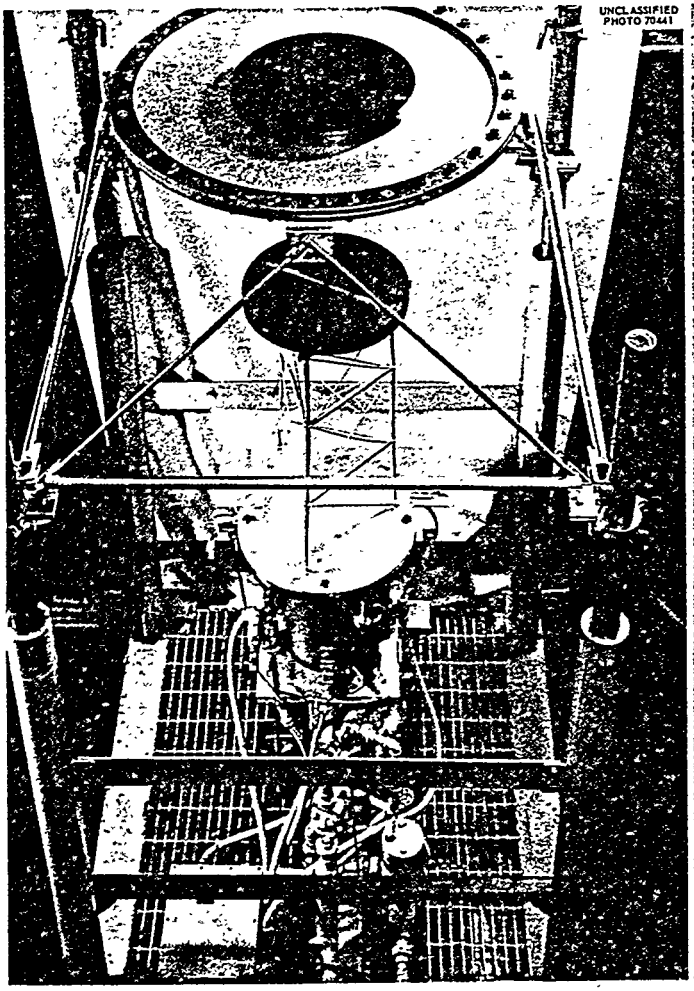

Typical 93.2 percent ^{235}U-enriched uranium metal assembly in cylindrical geometry. The upper half of the assembly is supported on a thin stainless steel diaphragm, and the lower half is on a low-mass aluminum stand. The cylinder is formed when the lower section is raised to meet the upper section.

reactor, a knowledge of the prompt-neutron lifetime in various types of assemblies adds greatly to the field of reactor technology. During 1963, prompt-neutron lifetimes were determined for a number of unreflected and unmoderated critical assemblies of uranium metal (93.2 percent uranium-235) in cylindrical geometry from measurements of prompt-neutron decay constants in the assemblies. The assemblies consisted of solid cylinders ranging in diameter from 7 to 15 inches and of cylindrical annuli having outside diameters as large as 15 inches. The upper section of each assembly was built on a thin stainless steel diaphragm held in position by an aluminum clamping ring, and the lower section was supported on a low-mass aluminum stand. The assembly was completed when the lower section was raised to meet the upper section. The prompt-neutron decay constants were measured at delayed critical by the Rossi α technique, in which the time behavior of prompt neutrons associated with a common ancestor is observed.

Values of the effective delayed-neutron fraction, β_{eff}, which are required to obtain the prompt-neutron lifetimes from the measured decay constants, were computed from transport-theory calculations using the S_n method of solution (see LA-2595) in the S_8 approximation and the six-group uranium-235 and uranium-238 cross sections of Hansen and Roach (LAMS-2543). The adequacy of the calculational method was demonstrated by the fact that the calculated and measured multiplication constants differed at most by ½ percent.

The lifetime determined for the solid cylinders is 6.25 ± 0.04 nanoseconds, which, within the limits of experimental errors, is independent, in the range studied, of the dimensions of the cylinders and agrees with the lifetime of 6.2 ± 0.1 nanoseconds obtained from earlier measurements at Los Alamos Scientific Laboratory for a uranium sphere (Godiva I). The lifetime for the cylindrical annuli varied from 7.0 to 8.0 nanoseconds; the increase over that for the solid cylinders is due to the time required for neutrons to cross the center void.

Similar experiments have been performed with pairs of interacting solid cylinders whose diameters were 7, 11, and 15 inches and whose flat faces were separated by as much as 10 inches. Although S_n calculations for these assemblies yielded multiplication constants that were within 1 percent of the experimental values, some difficulties were encountered in interpreting the change in the neutron lifetimes caused by the separation of the two units. The investigation of this effect is continuing with Monte Carlo calculations.

APPLICATION OF MONTE CARLO CALCULATIONAL TECHNIQUES TO THE STUDY OF FAST CRITICAL ASSEMBLIES

The O5R code, a general-purpose Monte Carlo reactor code developed at the Laboratory, has been widely applied to many neutron physics problems but, because of high computing costs and the lack of adequate cross-section data, it has rarely been applied to criticality studies. Still, this code is the only one existing which has a geometry routine that can be applied to almost any situation; for complex experimental assemblies, it represents the only means for performing corresponding calculations. It seems reasonable, therefore, that this method should be developed as a routine calculational tool for predicting the properties of critical assemblies, especially since more detailed microscopic cross-section data are now becoming available and the computing cost is decreasing. As a first step in this direction, O5R calculations were performed for several simple unmoderated and unreflected 93.2 percent uranium-235-enriched uranium assemblies, each of which had been made critical experimentally.

Where possible, cross-section values from BNL-325 were applied, and angular distributions from BNL-400 were used to obtain Legendre expansion coefficients which are utilized in O5R calculations to treat anisotropic scattering of neutrons. The calculations yielded multiplication constants that are in agreement with each other but are somewhat higher than the measured values. The sensitivity of the multiplication constant to errors in the cross sections is being examined in detail.

Reactor Fuels and Materials

RADIATION EFFECTS IN STRUCTURAL MATERIALS

In-Reactor Internal Friction Measurements of Precipitation in Alloys

Since precipitation in alloys is a phenomenon of fundamental and practical importance, it is of interest to determine how precipitation reactions are affected by radiation. This study has been aided by the development of an apparatus which measures low frequency internal friction during exposure in the reactor. The internal friction is a measure of the precipitation of interstitial solute atoms in body-centered cubic metals.

The apparatus uses a 0.005-inch-thick sample, 3/16 inch wide and 1.5 inches long, that is caused to vibrate in flexure by a voltage applied to a driver electrode. As the specimen vibrates, a vane attached to its end passes between capacitance plates which are connected remotely to a capacitance bridge and other electronic equipment. A signal proportional to the amplitude of motion is displayed on an oscilloscope screen and the internal friction is measured by the rate of decay of the signal after the driving voltage is removed.

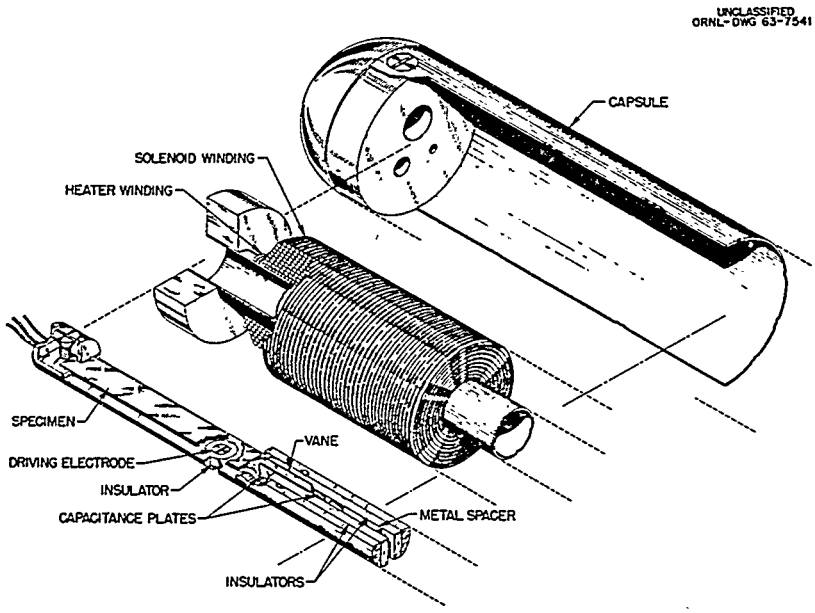

Flexure pendulum for the measurement of low-frequency internal friction during reactor irradiation. The specimen foil is set into flexural vibration by energizing the driver electrode. As the specimen vibrates, a vane attached to its end passes through capacitance plates. A signal from the capacitance plates, proportional to the deflection of the sample, is amplified remotely and displayed on an oscilloscope screen. The internal friction is measured by the rate of decay of the signal after the driving voltage is removed.

The in-reactor internal friction apparatus is being used to study the effect of irradiation on the precipitation of nitrogen in alpha iron. The distribution of nitrogen in iron and steel has an important bearing on mechanical properties. In particular, the creep strength of steels is thought to be related to the presence of nitrogen in solid solution, and the poorer creep properties of aluminum-killed steels may be due to the removal of nitrogen from solid solution by the formation of aluminum nitride.

Evidence has been obtained using the in-reactor internal friction apparatus that irradiation has the effect of accelerating the removal of nitrogen. Irradiated and unirradiated samples leave a fraction of nitrogen in solid solution during aging at 65°C after solution annealing and quenching. The nitrogen is removed considerably more rapidly for the samples irradiated below −120°C than for unirradiated samples. Two explanations of the irradiation-enhanced loss of nitrogen are being considered. The radiation may produce nucleation centers about which precipitation products precipitate. Another possibility is the trapping of nitrogen at vacancies produced by the irradiation.

The study of precipitation of nitrogen in iron is part of a general program in the Solid State Division to determine the effect of radiation on diffusion-controlled processes in metals and alloys.

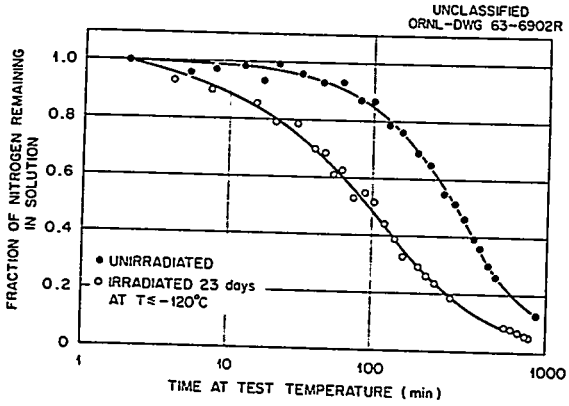

The fraction of nitrogen remaining in solid solution in alpha iron during aging at 65°C for an unirradiated sample and a sample irradiated below −120°C in the ORNL Graphite Reactor. The amount of nitrogen remaining in solid solution is determined from the height of the internal-friction peak.

Radiation-Enhanced Diffusion in Copper-Base Alloys

Ordering in alloys is a prime example of a diffusion-controlled phenomenon. Although the radiation-enhancement of ordering has been studied fairly extensively in the copper-aluminum system, no observations were previously made of the effect of prior cold-working. This factor has now been investigated. The radiation-enhanced reaction is retarded by prior cold-working; this is interpreted as an indication that dislocations produced by the cold-working serve as sinks for the radiation-produced defects and therefore reduce their effectiveness in stimulating the ordering.

The change in resistivity of copper–15 atomic percent aluminum upon irradiation at 100°C in the ORNL Graphite Reactor as a function of the percent reduction in area of prior cold-working. The samples were given prior cold-working treatments corresponding to 0 to 54 percent reduction in area. The decrease in resistivity is a measure of short-range ordering during the irradiation.

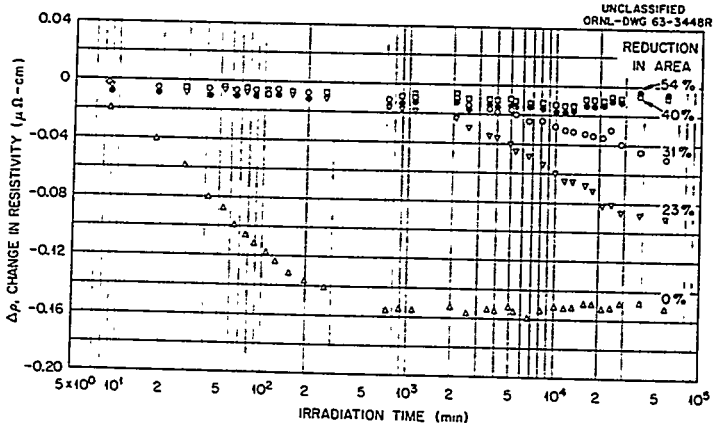

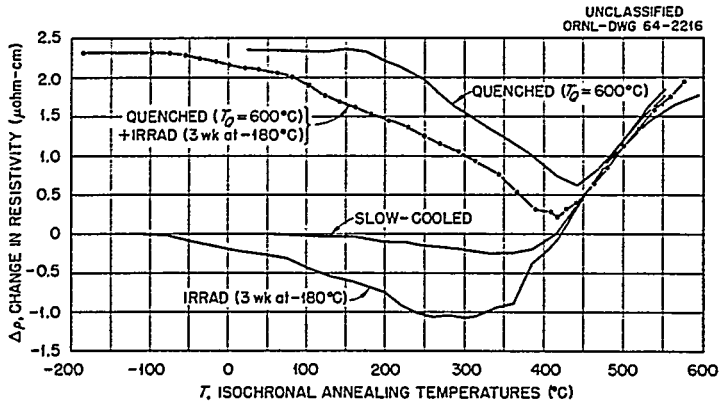

The change in resistivity of copper–62 atomic percent nickel as a function of isochronal annealing (holding for a fixed time at increasing temperatures) following various quenching and irradiation treatments. The decrease in resistivity is a measure of the segregation into copper-rich and nickel-rich zones. All resistivity measurements were made at liquid-nitrogen temperature.

Another type of diffusion-controlled reaction in alloys is the segregation process, as is exemplified by the copper-nickel system, where segregation is accompanied by a decrease in resistivity. A study is underway of the effect of quenching and irradiation on segregation in copper-nickel alloys. The differences in the annealing spectra for quenched and for irradiated samples suggest that a different defect is responsible for the enhancement of segregation in the two cases.

Tensile Properties of Irradiated Nickel

As part of an investigation in the Solid State Division of the effect of radiation on the mechanical properties of metals and alloys, a determination was made of the effect of high-flux reactor irradiations on the tensile properties of type 330 nickel. Sheet tensile samples, 1/16 inch thick, were prepared from base-plate, weld, and heat-affected zone material from two heats of starting stock. The irradiation facility was a partial fuel element in the Oak Ridge Research Reactor. The neutron flux was determined by measuring the activity of the induced Co^{58}, corrected for burn-up, in nickel wires included in the irradiation capsule. A value of about 10^{14} neutrons cm^{-2} sec^{-1} ($E >$ 1.0 million electron volts) was obtained assuming a fission spectrum.

The tensile tests were conducted remotely at room temperature in hot cells. The exposure to about 10^{21} neutrons/cm^2 ($E >$ 1.0 million electron volts) produced an increase in the yield

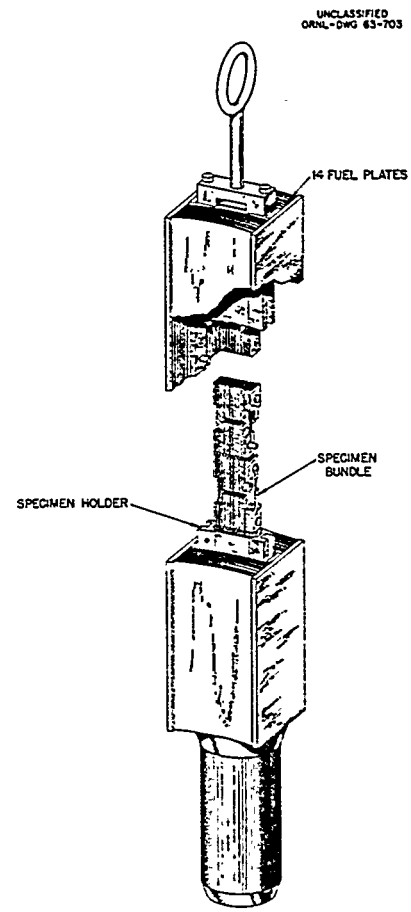

Partial fuel-element irradiation facility. A sample irradiation chamber is provided by an ORR fuel element in which five fuel plates are omitted. The neutron flux inside the specimen chamber was determined to be about 10^{14} neutrons cm^{-2} sec^{-1} with energies above 1 Mev.

Typical load-elongation and true stress–true strain curves for unirradiated and irradiated type 330 nickel. Smooth sheet tensile samples of base-plate material were used. The temperature of irradiation was below 100°C, and the integrated neutron flux was about 10^{21} neutrons/cm^2 ($E > 1$ Mev).

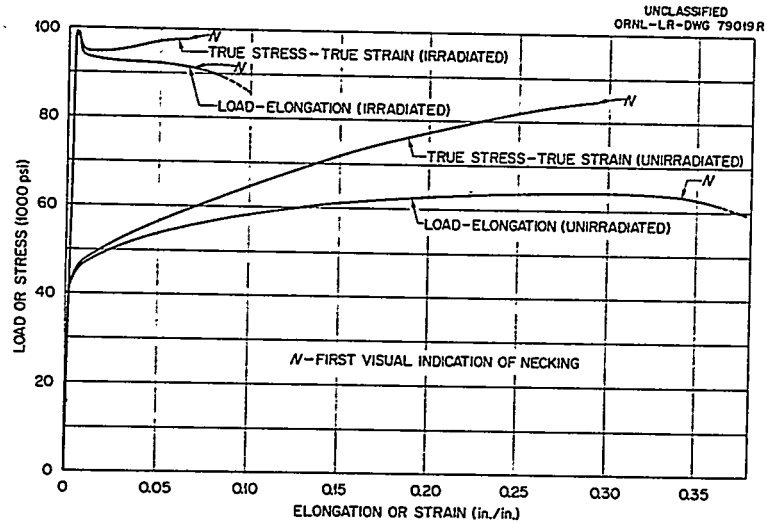

stress of more than a factor of two, a substantial decrease in the uniform and total elongations, and a reduction in the rate of work-hardening. However, the fractures appeared to be of the shear type even in the irradiated samples, with no tendency toward cleavage failures being noted. Also, in notched samples, there was no indication of an increase in notch sensitivity upon irradiation. These observations have a bearing on the selection of materials for use as structural members in radiation environments.

NONDESTRUCTIVE TEST DEVELOPMENT

Low-Voltage Microradiography

The Nondestructive Testing Group of the Metals and Ceramics Division has used very-low-voltage x rays, a helium atmosphere, and photographic emulsion detectors of extremely fine grain to develop advanced techniques for microradiography. In small or thin specimens, they can observe details and make measurements that are accurate to within less than 0.00004 inch. This capability has been particularly useful in the examination of uranium carbide particles, 0.010 inch in diameter, coated with pyrolytic graphite. Further modifications of this technique have enabled the microradiographic examination of samples of graphite or fuel particles, from reactor experiments, having

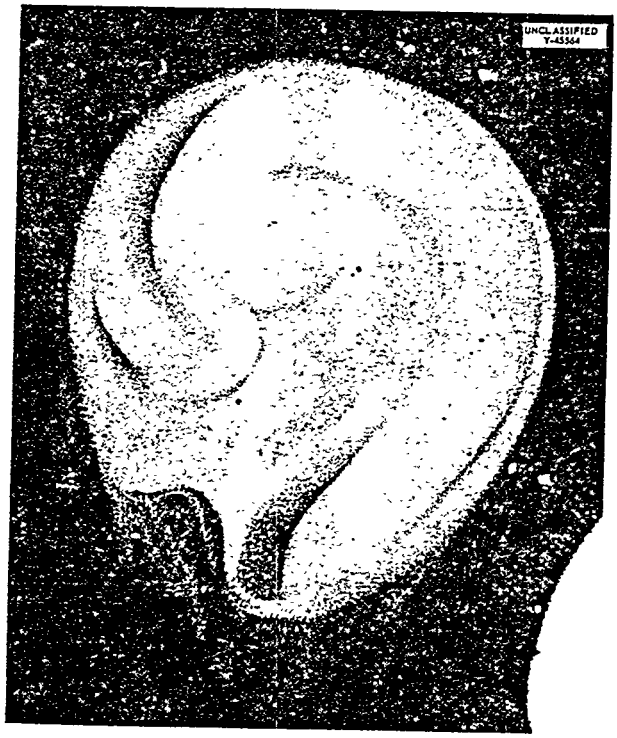

Microradiograph of a tomato seed (approximately 75X, reduced 51%). This photograph illustrates the detail and magnification achievable with low-voltage radiography. Note the excellent detail displayed in the cilia around the seed. This method is particularly useful for examining the coated fuel particles being developed for advanced gas-cooled reactors.

measured beta radioactivity as high as 3000 roentgens per hour at contact. These latter studies have opened the door to an area heretofore considered impossible – radiography in a radioactive background.

Ultrasonic Detection of Nonbond

The Nondestructive Testing Group of the Metals and Ceramics Division has expended considerable effort toward the development of techniques and equipment for the detection and evaluation of nonbond (lack of bonding) in clad structures. The studies have included through-transmission, reflection, ringing, resonance, and secondary-vibration techniques with both one and two transducers. In an important recent advance, this group has developed techniques and devices for the inspection of braze joints between heat exchanger tubes and headers, a previously impossible inspection. A probe bearing two crystals is inserted in the tube. One crystal transmits ultrasonic energy at the proper angle and frequency into the inner surface of the tube. Both entry angle and ultrasonic frequency are very critical and depend on the thickness and elastic properties of the tube. If there is a nonbond, energy will be detected by the receiver crystal; otherwise no signal is observed. Through proper electronic circuitry the presence of a nonbond can be announced by an audible or visual alarm and the area of nonbond recorded on a map of the tubular joint. This method has been applied successfully to the inspection of the heat exchanger for the Molten-Salt Reactor Experiment.

Use of Eddy Currents for Nondestructive Testing

Components for nuclear reactors must be thoroughly inspected before use to ensure an extremely low probability of failure. Many of the

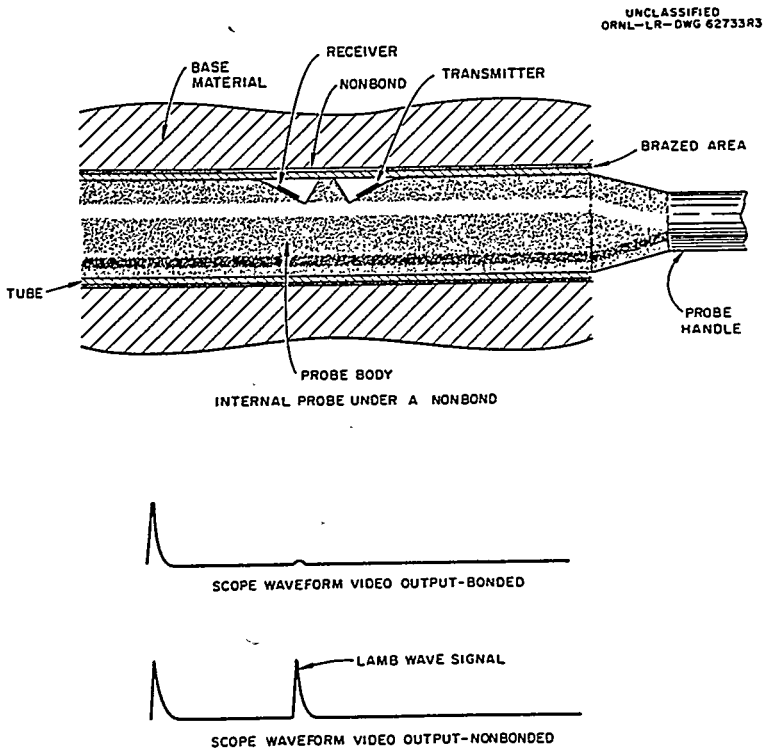

Ultrasonic technique for detection of nonbond in tube-to-header joint. One crystal of the probe transmits ultrasonic energy at a carefully chosen angle and frequency into the inner surface of the tube. If there is a nonbond, the second crystal detects energy. This technique has solved a previously impossible inspection problem.

Ultrasonic device for inspecting tube-to-header joints. This instrument, which has been used to examine the heat exchanger for the Molten-Salt Reactor Experiment, is shown on a mockup of the heat exchanger.

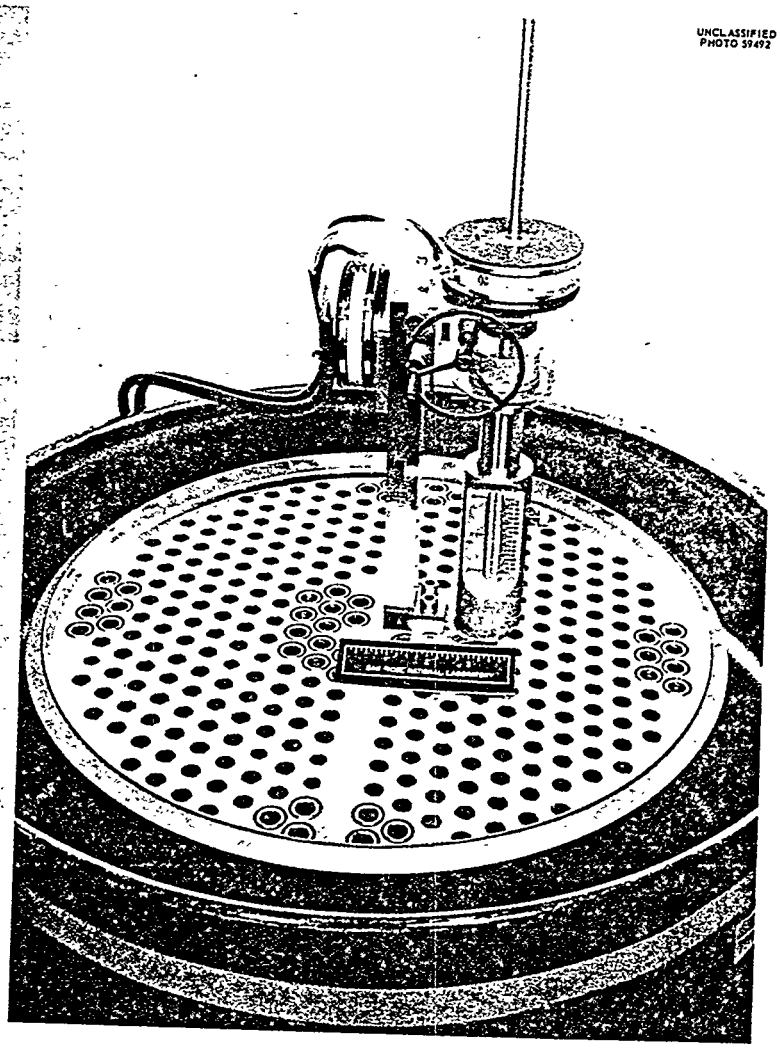

commonly used nondestructive inspection techniques utilize the eddy currents that are induced when a current-carrying coil is near an electrically conducting material. The Nondestructive Testing Group of the Metals and Ceramics Division has made two important developments that greatly increase the utility of eddy-current inspection. They have perfected a phase-sensitive measurement technique that eliminates many of the former limitations and devised a calculation method to enable systematic design of eddy-current coils for new applications.

All previous eddy-current equipment (used for measurement of dimensions, detection of discontinuities, etc.) has been very sensitive to variations in the spacing between coil and specimen. C. V. Dodd's new phase-sensitive equipment is not, but it is still as sensitive as older methods to the specimen variables. This new instrument will be of great value for rapid production inspection and remote (hot cell) operation, where consistent vibration-free positioning of the test coil cannot be maintained. To use the instrument for inspecting graphite spheres, Dodd invented a new scanning and manipulating device. As the spherical specimen is rotated about two axes, the probe scans the entire surface. This inspection would not be possible without the phase-sensitive instrument, since the specimen moves toward and away from the eddy-current probe due to its imperfect sphericity.

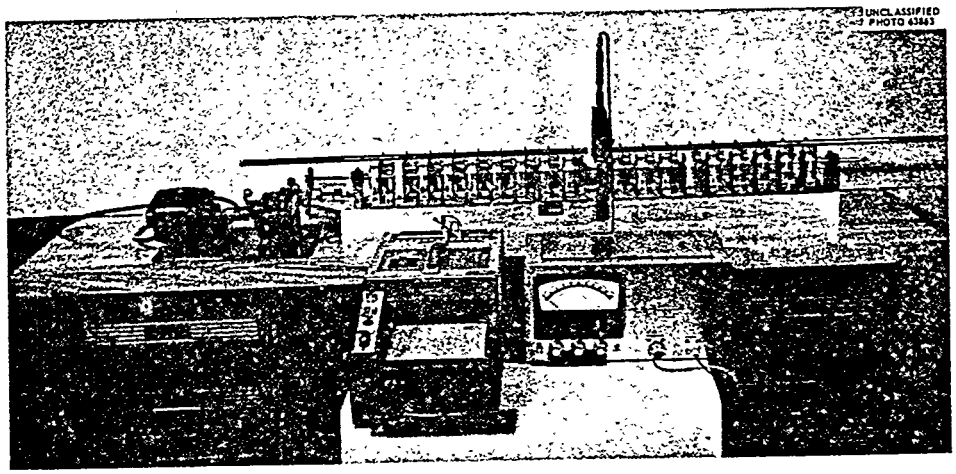

Phase-sensitive eddy-current apparatus being used to inspect tubing. The phase-sensitive technique overcomes the one basic difficulty of eddy-current inspection, sensitivity to variations in the coil-to-specimen spacing. The instrument as shown measures and detects flaws in tubing intended for reactor heat exchangers and fuel-element cladding. It is anticipated that the instrument will be capable of inspecting tapered tubing, which has been impossible.

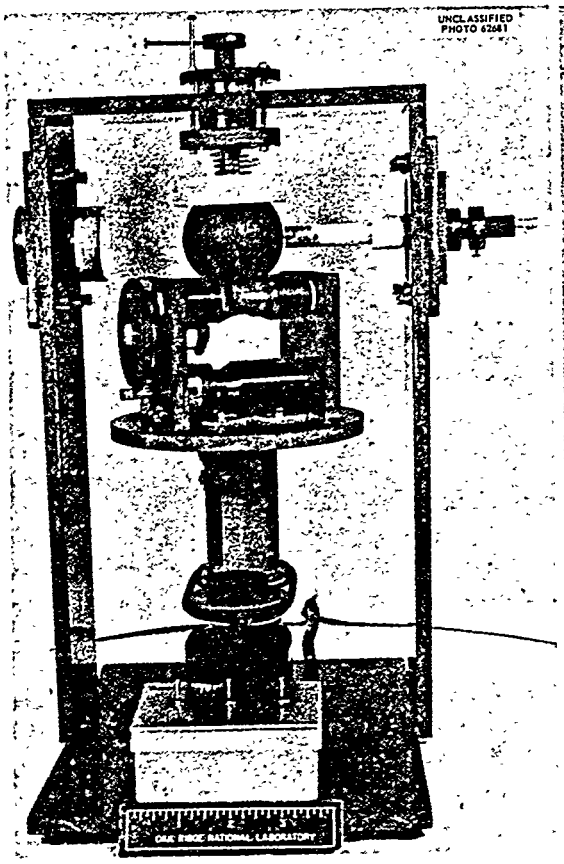

Scanning device for nondestructive testing of spheres. The detector head (in this case, an eddy-current probe) can seek flaws in the entire surface, enabled by rotation of the spherical specimen (in this case, a graphite-base fuel piece for the German AVR) about two axes. After replacement of the plastic rollers with ceramic, tests on heated specimens in this rig will be made to detect subsurface laminations.

Although eddy currents have been used for several years, most of the design and development work has been empirical. The new analytical approach uses a relaxation method to calculate the coil impedance as a function of the various parameters that affect it. The relaxation method consists of determining by appropriate differential equations the values of potential at every point throughout a lattice imposed on the coil-specimen system for a given set of parameters. Use of a high-speed computer enables the investigators to make the numerous necessary calculations rapidly and to begin a systematic study on the effect of the coil dimensions, electrical frequency, and specimen properties on the coil impedance. A further benefit that can be derived from this study is the calculation of the electromagnetic field strength as a function of the aforementioned properties. Thus this analysis will also enable accurate calculations of the vital parameters in many other areas in which the generation of an electromagnetic field is important – for example, induction heating.

Nondestructive Determination of Fuel Homogeneity

The Nondestructive Testing Group of the Metals and Ceramics Division has developed a working system for the nondestructive determination of fuel inhomogeneity in aluminum-base dispersion-core fuel plates. A tightly collimated beam of x rays is transmitted through the core section of the fuel plate. The emerging beam, which is attenuated according to fuel concentration, is detected by an NaI crystal coupled to a photomultiplier tube. The resultant electrical signal is directed to data-processing circuitry. The mechanical equipment allows complete scanning of the fuel plate and synchronous recording of the fuel concentration data. The apparatus is calibrated by standard shims of material having attenuation equivalent to that in the plate. These can be readily machined to any contour to match go-no-go conditions for any programmed fuel-loading variation. With this newly developed system, more rapid inspection for smaller inhomogeneities, with better accuracy and immediate

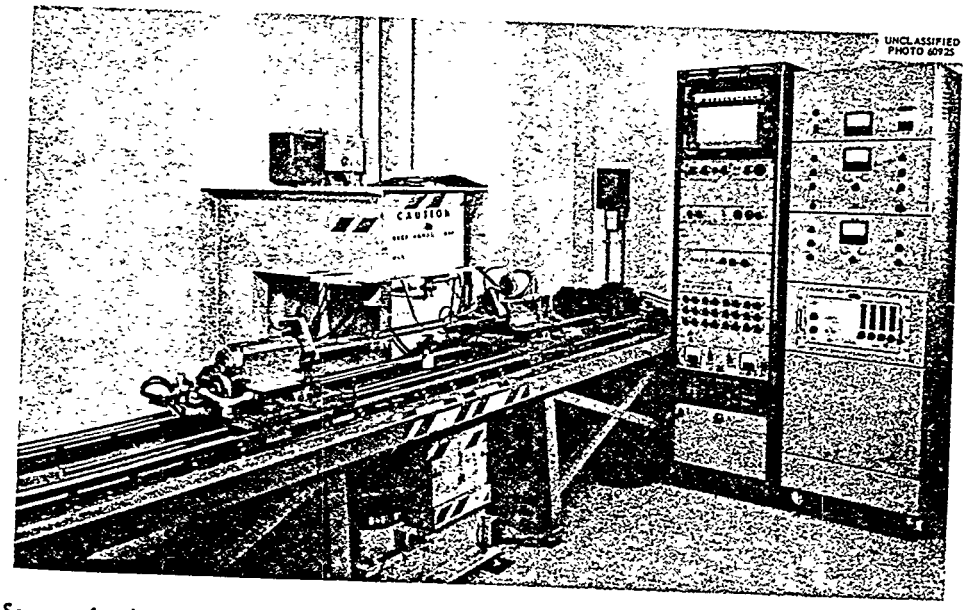

Scanner for detection and evaluation of fuel inhomogeneities. This instrument uses penetrating radiation to measure continuously the fuel density in rods or plates traversing the beam. To test thick specimens, a cobalt gamma source can be used instead of the x-ray unit shown.

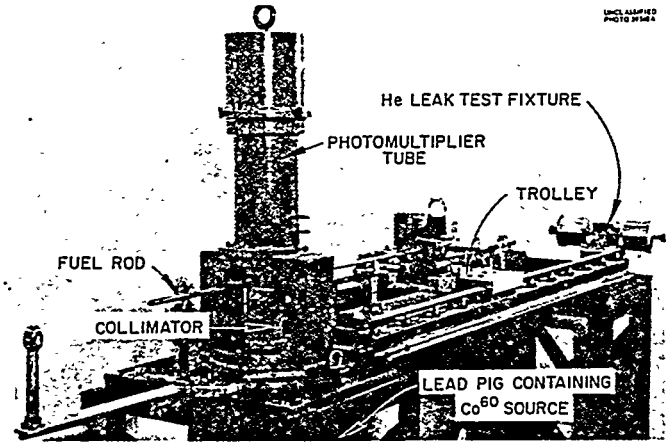

Gamma-ray scanner for detection of inhomogeneity in fuel rods. This instrument is used remotely in the Kilorod Facility to inspect fuel rods manufactured by vibratory compaction of $^{233}UO_2$-ThO_2 in Zircaloy-2 tubing.

interpretation, is possible. With further development this could become a powerful tool for assay of total fuel content. This method has been adapted by the Remote Fabrication Group to the inspection of fuel rods prepared by packing $^{233}UO_2$-ThO_2 powder into Zircaloy-2 tubes.

MECHANICAL PROPERTIES

Effect of Hydrogen on the High-Temperature Properties of Metals and Alloys

The strength, ductility, and other properties of metals in service are often affected by the gaseous part of their environment. This effect is the subject of a continuing program of research in the Metals and Ceramics Division. One phase of this program is a study of the high-temperature mechanical properties of several metals and alloys in hydrogen.

The creep-rupture properties of the materials in hydrogen and argon were compared. The materials studied were Inconel, nickel 200, nickel 270, electron-beam zone-refined nickel, high-purity copper, Armco iron, electrolytic iron, and type 304 stainless steel. All of the nickel and nickel-base materials and the copper exhibited inferior creep resistance in hydrogen; the iron and iro base materials were not affected by the chan in environment. The effect of hydrogen on pu nickel and copper was great; it decreased wi increasing impurity content. Three general c servations were made on the environmental effec

1. At the same stress and temperature, t minimum creep rate was greater in hydrogen th in argon.
2. The rupture life is less in hydrogen than argon at equivalent stress and temperature.
3. The rupture ductility is not affected.

Several additional experiments clarified t mechanism of the environmental effect. The included measurement of the permeation of hydr gen through Inconel, measurement of the surfac energy of nickel in argon and in hydrogen, co parison of the sintering rates of nickel powder argon, hydrogen, and vacuum, comparison of vo formation in diffusion couples of iron and nick annealed in argon and in hydrogen, comparison the diffusion of carbon in nickel in environmen of hydrogen and argon, measurement of the rate of diffusion of cobalt-60 in nickel in the sar gases, and transmission electron microscopy thin nickel creep specimens. Explanations base on surface and internal chemical reactions we discredited by one or more of these experiment. Direct observation by transmission electron micro copy revealed that in other gases dislocatior remained pinned, whereas when hydrogen w

present easy glide of dislocations occurred under low stresses. Since the phenomenon is reversible, the mechanism involves an interaction of hydrogen and the dislocations.

Radiation Effects in Fuel Cladding Materials

One of the most serious problems facing the technology of reactors using clad fuel elements concerns the ability of the fuel cladding to withstand the effects of neutron exposure. Since cladding failures sometimes occur at unacceptably low fuel exposures, the Mechanical Properties Group of the Metals and Ceramics Division is investigating the stability of cladding metals in long exposures to neutrons and seeking a cure for the failures. In their first experiments, austenitic stainless steels that are widely used in reactors are being irradiated in the Oak Ridge Research Reactor. Already a number of significant effects of irradiation temperature have been observed.

One of the major reasons for the large amount of scatter in the literature data on irradiation effects now appears to be a lack of awareness of the importance of specimen history, irradiation temperature, and test temperature. For example, stainless steels irradiated at the service temperature of pressurized-water reactors will show significant changes in rupture strength and ductility, depending on the temperature at which subsequent tests are performed. Likewise, stainless steels exposed to neutrons at temperatures from 600 to 850°C (the range of interest to superheat and gas-cooled reactors) exhibit very low ductility if tested at the irradiation temperature, but virtually no changes are observed if tests are conducted at room temperature.

Some encouragement that a solution to these problems exists is evolving from the discovery by this group that the degree of damage suffered by type 304 stainless steel (a common type, used as fuel cladding in the Experimental Gas-Cooled Reactor) can be altered by thermal pretreatment. Specimens annealed at a very high temperature before irradiation retained their ductility much

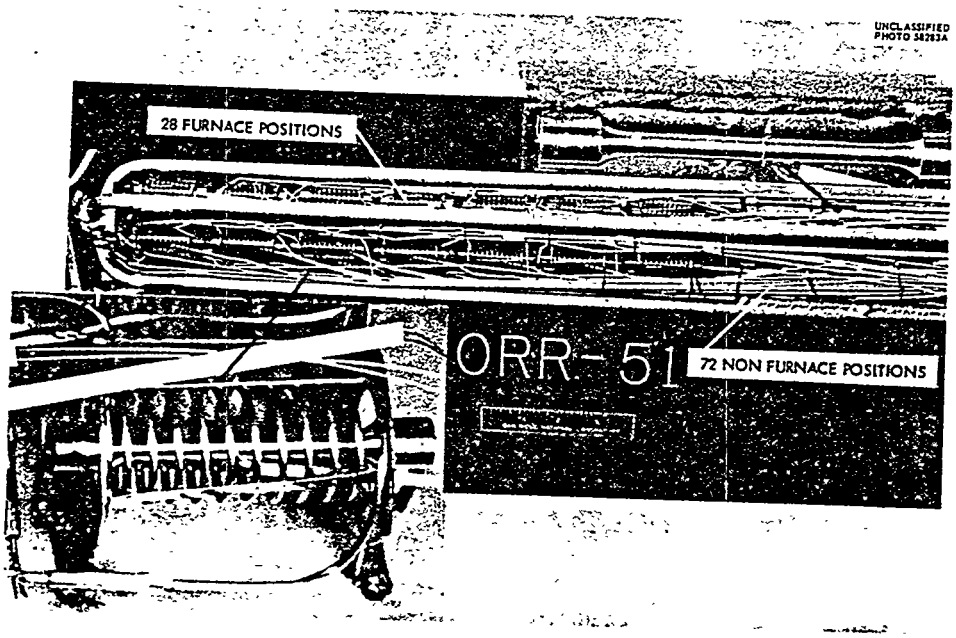

Rig used to irradiate tensile specimens (for mechanical strength determinations) in the Oak Ridge Research Reactor. Furnaces in this rig can heat 28 of the specimens at controlled temperatures above 550°C; the remaining 72 specimens are maintained at lower temperatures by prevailing radiation. The specimens are exposed to fast- and thermal-neutron fluxes of approximately 10^{14} neutrons cm^{-2} sec^{-1} each.

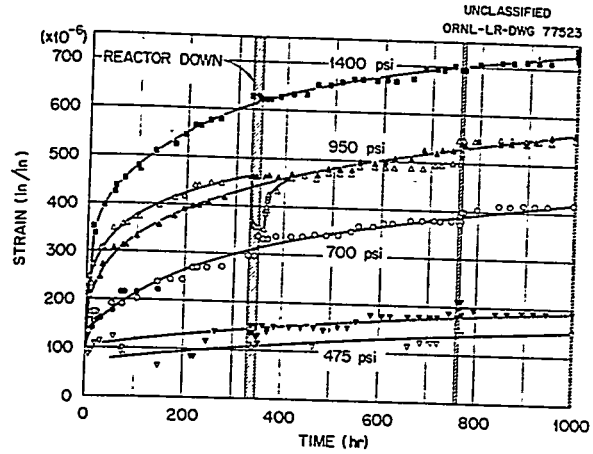

Typical examples of the creep of AGOT graphite under irradiation in the Oak Ridge Research Reactor. The figure shows the creep of duplicate specimens loaded to four stress levels and tested in a special rig.

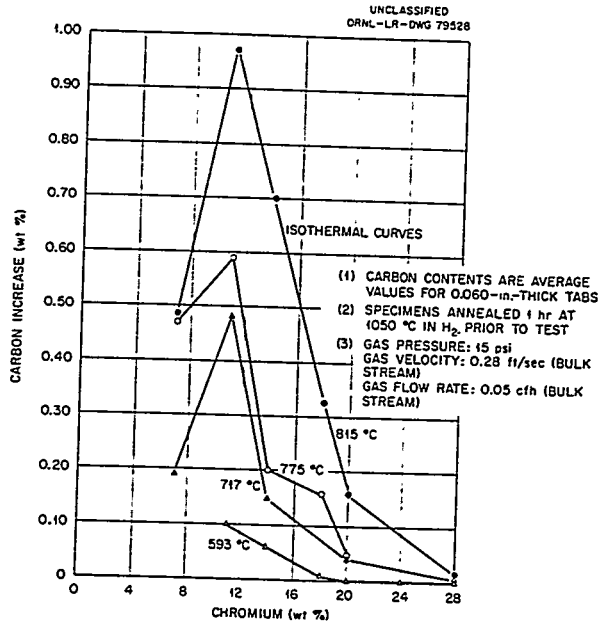

Influence of chromium content on the carburization of stainless steels containing 8 percent nickel, tested for 1000 hr at various temperatures in flowing CO_2. It can be seen that alloys containing less than 7 or more than 20 percent chromium do not absorb carbon under the conditions of these experiments.

Behavior of Stainless Steels in Carbon Dioxide

The coolant in a graphite-moderated gas-cooled reactor may be carbon dioxide or a gas containing CO_2 as an impurity. The Mechanical Properties Group of the Metals and Ceramics Division has observed that the common stainless steels absorb carbon in the presence of CO_2 at elevated temperatures, leading to a poor ductility in the steels under some conditions. Recently, this problem has been solved. The chromium content of these steels affects their absorption of carbon. Steels having chromium contents of from 7 to 20 percent absorbed carbon, whereas those having larger or smaller amounts of chromium did not. Thus we can now select stainless steels that are resistant to carburization in carbon dioxide gas.

ZIRCONIUM ALLOY DEVELOPMENT

During fabrication, anisotropy develops in the mechanical properties of metals with hexagonal crystal structure, such as zirconium, hafnium, titanium, magnesium, and beryllium, and many alloys of these metals. This anisotropy, which results from preferred orientation, has caused many difficulties in the fabrication of Zircaloy-2 and its use in reactor components. The Zirconium Alloy Development Group of the Metals and Ceramics Division has developed a very promising new approach to a solution of this problem. This approach analyzes the strain pattern present during plastic flow, using a knowledge of the deformation systems available in the material, the approximate flow strengths of each, and the preferred orientation existing at the point being considered. This analysis not only explains the strain behavior of the material, but it also indicates the texture that is desirable for a particular application and the manufacturing process necessary to produce it. This enables easier manufacture of high-quality mill products with improved yields, less resistance to the forming of structural shapes and parts, and an appreciable increase in the maximum allowable design stress (essentially doubled for pressure tubing in pressurized water reactors or fuel storage vessels in rockets). In some cases, all of these can be accomplished simultaneously;

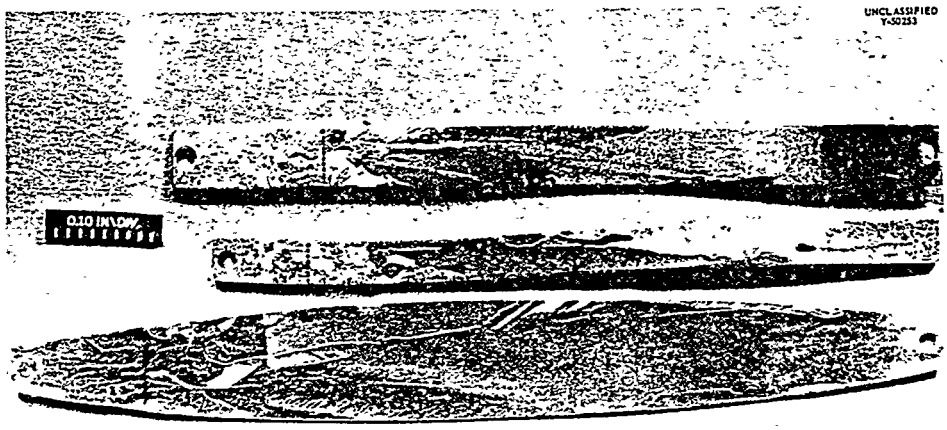

Single crystals of zirconium and Zircaloy-2 produced by an electron-beam technique in which a beta-phase zone is moved along the length of the specimen at about 1 centimeter per hour. Specimens were not polished or etched after crystal growth; brightness and texture variations are due to thermal etching, transformation relief, and orientation relative to the oblique light source used for photography. Undulations in the plane of the strips and twist about the longitudinal axis are present but do not show in this photograph. The superposed lines indicate the initial position of the electron beam. The beam was traversed from left to right as oriented above. Top: arc-melted iodide zirconium. Center: Zircaloy-2. Bottom: High-purity iodide zirconium.

in others, the best compromise can be more readily determined.

J. C. Wilson has developed several methods for growing single crystals of zirconium strip (up to 1 inch wide) and bar (up to 3/8 inch in diameter). Previous methods for preparing zirconium crystals required a heat-treating cycle of a month or more. Using electron-beam heating in vacuum, Wilson can grow comparable crystals in 10 to 100 hours. Contamination of the metal is reduced by the shorter growth time, and significant purification of crystals grown from the melt is indicated by a measured electrical resistivity ratio (the resistivity at 300°K divided by the resistivity at 4.2°K) of over 400; the highest ratio in the literature is now 240. Zirconium crystals have already proved valuable in studies of optical and hardness anisotropy, and new research on deformation and oxidation of zirconium is made possible by the availability of single crystals. Zircaloy–2 single crystals (up to 1/2 inch wide and 2 inches long) have been successfully produced for the first time. Significant differences in crystal growth rates and morphology were found in crystal-bar materials of similar purity. Wilson has successfully used floating-zone electron-beam zone refining to melt and purify zirconium directly from the crystal-bar stock (up to 1/2 inch in diameter) without intermediate melting or mechanical working. The purified material is being used to study grain growth and to serve as a reference material for other experiments on zirconium and its dilute alloys.

DIFFUSION IN HIGH-TEMPERATURE METALS

Many phenomena in solids are controlled by diffusion (atomic movement in the crystalline lattice). Some of these phenomena, which are important in nuclear and space systems, are high-temperature creep (deformation under continuous stress), recrystallization, annealing of radiation effects, and reactions with impurities. To improve understanding of these processes and to predict their

rates at temperatures beyond the range of measurements, T. S. Lundy and co-workers in the Metals and Ceramics Division are studying diffusion rates in metals that have the body-centered cubic crystal structure. Two very significant and unexpected findings have been made. The temperature dependence of diffusion is not as has been generally believed, and diffusion of solutes is much slower near the surface than in bulk material.

For years, the diffusion coefficient, like many measures of rate processes, has been assumed to obey the Arrhenius equation (that is, a graph of its logarithm against the reciprocal of the absolute temperature is a straight line, with a slope that measures the energy of activation of the process). T. S. Lundy, J. I. Federer, and J. F. Murdock have shown that this assumption is not valid over wide temperature ranges for either self-diffusion or impurity diffusion in beta-zirconium, beta-titanium, or vanadium. These results have reopened theoretical considerations of the mechanism of diffusion and the very fundamental question of the energy of activation of the process.

Development of an ultrafine sectioning technique for niobium and tantalum by R. E. Pawel and T. S. Lundy has enabled accurate measurement of near-surface diffusion in these metals. In this region, solutes diffuse at one-thousandth the rate they do in the bulk material. This discovery, although still unexplained, explains the discrepancies that exist between diffusion measurements made by different techniques. It obscures the validity of all diffusion measurements that depend on measurement of the decrease of radioactivity on the specimen surface.

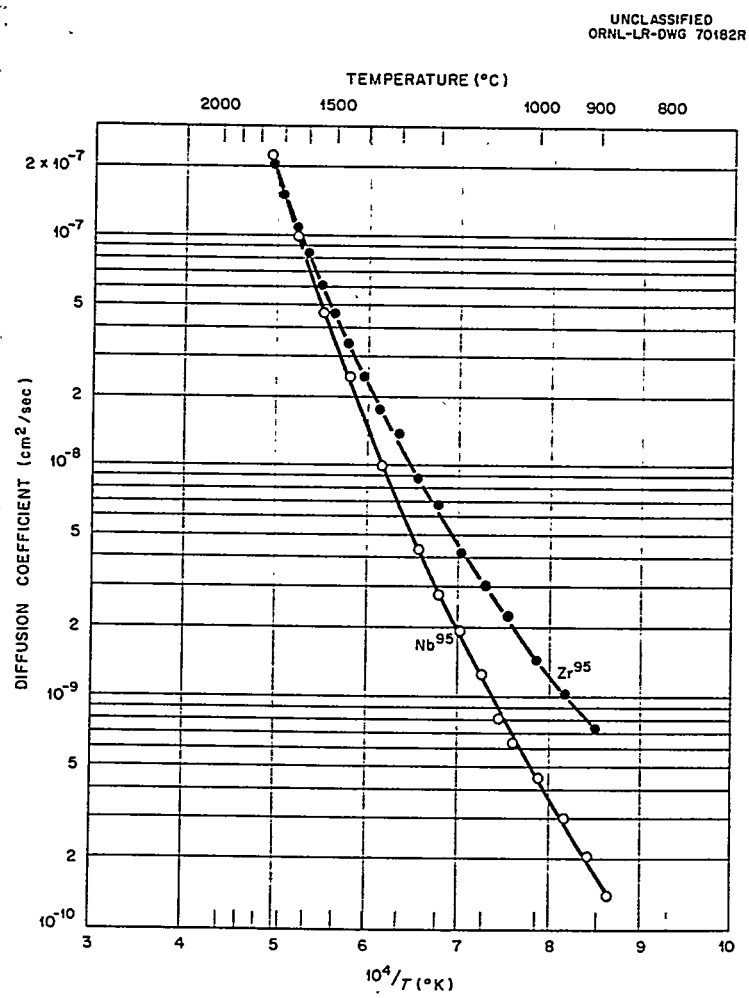

Temperature dependence of diffusion of zirconium and niobium in body-centered cubic zirconium. Generally, the temperature dependence of rate processes is assumed to obey the Arrhenius equation, in which case the data plotted on the scales shown should give straight lines. If the Arrhenius equation were derived from data taken near 900°C, it would predict diffusion rates at 1800°C one-tenth those observed.

CORROSION IN LIQUID-ALKALI-METAL SYSTEMS

In liquid-alkali-metal systems, such as are used to extract heat from high-temperature reactors, corrosion of structural metals is aggravated by the presence of oxygen in the liquid metal. Yet, except in the case of sodium, there are no proven methods of measuring the oxygen content of these coolants. The Metals and Ceramics Division has been attempting to extend the analytical procedures originally developed for sodium to the determination of oxygen in potassium, a coolant of interest in space reactors. However, it has not been possible to obtain quantitative and consistent recovery of oxygen from potassium by using these procedures. This is particularly true when the potassium is equilibrated at elevated temperature prior to analysis, as obviously must occur under service conditions. The Materials Compatibility Group of the Metals and Ceramics Division, with cooperation from the Analytical Chemistry Division, has now devised a reliable method. The potassium sample is contacted with zirconium metal at 815°C, and then the increase in oxygen content of the zirconium is determined.

When molten potassium contacts zirconium at elevated temperatures, oxygen that is invariably present in these metals is distributed between them in a known concentration ratio. For example, at 815° C the concentration of oxygen in zirconium is seven times that in potassium. Thus, when potassium is equilibrated with a zirconium specimen of known oxygen content, the gain in oxygen by the zirconium can be related to the original oxygen content of the potassium. This gain can be determined by the vacuum fusion method, in which one measures the amount of oxygen released when the zirconium sample is melted in a high-vacuum apparatus. Recent tests have demonstrated oxygen recoveries of essentially 100 percent from potassium by this method.

FUEL ELEMENT DEVELOPMENT

Pyrolytic Fabrication of Refractory Carbides

Boron carbide (B_4C) is used in nuclear technology as both a high-temperature bearing and a shield material. Silicon carbide is receiving considerable study as a coating material for imparting oxidation resistance to graphite, to graphite-base reactor fuels, and to various refractory metals. R. L. Heestand has discovered inexpensive methods of fabricating these materials by deposition from reacting vapors. The usefulness of boron carbide has been extended to previously impossible applications.

Boron carbide is so brittle and hard that it is difficult to machine to close tolerances or into complex shapes. The new technique circumvents these obstacles. A wide range of boron carbide mixtures can be deposited as homogeneous bodies of complex shapes and with polished surfaces. Also, the composition can be varied continuously across a single body to provide a very hard but brittle layer of B_4C on one surface and a soft and more ductile layer of essentially graphite on the other surface. For example, a hard inner surface can be deposited to any required dimension and with any surface finish; so expensive grinding is not needed. Such bodies appear ideal for high-temperature bearing applications.

Silicon carbide is deposited directly from silicon tetrachloride in Heestand's method rather than

Thin-walled high-density boron carbide (B_4C) tube prepared by pyrolytic deposition from vapors. Tubes of this type are desirable for shielding portions of in-pile experiments or equipment. Such boron carbide tubes are almost impossible to fabricate by other techniques.

made of the release of fission gas from nuclear fuels, the mechanism of this release has not been understood.

In the Metals and Ceramics Division, C. S. Morgan of the Sintering Studies Group and J. L. Scott and R. B. Fitts of the Fuel Evaluation Group have shown that stressing of irradiated UO_2 or ThO_2-UO_2 during heating released fission gas. Also, quenching of a similar specimen led to a burst of released fission gas on subsequent heating. These experiments were prompted by the observation that the kinetics of fission-gas release resembled markedly the kinetics of sintering of the fuel materials. Morgan and his group had previously demonstrated that plastic flow and dislocation movement were very important in the sintering of these materials. The present work shows that these processes appear to be important in fission-gas release.

RADIATION DAMAGE TO BERYLLIUM OXIDE

Beryllium oxide (BeO) has been considered for use as a moderator or fuel-matrix material in several advanced types of nuclear power plants. In the BeO irradiation program at the Oak Ridge National Laboratory, more than 600 sintered cylindrical specimens have been subjected to very high fast-neutron doses (0.3 to 8.0×10^{21} neutrons per square centimeter) at temperatures from 100 to 1100°C. The results showed that gross radiation damage (i.e., fracturing, powdering, and volume expansion) increased with increasing neutron dose and decreased with increasing temperature. There was significantly less damage to samples of low density and small grain size than to samples of high density or large grain size in irradiation experiments at 650°C or higher temperatures. Thus, the irradiation stability of BeO can be optimized by the proper choice of fabricational parameters and the reactor operating temperature, which should be at least 1000 to 1100°C in the maximum flux zone of a high-flux reactor.

Volume expansions ranging from 1 to 6 percent, dependent upon the neutron dose and temperature, were observed in the irradiated samples. The thermal conductivity and the crushing strength were found to decrease by about 50 percent after irradiation to neutron doses greater than 2×10^{21} neutrons per square centimeter. Most of the observed changes in physical properties can be explained by the separation of the boundaries between individual grains (crystals) of BeO as seen in photomicrographs of polished irradiated samples, although grain fracture and atomic displacements also play contributory roles.

Grain-boundary separation at low temperatures and low neutron doses is considered to result from strain on the boundaries by anisotropic expansion of individual grains. Because x-ray diffraction measurements and single-crystal studies indicate that grain expansion is much reduced at high temperatures, there is a possibility that grain-boundary separation at high temperatures (1100°C) and high neutron doses arises from the buildup of radiation-produced helium gas pressure at grain boundaries. This and other aspects of the BeO irradiation damage problem are actively being investigated.

Reactor Components

REACTOR CONTROLS DEVELOPMENT

Measurement of Shutdown Reactivity

Unlike most processes, the nuclear chain reaction is not completely quiescent when a reactor is shut down. Rather, the multiplication is reduced sufficiently below unity (the value for reactor criticality) that the fission rate is very low. The difference between the actual multiplication and criticality – the shutdown reactivity margin – is a measure of the safety of the shutdown reactor against accidental criticality. Unfortunately, in power reactors, extra shutdown reactivity margin can usually be obtained only by reducing the core life, and hence by increasing power costs. A measuring technique for continuous monitoring of shutdown reactivity margin would therefore contribute to both reactor safety and economic nuclear power.

We are developing an instrumentation technique to measure shutdown reactivity, making use of the variation of reactor dynamics with reactivity. The technique uses analysis of the inherent fluctuation (noise) in the reactor neutron population, which depends on both the source of noise and the reactor dynamic response to a noise source. Simple theories of the latter predict that the ratio of the fluctuation spectral densities in two appropriate frequency intervals is simply related to the reactivity.

Preliminary experiments in the Bulk Shielding Reactor (BSR), using laboratory-type instruments, were sufficiently promising that a special low-noise amplifier and a multichannel spectrum analyzer were developed for detailed experimental investigation. The amplifier has a noise (referred to the input) of 3.8 microvolts (root mean square), with a 3500-cycle per second bandwidth. Its gain stability is better than 0.1 percent in 60 hours. The analyzer includes the necessary filters to select ten frequency intervals, together with computer elements to square and time-average the signals in each channel.

An extensive checking and calibration program was carried out to establish that the measurements represented reactor dynamics rather than artifacts in instrumentation response. As an additional check, the system was tested, with its high-efficiency neutron detector, using a radioactive source. The expected uniform fluctuation spectral density was confirmed to within the statistical accuracy (0.2 to 3.5 percent) of the measurements.

Provisional results of the first set of measurements using the new instrumentation in the BSR confirm the predictions of the theory down to the minimum available reactivity of -15β. Further investigation will be aimed at understanding the limitations of the measuring technique, and extending it to reactors in which gamma radiation from the shutdown core would introduce an extraneous signal whose fluctuations would mask those of the signal to be measured.

Electrically Adjustable Compensated Ion Chamber

The new PCP-II ionization chamber series [ORNL-3191, p. 70 (1962)] has been extended by constructing gamma-compensated neutron-sensitive sections. The parallel circular plates (made of nickel) are 0.012 centimeter thick, spaced 0.1

centimeter apart in N_2 gas at 800 torrs, and arranged to form alternate sections, uncoated and coated with boron-10 (0.35 milligram per square centimeter). In the experiments described here, the test section had 16 signal plates, 9 positive high-voltage plates, and 8 negative high-voltage plates. The uncompensated sensitivities were 4×10^{-15} ampere per unit of neutron flux (neutrons per square centimeter per second) and 1.3×10^{-12} ampere per unit of gamma intensity (roentgens per hour).

The compensation can be changed by varying the ratio of the positive high voltage to the negative high voltage polarizing potentials. The signal plates are slightly smaller than the high-voltage plates, so the change in polarizing potential ratio creates a slight radial distortion of the electric field, and therefore the effective volume, near the edges of the plates. This technique has the advantage over methods previously used that both the neutron and gamma sections are well saturated at all polarizing voltages ordinarily used, so that the electrical compensation is not obtained at the expense of saturation. This results in a measured compensation factor independent of gamma intensity over at least four decades. In the test chamber installed in the BSR, with +300 volts applied, changing the negative high voltage from −300 volts to −200 volts changed the compensation from 2.4 percent overcompensated to 0.6 percent undercompensated.

The accuracy of manufacture permits attainment initially of compensation to better than 3 percent, and allows the final accurate adjustment to be made as precisely as desired by varying the voltage ratio.

Tests in the BSR using both "cool" and "hot" cores (as regards fission-product gamma-ray intensity, and therefore energy) showed that the compensation of the test chamber, located in water 15 to 40 centimeters from the core surface, varied less than 0.5 percent over a range of more than three decades. The signal from the compensated chamber followed the power of the BSR from source to full power – a range of $6\frac{1}{2}$ decades.

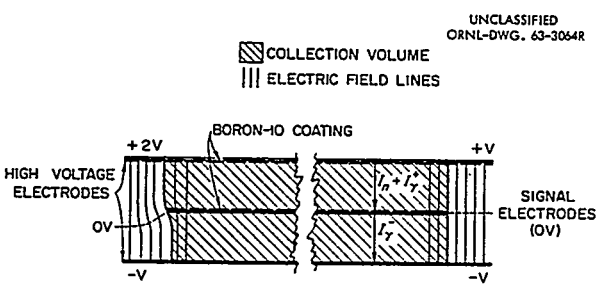

Diagram of adjustable electrical gamma compensation.

Use of Gamma Radiation as a Reactor Control and Safety Parameter

Several experiments with gamma-sensitive ionization chambers in the BSR and ORR have led to an improved understanding of the advantages and limitations of using gamma radiation with respect to the neutron flux usually used. The principal advantage gained by using gamma radiation is that the effect of changes in core and shielding configurations, at least in water-shielded reactors, is greatly reduced. The disadvantages are the fission-product signal, 20 ± 1 percent at equilibrium in the BSR, and the capture gamma rays produced by neutrons far from the core. The latter effect was observed whenever the ratio of the flux of neutrons to the flux of gamma photons exceeded 0.2 anywhere along the path between the core and the detector. Older experiments at SPERT (ORNL-3393-A and unpublished data) at periods as short as 3 milliseconds confirmed, as expected, that gamma-sensitive chambers would work well as safety detectors. The results of these experiments and several years' operating experience with gamma chambers in the ORR and BSR lead to the conclusion that the use of gamma radiation for reactor control and safety is feasible, and sometimes advantageous.

Modular Electronic Instruments

A system of modules has been devised, whereby each module is a functional unit of one or more transistorized electronic instruments for reactor use. In all, 24 modules have been designed and built in varying quantities, and the scheme is capable of almost indefinite expansion. The critical dimensions of the assemblies are compatible with presently developing international standards for reactor-control instruments.

The basic modular unit is approximately $1\frac{3}{8}$ inches wide, 5 inches high, and 11 inches deep; 12 of the units plug side-by-side into a drawer

which fits into the $5\frac{1}{4} \times 19$-inch standard relay rack. Single modules, two or more units wide, are easily accommodated. Interconnecting wiring and the components which establish the parameters (such as gain or trip-level of general-purpose modules) are located behind the plug-in connectors; this circuitry is quite complicated in some instances.

Modular regulators supply power to the instruments from input buses at ±32 volts, which can be supplied from commercial power supplies operating from the alternating-current line, or from storage batteries where operating continuity is required.

Modules designed so far include operational amplifier, trip amplifiers, magnet current controllers, servo amplifiers, logical elements for reactor safety systems, and the precision voltage regulators mentioned previously.

The 352 modules produced in the initial production will comprise the counting, regulating, and safety systems of the HFIR and the MSRE, now being constructed. We anticipate learning much from our first experience on these "second-generation" reactor instruments, and from the requirements of still more advanced reactor types, so that eventually the reactor instrumentation designer can assemble his instruments from proven building-block modules.

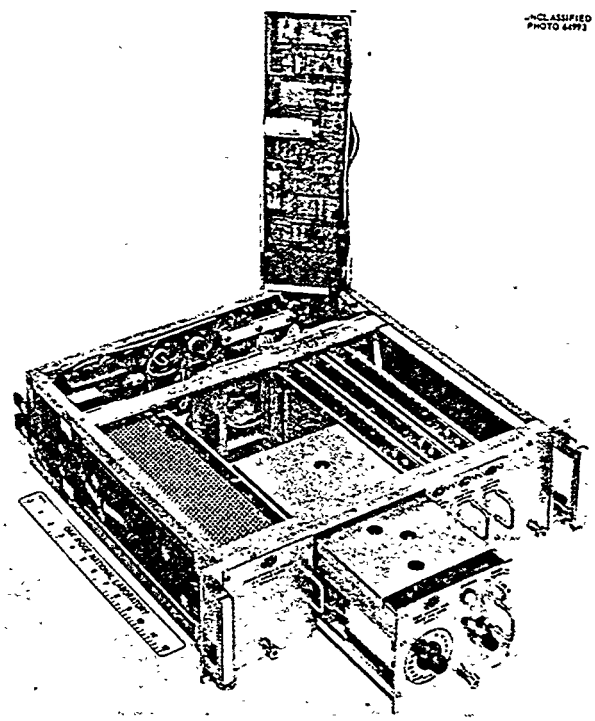

A typical drawer and modules.

Power Reactor Fuel Processing

CHEMICAL ANALYSIS OF ADVANCED REACTOR FUELS

A method was developed for the precise and accurate determination of microgram amounts of uranium. The ORNL high-sensitivity controlled-potential coulometric titrator is used to titrate as little as 2 micrograms of uranium with an error of less than 1 percent. Previously, milligram quantities of uranium were required for this titration.

With this new method, small samples of highly radioactive solutions can be titrated automatically and remotely in a hot cell with good precision and accuracy.

The special high-sensitivity coulometric titrator (Q-2564) designed and built at ORNL has a titration range of 1 to 100 microequivalents of material. A newly designed titration cell developed for these small quantities requires only 2 milliliters of mercury for the cathode and 2 milliliters of test solution. Metal rather than Tygon tubing for the argon purge gas is required since diffusion of oxygen through Tygon tubing caused a positive error. A blank and a faradaic background correction were found to be equivalent to 0.25 microgram of uranium. The reduction titration of uranium(VI) to uranium(IV) in 1 N H_2SO_4 at -0.325 volt versus saturated calomel electrode is terminated automatically at a background current of 0.5 microampere. The readout voltage from the instruments integrator is a measure of Q (coulombs of electricity and amount of uranium) consumed in the titration and is recorded as a function of time on a Brown recorder. Thus, the correction for faradaic current can be found by extrapolation of the curve to zero time.

This method is useful for the determination of microgram amounts of uranium in fuels and other materials of interest in the AEC program. The microtitration of other elements is also feasible.

Studies on the determination of carbon in aqueous and nitric acid solutions from the dissolution of carbide type fuels were continued. A gas chromatographic measurement of the CO_2 produced by oxidation of the carbon-containing compounds was incorporated into the procedure to effect an improvement in sensitivity of about 20-fold over the manometric measurement of CO_2. The interference of residual oxides of nitrogen is also eliminated by use of the gas chromatographic measurement.

Gas chromatography was used to resolve and determine the products from the reaction of carbide fuels with CCl_4 in the presence of air. With a 15-foot silica-gel column, only Cl_2 and $COCl_2$ were not resolvable from the expected reaction-product mixture of air, CCl_4, CO, CO_2, Cl_2, and $COCl_2$. Silicone-gum-rubber columns approximately 15 feet long appear to offer complete resolution of these compounds.

The oxides of nitrogen were determined gas chromatographically on a silica-gel column (3 feet long, 1 inch inside dimensions) programmed from 25 to 300°C. The order of elution under these conditions is NO, N_2O, N_2O_4, and NO_2.

Studies were initiated on the gas chromatographic determination of polynuclear aromatic hydrocarbons such as naphthalene, biphenyl, anthracene, and phenanthrene, which are expected to

be formed when uranium carbide is heated in nitric acid, and the resulting acids are decarboxylated at elevated temperatures. Silicone SE-30 and SE-52 are promising materials for this problem.

STUDIES ON THE DISSOLUTION OF CERAMIC FUELS FOR BREEDER REACTORS

Studies on the problem of dissolving commercially prepared plutonium dioxide–uranium dioxide (PuO_2-UO_2) fuel pellets that had been fired at high temperature showed that small amounts of fluoride in a nitric acid dissolvent will probably be required to effect a complete dissolution. When fabrication procedures produced a solid solution of plutonium dioxide and uranium oxide (i.e., a truly homogeneous distribution of PuO_2 and UO_2 molecules), the pellets could be dissolved in concentrated nitric acid in a reasonable time. However, if part of the PuO_2 was not completely mixed with the UO_2, a residue of plutonium remained after the bulk of the pellet had dissolved. The difficulty of producing a solid solution of PuO_2 in UO_2 during fabrication, and the uncertainty of the composition of the pellet after high irradiation, seem to justify the addition of fluoride to the dissolver. The presence of fluoride is of concern, however, because it greatly increases corrosion of the stainless steel equipment in the processing plants.

CHEMICAL PROCESS DEVELOPMENT: CARBIDE FUELS

Three head-end processes for the recovery of fuel values from uranium and plutonium carbide reactor fuels were investigated using specimens irradiated to burnups of up to 20,000 Mwd/metric ton. Solvent extraction behavior of the fuel solutions produced was examined in batch shake-out tests. Reaction with steam (pyrohydrolysis) at 750°C was the best method tested, although direct dissolution in boiling 13 *M* (60 percent) HNO_3 followed by oxidation of residual organic impurities in the resulting solution is also potentially useful. Hydrolysis with liquid water at 80 to 100°C is not feasible, since the irradiated carbides of uranium and plutonium are passive.

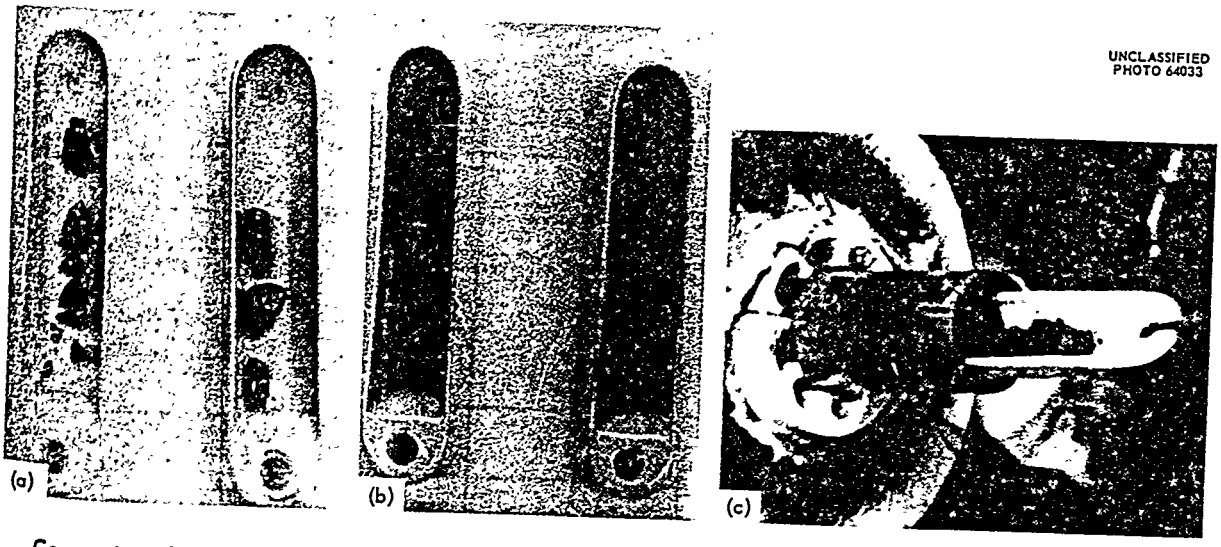

Conversion of uranium monocarbide to uranium dioxide by high-temperature steam. (*a*) Unirradiated uranium carbide before treatment with high-temperature steam (irradiated uranium carbide appears the same after boiling in water); (*b*) unirradiated uranium carbide after conversion to uranium dioxide by 750°C steam; (*c*) irradiated uranium carbide (16,000 Mwd per metric ton) after conversion by high-temperature steam.

By pyrohydrolysis at 750°C (air excluded), the uranium monocarbide was converted to UO_2 containing only about 0.03 percent carbon. The gaseous reaction products were H_2, CO_2, and CO. Cesium was the principal fission product volatilized, but the amount was very low (0.5 percent). This cesium was trapped when the excess steam was condensed. The UO_2 product dissolved easily in 6.5 *M* HNO_3 to yield a solution suitable as a feed for Purex solvent extraction. Batch extraction tests showed that greater than 99.9 percent of the uranium and plutonium could be recovered and separated from gross fission products by a factor of 10^4. The pyrohydrolysis process was also successfully demonstrated with irradiated 20 percent PuC–80 percent UC specimens.

Irradiated UC, PuC, or 20 percent PuC–80 percent UC could be dissolved directly in 60 percent HNO_3, but about 44 percent of the carbide carbon remained in solution, primarily as organic acids that interfered with solvent extraction. The organic impurities were largely eliminated by oxidative degradation. In solvent extraction tests of the treated solutions, uranium recovery was nearly quantitative, but up to 0.4% of the plutonium was retained by the solvent after stripping. The plutonium retention was attributed to residual organic impurities. Uranium and plutonium were separated from gross fission products by a factor of 3.4×10^4.

SELECTIVE REMOVAL OF THE FUEL FROM TUBULAR FUEL ELEMENTS BY THE CHOP-LEACH PROCESS

The chop-leach process, developed at ORNL, is a primary method of handling tubular, metal-clad fuel from nuclear power reactors preparatory to recovery of the fissionable material by the Purex (or Thorex) solvent extraction process. The chop-leach process involves the shearing of the fuel bundle into short lengths to expose the fuel oxide or alloy, after which the exposed fuel is dissolved by nitric acid. Only a minor fraction of the cladding dissolves. Development of this process (described on p. 302 in *Fundamental Nuclear Energy Research, 1962,* a special USAEC report) has been extended to include batch as well as semicontinuous leaching, since semicontinuous leaching of some fuels (e.g., metal-clad thorium-uranium oxide) is impractical.

The method is capable of processing, with the same equipment, any oxide or metal fuel clad with aluminum, stainless steel, or Zircaloy-2. Further, the cladding component is eliminated from the solutions in the solvent extraction system, thereby enabling an extraction column to process uranium at a greater rate. Finally, considerable advantage is found in the lowered cost of storing the cladding material as metal waste with relatively little radioactivity rather than as highly radioactive solutions.

The 250-ton prototype shear was used successfully to shear unirradiated stainless-steel-clad uranium oxide and thorium-uranium-oxide fuel assemblies about 6 inches square (containing up to 144 fuel tubes) into lengths of ½ inch to 2 inches. Zircaloy-2-clad fuel was sheared satisfactorily, showing no particular safety problems caused by the presence of Zircaloy-2 metal fines. Complex multitubular fuels of proposed designs which cannot be sheared intact can be disassembled and, after removal of the rods from the fuel assembly, can be satisfactorily sheared as a loose bundle. Tests with annular-type fuel, such as that used in the New Production Reactor at Hanford, were also satisfactory. The shear blade used in these tests made over 5000 cuts before chipping; this is equivalent to shearing half the core of an average-sized reactor. Fuel bundles have been sheared consistently to terminal lengths of 2 inches.

Batch leaching of stainless-steel-clad uranium oxide and thorium-uranium oxide was studied with a perforated basket of about 25 percent open area and 20-mil hole size. Leaching time for uranium oxide was 2 hours; leaching time for thorium-uranium oxide was about 20 hours.

The chop-leach process will be used by Nuclear Fuel Services, Inc., for processing fuels from reactors in the United States. Considerable interest in the chop-leach process has been expressed by workers in England, Germany, and Japan.

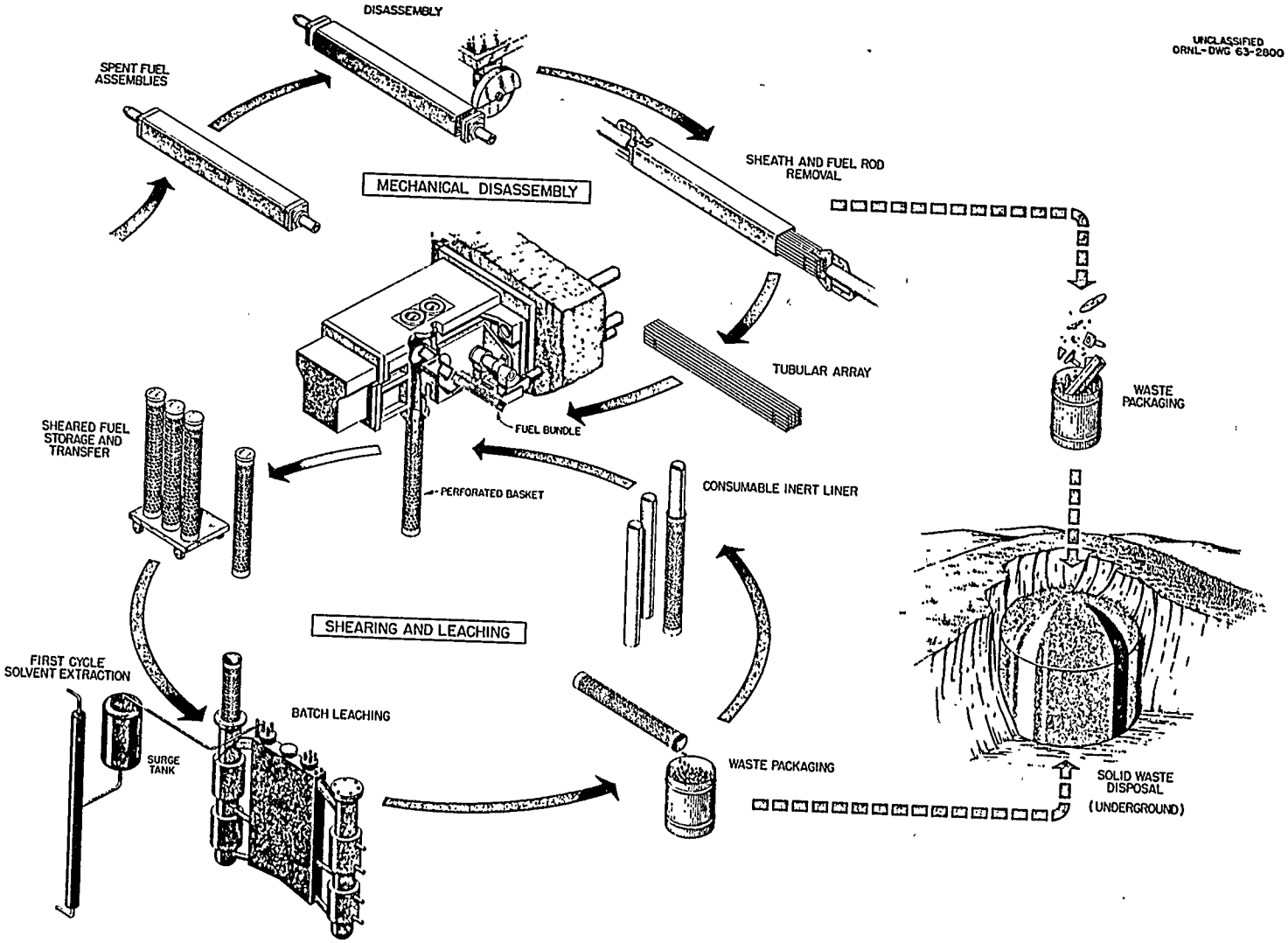

A typical shear-leach process for uranium oxide or thorium oxide fuel clad with stainless steel or Zircaloy-2. For existing Kanigen and Nicrobrazed fuels, the spent fuel assemblies are disassembled by sawing off the inert end fittings, sheath, and tube sheets. The resulting tubular array, which is usually in the form of subassemblies, is then sheared. The sheared pieces are collected in a perforated basket and leached in a batch leacher. The empty cladding is monitored and sent to underground waste storage along with the inert ends, sheaths, tube sheets, etc.

OXIDATION OF SPENT GRAPHITE-MATRIX FUEL ELEMENTS PRIOR TO RECOVERING THE URANIUM

One type of fuel element used in high-temperature gas-cooled nuclear reactors is a graphite structure in which carbon-coated uranium carbide and/or thorium carbide are dispersed. After irradiation, fuel of this type can be recovered by first removing the graphite by burning, a method developed and demonstrated at ORNL. The inclusion of fissionable-metal carbides and the formation of fission products in graphite necessitates the use of special equipment and more closely controlled operating procedures than those used for conventional carbon-burning processes. These requirements are met by the demonstration units operated at ORNL, which have high capacity, operate safely, and produce a residue suitable for further chemical processing.

The burning process has some restrictions, which have been considered in the ORNL development program. These are: (1) a maximum allowable combustion temperature, determined by the physical properties of fuel and fission product oxides; (2) the necessity of burning completely to carbon dioxide in order to avoid the hazard of carbon monoxide explosions; and (3) the necessity of using metal vessels with no refractory lining in order to prevent the holdup of fissionable materials and fission products in a slag not amenable to further chemical processing. Samples of neutron-irradiated Peach Bottom (High-Temperature Graphite Reactor) fuel, having burnups of about 10,000 Mwd per metric ton (U + Th), were burned in oxygen at 800 and at 1200°C. None of the zirconium or rare-earth fission products volatilized at either temperature; however, about 80 percent of the ruthenium vaporized at 800°C, and 97 to 99 percent at 1200°C; 25 to 35 percent of the cesium distilled at 800°C, and 67 to 88 percent at 1200°C. These volatile fission products were easily collected on 40-micron-porosity sintered-metal filters. A maximum temperature range of 1000 to 1200°C was chosen, because at these temperatures reasonable burning rates can be employed, the physical condition of the oxide residues is suitable for processing, and fission

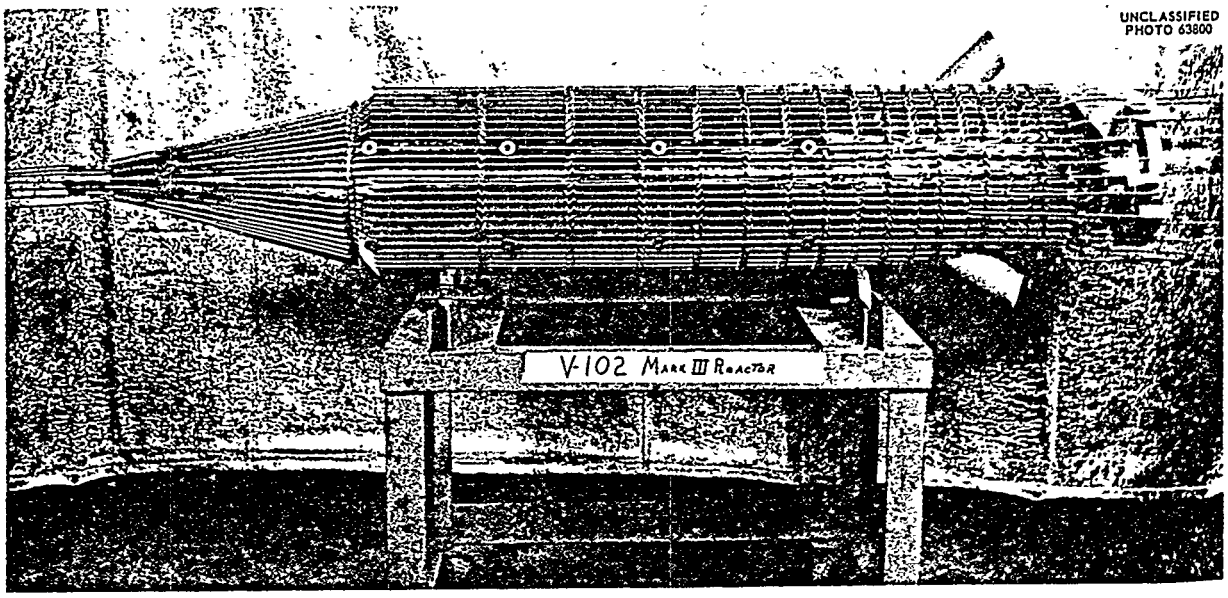

Air-cooled combustion reactor for graphite fuels. The cooling fins will be covered by a shroud to contain the cooling air. The reactor is mounted vertically, with the cone end at the bottom. Cooling air is forced up through the shroud. The large tubes protruding angularly are fuel feed ports, and the multiple small nozzles are air-oxygen inlets. The central pipe in the reactor, visible at the top, is an air-cooled core that removes heat from the center of the fuel bed. The reactor is 10 inches in diameter and 78 inches tall. It was made of nickel in the ORNL shops.

products, except ruthenium and cesium, are retained.

The fixed-bed reactors used for experimental work have been cooled by an air-water mist flowing in coils or channels welded to the outer walls of the vessel; a heat flux of 80,000 Btu ft^{-2} hr^{-1} has been measured. An air-cooled vessel with extensive fin cooling was designed, and it has adequate capacity at a flux of 15,000 Btu ft^{-2} hr^{-1} for the total cooling surface. Both types of cooling system were operated to keep the reactor wall temperature at 500 to 700°C during the oxidation.

The throughput was maximized by supplying the fuel bed with an air-oxygen mixture at a number of points so that the entire bed was burning. Combustion control was aided by the fact that the metal oxides in the fuel formed an ash film that tended to reduce the rate at which oxygen reached the unreacted carbon. This was quite beneficial; fewer gas inlets per unit of fuel volume were needed than would have been required to control the burning of pure graphite. A throughput of 10 pounds of fuel per hour was burned in a reactor 5 inches in diameter with a bed depth of 50 inches.

As an example of the process steps that can follow combustion (oxidation), the mixed uranium oxide–thorium oxides resulting from combustion were easily dissolved in a mixture of nitric and hydrofluoric acids to provide a solution suitable for the recovery of uranium and thorium by solvent extraction.

RECOVERY OF FISSILE AND FERTILE FUEL FROM THORIUM BREEDER REACTORS

The recovery of fertile and fissile fuel from thorium breeder reactors presents problems not common to reactors fueled with natural uranium or uranium slightly enriched in uranium-235. The difficulty centers around the difference in rates of decay of the radioactive isotopes involved. Protactinium-233, which decays to fissionable uranium-233 in the thorium reactor, has a 27-day half-life, whereas neptunium-239, the counterpart of protactinium-233 in the transmutation of uranium-238 to plutonium-239, has a half-life of only 2.4 days. Therefore, neptunium will have completely decayed before reprocessing (usually after 60 to 90 days of cooling), but protactinium will persist in significant quantity. In present processes for the recovery of thorium fuel, protactinium is either allowed to decay to uranium-233 during long storage periods prior to processing or relegated to a waste stream for recovery at a later date. In newly developed processes at ORNL, the protactinium may be preferentially adsorbed on unfired Vycor, or it may be simultaneously extracted with the uranium and thorium with 30 percent tributyl phosphate.

In the first method, the thorium fuel is dissolved in concentrated nitric acid that contains a small amount of fluoride and aluminum nitrate. When this solution is passed through a column containing pulverized unfired Vycor glass, the protactinium is sorbed on the glass. The protactinium is recovered from the glass by washing with an oxalic acid solution. The product contains less than 0.1 percent of the original fission products, with the exception of zirconium and niobium. The latter are acceptable contaminants.

In the second process, the Acid Thorex process for recovering thorium and uranium by solvent extraction is modified to include the recovery of protactinium by decreasing the concentration of thorium and increasing the acidity of the feed solution. As a result, the overall degree of separation from fission products is decreased, but the high-neutron-absorbing fission products are removed satisfactorily.

These processes have been demonstrated in laboratory equipment with fuel irradiated to tracer levels and are being tested at high irradiation levels in hot cells in order to verify the laboratory work.

FUSED-SALT FLUORIDE-VOLATILITY PROCESS FOR RECOVERING URANIUM FROM CERTAIN ALLOYED FUELS

Probably the highest degree of uranium purification ever obtained in a one-cycle nuclear-fuel recovery process was achieved in a series of experiments recently concluded in the Fluoride Volatility Pilot Plant at ORNL. The zirconium-uranium alloy fuel of the type used in both power and

military reactors was of high burnup (greater than 15 percent) and was decayed (cooled) only 6 to 13 months. (Experiments with long-decayed zirconium-uranium alloy fuel are described on pp. 307–8 in *Fundamental Nuclear Energy Research, 1962,* a special USAEC report.)

The fused-salt fluoride-volatility process involves dissolution of the zirconium-uranium alloy fuel elements in a fluoride melt with anhydrous hydrogen fluoride at an initial temperature of 650°C, which is gradually lowered to 500. The uranium-bearing melt is then contacted with fluorine at 500°C, which converts the uranium to uranium hexafluoride and converts some of the fission products to volatile fluorides. The UF_6 is further purified from these volatile fission product fluorides by a sorption-desorption cycle using a temperature-zoned movable bed of sodium fluoride pellets. Passage through a bed of magnesium fluoride for further purification and cold trapping of the UF_6 completes the process.

The outstanding degree of uranium purification achieved during the Fluoride Volatility Pilot Plant experiments with fuel decayed for a short time is shown by the decontamination factors obtained. (The decontamination factor is the ratio of the quantity of any specified fission product in the process feed to the quantity of that fission product in the process product. The higher the factor, the greater the degree of uranium purification.) In the experiment with fuel decayed 6 months, decontamination factors for the more important fission products that form nonvolatile fluorides (zirconium-95–niobium-95, strontium-90, and cesium-137) ranged from greater than 10^9 to greater than 10^{10}. In the same experiment, decontamination factors for the more important fission products that form volatile fluorides (tellurium, antimony-125, and ruthenium-106) ranged from greater than 10^8 to greater than 10^9. A decontamination factor of nearly 10^{11} was attained for zirconium-95–niobium-95 in the final experiment of the series. Fuel decayed 10 months was used in this experiment.

In addition to its capabilities for recovering enriched uranium from zirconium-uranium fuels, the process has been shown by laboratory-scale studies to be potentially useful for recovering enriched uranium from fuels containing zirconium dioxide, beryllium oxide, some stainless steel, thorium dioxide, and, most importantly, aluminum. The next program in the Fluoride Volatility Pilot Plant will be a demonstration of the recovery of enriched uranium and aluminum-uranium alloy fuels.

The process is also potentially applicable to recovering both uranium and plutonium from fuels containing low-enrichment uranium. Plutonium hexafluoride can be separated from UF_6 by selective sorption on beds of inorganic fluorides such as sodium fluoride and calcium fluoride. However, the removal of PuF_6 from fluoride melts by volatilization requires contacting the salt with a relatively large volume of fluorine.

Nuclear Safety

As a part of the Nuclear Safety research effort, an intensive study is being conducted to assess and characterize the many factors likely to contribute to the extent and nature of accidental release of radioactive fission products from nuclear reactors.

The out-of-pile fission product release program has emphasized the most nearly realistic simulation of reactor accident conditions, which include the most plausible atmosphere, irradiation level of the fuel, and time and temperature range of the heating cycle. This program has probably the only operating experimental facility of such capability anywhere in the atomic energy field.

The types of information which are being obtained include:

1. the percent of fission product release from power reactor UO_2 by melting, oxidation, and vaporization,
2. the rate of fission product aerosol settling, deposition, and washout in a confinement mockup tank,
3. the amount of individual fission products associated with airborne particles and the size distribution of such particles, and
4. the efficiency of collection of fission product aerosols by engineered adsorption filtration systems.

Radioiodine Distribution (Percent of Inventory in Fuel)

	Trace Conc. in Uncleaned Air[a]	Trace Conc. in Cleaned Air	High-Burnup Conc. in Cleaned Air
Amount of iodine deposited in confinement tank	46.5	23.8	25.3
Amount remaining airborne after 3 hours	31.0	29.6	57
Amount of iodine in penetrating (organic) form	3.7	0.4	0.1
Iodine loss through 1.5 inch charcoal bed	1.3	0.14	0.0002

[a]Twenty-five percent unfiltered air added after melting UO_2.

This program is conducted on a hot-cell basis on an intermediate scale (between laboratory and pilot plant) as required to provide the amount of fission products in realistic proportion to the confinement surface area and volume.

An example of fission product behavior characterized by this method is given in the table.

The change in particle concentration (number of separate particles) is shown as a function of time to illustrate the rapid agglomeration process. On the other hand, the plot of airborne activity shows no indication of significant settling or deposition as a function of time.

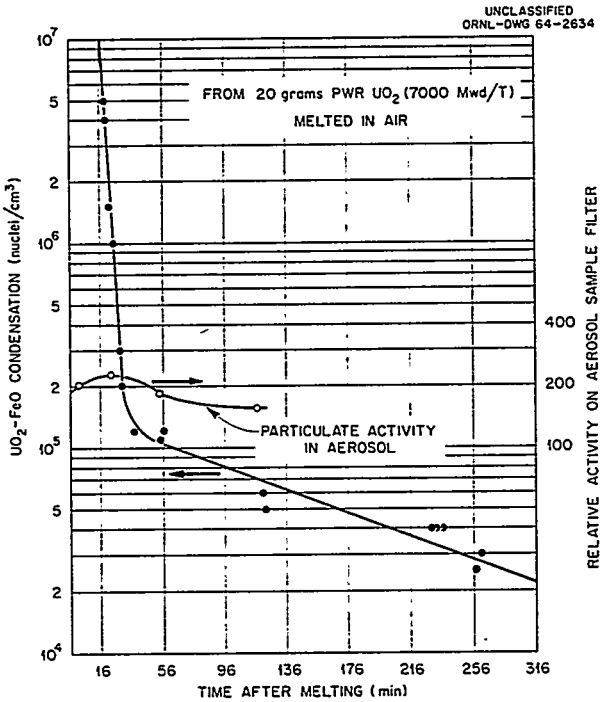

Study of the effect of agglomeration of particles on deposition of released fission products. An illustration of the rapid agglomeration of small particles vaporized into a confinement vessel by melting irradiated UO_2 in a stream of air and the small corresponding effect on deposition of the airborne radioactivity is shown in the two curves plotted on the same time scale.

RELEASE OF FISSION PRODUCTS ON IN-PILE MELTING OF REACTOR FUELS UNDER TRANSIENT REACTOR CONDITIONS

A program has been initiated in which UO_2 is melted under conditions that simulate the type of accident which could occur as a result of a prompt excursion associated with excess reactivity.

The objectives of the meltdown of UO_2 fuel pins in the Transient Reactor Test Facility (TREAT) are to measure and interpret the rapid release of fission products as a function of fuel type, cladding, atmosphere, burnup, and transient characteristics.

Two experiments have been performed in the TREAT reactor. In the first experiment, the UO_2 temperature rose above 2600°C, but the sample did not melt. In the second experiment, approximently 65 percent of the UO_2 became fluid and 10 percent flowed out of the pellet shell. The appearance of the displaced UO_2 could be described

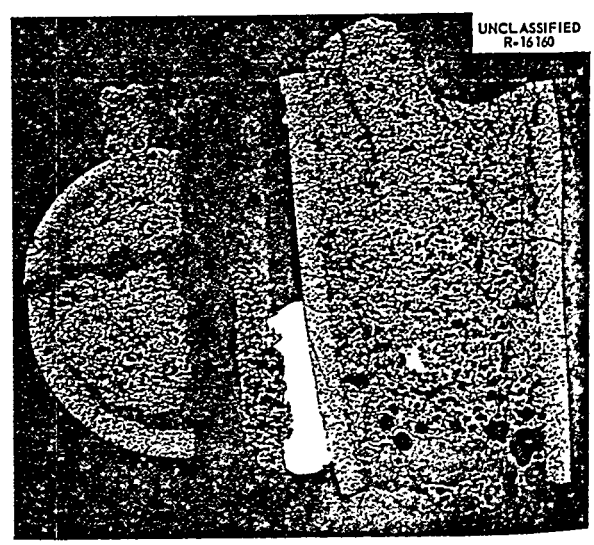

Two metallographic sections of a UO_2 fuel pellet that had been heated to melting by a fast transient in the pulsed TREAT reactor, showing the "foamy" structure of the melted UO_2. The white spot is a globule of stainless steel. The black spots are larger gas pockets.

as "foamy," which indicates that the material did not reach a highly fluid state sufficient to release the gas bubbles.

The fission product release data obtained were found to be highly biased by the precursor isotopes which form the initiation of the fission product chains. These results are more applicable to clean-core reactor incidents. Future experiments will emphasize other conditions including a pre-meltdown inventory.

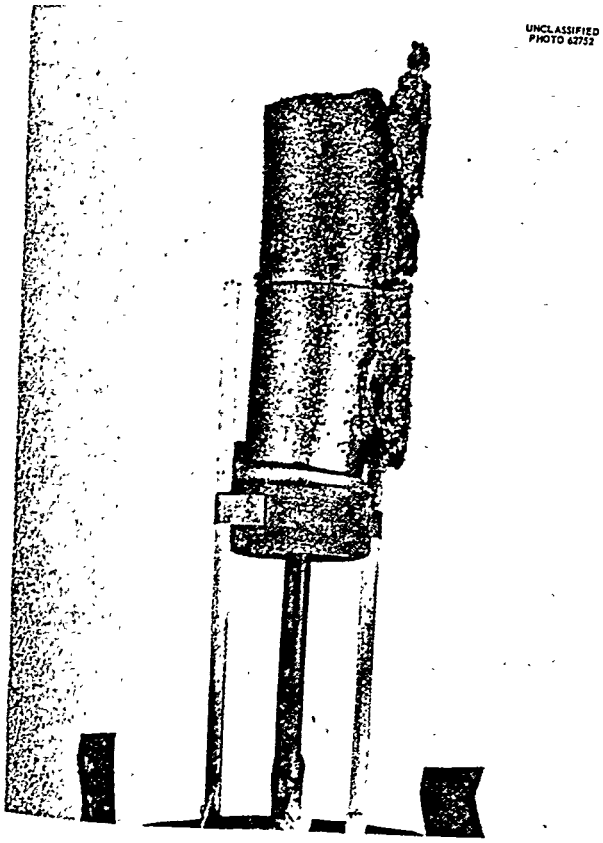

UO_2 fuel pellets which had been heated to melting by a fast transient in the pulsed TREAT reactor are shown with the top portion of the stainless steel cladding and the detached thermocouple. Fluidized, "foamy" UO_2 was displaced through a break in the side of the fuel.

FISSION PRODUCT RELEASE FROM MELTDOWN OF A CLUSTER OF CENTER-HEATED UO_2 FUEL PINS

The realistic simulation of a reactor loss-of-flow accident has been further approached on a small scale in out-of-pile experiments by melting trace-level irradiated unclad UO_2 fuel pins in a helium atmosphere by means of electrical resistance heat from centered tungsten resistors. The experimental technique has progressed from the initial arrangement for melting a single fuel pin of three UO_2 pellets to apparatus for melting a cluster of seven fuel pins consisting of four UO_2 pellets each.

Fuel pins, when arranged in a cluster, reduce heat loss from the center pin and may result in more nearly complete melting of the center pin. The cluster arrangement simulates a reactor loss-of-coolant accident with melted fuel in the center area but unmelted fuel toward the outer portions

A uranium oxide fuel pin that had been melted by heat from a centered tungsten resistor. The outer layer of the fuel pin is relatively intact, and the melted UO_2 has flowed out through cracks. A remarkable feature is the indication of grain growth by evaporation and condensation.

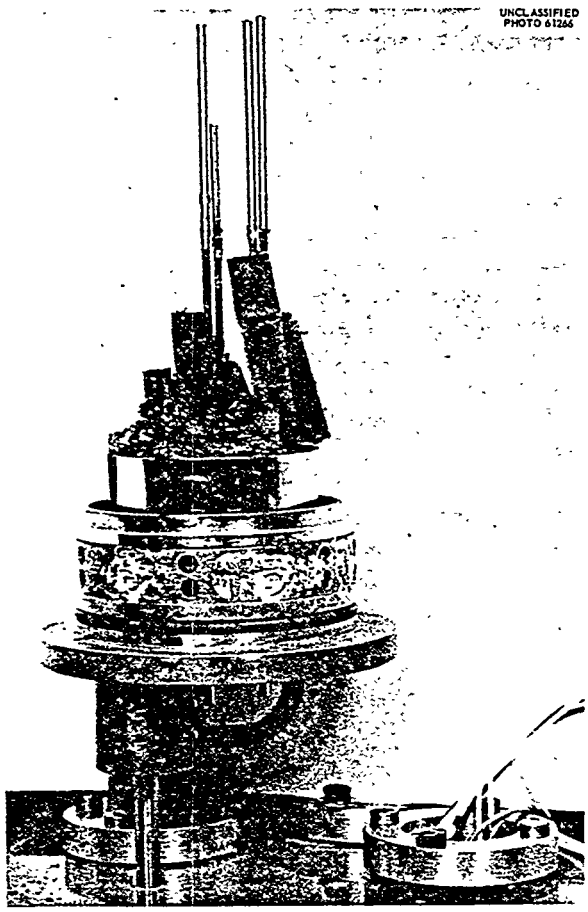

An assembly of seven fuel pins almost completely melted with the tungsten heater rods still standing, as well as portions of the outer layer of the UO_2 fuel pins.

of the reactor core. Thus in one integral experiment, the important effects of size and physical arrangement are simulated permitting observations on deposition of fission products on the unmelted fuel. The detailed analysis of the location of fission products in the residue of a cluster of seven pins of UO_2 after meltdown showed that a significant fraction of the released activities originally contained in the center pin had redeposited on the slightly cooler outer row of UO_2.

The analogy to a reactor is reasonable, although the further determination of larger fractions remaining in the primary vessel needs to be demonstrated on a greater scale of the meltdown.

IODINE CONTROL ON THE NUCLEAR SHIP "SAVANNAH"

The NS "Savannah" is provided with iodine adsorbers to prevent the accidental release of radioactive iodine to the environment. In-place tests of these adsorbers have been repeated at frequent intervals to provide continual assurance that they are capable of functioning with full effectiveness. These tests use radioactive iodine-131 or nonradioactive iodine-127 and have shown that an iodine removal efficiency greater than 99.8 percent can be expected.

Criticality Safety

An important requirement of any reactor development program is the safe and economic preparation and recovery of reactor fuels. Of concern are all operations with fissile elements outside reactors. The program at ORNL, primarily experimental but supported by reactor physics calculations, provides basic information describing critical configurations of fissile materials in various geometries and with associated materials of interest. The information guides the design of chemical and metallurgical processes, the specifications for storage and transportation, and the preparation of regulations necessary to ensure safety in nonreactor operations with fissile materials. In general, the studies are made with common materials in simple geometry, in order that data of the most general applicability will be obtained. These experiments are supplemented by tests of representative or specific items of equipment as demand requires.

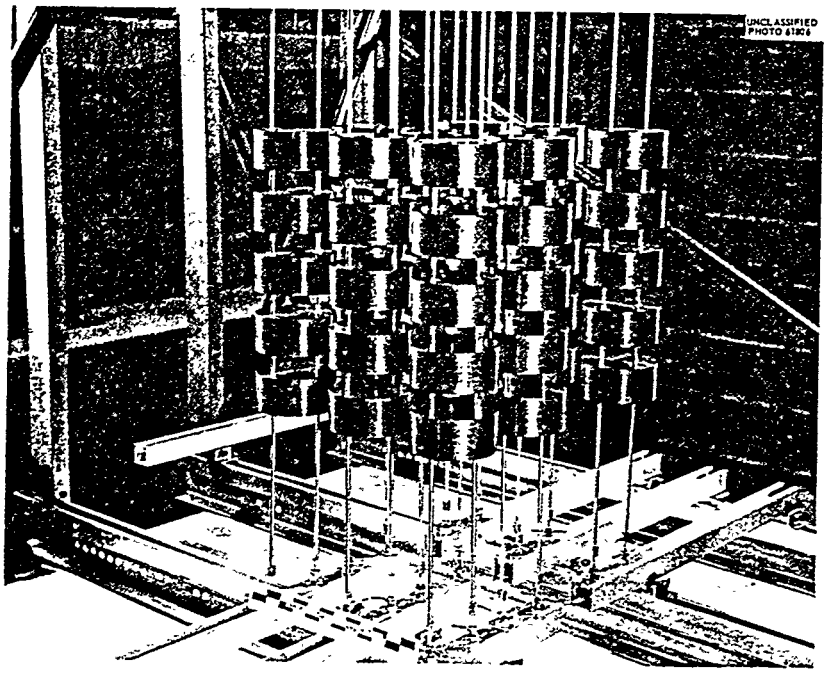

A typical unreflected and unmoderated array of enriched uranium cylinders used to study criticality safety in storage and transportation.

CRITICAL THREE-DIMENSIONAL ARRAYS OF NEUTRON-INTERACTING ENRICHED URANIUM METAL UNITS

A series of critical experiments with uranium metal cylinders, enriched to 93.2 percent in uranium-235 and arranged in three-dimensional arrays, was a part of a continuing program in support of criticality safety in the handling of accumulations of individually subcritical units of fissile materials. The units ranged from 10.5 to 26.2 kilograms in uranium mass and from 0.47 to 1.90 in height-to-diameter ratio. The critical surface separation between units was determined as a function of the number in an array. In addition, the critical uranium density (the ratio of the mass of a unit to the volume of the lattice cell it occupies in a critical array) was observed to depend on a number of factors. Changes in the k_{eff} of the individual units, if induced by altering their shape, produced inverse changes in the critical density, provided the array shape was unchanged. The critical density of the array varied with its shape in a manner similar to that resulting from corresponding changes in a single critical unit. Addition of a hydrogenous reflector reduced the critical density of the array by factors much greater than those observed for similar reflection of a single critical unit. In studies of the effect of moderator slabs between units, the density was found to be minimal when the units were separated by a hydrogenous moderator 4.9 centimeters thick. The separate effects of moderation and reflection of arrays are not additive. In several experiments it was observed that an array comprised of one-half of each of two different critical arrays was subcritical.

EFFECTS OF BOROSILICATE GLASS RASCHIG RINGS ON THE CRITICALITY OF AQUEOUS URANYL NITRATE SOLUTIONS

The processing and storage of large quantities of reactor fuels are of major concern to designers and operators of reactor complexes. Since the fuel is in solution in at least some stage of processing or recovery, the addition of effective neutron absorbers can result in considerable augmentation of both economy and safety. Commercially available borosilicate glass Raschig rings, known to be chemically compatible with many types of solutions, were investigated experimentally as neutron absorbers in uranyl nitrate solutions enriched to 92.6 percent in uranium-235.

The boron content of the glass varies from 0.5 to 5.7 weight percent, and the volume of the vessel occupied by the glass ranges from 20.9 to 30 percent. Results from exponential experiments, in which a critical layer of solution above the column of solution-ring mixture was used as a neutron source, provided estimates of the material buckling of the mixture as a function of solution concentration, boron content of the glass, and glass volume. It was shown, for example, that the material buckling is negative, and therefore the multiplication constant for an infinite volume is less than 1, if glass containing 4 weight percent boron occupies more than 22 percent of the mixture volume. With the same concentration of glass containing only 0.5 weight percent boron, positive values of the buckling result except for solutions more dilute than about 72 grams of uranium per liter (hydrogen to uranium-235 ratio approximately equal to 380).

Waste Disposal

CLINCH RIVER STUDIES

The discharges from the peaking power hydroelectric station at Melton Hill Dam – 2.2 miles upstream from the point of injection from White Oak Creek of the ORNL wastes into the Clinch River – will drastically change the flow regime in the river. The operation will cause White Oak Creek embayment to function similarly to a tidal estuary and release its water in discrete pulses when power is not being generated at Melton Hill Dam. Tracer tests, using rhodamine B, were run to determine the minimum dilution factors to be expected in the river under normal operating conditions. The power plant is not yet complete, so TVA released water through the gates to simulate normal summer operations. During the normal weekend shutdown at Melton Hill Dam, the highest concentration of tracer is ponded in the Clinch River. Consequently, the highest dye and, inferentially, radioactive concentration will be obtained downstream when this mass is transported by the next power wave. The minimum dilution measured at the water supply intake to the Oak Ridge Gaseous Diffusion Plant, 6.8 miles downstream, was 50 compared to a mean value of 450 during operations prior to the startup at Melton Hill Dam. Since the concentration of radionuclides in the water at this point had averaged 5 percent of the maximum permissible concentration values during the past few years, even at the minimum dilution the concentration of radioactivity is still within permissible limits for continuous use as drinking water.

Sediment Studies

The greatest thickness of radioactive sediment – 14.2 feet in the 1962 undisturbed cores from the Clinch River – was found 13.3 miles downstream from White Oak Creek. Measurement of vertical variations in gross gamma activity in the thick zones of radioactive sediment has revealed a recurring pattern in many of the cores; this pattern is being correlated with the releases from the Laboratory during the past 20 years.

Comparisons of the longitudinal distribution of radionuclides in the bottom sediments of the Clinch and Tennessee rivers have shown similar patterns for cesium-137, ruthenium-106, cobalt-60, and the rare earths. The similarity in distribution of these nuclides suggests that the mechanism controlling their distribution is a sedimentation process rather than a chemical process. However, the longitudinal distribution patterns of zirconium-95, niobium-95, and of strontium-90 were not similar, nor did their patterns compare favorably with the patterns for the other radionuclides.

Safety

Analyses of fish taken from the Clinch River show that no more than 2.5 percent of the maximum permissible intake (MPI) could be received by a person eating 37 pounds of fish per year from East Tennessee rivers. This MPI is that given by the International Commission on Radiological Protection and by the National Committee on

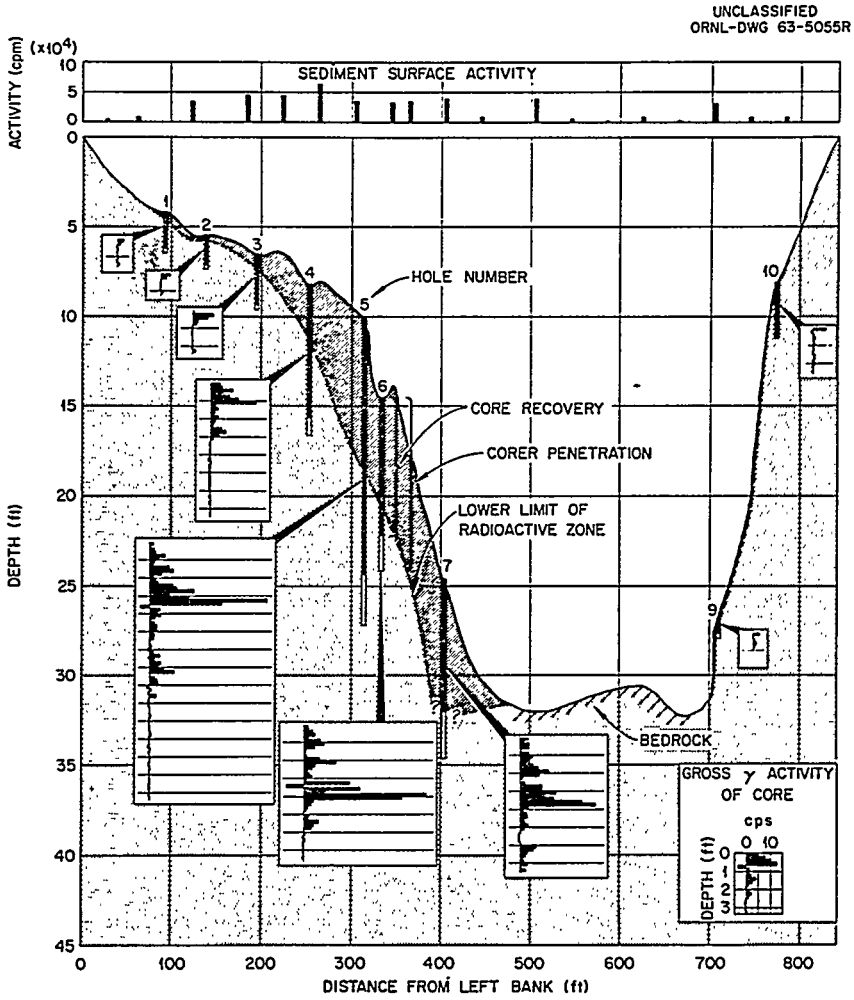

Cross section 7.5 miles upstream from the mouth of the Clinch River, showing penetration, recovery, and gross gamma radioactivity variations with depth for 1962 bottom sediment core samples (vertical exaggeration 20:1). Radioactive river bottom sediment is thickest on the less steep side of the stream channel at downstream sections. A recurring pattern of variation in radioactivity with depth appears to reflect variations in the amount of radioactivity released annually to the river.

Radiation Protection for the population at large. Radiation levels, adjacent to filter beds in water plants on the Clinch River upstream and downstream from the point of entry of White Oak Creek, are at background.

MINERAL EXCHANGE STUDIES

Studies of Cesium Selective Minerals

Many naturally occurring minerals, with and without treatment, have been studied in order

to understand the mechanism of selective retention of cesium and to improve waste-disposal operations. Explanations for the sorptive behavior of cesium, based on the structure of the minerals, were offered; but, since many different minerals and treatments were involved, these explanations were not accepted as completely satisfactory. More recently, cesium sorption curves, typical of responses by all the other minerals previously studied, were obtained with a single material, hydrobiotite, when suitably altered.

These responses are: (1) the amount of cesium sorbed by natural hydrobiotite decreases initially and then increases with higher amounts of cesium until the material is fully loaded (this type of response is similar to that observed when vermiculite is used); (2) with potassium-saturated hydrobiotite, there was a continuing decrease in sorption with increasing cesium concentration (this type of curve is also obtained with the minerals: illite, muscovite, biotite, and heated montmorillonite); and (3) hydrobiotite treated first with stable cesium shows a constant amount of sorption over a wide range of cesium concentrations (this type of curve is typical for kaolinites and natural montmorillonites).

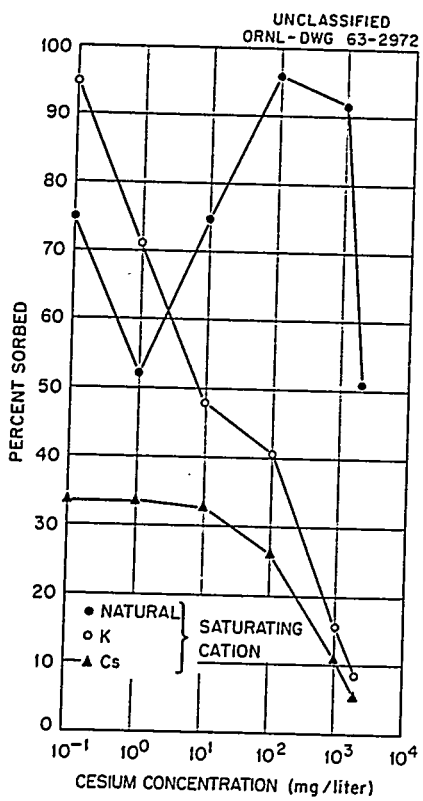

Cesium removal by hydrobiotite saturated with several cations. From the use of curves such as these, the best material for removing cesium from waste solutions can be selected. Studies at ORNL have helped in explaining the slow movement and the strong retention of cesium released to the ground.

When the atoms of the different minerals arrange themselves, they differ principally in how they stack. Both montmorillonite and the hydrobiotite materials stack themselves in their natural state with ample room for water molecules between layers of groups of atoms. Cesium ions, when they are present, will attach themselves on the surface or go in between the stacks. With montmorillonite, the stacking arrangement of 14 angstroms is not favorable for cesium and not very much cesium is sorbed. The stacking is similar with natural hydrobiotite and vermiculite, but the atoms making up these minerals are different from those of montmorillonite. Because of this difference in the atomic composition, their affinity for cesium increases as more cesium goes on the mineral, unlike the response of montmorillonite which remains insensitive to increases in cesium. The continual increase in affinity is caused by the conversion of the stack from the "water" type mentioned above to the dehydrated or illite type. Hydrobiotite if first treated with potassium, and montmorillonite if heated to 700°C, become permanently dehydrated, and their stacking pattern is similar to that of illite.

The minerals mentioned above are common components of our soils; consequently, by analyzing the soil for its mineral content, it is possible to predict the sorption one might expect in the event of contamination. These studies are also useful for clay mineral identification. Small amounts of clay impurities can be identified by direct observation or by observing the response after heating or potassium treatment. Studies of several "pure" clay minerals revealed impurities heretofore unknown or only suspected.

An understanding of the mechanism of cesium sorption has been useful in explaining the low uptake of cesium by plants observed by ecologists

and in producing efficient sorbents for waste decontamination. Similar studies are continuing with reactions of strontium and the results are encouraging.

DISPOSAL OF RADIOACTIVE WASTE IN GEOLOGIC FORMATIONS

Disposal in Natural Salt Formations

The major effort in the Oak Ridge National Laboratory studies on the disposal of high-level solid radioactive wastes into underground salt formations is the design, construction, and operation of a field demonstration in a Lyons, Kansas, salt mine. This demonstration, to be initiated early in 1965, will use 14 Engineering Test Reactor fuel assemblies, contained in seven cans and located around a center can in a circular array of holes in the mine floor, to simulate the heat and radiation anticipated in wastes solidified by the proposed high-level waste treatment processes. Fuel assemblies are being used because pilot plant solidification of wastes containing the required activity levels will not be initiated for at least 2 years. The demonstration will last for 2 years, during which time the fuel assemblies will be exchanged for fresh assemblies three times to increase the radiation dosage to the salt and to perfect handling equipment.

The engineering and scientific objectives of the demonstration are the development of the waste-handling equipment and techniques; determination of possible effects of radiation on hole closure, floor uplift, and mine stability in an area where the salt temperatures range from 100 to 200°C; the determination of possible radiolytic production of chlorine; and the measurement of creep and plastic flow of salt at elevated temperatures. This information will be used later in the design of an actual disposal facility.

As presently planned, the fuel assemblies, after canning in Idaho, will be shipped by rail in a

Simplified cross section of the demonstration experiment of high-level radioactive solids disposal in salt. The shipping cask is transferred from the railroad car and erected over the waste-charging shaft. The cans containing the fuel elements (used to simulate radiation and heat generation in solid wastes) are lowered one at a time down the shaft into the underground transporter. The transporter moves the cans from the waste shaft area to the experimental area where they are lowered into storage holes drilled in the salt.

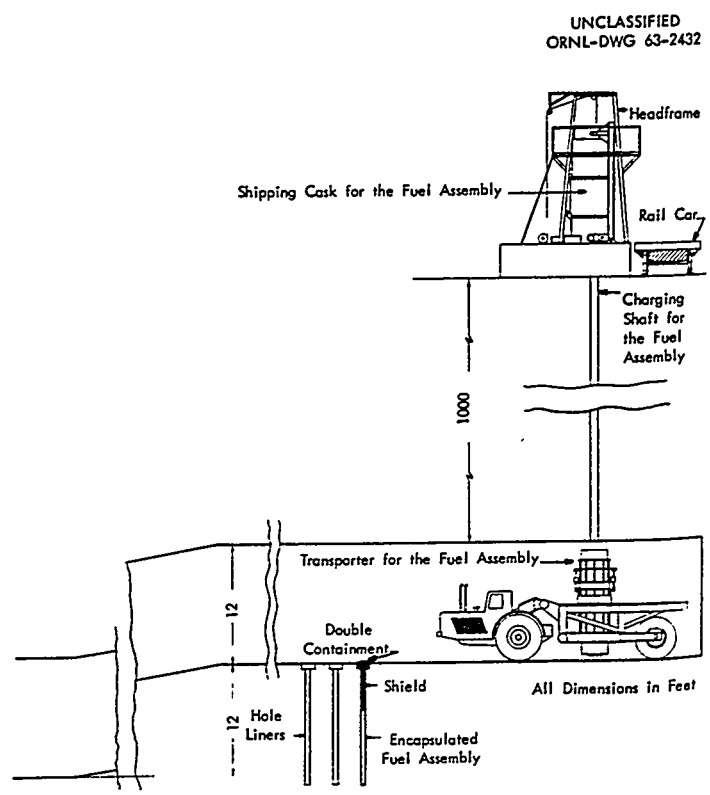

modified carrier. At Lyons, the carrier will be removed from the rail car and up-ended over a cased, vertical shaft extending to the mine approximately 1000 feet below. The canned assemblies will be lowered, one at a time, through the shaft and into a movable shielded cask, mounted on a fuel assembly transporter. The transporter will move to the experimental area where the cask will be positioned and lowered over the designated hole in the floor. The can will then be lowered through the bottom of the cask into the storage hole. These holes will have metal liners to ensure that the fuel assemblies can be removed from the salt for return to Idaho at the completion of the experiment.

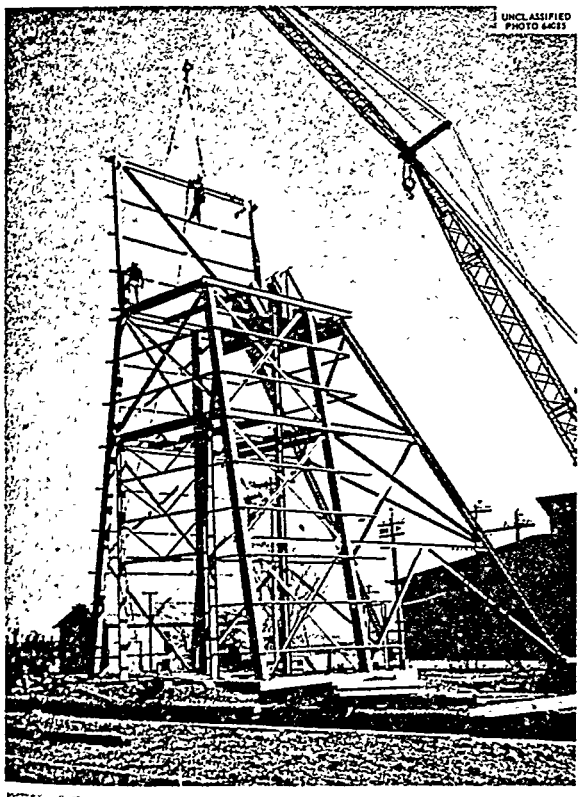

New headframe being erected at the Carey salt mine in Lyons, Kansas. The headframe is 45 feet high and is designed to lower experimental and mining equipment down the main hoisting shaft.

Renovation of the existing mine facilities for the demonstration is currently under way. A new headframe has been erected to allow lowering of the experimental and mining equipment into the mine. As soon as this topside work has been completed, underground preparations, including mining of the experimental area, will be initiated.

Disposal in Permeable Formations by Well Injection

Large volumes of liquid may be isolated from flowing surface and ground waters by injection into deep permeable formations. The use of wells to dispose of brine in deep permeable formations is a current practice in the petroleum industry. An advisory committee is continuing to review and coordinate the activities of several agencies participating in developing this method for disposal of radioactive wastes. ORNL, the U.S. Bureau of Mines, the University of California, and the U.S. Geological Survey are represented on this committee.

In a geologic formation used for disposal, the radionuclides move along the same pathways as water, but the rate of movement of the radionuclides is reduced by sorption of the radionuclides by the geologic formation or by other processes such as filtration or precipitation.

In an ideal situation, where a uniform sandstone of moderately high water-transmitting properties is separated from other usable geologic strata by thick impermeable beds, flow from a central injection well would occur laterally in a nearly radial fashion. Movement of radionuclides laterally would be reduced by interaction of the radionuclides with the formation, and radioactive decay would lower the activity of low- and intermediate-level wastes to innocuous levels before extensive movement had occurred — probably within 1000 feet of the injection well. Vertical movement of radionuclides would be much less rapid than lateral movement because of the reduced rate of water movement through the less permeable strata in addition to the higher sorptive properties likely to be associated with the finer-grained capping formations.

In actual operations, the receiving formation will have somewhat less than ideal properties of water transmission and radionuclide sorption. It is for

this reason that field testing of methods for predicting radionuclide migration based on known properties of the formation must be conducted. Although the results of radionuclide migration from a single field test cannot be applied directly to an operating system, the methods of predicting the behavior of their migration can be used as guidelines in preoperational evaluation of a proposed disposal site.

Previous studies of strontium exchange by sandstones indicated that strontium behaves similarly to calcium and that sodium has a relatively minor effect on strontium exchange. When Versene (ethylenediaminetetraacetic acid) is added to solutions passed through mineral columns, the Versene forms a more stable complex with calcium than with strontium. As a result, the concentration of ionic calcium is reduced and the uptake of strontium by the mineral is increased, resulting in a slower rate of migration of the radioactive strontium. Other chelating reagents would also be useful in promoting the relative sorption of strontium compared to calcium, provided the calcium complex is more likely to be formed than the strontium complex.

Studies at ORNL indicate that cesium moves more slowly than strontium. Thus, since strontium has a greater hazard potential, its movement in the disposal formation will be more critical than that of cesium.

Hydrofracturing Pilot Plant

Various nuclear processes at ORNL generate about four million gallons per year of intermediate-level waste solution. This waste has a specific activity of about 0.015 curie per gallon and contains appreciable quantities of cesium-137 and strontium-90 isotopes with long half-lives contributing considerably to their biological hazard. It is planned to concentrate this waste solution in an evaporator and store the concentrate in underground tanks pending the development of a suitable process for permanent disposal.

The shale fracturing experiment is a test of such an ultimate disposal method. This experiment will consist of the injection of several forty-thousand-gallon batches of waste solution, mixed with cement and other additives, into an impermeable shale formation at an approximate depth of 900 feet. The injection pressure of the waste-cement mix will be sufficiently high to propagate a thin horizontal crack in the shale. As the injection of the waste-cement grout continues, this crack will be filled by the grout and extended further so that a thin, approximately horizontal grout sheet several hundred feet across will be formed during the course of the injection. Shortly after the completion of the injection the mix will set, thereby permanently fixing the radioactive wastes in the shale formation. Subsequent injections will form parallel sheets above the first, and 5 to 10 feet apart.

The site selected for the shale fracturing experiment is near ORNL. Here at several depths there are thick beds of shale that are nearly horizontal and extremely impermeable to water. Previous tests have shown that when cement grouts are injected into these beds the grout sheets that are formed are parallel to the inclination of the beds and exhibit no significant vertical movement.

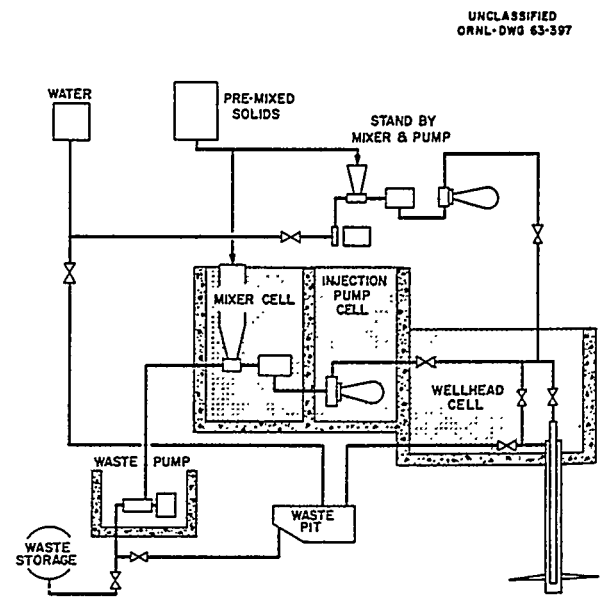

A schematic flow diagram of the shale fracturing experiment. The radioactive waste solution is pumped to the mixer cell, blended with solids, and pumped down the well and out into the shale formation. A standby mixer and pump will be used to clear grout from the well in the event of equipment failure. A recirculating waste system is provided for washing, slotting the injection well, and other purposes.

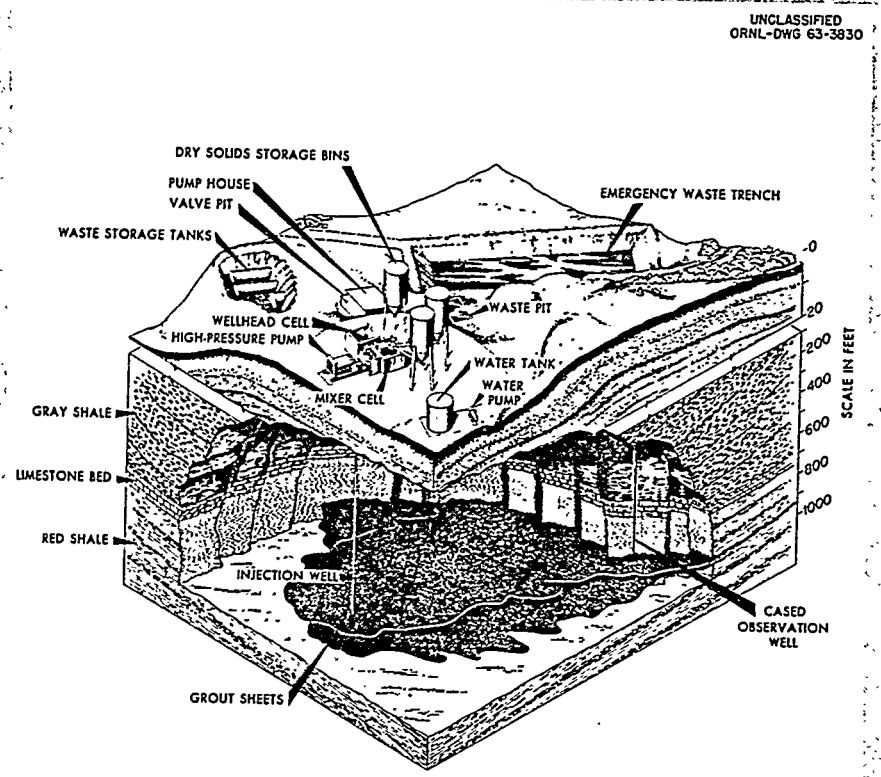

An isometric view of the shale fracturing experiment showing both the surface plant and the formation of the underground grout sheets. The radioactive waste solution is pumped from the storage tanks to the mixer cell where it is mixed with dry solids from the storage bins. The resulting grout is pumped down the injection well. A gamma-sensitive probe in the cased observation well will detect the grout sheet and thereby help establish its extent and vertical inclination.

copy rec'd JAW 11/12/92

The grout sheets were about $\frac{1}{8}$ inch thick, roughly circular in shape, and several hundred feet in diameter.

The mixes that are currently being considered for use with the shale fracturing experiment are cement-base mixes that contain a retarder to delay the time of setting and an extender to keep the cement in suspension. These mixes can be pumped for as long as 30 hours, will retain more than 98 percent of the associated water when they set, are usable with waste solutions with a wide range of concentrations, and are relatively cheap.

The equipment used for the injection of each batch of waste consists of a waste transfer pump and spare, four bulk storage tanks to store the cement and other solid constituents of the mix,

a jet mixer, a surge tank, a high-pressure injection pump, a standby injection pump and mixer, and assorted valving and special equipment. The mixer, surge tank, injection pump, and wellhead valving will be installed in cells to reduce the radiation exposure of the operators and limit the area that would become contaminated in the event of a leak in the equipment or piping. All necessary control operations will be carried out from the outside of the cell during an injection.

A series of four test injections is planned for the spring of 1964 to evaluate the mixes that have been developed, to obtain information on the performance of the surface plant, and to confirm the size and orientation of the grout sheets that are formed. The successful completion of this test series will establish the fracturing process as a demonstrated method for ultimate disposal of actual waste solutions.

FOAM SEPARATION STUDIES

Removal of Strontium from Process Waste Water Low in Radioactivity

Basic engineering at ORNL on the removal of strontium from waste low in radioactivity by foam separation have established the practicality of this relatively new operation. This information is being incorporated into the flowsheet for a pilot plant that will demonstrate a process for the decontamination of low-radioactivity-level process waste water at ORNL. The foam separation process uses differences in surface activity to separate components of a solution. The strontium is made surface active by chemically attaching it to an organic surfactant (sodium dodecylbenzenesulfonate is presently being used). The waste solution is fed to the top of a rising column of foam to provide a countercurrent flow of surface against liquid. The operation can be analyzed in a manner similar to the analysis of distillation or solvent extraction, if the surface is considered analogous to the second phase. Satisfactory gas spargers for forming foams, liquid distributors for introducing feed, and foam condensation equipment have been developed. Foam-drainage conditions, flow capacities, and unit performance have been studied on columns 6 and 24 inches in diameter. One-centimeter heights of transfer, indicating very efficient mass transfer, have been realized.

The low-level-waste pilot plant will remove most of the calcium and magnesium before the foam separation step by precipitation with sodium hydroxide and sodium carbonate. The foam column will be 4 square feet in cross section and 6 feet high; it will process 3 gallons per minute. The system will provide an overall decontamination factor of 1000.

HIGH-ACTIVITY-WASTE CALCINATION

In an effort to manage more safely the highly radioactive waste solutions produced by the processing of nuclear reactor fuels, the Oak Ridge National Laboratory has been studying methods for reducing the wastes to solids. The pot calcination process, which is the simplest and most straightforward of these processes, has been under development for several years. Simulated nonradioactive waste solutions have been used, but highly radioactive wastes will be used in the demonstration pilot plant at the Hanford Atomic Products Operation.

In the pot calcination process, the nitric acid is steam-stripped from the waste in an evaporator which produces a concentrated solution for feed to a heated calciner pot. The calciner pot is an upright cylinder, 8 to 18 inches in diameter, depending on the heat-generating properties of the waste, and 6 to 8 feet tall. The solids are retained, denitrated, and calcined in the pot; the vapors from the pot are condensed and returned to the evaporator. The pot, becoming the permanent container for the solid waste, is then disconnected from the system and is sealed and stored. The three most important waste types (Purex, Darex, and TBP-25) have been tested and show average rates of about 5 gallons per hour per pot. The residual nitrate in the solids is less than 300 parts per million, and the volume of the calcined solids is about an eighth of the liquid waste volume. The engineering studies on simulated waste have been successfully completed.

Since it is desirable that the final storage site be suited to storage of this type of waste (e.g., a special salt mine), and since it is unlikely that

such a site would exist at the processing plant, shipment of the pots seems unavoidable. This operation is probably the most hazardous in the waste management scheme. To reduce the risk in this operation conversion of the waste to leach-resistant glass, rather than a calcine, is being pursued. Purex and TBP-25 simulated wastes have been converted to glasses in pot calcination equipment by simply adding chemicals to cause the solids to fuse at high temperatures. This modification of the pot calcination process gives a lower processing rate.

Glass has more effectively been formed from aluminum TBP-25 waste in a continuous waste melter, which is fed with evaporated waste solution to which phosphoric acid and lead nitrate have been added. In this equipment, a rather large shallow pool of molten glass is maintained, onto the surface of which the aqueous solution is fed. A thin solid crust is formed, from the top side of which evaporation and calcination take place while the bottom is continuously being melted. There is no violent reaction when the liquid is introduced in this manner. The present melter uses a horizontal vessel (8 inches in diameter and 40 inches long) with a 25-kilowatt heat source. The molten glass is withdrawn continuously and is allowed to solidify in a final storage vessel. The off-gas from the melter is returned to the evaporator, as in the pot calcination process.

TBP-25 aluminum glass prepared in an 8-inch-diameter calciner pot by the rising-level procedure. Phosphate and lead have been added to the aluminum nitrate waste to cause it to melt.

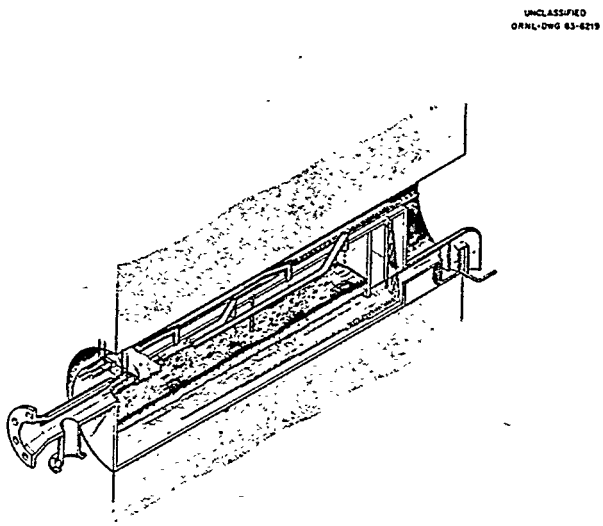

High-level waste continuous melter. Evaporator-concentrated liquid waste is fed directly onto a pool of molten glass through water-cooled feed lines. The liquid waste calcines and then melts. The melt is withdrawn continuously into a final storage vessel.

ENGINEERING, ECONOMIC, AND SAFETY EVALUATION

Evaluations of Waste-Management Methods

A study of the relative safety and cost of alternative methods for the management of radioactive wastes from power reactor fuel processing provides a means for selecting the best combination of operations and can indicate which methods should be developed for a nuclear power industry. One series of operations believed to represent acceptably safe management consists of interim storage of the wastes as liquids in tanks, followed by pot calcination of the wastes to produce relatively small volumes of thermally stable solids, interim storage of the pots, and, finally, shipment of the pots to salt mines for permanent disposal.

Studies at ORNL indicate that these sequential management steps should range in cost (in units of mills per kilowatt-hour of electricity delivered by the reactor plant) from 0.002 to 0.01 for interim

liquid storage, 0.009 to 0.050 for pot calcination, 0.002 to 0.005 for interim storage of the pots, 0.004 to 0.040 for 1000-mile shipment of the pots, and 0.006 to 0.030 for final disposal in salt. It was estimated that final disposal of the pots in concrete vaults would cost five to seven times as much as their disposal in salt. The range of total costs for these steps was from 0.025 to 0.095 mill per kilowatt-hour, and the optimum cost was about 0.030 mill per kilowatt-hour. The latter is only about 1 percent of the total reactor fuel cycle cost and represents an acceptable contribution to the expected cost of nuclear electricity.

The effects of fission product removal on total waste-management costs were estimated according to optimistic expectations of future processes for separating the fission products. The cost of managing wastes that are 90 to 99 percent depleted in fission products is about 70 percent as much as the cost of managing wastes from which no fission products have been removed. This difference is not enough to pay for the separation and handling of fission products; consequently, fission product removal must be justified and paid for by the market for fission product radiation and heat sources, with only a marginal credit from the reduced cost of waste management.

Studies and Evaluations

STUDIES RELATING TO SHIPPING CONTAINERS FOR SPENT REACTOR FUEL

The Laboratory has been testing casks used to contain and shield irradiated reactor fuel assemblies during shipment. The purposes of the tests are to determine resistance of containers to impact and to gather data to aid in establishing federal regulations covering the structural integrity of such casks. Attempts have been made to correlate the data from model casks so that damage to full-scale casks can be accurately predicted. Over 50 drop tests were made.

Five cylindrical steel-shelled, lead-filled casks each weighing approximately 1.3 tons and two similar casks each weighing 6 tons were dropped onto a 4 ½-inch-thick slab of armor plate backed up by more than 5 feet of reinforced concrete. Drops were made with the cylindrical casks in a horizontal attitude, at a 45° angle, on end, and onto a piston. Many casks were equipped with strain gages, accelerometers, and compressometers and were coated with a brittle lacquer, which cracked under high stress on impact. The two major results were:

1. The casks did not rupture when dropped 15 feet onto a solid surface, with any surface of the cask perpendicular to the direction of fall. With adequate welds and an optimized design, they should be able to withstand a 30-foot drop.

2. The damage resulting from testing the casks of two different sizes under identical conditions showed a great amount of similarity. Until reliable mathematical methods are established to determine impact resistance, model testing may provide an adequate and inexpensive method of evaluating the behavior of a prototype cask on impact.

To evaluate temperature control for pin-type fuel elements, it is necessary to be able to predict temperature variations under given conditions throughout the tube bundles which make up the elements. Mockup stainless steel pin-type fuel elements were provided with internal resistance heaters and placed in cavities that simulate the inside of shipping containers. Heat transfer from pin to pin in air was studied in bundles that contained up to 64 closely spaced pins. It was determined that, even at temperatures above a few hundred degrees Fahrenheit, heat loss to the inside walls of the cask is primarily by radiation rather than convection. Temperatures throughout the bundle can now be predicted with a reasonable degree of confidence.

A manual summarizing all available data on reactor assembly fuel shipping is being written to assist persons interested in such work.

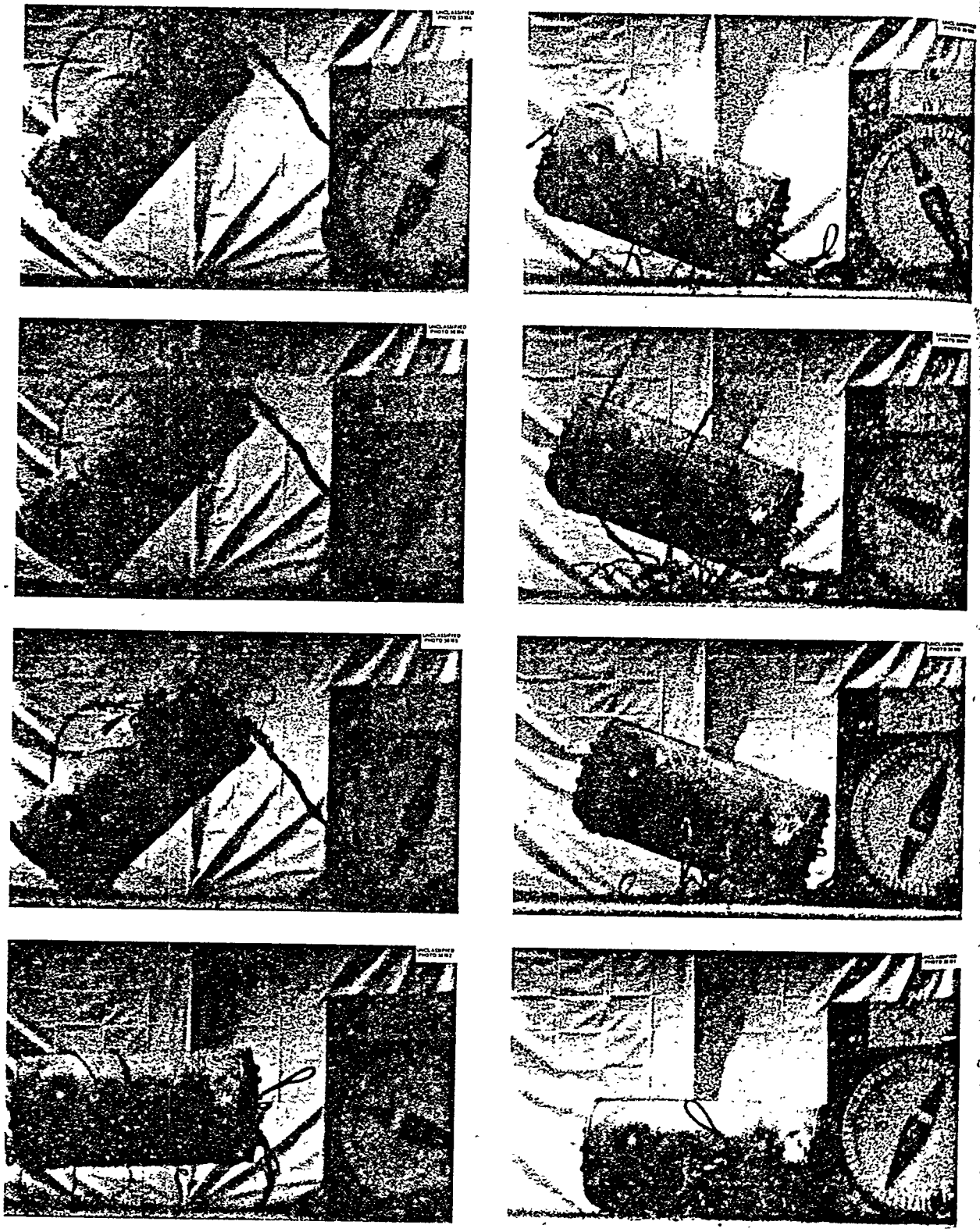

Drop test of a model fuel-shipping cask. This sequence of pictures shows the initial impact of the cask (top to bottom at left) and the subsequent bounce before the cask came to rest (top to bottom at right). In this test, the 1.3-ton cask was dropped at a 45° angle from a height of 15 feet onto a 4½-inch-thick armor plate set in a 5-foot-thick slab of reinforced concrete. The drop resulted in a faint hairline crack in a poor weld area at the point of initial impact.

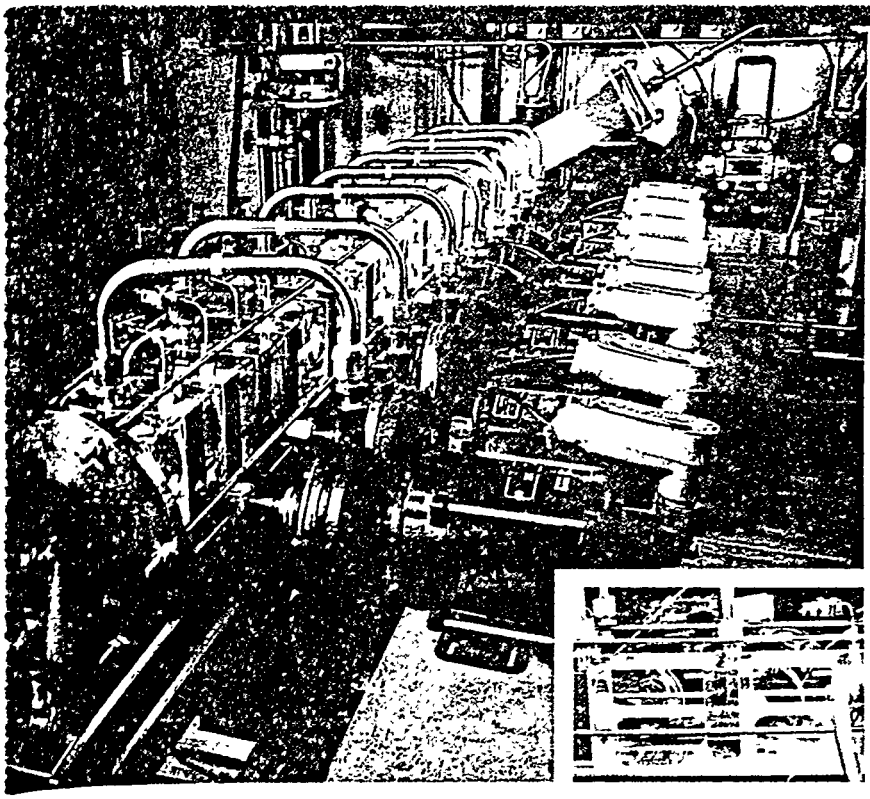

Physical Research

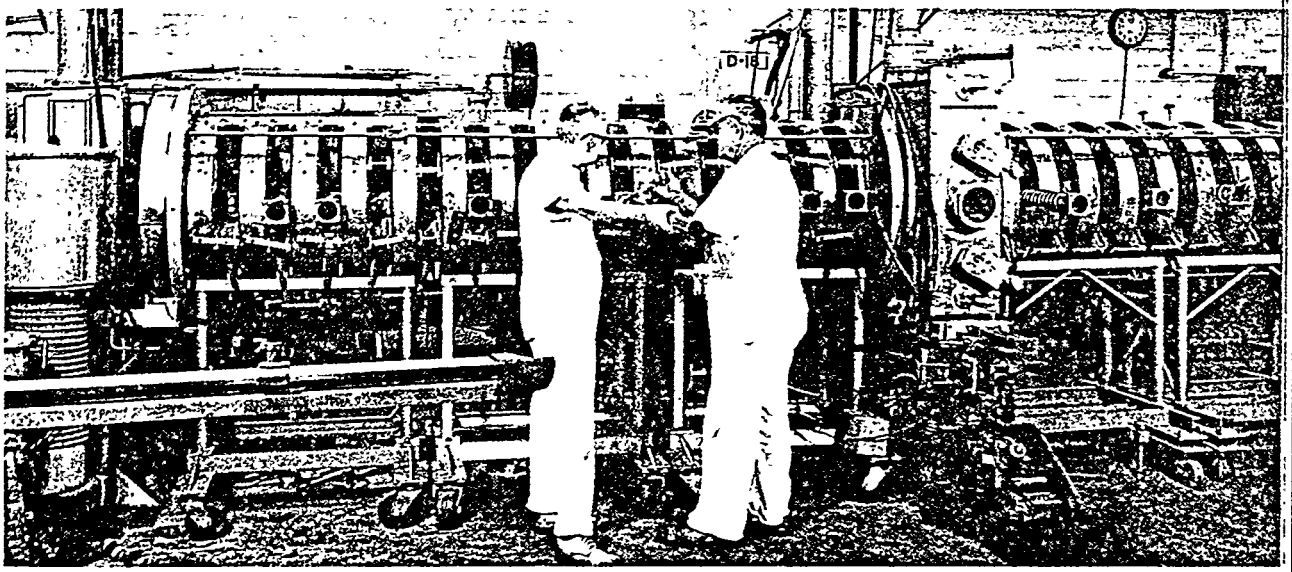

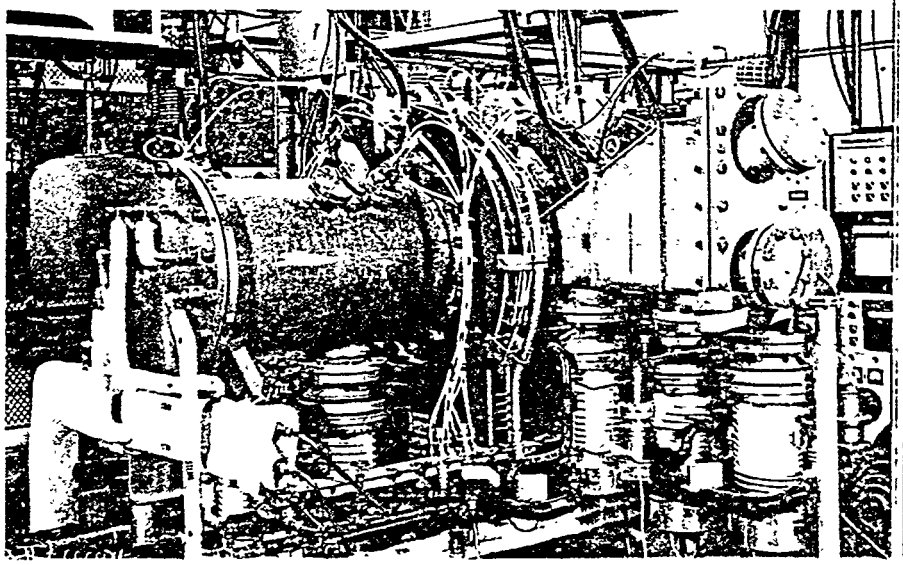

Physics and Mathematics

NEUTRON CAPTURE AND COSMOLOGY

Nuclear power, nuclear weapons, and cosmology have a lot in common. The detailed knowledge of nuclear structure, vital to the understanding of these processes, is that common bond. Fundamental knowledge about a particular nuclear reaction, neutron capture in the kilo-electron volt energy range, is directly applicable both to the study of stellar nucleosynthesis (formation of elements in the universe) and to the design of more efficient nuclear reactors. During the past several years, physicists at the Physics Division's High-Voltage Accelerator Laboratory, in collaboration with colleagues at the California Institute of Technology and Rice University, have been studying capture reactions with both nucleosynthesis and reactors in mind.

The region of common interest corresponds to neutron temperatures of (3–8) $\times$ 10^8 °C, typical both of the interiors of red giant stars and of the energies of neutrons in fast reactors. Investigations of the origin of elements heavier than iron have led to two proposed mechanisms. One has to do with sudden events such as supernovae and is therefore difficult to investigate directly. The other, called the "*s*-process," is characterized by slow reaction times as found in red giant stars and is subject to quantitative investigation as outlined in this report. Special techniques have been developed here to produce these neutrons and to measure their energies and reaction rates. In fact, these new beam-pulsing and time-of-flight techniques, described in another section of this report, are being applied to many other measurements in nuclear physics. Some of the most interesting capture studies involve small samples of separated stable isotopes. *In order to perform the measurements, techniques were developed to measure within a few percent the speed of a neutron traveling at five million miles per hour over a flight path of only 3 inches!*

A sensitive experimental test of the *s*-process synthesis hypothesis was first proposed by W. A. Fowler and associates at the California Institute of Technology. Briefly, the process calls for a close correlation between capture cross section and universal abundance for a large number of nuclides lying in the mass table along the valley of beta-decay stability. Correlations between different elements cannot be established very accurately, largely because of historical chemical fractionation problems. However, studies of correlations between *isotopes* of a given element completely avoid this problem and provide a very quantitative testing ground.

The first test, proposed by Fowler, was with isotopes of tin, electromagnetically enriched at ORNL. The results, namely the inverse correlation between isotopic abundance and capture cross section near 25 kilo-electron volts, were in disagreement with Fowler's predictions, but the apparent disharmony was brought into quick accord by a reestimate of a contribution due to another stellar synthesis process (apparently due to supernovae). A completely unambiguous test was next devised at ORNL by measuring capture in certain samarium isotopes. In this case no "contamination" due to other processes was possible, and remarkable agreement with the hypothesis was

Summary of Neutron Capture in Isotopes of Samarium at 30 (±7) Kilo-electron Volts

The *s*-process hypothesis of stellar nucleosynthesis of heavy elements identifies certain stellar interiors as the location of synthesis via capture of approximately 25 kilo-electron volt neutrons. The theory predicted that the product of cross section times isotopic abundance for samarium-148 and samarium-150 should be equal. The experimental results (column 4), when multiplied by abundance, gave excellent agreement with the prediction. Once the *s*-process contribution was determined, the *r*-process contribution was found by subtraction.

A	N (atom %)	Class[a]	σ_c(mb)	$N_s\sigma_c$	N_s (atom %)	N_r (atom %)	A
144	2.87	*p(m)*	119 ± 55				
147	14.94	*rs*	1173 ± 192	(2850)	2.4 ± 0.4	12.5 ± 0.4	147
148	11.24	*s-o*	258 ± 48	2930 ± 540			
149	13.85	*rs*	1622 ± 279	(2850)	1.8 ± 0.3	12.1 ± 0.3	149
150	7.36	*s-o*	370 ± 72	2770 ± 535			
152	26.90	*rs*	411 ± 71	(2850)	6.9 ± 1.0	20.0 ± 1.0	152
154	22.84	*r-o*	325 ± 61	0	0	22.84	154

[a]Symbols designating nucleosynthesis production mechanism are: *p(m)*, photonuclear and proton capture; *r*, rapid process; *s*, slow process; *s-o*, pure *s* process; and *r-o*, pure *r* process.

found. The confidence gained in these results has already led to new independent estimates of the chronology of our galaxy.

The capture measurements also showed that samarium as found on the earth has *not* been subjected to any significant thermal flux of neutrons. Such a flux had been proposed as a means of accounting for certain light-element isotopic abundances.

The results of these measurements have provided a secure experimental basis for the *s*-process theory of heavy-element synthesis in stellar interiors and have helped to show the relative importance of supernovae in the synthesis of the heaviest elements. One new understanding that has emerged with quantitative proof is that most of the material of the earth was formed by means of many round trips through star formation, explosion, and re-formation into new stars. Many of these same capture measurements have already been utilized in advanced reactor design and have enabled the designers to make more intelligent choices of structural materials as well as more accurate estimates of neutron economy.

ACCELERATOR TERMINAL PULSING AND KLYSTRON BUNCHING

Studies of nuclear structure are of fundamental importance in the understanding of nuclear physics and the development of nuclear power. Of all nuclear reactions that are studied in the investigation of nuclear structure, neutron reactions are most directly related to the knowledge required to advance nuclear technology. However, since the neutron carries no charge, the traditional and highly refined methods of energy measurement developed for charged particles are not applicable. Instead, the time-of-flight method for measuring neutron energies has been gradually developed until it now plays a dominant role in most neutron experiments. This detection method depends on a measurement of the time taken by the neutron to cover a given distance; from this measurement the velocity and, hence, the energy is deduced. Neutrons in the kilo-electron volt and million electron volt energy range are usually produced by bombarding suitable targets with repetitive bunches of accelerated charged particles, such as

Cross-sectional diagram of Van de Graaff terminal pulser-buncher. Terminal pulsing was first developed at ORNL using a radio-frequency ion source. The duoplasmatron ion source was adapted more recently since it is capable of higher gas efficiency and beam quality. The beam is swept in a Lissajous pattern at the pulse aperture by mixing oscillations of 3 and 1 megacycles per second. This sinusoidal sweeping produces a 1 megacycle per second pulse with variable length (3 to 20 nanoseconds). For higher peak ion currents or bursts down to less than 1 nanosecond in time, a properly phased klystron bunching voltage is applied immediately below the sweep aperture which causes the pulse to coalesce in time at the target.

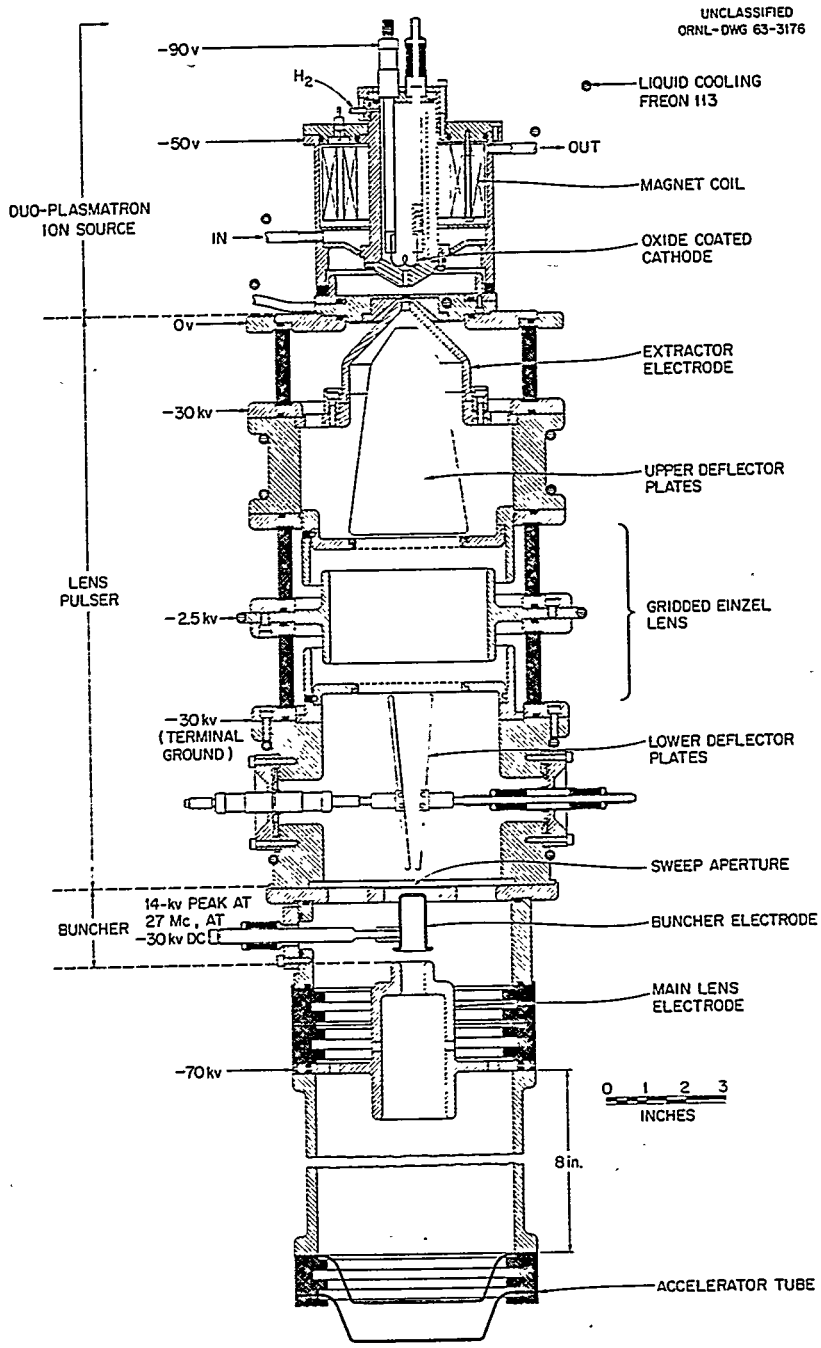

protons, which are sharply defined in time. The accuracy of the time-of-flight method is thus directly related to how sharp and how intense one can make the accelerated charged-particle bunches.

Special new techniques for producing extremely short and intense bursts of neutrons have been developed in the Physics Division's High-Voltage Accelerator Laboratory. An extra benefit from these developments is that they have greatly extended the productive lifetime of many Van de Graaff accelerators by virtue of their increased versatility and new capabilities. The principal technique is that of ion beam pulsing at the high-voltage end of a Van de Graaff accelerator, developed at the High-Voltage Accelerator Laboratory. This involves the formation of short bursts of ions just prior to their acceleration by means of sinusoidal sweeping of a high-quality ion beam across a small aperture. A new development in 1963 was the preacceleration *klystron buncher*, which helps produce extremely short bursts of ions less than 1 nanosecond ($<10^{-9}$ second) in duration. The buncher produces a small energy spread in the input pulse which causes it to coalesce in time at the target. Klystron bunching has thus replaced an earlier, considerably less versatile, technique for doing this (used at other laboratories) that was almost ten times more expensive. The earlier technique was a postacceleration magnetic buncher. It is estimated that the taxpayer's investment in this development will be amortized several times over each year in new research equipment costs alone, in addition to the scientific values that are already evident.

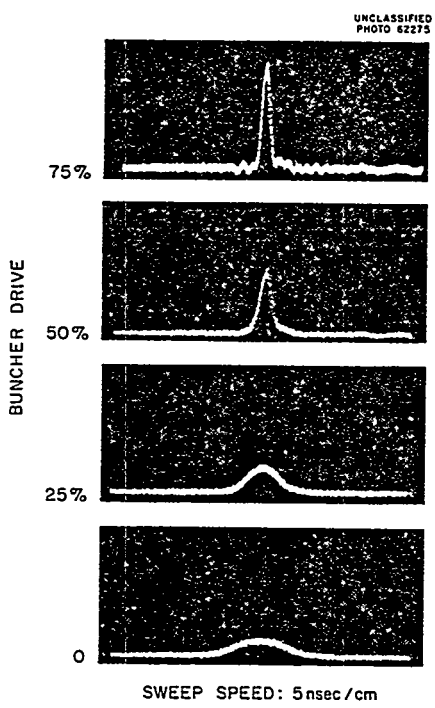

Response of a proton burst from the terminal pulser-buncher as a function of buncher amplitude. The bottom pulse has a full width at half maximum of about 5 nanoseconds. At 75 percent bunching oscillator amplitude the pulse width has decreased to less than or equal to 1 nanosecond, and its height increased proportionally (about a factor of 10). The oscillations apparent in the uppermost photo are due to an electronic "ringing" and do not represent pulse satellites.

Free Neutrons and Gravity

Prior to 1963 the most accurate measurement of the gravitational constant, *g*, for free neutrons had an uncertainty of 7.5 percent. Motivation for a careful measurement of this constant was enhanced by a recent theoretical suggestion that *g* might differ for the two vertical spin projections ($\pm\frac{1}{2}$) of the neutron. Low-energy neutrons from the ORR were first diffracted through a beryllium filter, which defined their spin projection and energy. Then, after passing through spatial defining slits, their fall under the influence of gravity was measured over a 180-meter flight path. The results of the measurement gave a value of *g* accurate to 0.3 percent and indicated (1) excellent agreement with values for *g* using microscopic bodies, and (2) that the suggested spin orientation dependence is not confirmed.

GAMMA RAYS FROM RESONANCE NEUTRON CAPTURE

When a neutron is absorbed by a nucleus, the process is almost always followed by a burst of gamma rays that emerge as the new nucleus settles down. In the past the study of gamma rays from capture of thermal neutrons has provided abundant information about excited states of the product nuclei and also some systematics about the capture process itself.

Experimentalists have always wanted to study gamma rays from resonance neutron capture because the quantum description of the initial conditions is uniquely known (frequently not so for thermal capture), and the initial conditions can be varied for a given nucleus by varying the neutron energy. This kind of experiment has finally become possible by using the high-current pulse Van de Graaff and high-efficiency gamma-ray detectors, both developed at ORNL.

It has been sometimes said that low-energy nuclear physics research is a dying field since we know so much about the subject. Our first experiment with this new equipment, the spectra of gamma rays from 27 kilo-electron volt resonance capture in (fluorine-19 + n) is a case in point. All previous experience led us to expect a preponderance of high-energy transitions leading to, or near the ground state of, fluorine-20. We observed, however, that in fact these transitions are almost totally absent. Thus the study of spectra from resonant capture is shedding new light on neutron capture reactions, a subject of fundamental importance in the understanding of nuclear structure and therefore the exploitation of nuclear forces.

Nuclear Reaction Theory

The attempts to provide a formal mathematical description of nuclear interactions have led to several highly successful "models," such as the "shell model," the "collective model," the "optical model," and others. Each model is successful only over a limited range of nuclei, energy, etc. In addition to gains in fundamental insight into the nature of these processes, these models can save us money; that is, they can in many cases be used to *calculate* an effect instead of measuring the effect (normally a much more expensive job). For example, a few well-chosen measurements of neutron elastic scattering can be used with the optical model to accurately compute cross sections for many nuclei over a wide energy range. The models can also guide the experimentalist toward the more valuable and critical experiment.

During 1963, several forms of the optical model were developed to higher degrees of sophistication and thus have higher accuracy and wider application. For example, the highly successful application of distorted-wave analysis to low- and medium-energy reactions was further refined to

Gamma rays from 27 kilo-electron volt neutron capture in fluorine-19. Since this well-known p-wave level has $J^{\pi} = 2^{-}$, $E1$ transitions are allowed to and near the ground state. We observed, to our surprise, that such transitions are virtually missing, and instead the nucleus decays by $E1$ and $M1$ radiation to higher-lying states. The vertical spikes along the abcissa indicate positions and relative intensities of gamma rays from thermal (2^{+}, 3^{+}) capture.

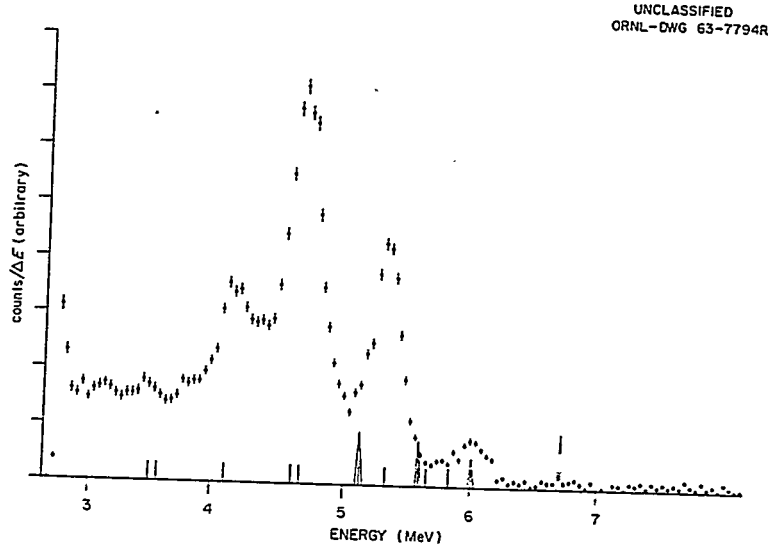

include a spin-orbit portion to the interaction. The complex computer codes that result from such calculations are being used to analyze literally hundreds of experimental results obtained in many laboratories.

NUCLEAR RECOILS FOLLOWING RADIOACTIVE DECAY

When a nucleus undergoes the nuclear transformation known as beta decay, the process involves the beta particle (an electron), the very elusive neutrino, and the recoiling product nucleus. An important question that arises from fundamental nuclear theory can be stated thus: Do the electron and neutrino leave the nucleus in the same direction or in opposite directions? Physicists at Oak Ridge National Laboratory have determined an accurate answer to this question in a unique "neutrino detective" experiment.

The neutrino is extremely difficult to detect in a direct sense, but it leaves evidence behind that enables the physicist to infer what happened. This evidence can be uncovered if one can measure the angles at which the electron and nucleus recoil and also the energy of the recoiling nucleus. In order to do this, the physicists had to work with highly radioactive gases at very low pressures in a spectrometer developed for this purpose. The results of the experiments on helium-6 and neon-23 beta decay show that the electron and neutrino emerge from the nucleus in opposite directions. Furthermore, no evidence was found for any other emission mode, in agreement with the current "universal theory" of beta decay.

The spectrometer has proved sensitive and accurate enough to be used in the further study of secondary effects in beta decay. While these effects are "secondary" in a phenomenological sense, they are of fundamental importance in learning just how the nucleus is held together.

DATA INFORMATION AND EVALUATION CENTER

The rapid accumulation and increasing publication rate of scientific information are well known, and numerous efforts have been made to keep summary and reference collections up to date, particularly in the field of nuclear structure. Without the services of *good* data-summary information, an experimentalist in nuclear structure must either digest about ten relevant papers each working day or else slowly lose track of activities outside his immediate field of research. The collecting and summarizing of data needs the services of active scientists in the field, since value judgments must be made. To this end a significant amount of activity in data accumulation and evaluation has evolved at Oak Ridge National Laboratory. A charged-particle cross-section center is located where physicists active in the field can lend part-time support. The Nuclear Data Center, formerly located in Washington, is now located at ORNL. Several ORNL scientists spend a fraction of their time at other data centers, such as the neutron cross-section center at Brookhaven, as advisors in their own field of specialization. The publications from these centers serve to help the physicist maintain a broad acquaintance with his general area of interest and to give an outsider relatively easy access to needed scientific data. They do not replace, however, the indispensable frequent personal contacts within a given specialty.

SHIELDING AGAINST HIGH-ENERGY RADIATIONS

Studies of shielding against high-energy radiations are being conducted at the Laboratory with a twofold purpose: the prediction of radiation levels in the vicinity of particle accelerators and the prediction of radiation doses to which astronauts will be subjected. Because each of these problems is concerned with shielding against protons and electrons, much of the research is common to both, but there are important differences. For example, the energies of protons from solar flares or from a Van Allen belt which must be considered in space-vehicle shielding are usually less than 1 Bev, whereas the energies of particles from an accelerator beam can be much greater. (Calculations for the proposed Stanford accelerator have been for energies up to 45 Bev.) Also, the shields proposed for space vehicles

are relatively thin, while those in accelerator designs are very thick.

The ultimate goal in these studies is to develop methods for calculating the effectiveness of any proposed shield. Such calculations must accurately predict not only the attenuation of the primary source, but also the attenuation of the many secondary radiations born in the shield as a result of interactions of the primary particles. But for the calculations to be reliable, the cross sections for the interactions must be available: that is, the secondary particles and their energies and angular distributions must be known. Unfortunately, there is a dearth of such information, and for the extremely high energies encountered in accelerator shielding the basic physics is not even known. Thus one of the goals of the studies at ORNL is to supply the required cross-section data.

For space-vehicle shields it appears that the secondary particles to be considered are neutrons, protons, and gamma rays. For accelerator shields, pions and muons must also be included. Since any attempt to measure all the reactions in which these secondaries are produced would be impractical, methods are being devised for calculating them. The calculations must, of course, be validated by comparison with experimental values for at least a few energies, and where no such values are available they are being obtained through experiments performed at various accelerator facilities.

Thus far experiments have been performed at the Harvard University Synchrocyclotron for 160-Mev protons incident on targets of beryllium, carbon, oxygen, aluminum, cobalt, and bismuth. The spectra of secondary gamma rays from these materials were measured with multiple-crystal scintillation spectrometers, and the spectra of neutrons and protons were obtained with proton-recoil spectrometers and by time-of-flight techniques. In addition, measurements were made of the total energy deposited at various points within a spherical, water-filled Lucite phantom, 42 centimeters in diameter, by secondary particles from these targets.

In an additional experiment, performed in cooperation with the Rutherford High-Energy Laboratory, nuclear emulsions were placed at various positions in a steel shield exposed to a narrow 9-Bev proton beam. The exposed emulsions were scanned for shower-track intensity, defined as the number of charged particles above a certain energy crossing the unit area per incident beam particle, and for star density, defined as the number of interactions per unit volume.

As discussed previously (ORNL-3350, p. 97), Monte Carlo intranuclear cascade calculations are being performed to predict the needed cross sections. Results are available for neutrons and protons incident on carbon, oxygen, aluminum, chromium, copper, ruthenium, cesium, tungsten, lead, and uranium at energies between 25 and 400 Mev. Substantial progress has been made in extending the energies to 2 Bev.

A Monte Carlo transport code which uses the intranuclear cascade data to compute the energy deposited in tissue by both protons and neutrons has been completed for source energies up to 400 Mev. Calculations with the code have yielded the first defensible flux-to-dose conversion factors for this energy range.

A one-dimensional transport code (ORNL-3350, p. 97) has been developed for calculating the penetration of high-energy particles through the thick shields proposed for accelerators. For such deep-penetration studies the truncation error is of major concern, and its effect was investigated by comparing results obtained with the code with those from an analytic solution for a very special case. The agreement between the two methods tends to prove the numerical reliability of the code. It has been applied to a number of cases of interest to accelerator shielding, but the input cross-section data are still too crude to consider the results to be anything but approximate.

The one-dimensional transport code has also been used to obtain preliminary estimates of the attenuation of solar-flare protons by aluminum shields. It was found that for typical flare spectra the dose from secondary particles becomes comparable to the dose from the primary protons only for relatively thick shields (>50 g/cm^2).

The tissue doses obtained with the Monte Carlo transport code were combined with the primary proton flux computed with the one-dimensional code to construct a series of "importance functions" which show the relative importance of various energies in a solar-flare proton spectrum. The importance always increases with decreasing proton energy (to the lowest energy that can now be calculated), and this fact has strongly influenced the plans for further calculations and experiments.

MASS SPECTROMETRY

A method was devised for determining gas contaminants in quartz capsules that contained UO_2-Al fuel pellets. Space and equipment for the high-alpha, double-magnet mass spectrometry laboratory were put in order. A routine based on a daily isotopic standard was devised and used to analyze about 200 potassium samples. A manual, *Isotopic Mass Spectrometry of the Elements,* is being published.

THERMAL DIFFUSION ISOTOPE SEPARATIONS

The thermal diffusion program is responsible for the development of techniques and equipment required for enriching isotopes in elements especially adaptable to the thermal diffusion process.

The most notable characteristic of our work in thermal diffusion development was a shift of attention to the "middle" isotopes of neon (neon-21), argon (argon-38), and xenon (xenon-124) after previously enriching the "end" isotopes only. Achieving enrichment in the "middle" isotope of an element requires more complicated equipment and closer control of variable conditions affecting the separation factors than is the case for "end" isotope enrichment.

By the end of 1963, we had obtained enrichments of 30.8 percent neon-21 (0.257 percent natural abundance), 23.1 percent argon-38 (0.063 percent natural abundance), and 4.4 percent xenon-124 (0.096 percent natural abundance). A newly installed calrod-heated system, replacing an antiquated hot-wire system, enriched krypton-86 from 17.37 percent to 81.2 percent in a six-month period; our goal is greater than 99 percent krypton-86.

MATHEMATICS AND PROGRAMMING RESEARCH

In order that the programming language ALGOL 60 might be used for writing programs for the Control Data 1604-A computer at ORNL, a translator program was written for the 1604-A in cooperation with Control Data Corporation. The translator has been checked out and put into operation. Programmers at the Laboratory may now make use of existing programs in ALGOL 60, many of which are continually being published in technical journals, and may also write their own programs in this language. ALGOL 60 is in wide use in scientific programming in Europe and the Soviet Union. The Laboratory is a member of a cooperative group known as ALCOR, with a considerable European and smaller American membership, which exists for the purposes of exchanging experiences with ALGOL 60 and making common use of programs written in this language. The translator for the 1604-A gives the Laboratory one of the finest implementations of ALGOL 60 in the ALCOR group.

Much of the development work on the translator is of theoretical interest. In parallel with its application to the 1604-A translator, the theoretical aspect was examined independently of any particular computer, carrying on work in this area which began when an ALGOL translator was written for the Oracle, the previous computer at ORNL. The documentation of both the theoretical and applied work is written largely in ALGOL 60 itself, which makes it readily accessible to those interested.

Electronuclear Research and Development

ACCELERATOR DEVELOPMENT

Introduction

The immediate goal of the accelerator development work of the Electronuclear Division is to make the Oak Ridge Isochronous Cyclotron (ORIC) a first-class research tool. For this purpose we are installing and inventing instrumentation which includes equipment for time-of-flight energy analysis, beam position indicators, an elaborate beam handling system, and a high-resolution magnetic spectrometer. The cyclotron is being developed to provide the experimenter with precise beams of a wide choice of particles accelerated to a broad range of exact energies.

The long-term goal of this program is to build a high-intensity proton accelerator (100 microamperes to several milliamperes) at an energy in the vicinity of 1 Bev. Whether the Mc^2 Cyclotron concept or the new Separated-Orbit Cyclotron idea will prove most advantageous, considering both research capability and cost, is as yet undecided. It is clear, however, that a high-intensity accelerator in this energy region will be a challenge to the designer and a boon to the experimenter.

The Oak Ridge Isochronous Cyclotron

The Oak Ridge Isochronous Cyclotron (ORIC) was brought up to full power operation, and a novel beam extraction system was developed to provide high-quality external beams. This versatile variable-energy cyclotron had previously been test operated with a temporary radio-frequency power supply.

The installation of the final stage of the radio-frequency power supply was completed in early 1963, and the internal beams of deuterons and alpha particles were brought up to full design energy, about 39 and 78 Mev. The first two elements of the beam extraction system, the electrostatic deflection channel and the coaxial magnetic channel, were installed, and the beam was deflected onto an internal probe. At this point the characteristics of the deflected beam were measured so that the design of the final extraction element, the compensated-iron channel, could be completed.

The development of an entirely new mode of beam deflection in ORIC has resulted in the extraction, with unusually high efficiency, of a high-quality beam. A carefully placed asymmetry in the magnetic field, introduced near the center, produces a controllable coherent radial oscillation in the beam and increases the spacing between orbits at the entrance of the electrostatic deflection channel. This minimizes the amount of beam lost by striking the septum which separates the deflected beam from the circulating beam.

An extracted beam of molecular hydrogen at 36 Mev is produced with an extraction efficiency of about 60 percent. This may be compared with

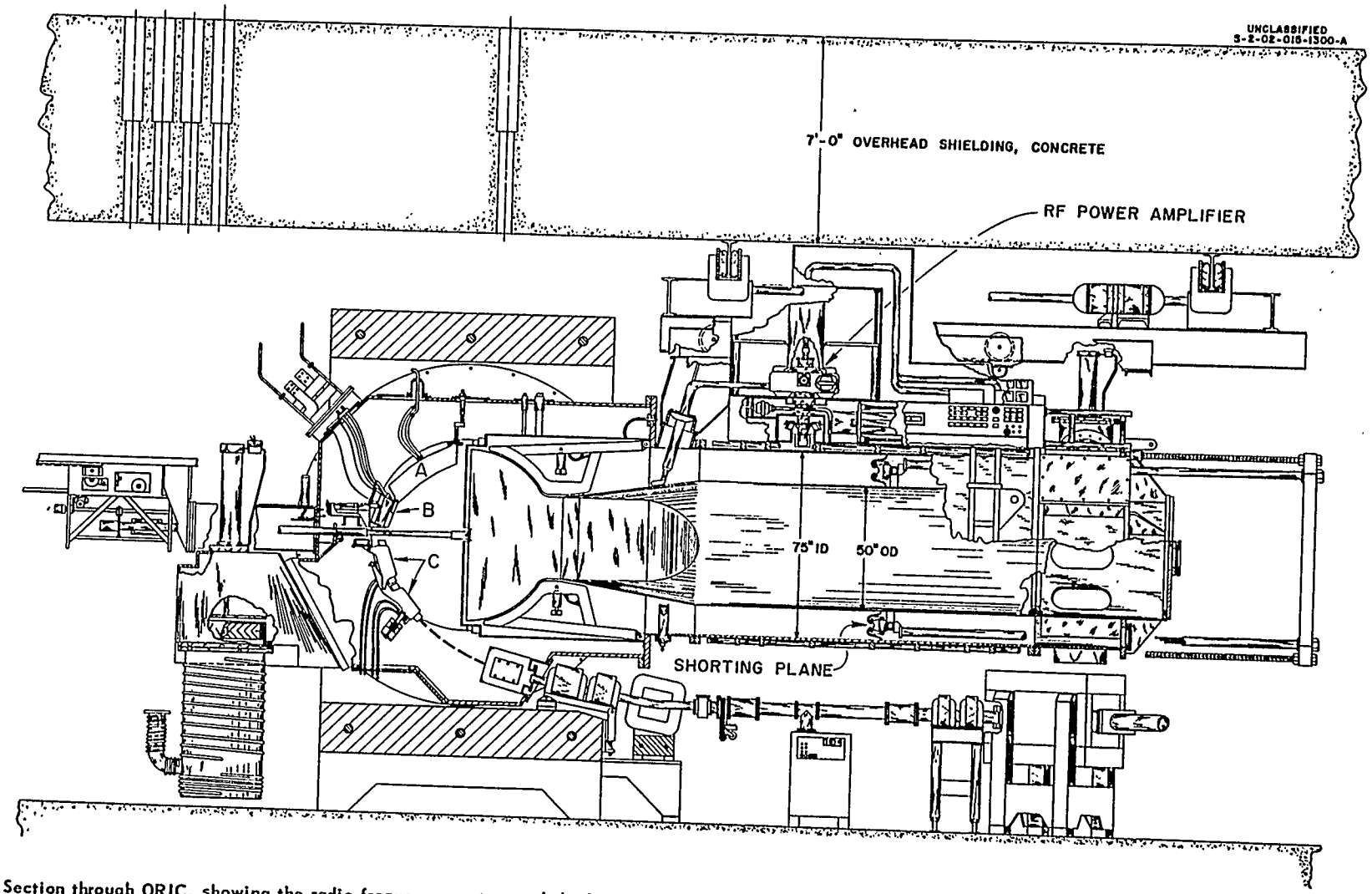

Section through ORIC, showing the radio-frequency system and the beam extraction system. The collar-shaped shorting plane, parts of which are shown in cutaway view just above and just below the 50-inch dee stem, can be moved along the dee stem to tune the dee for the desired operating frequency. The beam of accelerated ions spirals outward from the center of the magnet, in and out of the single dee, until it enters the deflector channel (*A*). The coaxial magnet (*B*) and the compensated-iron channel (*C*) neutralize the magnetic field very locally, enough to provide the deflected beam an escape route into the series of positioning and focusing magnets leading to the switching magnet at the lower right. This magnet is used to direct the beam toward the various target locations.

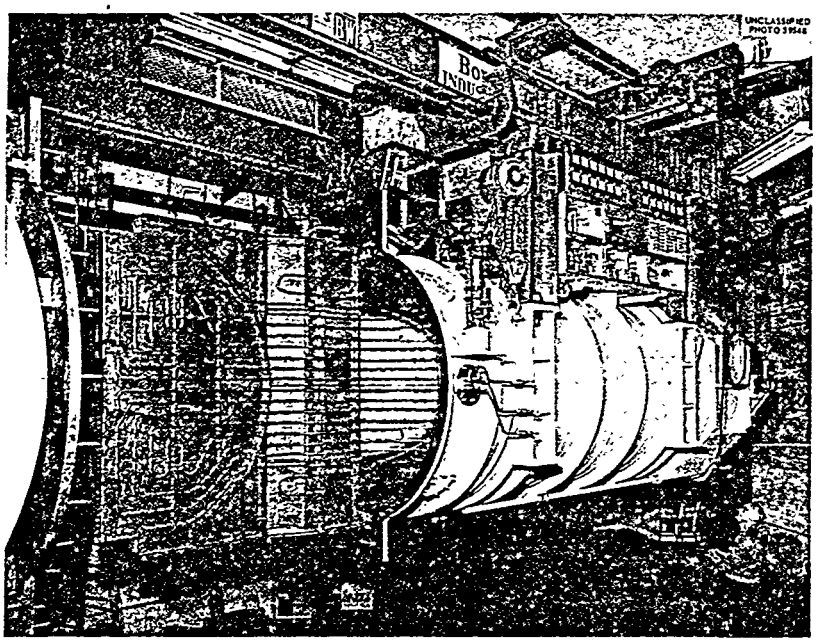

The radio-frequency system of ORIC. The resonator can be removed from the magnet (at the left) as a single unit for easy servicing. The dee and the liner which encloses it are formed from water-cooled copper sheet. The 500-kilowatt power amplifier is mounted on top of the copper-lined steel resonator tank, which is designed to include the dee stem within the vacuum chamber.

the usual 5 to 10 percent for frequency-modulated cyclotrons of this energy range and with 20 to 30 percent for conventional machines of lower energy.

The small energy spread and small angular divergence of this high-quality beam will facilitate the delivery of beams with the desired characteristics to the various target areas and will markedly improve the precision of nuclear-reaction measurements.

Proposed High-Intensity Proton Accelerator

The preliminary design of a new research facility for the production and use of intense beams of protons, neutrons, and pi and mu mesons was completed (and a proposal document, ORNL-3540, was prepared). The accelerator, the Mc^2 Cyclotron, is an eight-sector isochronous cyclotron with a maximum internal proton energy of 900 Mev; an external beam would be obtained by extraction at an energy of 810 Mev. Due to the relativistic increase of mass with velocity ($E = Mc^2$) the mass of a proton accelerated to this energy is, in effect, about doubled. The facility will provide well defined beams with intensities up to 6×10^{14} protons per second, 10^9 pions per second, and 10^7 muons per second. These intensities are at least 1000 times as great as intensities now available at this energy level.

The research program currently envisions that the accelerator will be primarily used for the study of nuclear structure by means of inelastic scattering and nuclear reactions produced with highly monoenergetic proton beams. The accelerator and its associated facilities will also enable new and more precise investigations of both weak and strong interactions of the elementary particles. More refined studies of muonium, mesic atoms, and mesic molecules will be possible. In addition to its use for physics research, the facility can be an important tool for fundamental research into the effects of high-energy radiation on biological systems, including applications in radiation therapy and the problems of space radiation. Facilities for cancer therapy and for neutron time-of-flight studies can be added to the proposed research complex.

The design of the eight-sector isochronous cyclotron is based on several years of research and development effort, including extensive modeling of the magnet and radio-frequency systems. The performance characteristics of the cyclotron were proved through the construction and operation of an electron-scale model, Cyclotron Analogue II. This electron cyclotron fully demonstrates the validity of the theoretical and design work; the beam is readily accelerated to

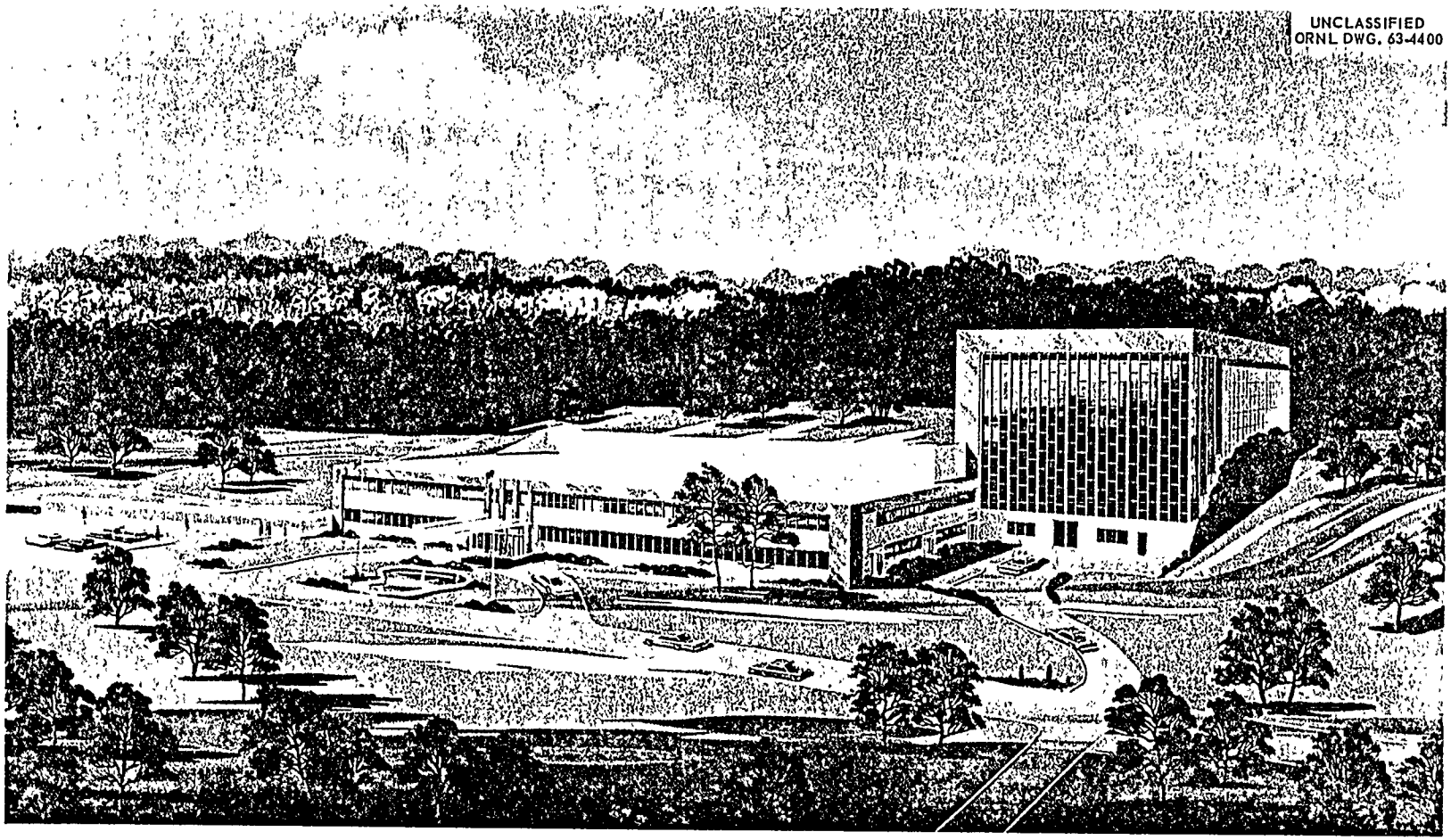

Architect's rendition of proposed Mc^2 Cyclotron laboratory. The 810-Mev isochronous cyclotron would produce proton beams of such high intensity as to require massive shielding. The architect (G. Edward Sakrison, American Institute of Architects) has taken advantage of the hillside site to provide earth shielding for three underground experiment halls (about 3.5 million cubic feet) extending back from the laboratory-office building at the left. The cyclotron and necessary crane facilities are placed in the taller building at the right.

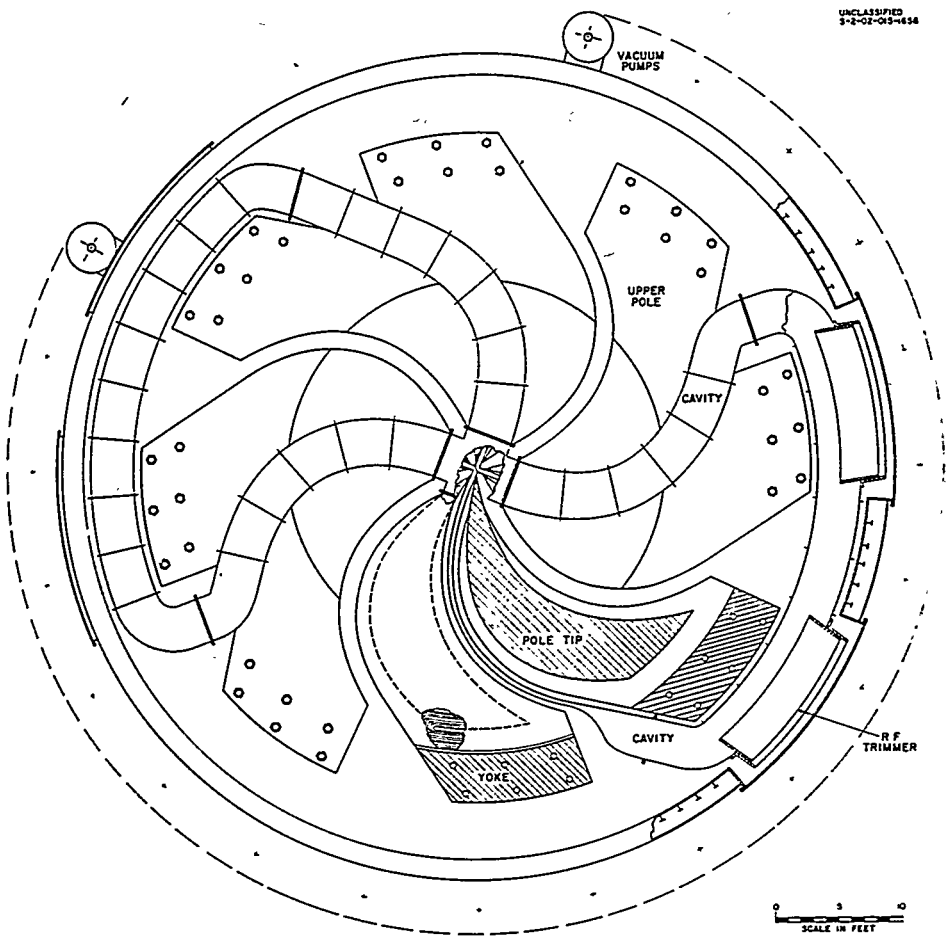

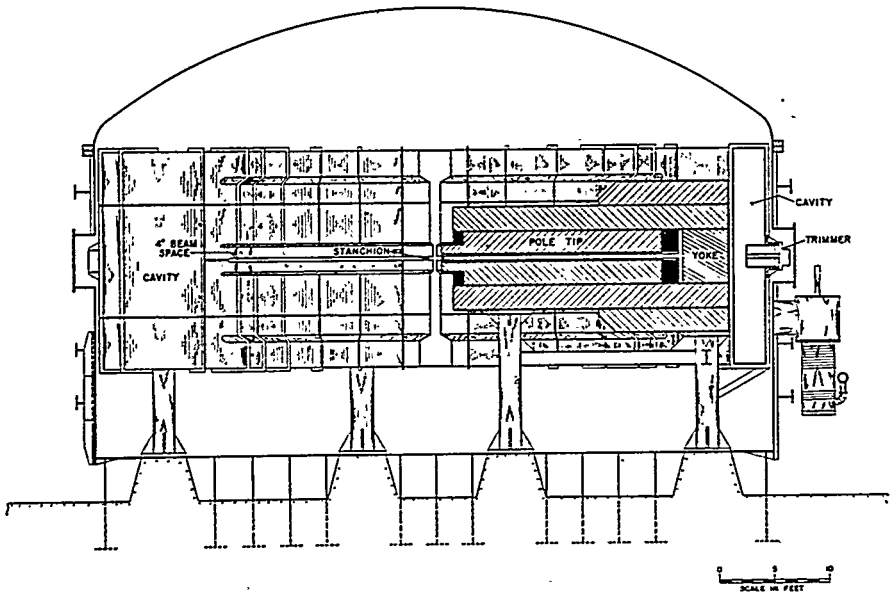

Plan and section of Mc^2 Cyclotron. The magnetic field of the 53-foot eight-sector magnet varies azimuthally and increases radially from 4500 gauss at the center to 18,000 gauss at the maximum orbit. This magnet configuration permits the use of two radio-frequency cavities operating at a fixed frequency to accelerate an intense beam of protons, at a gain of 1 Mev per turn, to over 800 Mev.

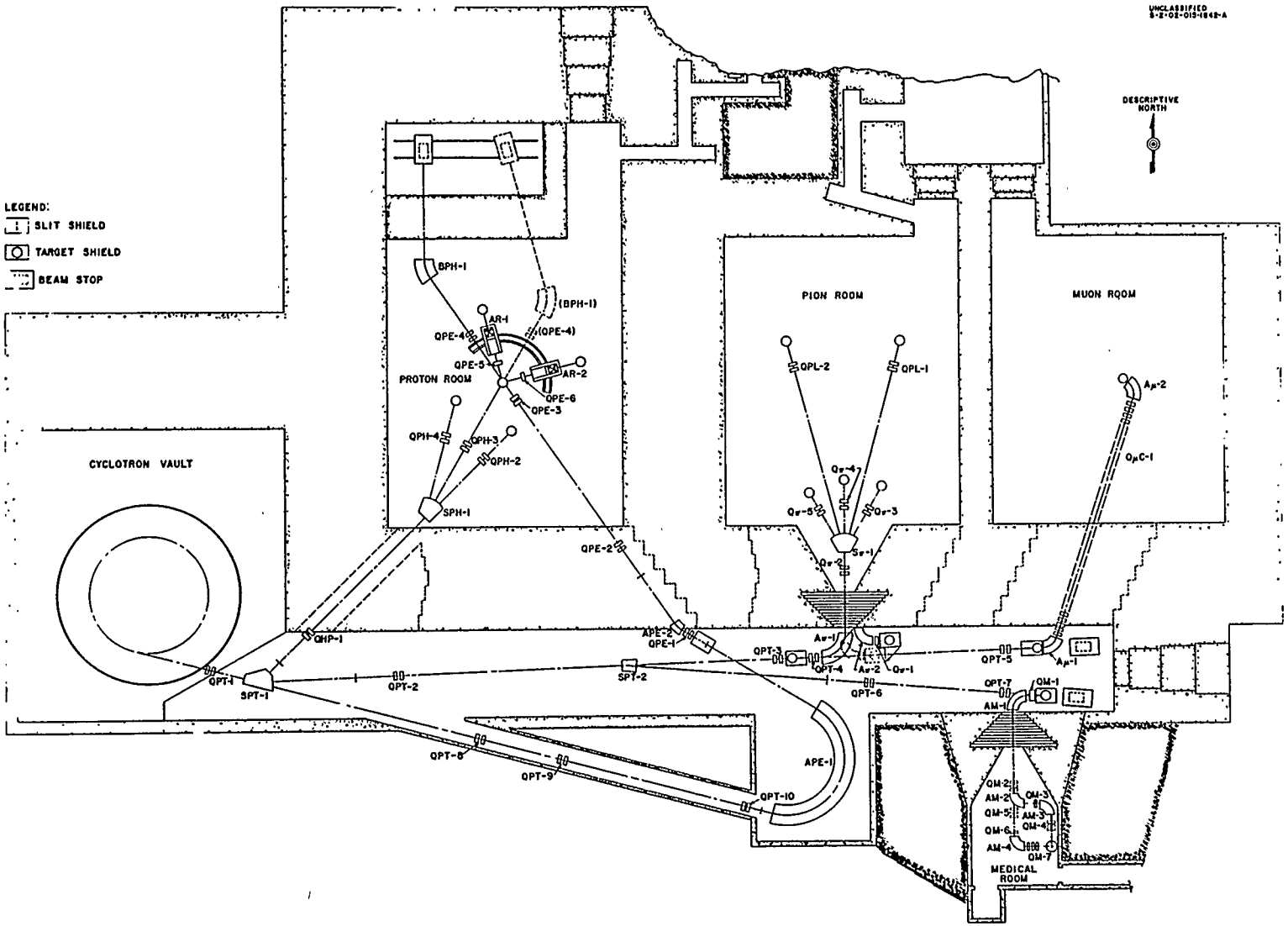

Plan view of Mc^2 Cyclotron vault and experiment areas. The extensive ion optics system is designed for the safe and efficient exploitation of the intense beam of 810-Mev protons and the secondary beams it will generate. The system includes a high-resolution beam analyzing magnet, several steering magnets, beam transport quadrupoles, and a muon channel. Studies indicate that as much as 40 feet of concrete will be required to shield occupied areas from the intense radiations. The experiment rooms shown are underground, covered with at least 25 feet of earth.

full energy without appreciable losses, and 80 to 90 percent of the beam can be extracted from the machine. The hazards due to residual radiation induced in the Mc^2 Cyclotron and associated facilities were evaluated. These studies, based on data from experiments at the CERN Synchro-Cyclotron and on computer calculations, show that the radiation problems encountered at the desired beam intensities can be managed.

Cyclotron Analogue II

During the past year beam-extraction studies with this operating electron-scale model cyclotron have further demonstrated the practicability of the proposed Mc^2 Cyclotron. An extraction efficiency of over 85 percent is achieved. The electrons are extracted from the circulating beam by exploiting an instability in their radial motion

Cyclotron Analogue II. The performance of this eight-sector electron model of the proposed Mc^2 Cyclotron has verified exactly the beam dynamics predicted from design studies. Electrons are extracted at an energy of 440 kev, which is comparable to 810 Mev in the large proton accelerator.

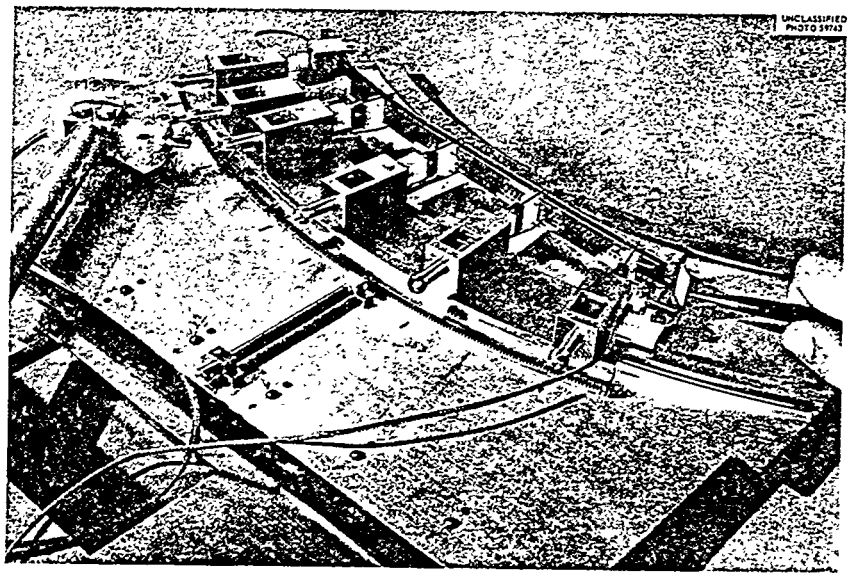

Extraction mechanism of Cyclotron Analogue II. The electron beam enters the 8-in. deflector channel, from the left, and strikes the small fluorescent screen indicated at the right. A 2000-volt potential between the two sides of the channel deflects the beam away from the circulating orbit. Since the magnetic field in this new type of cyclotron varies azimuthally to provide focusing forces, the beam path is no longer a simple circle. The ingenious mechanism shown above, with its many remotely controlled adjustments for making the channel fit the beam path, was used to determine that high deflection efficiency is possible. The demonstrated deflection efficiency of over 85 percent suggests that even when the Mc^2 Cyclotron is operated at high beam intensity the interior would not be unreasonably activated by straying high-energy protons.

which occurs near the maximum energy. A small variation in the magnetic field strength, introduced locally near the extraction radius, causes the radial separation between successive revolutions of the beam to increase rapidly; thus, a large fraction of the beam enters the extraction channel. Since the Analogue closely models the particle dynamics anticipated in the Mc^2 Cyclotron, it is expected that a continuous beam in excess of 100 microamperes of 810-Mev protons can be extracted without unreasonable activation of the inner parts of the cyclotron by stray protons.

Residual Radiation Studies

No large accelerator has ever been operated at the beam intensities desired in the Mc^2 Cyclotron. Therefore, a detailed evaluation of the problem of induced radioactivity was necessary before handling facilities could be planned for safe operation and maintenance of the cyclotron and its components.

Calculations of the residual radiation levels are based on published data on spallation cross sections. A computer program was written (ORNL-3554) for determining the radiation levels near slabs of various materials after irradiation with high-energy protons or neutrons. The residual radiation dose rate was determined by combining the dose rates calculated for all the spallation products.

Experimental verification of the calculated dose rates was obtained in cooperation with the staff of the 600-Mev Synchro-Cyclotron at CERN. Selected materials were exposed at 30 widely distributed locations throughout the cyclotron and the decay curves of the induced activities were determined. The activity obtained varied with location, of course, but the average of the activities measured 15 days after cyclotron shutdown

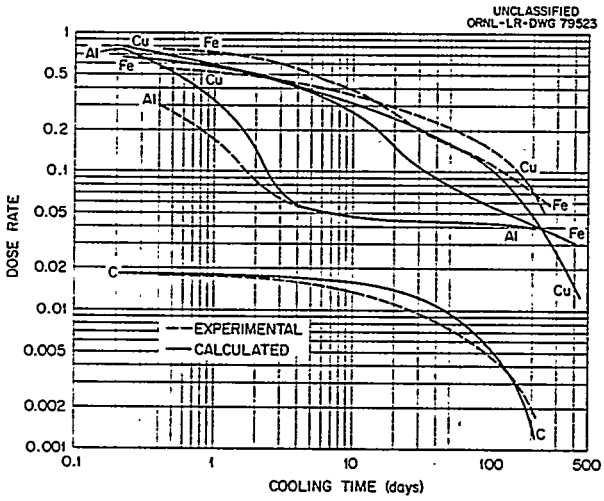

Residual radiation decay curves. Experimental data are for gamma radiation from samples which had been exposed for three months within the CERN 600-Mev Synchro-Cyclotron. Calculated data are for samples 1 millimeter thick, exposed to an assumed 1-microampere, 600-Mev proton beam for three months. For the comparison all curves are normalized where the curves for aluminum flatten (where sodium-22 is the dominant activity in aluminum).

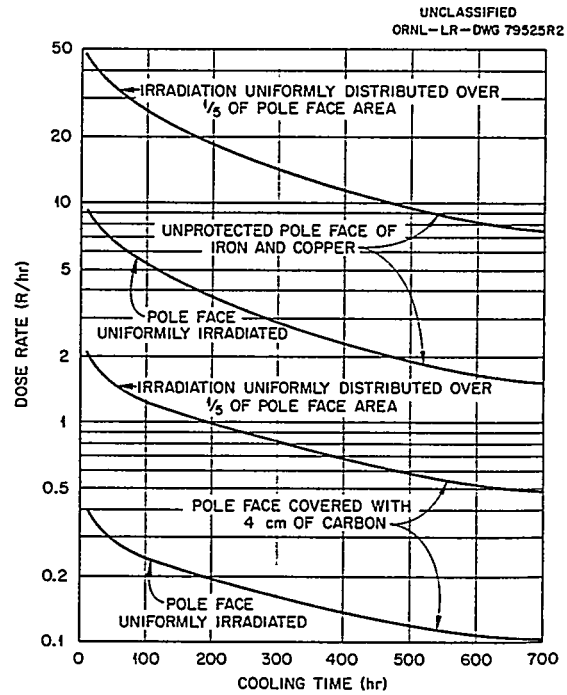

Calculated maximum residual radiation levels expected in the Mc^2 Cyclotron. The cooling time is assumed to begin after 1000 hours of operation during which 10 microamperes of high-energy protons were scattered from the beam-extraction apparatus into the pole faces. Carbon shields can be used to control the activation problem; 4 centimeters will reduce the residual radiation by a factor of 20.

agreed well with the dose rate calculated for the same cooling time. Since the calculated and experimental data for all materials agree within a factor of two, we conclude that the calculation method can be used with reasonable confidence. The radiation levels will require the development of some special handling equipment and procedures, but we are confident that the problem is manageable.

Separated-Orbit Cyclotron

The basic theory of a new fixed-frequency, fixed-field, high-energy accelerator, the "Separated-Orbit Cyclotron," was developed during 1963 and is being evaluated by the Electronuclear Division. This concept was initiated by F. M. Russell, Rutherford Laboratory, England, during his exchange year at ORNL. It combines the best features of the fixed-frequency cyclotron, the alternating-gradient synchrotron, and the linear accelerator. Phase stability is achieved in the new design, a feature unique for fixed-frequency accelerators.

The essential innovation is that the magnetic field is designed so that the orbits of the circulating ions are separated axially as well as radially, in a spiral-helix configuration. The usual resonance problems which arise when successive revolutions of the accelerating particles occur in a common magnetic field are thus eliminated. The residual coupling and error resonances can be bypassed by changing the magnetic field properties stepwise along the orbit. The proton beam is accelerated in radio-frequency cavities spaced uniformly between the alternating-gradient magnet elements around the machine. Each cavity provides acceleration for all of the orbits, as in a cyclotron. This feature results in a relatively modest radio-frequency power requirement and enables the accelerator to be operated continuously rather than in the pulsed manner of the conventional linear accelerator. Additional advantages are that the beam can easily be injected and extracted; the final energy can be varied by extracting at chosen points along the orbit.

The Separated-Orbit Cyclotron combines the desirable features ordinarily associated with the cyclotron, such as modest radio-frequency power, compactness, and continuous beam, with the flexibility and the 100-percent beam-extraction capability characteristic of linear accelerators.

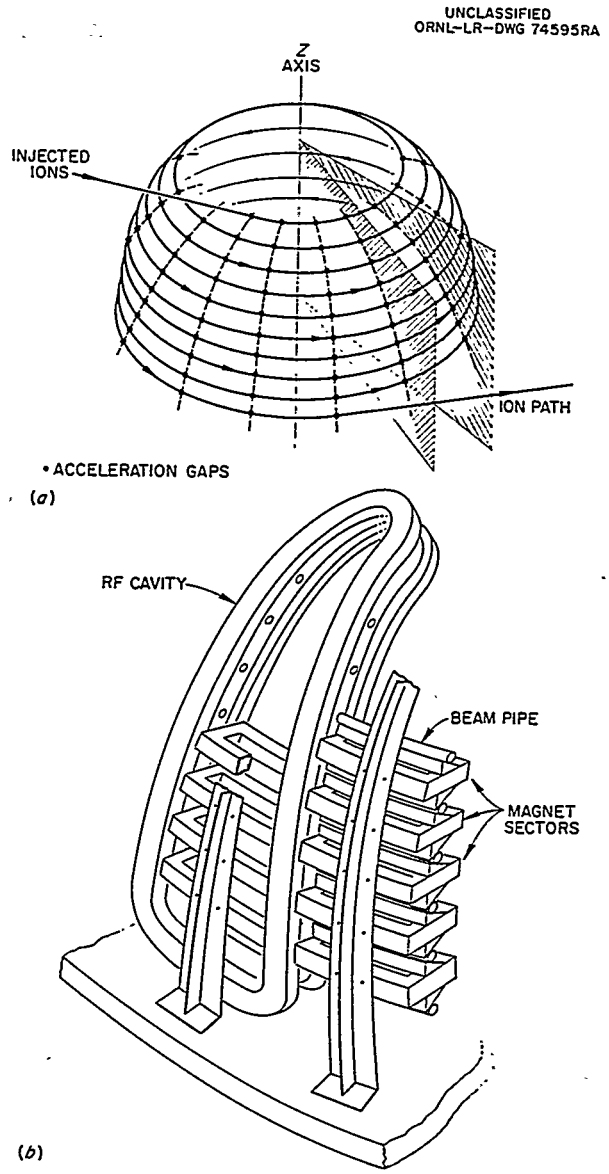

The Separated-Orbit Cyclotron. In this newly conceived accelerator the ions move at a constant orbital frequency along a spiral, helical beam path, as shown in the upper drawing. Acceleration is provided by radially disposed radio-frequency cavities. In the conceptual design, suggested by the lower sketch, alternating-gradient magnet sectors are stacked in and between radio-frequency cavities. A well-focused beam of ions is accelerated through the spiral beam pipe. It is believed that, with development, the Separated-Orbit Cyclotron may prove superior to existing types of machines for the acceleration of very intense ion beams to high energies, billions of electron volts.

It appears to be suitable for obtaining intense beams at energies well beyond the energy of the proposed Mc^2 Cyclotron. A detailed evaluation of the machine is in progress to determine the optimum arrangement of the radio-frequency system and magnet and the optimum injection energy, and to delineate tolerances in the mechanical and electronic components.

Superconducting Magnet Studies

If large accelerator magnets could be developed to take advantage of the unusual properties of superconducting alloys, their power requirements should be greatly reduced. For this reason the Electronuclear Division has designed and built a superconducting solenoid to investigate the basic problems which seem to limit such an attractive application.

A property of superconductors which limits their use is that their zero resistance is suddenly lost whenever either the current or the magnetic field strength is increased above certain critical values. These critical values may become even lower when the wire is wound to form a large magnet coil.

The structural and environmental factors affecting this transition from superconducting to normal resistance are being evaluated in a nine-section superconducting solenoid, with three concentric coils in each of three stacked layers. The unit contains 30,000 feet (8.5 pounds) of niobium-zirconium wire, 0.01 inch in diameter. To determine the current and magnetic field conditions under which transitions are initiated, the solenoid is arranged so that the nine sections can be energized and monitored separately. A copper secondary is wound bifilarly with and protects the niobium-zirconium wire; the shorted secondary serves to dissipate surges of energy during the sudden transitions.

An unusual effect has been observed by using different currents in the various sections of the magnet. With all coils carrying equal currents, the transition occurs at a current of 14 amperes, which limits the magnetic field to only 23,000 gauss. When the currents in the outer coils of the magnet are reduced, however, the current in the central coil can be increased to as much as 26 amperes; the central field is then 32,000 gauss. This observation is contrary to the usual concept that it is the high-field region of the magnet which determines the maximum current.

The ORNL Nine-Section Superconducting Solenoid. The solenoid is being lowered into a vacuum-insulated chamber. Liquid helium is used in the chamber to maintain the low temperature, 4.2°K (−269°C or −452°F), necessary for the operation of the superconductor. The unit produces a magnetic field of 32,000 gauss at the center of the 2-inch bore. The nine-section design makes it possible to localize the current-field conditions in which transitions are initiated.

NUCLEAR PHYSICS

Introduction

The nuclear physics program of the Electronuclear Division encompasses both theoretical and experimental work. In the former the immediate goals consist of an elaborate shell model calculation and a program of optical model and distorted wave analyses of elastic and inelastic

scattering, including polarization effects. In the long run we hope that the theoretical effort will include some interpretation of collective aspects of the nucleus, as well as the few-nucleon problem.

The immediate goals of the experimental program are directed toward the exploitation of ORIC. To this end experiments are designed to investigate direct interactions with protons, deuterons, ^{3}He, and lithium ions. An experiment has been designed to measure the differential cross section of the elastic and inelastic scattering of polarized protons from a number of targets. Heavy-ion reactions, both of the direct variety, that is, transfer reactions, and those leading to a statistical evaporation of reaction products, will be studied. The purpose of the many-pronged experimental program is to extract information which is pertinent to the shell model from direct reactions, to the statistical model from evaporation reactions, to the collective model from the radioactive decay schemes of the rare earths, and pertinent to the optical model and the theory of nuclear reactions from scattering of polarized and unpolarized particles.

The very long-range objective of the experimental program is to use the high-energy protons and other particles available from the proposed Mc^2 Cyclotron or the Separated-Orbit Cyclotron for nuclear physics. For example, the study of inelastic scattering of high-energy protons should make it possible to separate the interaction from the nuclear form factors and thus to obtain clear-cut information about the latter.

Elastic Scattering of Helium-3 Ions

In the past few years, experiments have been performed on the scattering of helium-3 ions from various nuclei. In the absence of a fundamental theory for the scattering of complex particles, analyses of this type of data have necessarily used the optical model. While no fundamental proof of the validity of the model as yet exists for complex particles, phenomenological studies of the scattering of alpha particles and deuterons have demonstrated its applicability.

A compelling reason to establish the optical model for helium-3 ions is to enable the study, through the distorted-wave approximation, of reactions in which helium-3 is a participant. An example is the (^{3}He,d) reaction which appears to be the most straightforward way of studying single particle proton states of nuclei. To assign physical meaning to an optical model for helium-3 scattering, a minimal condition is that the main features of the scattering be reproduced by a model in which the parameters are smoothly dependent on target mass and projectile energy. Previous studies have not satisfied this condition.

We are systematically analyzing the available data on elastic scattering of helium-3. We have prepared an automatic search program and, to date, we have established that the optical model shows a smooth dependence on the mass number of the target, provided that the absorptive potential is surface localized.

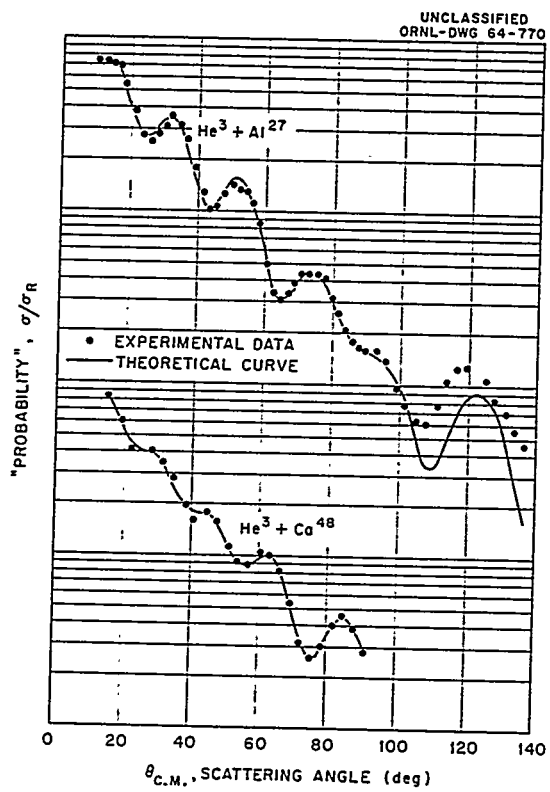

Theoretical interpretation of elastic scattering. Theoretical curves calculated at ORNL on the optical model for the elastic scattering of helium-3 ions from aluminum-27 and calcium-48 agree closely with data obtained experimentally at Los Alamos Scientific Laboratory. When such theoretical studies successfully interpret the experimental data from the various laboratories, they are then useful in guiding further research toward an understanding of nuclear processes.

Fluctuations in Nuclear Cross Sections

It has long been known that many nuclear phenomena may be predicted by statistical considerations. For example, calculating the average cross section for decay of a compound nucleus into one of its possible final systems is basically a problem in probability theory, and accurate results can be obtained from statistics.

It has only recently been fully realized, however, that the average quantities are themselves statistical. Individual cases, when closely examined, should be expected to deviate at random from the predicted average behavior; a nuclear cross section plotted as a function of energy should wiggle up and down rapidly and erratically. Such fluctuations have in fact been observed in a number of reactions and are now well established experimentally.

Mere discovery of an effect is not sufficient to transform it from a curiosity to a phenomenon worth full investigation. The impetus for further work comes from the prediction that the strength and the rapidity of the *fluctuations* may be used to ascertain important *average* properties of nuclear systems which are otherwise difficult or impossible to measure by present experimental techniques. For example, the number of wiggles observed over a given range of bombarding energy can be used to estimate the average lifetime of a compound system. In experiments in which carbon was bombarded by oxygen ions accelerated by the Oak Ridge Tandem Accelerator, this quantity turned out to be about 10^{-20} second, a fantastically short time, shorter by a factor of about a million than the shortest time intervals that can be measured by even the most advanced techniques.

Of even greater value is the prediction that one can estimate what fraction of a given reaction proceeds by a prompt mechanism (direct interaction) and what part goes by a delayed process (compound nucleus). For many years nuclear physicists have spoken loosely of direct vs compound processes without having a really quantitative way to define these terms. Now, however, it is possible to determine precisely what fraction of the time some particular reaction proceeds by a direct interaction. This type of analysis has shown that the reaction $^{12}C(^{16}O, \alpha)^{24}Mg$, where the ^{24}Mg is left in its ground state, proceeds primarily by a compound-nucleus process.

Fine Details of the Shell Model in the Mass Region $90 < A \lesssim 100$

The nuclear shell model in its simplest form is not adequate to explain the detailed level spacings in nuclei. To make accurate predictions it is necessary to add residual interactions between pairs of particles.

The recent determination at ORNL of energies and spins of the low-lying levels of $^{92}_{41}Nb_{51}$ (41 protons and 51 neutrons) specifies the effective residual interaction of a proton in the $1g_{9/2}$ shell with a neutron in the $2d_{5/2}$ shell and (thereby) completes the set of effective interactions which are extremely useful in determining the properties of low-lying excitations of nuclei in this mass range. The other two effective interactions – that between two protons in the $1g_{9/2}$ shell and that between two neutrons in the $2d_{5/2}$ shell – were known from the spectra of $^{92}_{42}Mo_{50}$ and $^{92}_{40}Zr_{52}$.

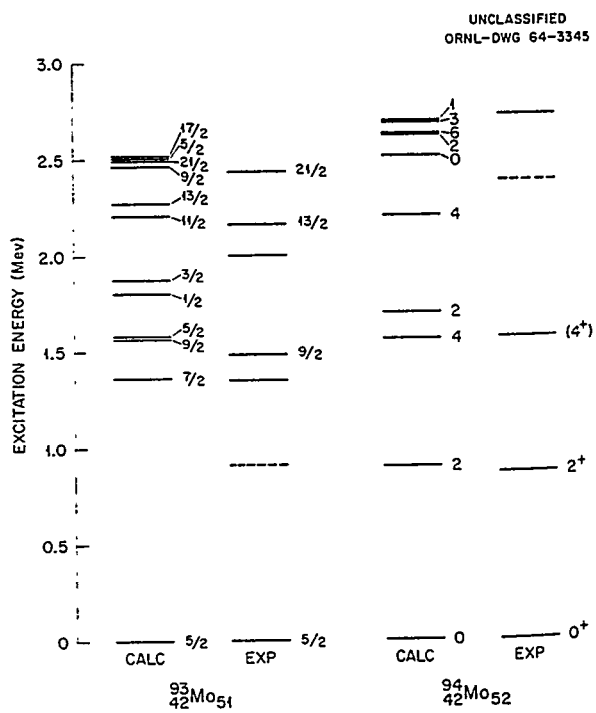

Comparison of the experimental energy spectra of molybdenum-93 and molybdenum-94 with the calculated spectra. The good agreement with existing data should encourage further experimental work to check the predictions of the calculations.

The low-lying energy levels of nuclei with $90 < A \lesssim 100$ are expected to belong, predominantly, to a configuration having protons in the $1g_{9/2}$ shell and neutrons in the $2d_{5/2}$ shell and hence are determined by the above set of (p,p), (p,n), and (n,n) interactions.

We have calculated the energy spectra of the isotopes of niobium and molybdenum and find good agreement with existing experimental information. More definitive experiments, determining properties such as energies and spins of the various states and the rates of electromagnetic transitions between these states, are very desirable for a detailed comparison with the predictions of the calculation.

Systematic, intensive studies, both experimental and theoretical, of nuclei in this region of the periodic table are beginning, in order to provide a better understanding of their structure.

Useful Diagrams for Representing Nuclear States

An objective of nuclear structure studies is to provide quantitatively valid descriptions of atomic nuclei. These nuclei are believed to be assemblages of protons and neutrons which interact with each other; the interactions are described by quantum mechanics. Therefore, the ultimate picture that one can hope to get will be in the form of quantum mechanical operators and state vectors (or wave functions).

A complete microscopic description of a system of more than a very few particles is not practically obtainable; approximations must be made. A well known and extremely useful approximation to the nuclear structure picture is the nuclear shell model. In this model the interaction energies of any particle with all the other particles are replaced by a potential which is the same for all particles. This results in a picture consisting of a set of characteristic states (characteristic of the chosen potential) which are available for occupancy by the particles. An energy state of a given nucleus is thus represented by a particular pattern of occupancy of these characteristic single-particle states.

Although this picture provides a tremendously simplified view of nuclear structure, it may still be quite complicated. For example, there are 63,504 possible distinct rearrangements of five neutrons and five protons with ten single-particle states available to each. (This would apply, for example, to five neutrons and five protons in the $g_{9/2}$ shell.)

Sheer numbers is not the only problem. Even when only a few wave functions exist, it may be difficult to see the connection between the wave functions that one can write down and the physically observed processes. Consider, for example, the valuable technique for studying nuclei by using pickup and stripping reactions to remove or to drop in one or two nucleons. Unless the wave function is cast into a representation that abstracts the "picked up" or "dropped in" particle (or particles) and the remaining nucleus, one will have difficulty understanding the relationships between the reaction data and the nuclear model. The process of abstracting these parts may not be easy, for the rules of quantum mechanics tell us that all particles must be treated as equal. We must be careful not to favor any particles in separating the picked-up particle (or particles) and the remaining nucleus. Also, the Pauli exclusion principle, which specifies that no two particles may occupy the same state, must be obeyed.

At ORNL a new kind of diagram has been introduced to represent the nucleus; it can be used for quantitative calculations as well as for visualization of the nuclear states and reactions. In this diagram single-particle, shell-model states appear as slots into which particles may be placed. The proper number of particles are distributed appropriately among the slots to describe a particular nuclear state. This description of a particular nuclear state is, in general, a sum of such diagrams with appropriate weighting factors. Quantum mechanical operators, in this representation, move the particles from slot to slot and change the weighting factors. The diagrams, being in essence binary numbers, are easily incorporated into computer programs.

With these diagrams a pickup reaction, for example, can be mocked up quite easily. One writes the diagram for the target nucleus, removes the picked-up particle, and compares the remaining diagram with the diagrams for the various states of the final nucleus. In this way the probabilities for exciting the several final states are determined.

This technique is far less cumbersome and more visual than techniques which have been used in the past. A particular advantage is that the technique satisfies the requirements of the Pauli exclusion principle and of indistinguishability of particles by the very nature of the diagrams, while the requirements appear as complicated restrictions on the wave functions in other representations.

The new diagrams have been especially helpful in understanding isobaric-spin analog states and the relationship of isobaric spin to nuclear states found by pickup and stripping reactions. The isobaric-spin formalism is introduced by providing matching sets of slots in the diagrams for protons and neutrons. Isobaric-spin operators move particles from proton slots to neutron slots and from neutron slots to proton slots. The method has been applied to understanding several spin-1/2 levels in the zirconium-89 nucleus. The remarkable result is that the isobaric-spin formalism, which seems at the outset to be no more than a formal computational trick, provides a simple and accurate description of the nucleus. Specifically, a state at 0.588-Mev excitation in zirconium-89, which is reached by the reaction $^{90}Zr(p,d)^{89}Zr$, is found to be pure $T = 9/2$ (where T stands for total isobaric spin), while a simple picture of the reaction which treats the neutrons and protons separately would indicate a mixture of $T = 9/2$ and $T = 11/2$.

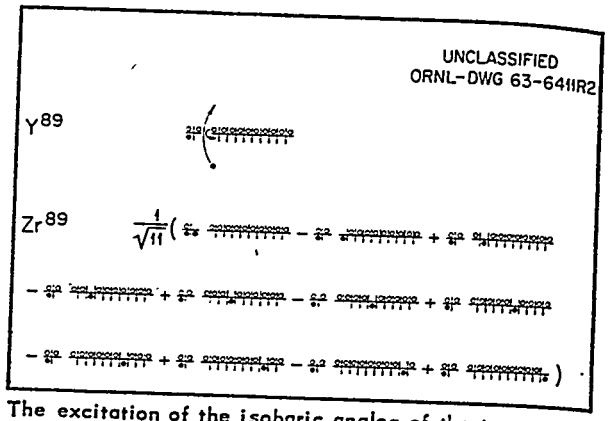

The excitation of the isobaric analog of the target with a (p,n) reaction as depicted by a new type of diagram. The incident proton, under the influence of nuclear forces in the yttrium-89 nucleus, becomes a neutron while a neutron in the nucleus becomes a proton, thus conserving charge. The process may occur with any of the neutrons for which the corresponding proton states are not occupied; thus a summation over these states is shown. The alternation in sign in the sum is to satisfy certain rules of quantum mechanics. The slots above the center line represent neutron states; those below represent proton states.

Chemistry

ANALYTICAL CHEMISTRY RESEARCH

Gas-Chromatographic Determination of Trace Contaminants in Helium

Studies in process gas chromatography were continued for application in the Gas-Cooled Reactor Program. A Beckman model 120A process chromatograph with infrared analyzer was adapted for use in hydrogen autoclave tests to determine methane, nitrogen, carbon monoxide, and carbon dioxide. A Greenbrier model 112 instrument was used to monitor gases (H_2, CO_2, CO, O_2, N_2, CH_4) in a high-temperature steam-graphite loop.

A simple and highly sensitive detector has been developed for the gas chromatographic determination of concentrations below the parts per million range of permanent gas impurities in helium. Gas chromatographic detectors are used to measure impurities such as hydrogen, oxygen, nitrogen, methane, carbon monoxide, and carbon dioxide in a stream of helium as they emerge from a chromatographic column as separate peaks at characteristic intervals. This technique has been shown to be applicable to the analysis of helium samples both in the laboratory and in automatic in-line analysis, but has been limited to concentrations above 1 part per million by the insensitivity of conventional thermal conductivity detectors. After several alternate types of detectors were evaluated, this modified helium breakdown detector was found to be the most sensitive for these contaminants.

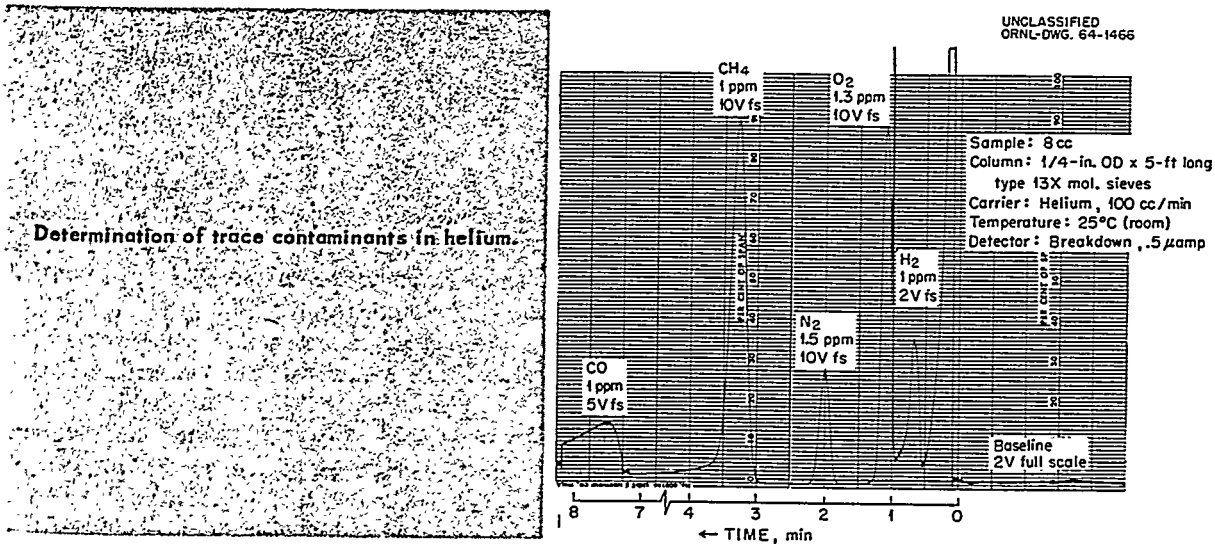

Determination of trace contaminants in helium.

This detector consists of a compact cell in which the gas from a chromatographic column passes between closely spaced concentric electrodes which carry a constant current of 1 microampere. With pure helium, a potential of about 500 volts is developed across these electrodes. When traces of impurities are introduced, this voltage is decreased by as much as 100 volts. Conservatively estimated detection limits range from 0.1 part per million for hydrogen to 0.005 part per million for oxygen and methane. At this time the maximum concentrations that can be measured are about 10 parts per million; but techniques to extend the range either by dilution or by combination with a less sensitive detector in an automatic instrument are being investigated.

This analytical technique is being developed primarily for the measurement of impurities in helium from advanced gas-cooled reactor development tests but has already been applied to the determination of carbon tetrafluoride, krypton, and xenon in Molten-Salt Reactor Experiment investigations. Potential applications include the analysis of atmospheres for environmental studies of metallurgical specimens, the investigation of diffusion of gases through metals (for example, in the development of space power sources), and the establishment of purity of gases for inert-gas welding of refractory metals.

EFFECTS OF RADIATION ON ANALYTICAL METHODS

Radiolysis of Chloride Solutions

Concentrated solutions of LiCl, used in separations of the transuranium elements, have been observed to lose their acidity as a result of radiolytic decomposition. One product of the loss of acidity is chlorine. A detailed study of this phenomenon has been carried out with the findings that such behavior is not unique to the concentrated LiCl system but that other chloride systems behave the same way within certain limits.

Such radiolysis apparently takes place only in acid chloride systems when the lower concentration limit is 1.4 *M* chloride. The *G* value for the loss in acidity is about 0.5 over a wide range of composition. However, the *G* value for the production of Cl_2 varies directly with total chloride content. The production of Cl_2 seems to reach a steady-state level which is chloride dependent.

The production of chlorine in such systems could be expected to be a serious impediment to the use of reagents which are readily oxidizable. This is particularly the case with many chromogenic reagents. The loss in acidity of such systems on irradiation is probably less serious, although it would tend to become serious in very high radiation fields.

Effect of Gamma Radiation on Arsenazo III Solutions

Arsenazo III (the disodium salt of 1,8-dihydroxynaphthalene-3,6-disulfonic acid-2,7-bis(azo-2)-phenyl arsonic acid) is an extremely useful chromogenic reagent for the colorimetric determination of the members of the lanthanide and actinide families. Because of its use for the determination of such elements and/or their isotopes, a study of its stability, under conditions of radiation, was carried out.

Aqueous solutions of arsenazo III, both neutral and acidic, were irradiated in a cobalt-60 gamma source. The decrease in the arsenazo III concentration, caused by such radiation, was followed photometrically. Hydrochloric, sulfuric, and acetic acid solutions of arsenazo III have been studied. An example of the data obtained is that the rate of decomposition of a 1×10^{-4} *M* solution of arsenazo III, due to radiation, in 1 *N* HCl and 9 *N* HCl is, respectively, 2×10^{-6} and 9×10^{-7} mole per liter per kilorad of absorbed gamma radiation. This indicates that the acid concentration is an important factor in the sensitivity of this reagent to radiation. The same concentration of arsenazo III (1×10^{-4} *M*) in 1 *N* acetic acid shows a decomposition rate of 9×10^{-8} mole liter^{-1} kilorad^{-1} when the dose is below 72 kilorads. Above this level of radiation the rate of radiolytic decomposition increases to 2×10^{-6} mole liter^{-1} kilorad^{-1}. Upon termination of the irradiation, decomposition continues as a postirradiation effect.

Such data will be of great use in determining the usage of this chromogenic reagent in the presence of radiation. Potential applications of such results are in the analytical chemistry of various

experimental reactor programs in progress at various AEC installations.

Effect of Gamma Radiation on the Nickel-Dimethylglyoxime Reaction

The reaction between nickel and dimethylglyoxime to form a red-colored complex, absorbing at approximately 465 millimicrons, is very widely used for the determination of trace amounts of nickel. Since the determination of nickel is of interest in many reactor programs, it is axiomatic that its determination under conditions of high radiation is necessary. Therefore, the study of this reaction and the effect of radiation upon it was accomplished. The results may be summarized in brief by the following statements:

1. The extent of radiation damage to the dimethylglyoxime reagent itself is a function of its concentration. The *G* value changes twofold when the concentration is varied tenfold.
2. The effect of radiation on dimethylglyoxime reagent may be minimized by use of an alcoholic medium.
3. The nickel-dimethylglyoxime complex is much more sensitive to radiation than is the dimethylglyoxime itself. However, on removal from the radiation field, the nickel-dimethylglyoxime complex re-forms and the absorbance of a given sample regains its original value.

The results of this work point up strongly the necessity for making such a study *in situ* and demonstrates how the study of radiation effects may lead to valuable knowledge of the reaction itself.

ANALYTICAL INSTRUMENTATION

Several instruments were modified for specialized applications. Detailed design information was provided for the modification of an ORNL model Q-1988 controlled-potential and derivative polarograph for molten-salt voltammetry, and of a model Q-1988A for use at fast scan rates with dropping-mercury electrodes having drop times of ½ second or less. A Beckman model B spectrophotometer was modified for continuous recording of the titration of free fluoride ion. The time per analysis was reduced from 75 to 15 minutes, and the precision of analysis was improved. For a fused-salt application, the precision chronopotentiometer was altered to function with system ground isolated from earth ground. Also, an improved constant-current supply was incorporated in the modified instrument.

A direct-current preamplifier and an alternating-current to direct-current converter, both having high input impedance and providing buffering to the voltage source being measured, were designed for the Non-Linear Systems, Inc., model V35A digital voltmeter. The converter can serve as a standard for alternating-current voltage measurements because of its direct-current calibration.

The design, construction, and evaluation of the high-sensitivity, direct-reading linear recording conductometric titrator was completed. A proportional temperature controller that provides essentially stepless control of titration cell temperature to within ±0.01°C was designed to supplement the automatic temperature-compensation circuit for high-sensitivity work. The performance of the conductometric titrator on about 40 different chemical systems met, or exceeded, design criteria.

The controlled-potential alternating-current polarograph was rebuilt with a new potentiostat having improved performance characteristics. Test runs made with a dropping-mercury electrode on solutions that contained 10^{-4} *M* Cd^{2+} in 0.1 *M* KCl show that the instrument achieves excellent rejection of the double-layer charging current. Other tests indicate that excellent resolution of the In^{3+} and Cd^{2+} waves ($\Delta E_{1/2}$ = 38 millivolts) is obtained.

A model VII high-resolution flame spectrophotometer, which uses a single multiplier phototube (EMI type 9558QA) to cover the entire wavelength range from 2000 to 8700 angstroms, was designed and put into service for emission photometry. Either instantaneous or integrated flame-emission intensities can be recorded for measurement. The unit can also be used with an absorption source assembly for atomic absorption work.

An investigation has been completed of the feasibility of polarography for the direct determination of metal complexes in the organic phase following solvent extractions. The ORNL model Q-1988-FES direct-current polarograph was used to produce controlled-potential regular and first-derivative polarograms of cadmium and uranium in several solvent-extraction systems, including

those of the ion-association and chelate types. The average-current and derivative computer circuits were modified to permit the use of a ½-second Smoler-type vertical-orifice dropping-mercury electrode and the use of scan rates up to 3 volts per minute. A quantitative method for the determination of microgram quantities of uranium in tri-*n*-octylphosphine oxide extract was developed. Polarography in the organic extracts from solvent extraction offers the following advantages: (1) the substance to be determined can be concentrated selectively, (2) matrix elements that interfere are removed, and (3) a separate stripping step into an aqueous medium is not required. Also, the possibility exists of performing polarographic analysis on species unstable in water.

A controlled-potential voltammeter was designed and built for operation in molten-salt (including molten fluoride) systems. The voltammeter design uses several operational amplifier modules to achieve the necessary functions. The cells, fabricated from graphite or metal, contain a stationary polarized electrode, a counter electrode, and a reference electrode and may have a variable, uncontrolled resistive leakage to earth ground. For the uninsulated cell vessels, system ground must float with respect to earth ground. Performance tests of this voltammeter are in progress. Another controlled-potential instrument that will have chronopotentiometric and stripping-voltammetric functions in addition to the voltammetric function is to be designed.

VOLTAMMETRIC STUDIES IN MOLTEN FLUORIDE SALT SYSTEMS

In connection with the Molten-Salt Reactor Experiment (MSRE), it would be very desirable to carry out analyses of the molten fuel directly. However, to monitor such substances as corrosion products (iron, nickel, and chromium) and to gain information on the oxidation states and electrochemical behavior of other species in the molten fluorides is certainly a challenging analytical problem. Electroanalytical methods have proved valuable for *in situ* analysis of molten chloride and nitrate salt systems, and it is to this end that a program on voltammetric studies of reducible species in molten fluorides was initiated in mid-1962 and continued during 1963.

The melt (approximately 40 milliliters) is contained in a graphite cell (2 inches in diameter by 4 inches long) which is enclosed in a quartz jacket to maintain a vacuum or controlled atmosphere. An ORNL model Q-1988 controlled-potential polarograph was utilized to record the current-voltage curves. This instrument was modified to produce scan rates from 50 millivolts per minute to 10 volts per minute and to measure cell currents to 5 milliamperes. A stationary indicator electrode coupled with a platinum quasi-reference electrode comprised the measuring system. A third platinum electrode which was isolated served as the counter electrode. Indicator electrodes fabricated from platinum, gold, silver, tungsten, and pyrolytic graphite were utilized. Pyrolytic graphite is the most favorable indicator electrode material tested so far. The electrode is encased in hot-pressed boron nitride to insulate the layered edges of the "*c*" planes, so that only the impervious surface of the "*a*" plane is exposed to the fluoride melt.

The voltammetry of iron(II) and nickel(II) in molten LiF-NaF-KF (46.5-11.5-42 mole percent) was investigated. These electroactive species are of interest because they are corrosion products associated with MSRE-type fuels. The reduction of iron(II) to the metal occurs at approximately −0.6 volt versus the platinum quasi-reference electrode, whereas nickel(II) is reduced at −0.2 volt. Current-voltage curves recorded at slow scan rates (50 millivolts per minute) are S shaped, which indicates that the mass transport process to the electrode is governed by both diffusion and convection. At faster scan rates (greater than 50 millivolts per minute), however, the curves are peak shaped, which is in agreement with theory for a diffusion-controlled process at a stationary microelectrode. In either case, the limiting current is proportional to the concentration of reducible species over the range tested, approximately 30 to 300 parts per million of iron and 20 to 80 parts per million of nickel.

For peak-shaped polarograms, the relationship between peak current and scan rate at 500°C is given by

$$i_p = 2.29 \times 10^5\, n^{3/2} C A D^{1/2} v^{1/2} ,$$

where

i_p = peak current,

n = electron change,

C = concentration of electroactive species,

A = electrode area,

D = diffusion coefficient of the reducible species,

v = rate of voltage scan.

For both iron and nickel, plots of i_p versus $v^{1/2}$ resulted in straight lines, and from the slope of the lines, D values of approximately 1×10^{-6} square centimeter per second were calculated. The diffusion coefficients are approximately ten times smaller than normally found in aqueous solutions. This is believed to be due in part to increased complexation effects in fluoride melts and also to the increased viscosity of the melts.

Anodic stripping voltammetry was investigated as a means of evaluating low levels of nickel (less than 10 parts per million) in the melt. In this method, the nickel is plated onto the pyrolytic-graphite electrode and then anodically removed under controlled conditions. The area under the stripping curve (reverse current-voltage curve) is related to the concentration of nickel in the melt. Well-defined stripping curves were observed for nickel at the 4 parts per million level, and as little as 1 part per million could be detected. This approach, therefore, appears to be somewhat more sensitive than conventional wet chemical analysis for nickel in fluoride salts for which the lower limit is approximately 5 parts per million.

Current-voltage curves were obtained for the reduction of zirconium(IV) and the oxidation of uranium(IV) in fluoride melts. From an analytical point of view, however, erratic results were obtained when attempts were made to correlate the magnitude of the limiting current with the concentration of these constituents. This is believed to be due in part to oxide contamination of the melt which caused partial precipitation of ZrO_2 and UO_2. Further work is contemplated in this area.

It is planned to continue the controlled-potential voltammetric studies and to utilize additional techniques such as chronopotentiometry and potentiometric measurements. A better insight can be gained on the overall electrode process through different techniques.

As experience is gained with the pyrolytic-graphite electrode, it is anticipated that improvements in design and construction will enhance its usefulness in molten fluoride salt systems.

MOLTEN-SALT SPECTROPHOTOMETRY

Advances in Apparatus

A new high-temperature cell assembly, fabricated from nickel metal, is now in operation. The design of this furnace is such that no insulation material is in the compartment where samples are melted. The atmosphere surrounding the sample is therefore much more inert than had been the case in the original furnace. Initial evaluation of the newly developed captive liquid cells was completed. These cells are cylindrical metal containers with specially designed holes placed in the side of the container. A corrosive liquid, such as a molten fluoride salt, which wets the walls of the container is held in the container above the holes so that spectrophotometric observations of the liquid can be made through these holes. The liquid path length in the hole is slightly larger than the outside dimensions of the cell and is reasonably constant, ±3 percent. This apparatus is used for spectrophotometric studies of molten fluoride salts to ascertain analytical possibilities of such measurements for use with molten-salt reactor melts and to investigate the chemistry of molten fluoride solutions which is of value to the above reactor program and other programs where molten fluoride salts are being or will be used.

Reactions of Active Metals with Molten LiF-NaF-KF

The reaction of metals (such as uranium, zirconium, lithium, magnesium, yttrium, chromium, and iron) with LiF-NaF-KF (46.5-11.5-42.0 mole percent) has been studied spectrophotometrically in order to evaluate the stability of these metals with alkali fluorides and therefore provide a basis for predicting possible reactions of these metals with molten-salt reactor melts. All metals except chromium and iron reacted with the melt in the

following way:

$$MF + \frac{1}{n} R^0 \rightarrow \frac{1}{n} RF_n + M^0 ,$$

where MF is NaF or KF and R^0 is an active metal. The alkali metal vapors are identified by their characteristic resonance absorption spectra.

With uranium, it was observed spectrophotometrically that both U^0 and U(III) were unstable with respect to U(IV) in the alkali fluoride eutectic. Although U(III) is not stable in this melt, the spectrum was obtained, and estimates of the molar absorptivities of several absorption peaks were made, approximately 500 liters $mole^{-1}$ cm^{-1} at 420 millimicrons and approximately 40 liters $mole^{-1}$ cm^{-1} at 890 millimicrons. In the absence of interfering ions, U(III) could therefore be determined spectrophotometrically at concentration levels of under 100 parts per million at a wavelength of 420 millimicrons. It is of interest to note that soluble lower-oxidation-state zirconium was not observed in the reaction of Zr^0 with LiF-NaF-KF.

Coordination of Dissolved Ionic Species in Fluoride Melts

Although the application of ligand-field theory to the interpretation of absorption spectra is not specifically a problem in analytical chemistry, it is of definite value in a physical and an analytical sense. By means of such considerations, various oxidation states of transition-metal ions can be identified, and information concerned with the coordination of these ions in melts of interest can be obtained. In cooperation with the Metals and Ceramics Division a detailed study was made of the spectrum of NiF_2 in LiF-NaF-KF. A fit of the experimental transition energies to theoretical energy levels is very satisfactory for an octahedral configuration of Ni(II) in the melt having a cubic ligand field parameter (Dq) of -650 cm^{-1} and Rocah's interelectronic repulsion parameter (B) of 950 cm^{-1}. Work of this nature has not been undertaken previously in molten fluoride salts. Spectral absorption data are now being obtained for Fe(II) and Cr(II) in LiF-NaF-KF and LiF-BeF_2-ZrF_4 for similar interpretation.

CHEMICAL ENGINEERING RESEARCH

High-Performance Solvent-Extraction Equipment

As the fuel burnups in power reactors steadily increase, radiation damage to the solvents used in fuel recovery by solvent extraction becomes increasingly important. An obvious method of reducing this damage is to reduce the time of exposure of the solvent to a high radiation field.

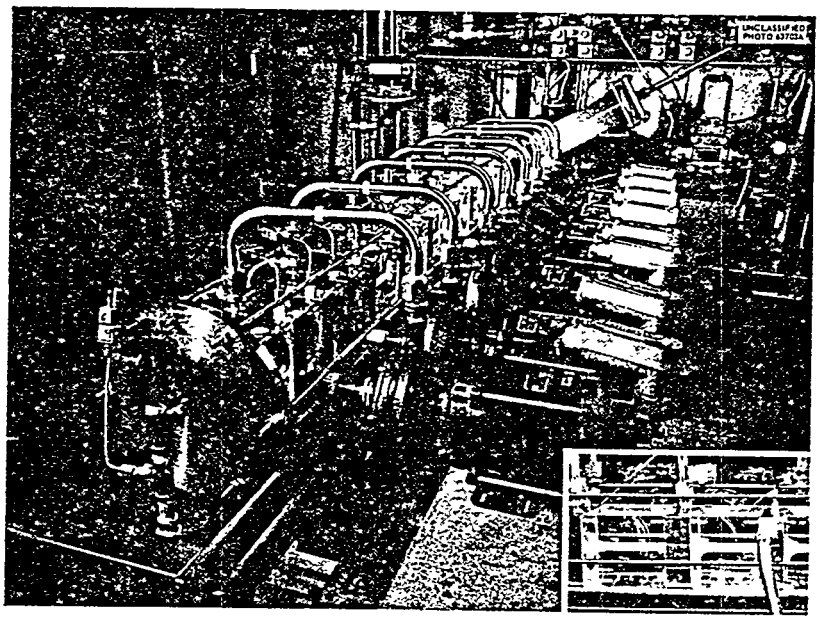

This experimental stacked-clone contactor is extracting uranyl nitrate from an aqueous solution into a tributyl phosphate solvent phase. The liquids remain in each stage less than 4 seconds. The insert shows the clone cavity cut in a clear plastic block. The swirling action of the liquid which separates the two immiscible phases and causes countercurrent flow is generated at a tangential inlet port within the stainless steel section. Each stage requires a pump to drive it. When applied to radiochemical processing, these pumps will be made an integral part of the unit, eliminating the need for connecting lines.

The Oak Ridge National Laboratory has been developing a solvent extraction device called the stacked-clone contactor, which reduces this exposure time to a tenth of that in the pulsed columns currently being used. The device uses hydroclones (liquid cyclones) and achieves a stable countercurrent flow of aqueous and organic phases by an inherent flow pattern of the hydroclones known as the "induced underflow effect." Although each stage of the experimental model requires a separate pump to drive it, no interstage flow control is required. Whereas conventional pulsed columns have holdup times of about 20 seconds per theoretical stage and require several hours to reach steady-state operation, the stacked-clone contactor has holdup times of about 3 seconds per theoretical stage and will reach steady-state operation in less than 10 minutes. The extremely rapid response of this device promises, in application to fuel recovery plants, a great reduction in "turn-around time" for the processing of different types of fuels. The very small inventory and the ease of startup and shutdown of the stacked-clone contactor may make possible a policy of operation heretofore unattempted.

SYSTEMS AND MATERIALS CHEMISTRY

Recovery and Separation of Fission Product Elements

Because of the increasing demand for radioactive fission products (e.g., strontium-90, cerium-144, and cesium-137) for space and industrial uses, studies have continued at ORNL on methods adaptable to the large-scale recovery of these elements from reactor fuel process waste solutions. Several new solvent extraction processes have been developed and are in use or have been tested successfully on a small scale. These include: recovery and separation of strontium and mixed rare earths by extraction with di(2-ethylhexyl)-phosphoric acid; recovery of zirconium-niobium by extraction with di(2-ethylhexyl)phosphoric acid; recovery of cesium by extraction with substituted phenols; and pretreatment of wastes by extraction with amines to remove bulk contaminants, such as nitric acid and iron, to produce better feed liquors for the recovery of fission products. These new developments have led to a versatile integrated solvent extraction flowsheet for the recovery and purification of nearly all the important fission products in waste liquor. Additional studies have shown the feasibility of recovering, with the same extractants, other valuable waste components, such as technetium, neptunium, and plutonium.

Recovery and Separation of Alkali Metals

A process developed at ORNL for recovering fission product cesium from reactor fuel waste liquors by solvent extraction with substituted phenols and stripping with dilute acid has been adapted to the recovery of macro amounts of cesium from ores. The process provides a simple and economical route to the production of high-purity cesium salts and is expected to be helpful in satisfying the expected large demand for cesium in the 1970's for ion-rocket propulsion and power-generation systems. The process is also applicable to the recovery of rubidium.

Purification of Transplutonium Elements

The production of increasing quantities of the transplutonium elements requires the development of new methods of purifying them of the much larger quantities of other elements produced simultaneously by fission. A problem of special importance is the removal of the lanthanides, which are in most respects very similar chemically to the transplutonium elements. One process for accomplishing this utilizes the selective extraction of the transplutonium elements by amines from highly concentrated chloride solutions.

Recently, an alternative method for separating these groups of elements was developed. It consists in preferentially extracting the lanthanides with di(2-ethylhexyl)phosphoric acid from an aqueous solution containing an aminopolyacetic acid (a complexing agent). Best results are obtained with an alkali-metal salt of diethylenetriaminepentaacetic acid in an aqueous solution of a carboxylic acid, such as lactic acid. The transplutonium elements are subsequently recovered from this solution by extraction with the same reagent, after the strength of the complexing agent is reduced with a small amount of nitric acid. The aqueous solutions used in this process are satisfactory from the standpoint of concentration of

chemicals required and their corrosive action on equipment.

Acid Recovery

A process was developed at ORNL for recovering sulfuric acid from waste streams (thereby making the waste disposal easier) by extracting the acid with long-chain alkylamines and stripping the acid from the solvent with water. Certain tertiary amines with branching close to the nitrogen, such as *N*-benzyl-di(2-ethylhexyl)amine, showed the best balance between acid-extraction power and amenability to water stripping. Also, relatively pure phosphoric acid can be recovered from commercial phosphoric acid by the same method, if amines with less branching on the alkyl chains are used.

Fundamental Extraction Chemistry

A continuing program at ORNL is devoted to the study of fundamental chemistry of reactions in solvent extraction processes and of the complex combinations of chemicals that are found in the aqueous and organic phases. Recent advances include: identification of thorium sulfate complex compounds that form in the aqueous phase and an evaluation of their formation constants; identification of complex compounds and their interactions in the extraction of sodium and strontium by dialkylphosphoric acid; evaluation of activity coefficients of solvent extraction agents in organic phases; and rate-of-transfer measurements, which help to identify the actual chemical forms in which metal ions are extracted.

Recovery of Thorium from Granitic Rock

Future demand for uranium and thorium as nuclear fuel will require eventual development of very low-grade ores. Previous studies at ORNL (see *Atomic Energy Research, 1961,* a special USAEC report, December 1961) showed that thorium can be recovered for several hundred dollars per pound from the most abundant rock in the earth's crust (granitic rock) when the thorium content is only 12 parts per million, the average value. Such costs are acceptable for a successful breeder power-reactor system.

Lower recovery costs are attainable with higher-grade granites. In this respect, recent studies at ORNL in cooperation with Rice University showed the Conway granite formations in New Hampshire to be an especially attractive future source of nuclear fuel. These deposits contain tens of millions of tons of thorium at an average concentration of about 55 parts per million. Lower, but still impressive, tonnages of uranium are also present. Process evaluations indicated that much of the thorium and uranium can be recovered from this material for less than $75 per pound. A significant portion may be obtainable at costs of $30 to $40 per pound. This single formation constitutes a hundredfold increase in known resources of moderate-cost thorium within the United States.

RADIOLYSIS OF METALLIC FLUORIDES

The effects of energetic radiation on solids have been under intensive study for a little more than 17 years. The mass of accumulated information is enormous; the number of well-established principles is less impressive. A new and unexpected phenomenon, the generation of considerable quantities of elemental fluorine as a gas, has recently been observed as a consequence of the self-irradiation of metallic fluoride mixtures containing fission products at temperatures well below the melting point of the material. Because the mixture of radiation types and intensities from fission products makes the results difficult to interpret, it was decided to make use of the so-called pure radiations in three programs which are now under way in the Reactor Chemistry Division. High-speed electrons from a Van de Graaff generator, high-energy gamma rays from a cobalt-60 source, and soft x rays from conventional skin-cancer-treatment equipment are used to irradiate the fluoride mixtures. The irradiated samples themselves are not radioactive; they can be removed from the sources of radiation and then handled by ordinary laboratory techniques.

Use of gamma radiation from a cobalt-60 source has produced fluorine gas at measurable rates during irradiations at temperatures up to 110°C; at 150°C, any fluorine gas which had been generated appeared to recombine with the remaining

salt constituents; at 130°C, the rate of recombination appeared to be roughly equal to the rate of fluorine generation.

A similar mixture of the fluoride salts (of lithium, beryllium, zirconium, uranium, and thorium), a mixture which could be used as a fuel in a molten-salt reactor, was bombarded with high-energy electrons at or near room temperature. Significant amounts of fluorine were released from the samples. Exposure of the fluoride salt mixture to x rays from a conventional 250-kilovolt generator also led to the evolution of fluorine; the particle size of the salt mixture appeared to be an important parameter in that large particles yielded much less fluorine than the small particles (possibly because of the larger surface area of the latter). Tests with x rays were made on a variety of pure metallic fluorides; lithium fluoride and zirconium fluoride failed to yield fluorine, while thorium fluoride (quite similar crystallographically to zirconium fluoride) liberated fluorine readily.

PYROLYSIS OF BIPHENYL

Biphenyl is the simplest member of the series of aromatic organic compounds (polyphenyls) which seem most useful as coolants for reactors moderated with heavy water. The principal advantages of these coolants are that they can be used at a moderately high temperature but at a low pressure and that they can be used in low-capital-cost conventional petroleum-refinery equipment. A disadvantage which limits their use is their tendency to be decomposed by the combination of high temperatures and high radiation fields. The thermal decomposition of biphenyl was studied by W. T. Rainey and co-workers in the Reactor Chemistry Division to provide a better understanding of the mechanism of the reaction as a prerequisite to an ultimate understanding and control of the decomposition by the combined effects of temperature and radiation.

Temperatures as high as 435°C, just above the limit of present usefulness of organic coolants, were used in the study. The extent of decomposition was limited to less than 1.5 percent of the starting material in order that the products of the initial steps in the reaction might be isolated before the onset of secondary or complicating reactions. Analytical procedures were developed in cooperation with the Analytical Chemistry Division which were able to account for all the reaction products. The primary products were benzene, hydrogen, terphenyl, and quaterphenyl. Simple kinetic equations were developed which described the effects of time and temperature. The presence of oxygen increased the amount of decomposition, while water, in the form of steam, was without effect. Some surfaces were found to increase the decomposition by "cracking" reactions similar to petroleum technology, but other surfaces were found to inhibit the decomposition. The results of studies such as this, ultimately including the effects of radiation, should make it possible to realize the potential advantages of organic reactor coolants.

NUCLEAR METHODS OF CHEMICAL ANALYSIS

Neutron Energy Distribution from ^{241}Am-Be Neutron Sources

^{6}LiF-Si sandwich neutron detectors were employed to determine the energy distribution of neutrons emitted by ^{241}Am-Be neutron sources. The response of the detectors was examined using 14.7-Mev T(d,n)He and ^{210}Po-Be neutron sources while varying the coincidence criteria of the energy (triton plus alpha) summation. It was determined that the background due to fast-neutron reactions on silicon is inversely proportional to the coincidence gate. For neutrons of energy above 6 Mev, coincidence circuits with a gate width of greater than 100 nanoseconds were essentially useless.

Chemical Effects of Isomeric Transitions in Tellurium

Nuclear isomers can oftentimes be chemically separated if the isomeric transition is highly internally converted. The efficiency of the separation can be simply determined, independently of detection efficiency, by gamma-ray spectrometry. The experimental efficiencies are all approximately unity for the isomers of tellurium-127, -129, and

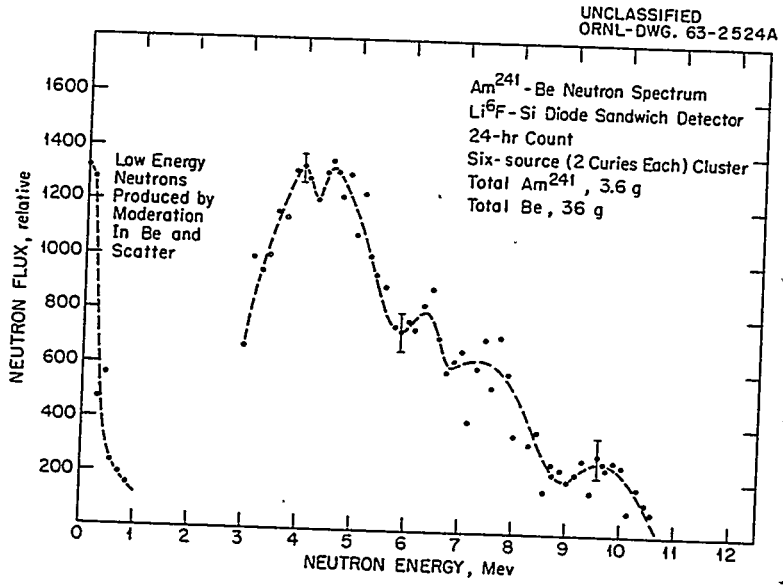

Americium-241–beryllium neutron spectrum. ^{6}LiF–silicon diode detector; 24-hour count of six-source cluster. Total americium-241, 3.6 grams; total beryllium, 36 grams.

-121 in 6 *N* HCl. Furthermore, the ratios of the separation efficiencies for tellurium-127 and tellurium-129 are close to unity in such media as solid telluric acid, H_2O, 6 *N* $HClO_4$, and 6 *N* NaOH. These results suggest that the chemical properties of the unstable tellurium species formed in internal conversion are essentially independent of the details of the nuclear decay and are the same in a given chemical environment for all tellurium nuclides that decay via highly converted isomeric transitions. The separation efficiency (*S*) for tellurium-127 was also observed to vary in a smooth manner with pH, as

$$S = e^x/(1 + e^x) ,$$

where x is a simple linear function of pH.

Activation Analysis of High-Purity Materials

A method has been developed for the comprehensive analysis of trace impurities in high-purity materials that are to be used in the construction of nuclear reactors. Samples of beryllium, aluminum, iron, and graphite have been analyzed for as many as 62 elements by measuring the gamma activities of the radionuclides produced by neutron activation. Ten elements are determined by nondestructive measurement of short-lived nuclides produced by 10-second irradiations in the pneumatic facility of the ORR. Gamma-emitting nuclides of chlorine, bromine, and iodine are measured in a second portion of the sample that has been irradiated for 20 minutes. Forty-nine elements are determined in a third portion of the sample that has been irradiated for 16 hours and subsequently been divided chemically into six groups of elements to facilitate resolution of gamma activities.

The method can be extended to the analysis of less pure materials by the use of additional chemical separation steps to ensure accurate discrimination of all gamma activities.

14-Mev Neutron Reactions

The first section of a gamma spectral catalog has been completed covering the elements $Z = 3$ to $Z = 30$. The catalog details the reactions observed when 1 gram of the element is irradiated at an unmoderated 14-Mev neutron flux of 5×10^8 neutrons cm^{-2} sec^{-1}. The reactions are listed, and cross sections are calculated when possible. The resultant gamma spectra are normalized to that spectrum which will be recorded when 1 gram of the natural element is irradiated for a short time (0.16–10 minutes). If more than one radionuclide is produced, a spectral decay is presented for two irradiation times. The spectra are most

useful to predict direct gamma spectral analysis sensitivities.

The second section, $Z = 31$ to $Z = 60$, is presently in progress.

Nuclear Methods

Second-order interference was studied in 23 cases of activation analysis. This error is caused by second-order nuclear reactions, that is, when the product of a neutron capture undergoes an additional neutron capture. The calculations were run in an IBM 7090 computer, and interference was plotted versus irradiation time. A total of 39 curves were drawn; they should prove useful to correct analytical results. This work and two comprehensive monographs, developed for radioactivity calculations, were sent to *Nucleonics* as separate papers.

A rapid method to estimate 14-Mev neutron-generator spectra was developed. It is based on (1) neutron energy tables for the reaction $^3H(d,n)^4He$, (2) neutron scattering data, and (3) probability calculations. The influence of the neutron spectrum in 14-Mev neutron-activation analysis and cross-section measurements can now be rapidly evaluated and has been shown to be significant. The method will be presented at the 1964 Annual Meeting of the American Nuclear Society.

X-RAY AND SPECTROCHEMICAL ANALYSIS

An x-ray fluorescence procedure was devised for determining Gd_2O_3 in Gd_2O_3-Al_2O_3 ceramics. Procedures were worked out to compensate for neighboring absorption-edge effects in x-ray absorption-edge analysis. A disposable cell was designed for the x-ray absorption-edge analysis of radioactive solutions. In atomic absorption analysis, studies were made of the effects of hollow-cathode current and absorption-tube length on absorbance. Tin was detected by this method at the 0.5 microgram per milliliter level. The ammonium phosphomolybdate adsorption–flame photometry method was adapted for the determination of cesium in seawater. Further studies of volatilization losses during the ashing of tissue have confirmed previous results and have failed to show evidence of loss of vanadium. Installation of a punched-tape readout on the Quantometer has reduced analytical time by one-fifth.

AQUEOUS SOLUTION CHEMISTRY

A broad program of research is being conducted in the Chemistry Division to study the properties of aqueous solutions over wide ranges of temperature and concentration. Many different techniques are being used in implementing this program, including spectrophotometric, electromotive force, solubility, and ion exchange studies.

A spectrophotometer chamber and cell assembly for the Cary model 14 spectrophotometer which allows simultaneous liquid-gas equilibration and investigations from 0.25 to 2.7 microns has been used routinely from below –70 to 280°C and from 0 to 2000 pounds per square inch absolute. The spectral variations with temperature and comparisons of the liquid and vapor spectra of H_2O, D_2O, and ethanol clearly indicate greater hydrogen bonding than in the case of ammonia, which in turn shows much more intermolecular attraction in the liquid state than does carbon dioxide. The aqueous mineral acids H_2SO_4, HNO_3, and $HClO_4$ have been shown to be suitable solvents for spectrophotometric studies of metallic ions in titanium cells with sapphire windows. At concentrations of about 0.1 *m*, the windows should last at least several days at 250°C and, of course, much longer at lower temperatures.

Electromotive force studies have been used to measure the activity coefficient of hydrobromic acid in hydrobromic acid–sodium bromide mixtures to unit ionic strength and 150°C. From these results and those in the literature for pure potassium bromide solutions, the activity coefficient of potassium bromide in the mixtures was evaluated to 90°C. The deuterium gas electrode has been used to determine the activity coefficient of deuterium chloride in heavy water to 225°C and unit molality. A study of the activity coefficient of hydrochloric acid in hydrochloric acid–sodium chloride mixtures to at least 225°C is now in progress.

The second dissociation constant of deuteriosulfuric acid has been computed from 25 to 225°C from data on the solubility of silver sulfate in deuteriosulfuric acid solutions. In addition, the

thermodynamic constants for the reaction $DSO_4^- = D^+ + SO_4^{2-}$ have been evaluated.

The structure of the aqueous pertechnetate ion, TcO_4^-(aq), has been shown to be tetrahedral by Raman and infrared spectroscopy. Interpretation of the Raman spectrum of the ion, required for the structure determination, was greatly facilitated by observing the Raman spectra of powdered crystals of $KTcO_4$ and several salts containing tetrahedral oxyanions which surround technetium in the periodic table. The excellence of the Raman crystal spectra, together with the infrared spectra observed, also made possible refinement of the interpretation of the Raman spectra of the aqueous oxyanions of several of these salts (specifically ReO_4^-, WO_4^{2-}, and MoO_4^{2-}).

The identification of niobium(V) species in hydrofluoric acid has been accomplished by a direct comparison of the Raman spectra of the solutions and of crystals containing fluoro complexes of niobium. The Raman spectra of crystalline $K_2NbOF_5 \cdot H_2O$, $CsNbF_6$, and K_2NbF_7 show that the $NbOF_5^{2-}$ ion is present in solutions made by dissolving K_2NbF_7 in 1 to 35 percent HF and that the NbF_6^- ion is present in solutions containing 25 to 50 percent HF. The infrared spectrum of $K_2NbOF_5 \cdot H_2O$, when compared with the Raman spectrum, shows that the $NbOF_5^{2-}$ ion rather than the $Nb(OH)_2F_5^{2-}$ ion is present in the crystal.

A broad, systematic study has been completed on the cation exchange adsorption of elements from HCl, $HClO_4$, and $HClO_4$-HCl-HF mixtures. Many of the elements show excellent adsorption, particularly at high ionic strength. The data permit conclusions concerning chloride and fluoride complexing of many of the elements and serve as a basis for numerous separations.

Cation and anion exchange measurements have been carried out with a number of elements in mixed solvents, for example, HCl-water-methanol or HCl-water-acetone. In many instances, column separations are markedly improved by use of these mixed solvents. In studies of the properties of inorganic exchangers, zirconium(IV) antimonate was found to have excellent adsorptive properties and high selectivity for Na^+. The material also shows an unusually high selectivity for Ca(II) and Sr(II) in comparison with Mg(II), which permits their removal from moderately large volumes of 0.1 *M* Mg(II) solutions. In acidic media, zirconium(IV) antimonate was found to be a poor adsorbent for cations.

NUCLEAR CHEMISTRY

The long-term goal of nuclear chemistry research is the interpretation of nuclear energy level structures and nuclear processes in terms of fundamental theoretical concepts. Before this goal is attained, much nuclear data must be taken and systematized. Theories of nuclear processes must be proposed which not only explain existing data but predict new phenomena which are susceptible to observation and measurement. The knowledge gained in this process not only has intrinsic interest, but it is fundamental to the development of nuclear technology.

The areas of interest include studies of the nuclear chemistry of the transuranic elements. This area forms a logical subdivision of the field because it requires a knowledge of the chemical properties of the actinide elements, and because skill in handling high levels of alpha radioactivity is required. This work is part of the national transuranic program which also includes the HFIR and TRU projects at ORNL.

Another area of interest has centered around nuclides which are of special importance in reactor technology. The interest here is in the half-lives, decay schemes, and neutron cross sections of fissionable isotopes and fission products. Fission yield curves, independent fission yields, and delayed neutron emission are also of interest in this program.

A third area of interest in nuclear chemistry is nuclear spectroscopy. Here the goal is the elucidation of nuclear energy level diagrams and the assignment of spins and parities to the levels. The techniques involve the study of nuclear energy levels by use of low-energy particle scattering, as well as the study of levels populated by radioactive decay.

One of the more fruitful techniques used in the determination of nuclear energy levels involves the bombardment of a target nucleus with a particle of known energy, and detection of a scattered proton with a semiconductor detector. Energy levels in nickel-62, nickel-64, copper-63, copper-65, cadmium-115, and cadmium-117 were studied in 1963 in cooperation with members of the Physics Division. The work on cadmium-115 was particularly rewarding because it could be related to current work on the decay scheme of silver-115 at MIT.

A 12.000 ± 0.005 Mev deuteron beam from the ORNL Tandem Van de Graaff accelerator was used to bombard a cadmium-114 target. The protons from the $^{114}Cd(d,p)^{115}Cd$ reaction were detected with lithium-drifted silicon detectors which gave an overall energy uncertainty of ±20 kev. About twenty new energy levels of cadmium-115 were discovered.

It was possible to assign definite orbital angular momentum quantum numbers (l) to eight of these levels. This was done by measuring the angular distributions of the different proton energy groups and comparing the results with the predictions of the distorted-wave theory of nuclear reactions. Since the nuclear spin $j = l \pm \frac{1}{2}$, these measurements give definite parity assignments and limit the choices for the spin of a given energy level to two. In the case of cadmium-115, the ambiguity in the spin assignments could be removed by using the MIT results on the silver-115 decay scheme.

The experimental level structure was compared to that computed for cadmium-115 by Kisslinger and Sorenson on the assumption of a short-range pairing force between like nucleons, plus a quadrupole interaction between all nucleons. There was fair qualitative agreement between theory and experiment on the number of levels of a given spin but quantitative disagreement on the energies of these levels. Although part of the discrepancy may result from errors inherent in the analysis of the data, the experimental results indicate the need for further development of the theory.

RADIATION CHEMISTRY

Formation of Ozone in the Radiolysis of Liquid Oxygen and of Oxygen-Nitrogen Solutions

Ozone is the only stable product of the radiolysis of oxygen. We found that on irradiating liquid oxygen, ozone is produced with a yield of 12.5 molecules for every 100 electron volts of energy absorbed. This yield represents a conversion of 21 percent of the radiation energy to chemical energy, and is one of the most efficient reactions known. The production of ozone, therefore, is a possible chemonuclear process, and it is important to understand the mechanism. But the possible production of ozone is not the only reason for studying oxygen, and perhaps not the most important. Oxygen is extremely interesting to radiation chemists because it is a small molecule with a high electron affinity and relatively low ionization potential, and it readily enters into many important reactions induced by radiation. In addition to studying the radiolysis of pure liquid oxygen and developing a mechanism for ozone formation, we also irradiated mixtures of liquid oxygen and nitrogen in all proportions. Again, the principal product is ozone, but small amounts of oxides of nitrogen are also produced. It was discovered that a large fraction of the energy absorbed by the nitrogen was effective in making ozone. Even when the oxygen concentration is only 0.005 percent, the ozone yield is still about 20 percent of that for pure oxygen. This means that some type of "energy transfer" occurs. On this basis, a mechanism was developed which accounts for the ozone yield over most of the concentration range. For making these measurements, special silica Dewar vessels were designed which allowed irradiation of the cold liquid, and subsequent measurement of the ozone by optical absorption *in situ*. This technique avoided possible decomposition of the ozone in the transfer and other operations required in the chemical methods usually employed for analysis.

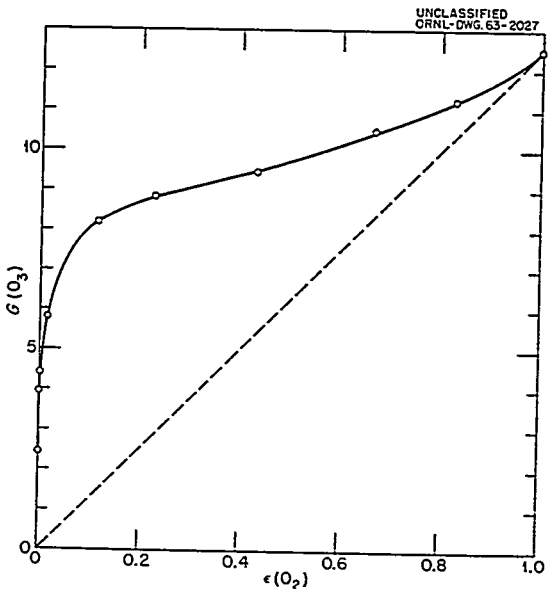

Ozone yield $G(O_3)$ from the radiolysis of oxygen-nitrogen at 77°K vs electron fraction of oxygen $\epsilon(O_2)$.

"Thermal Spikes" in Radiation Chemistry

Radiation chemistry is unique among the various branches of kinetics in two important aspects. First, a wide variety of states are excited, including very high states which cannot be excited by photochemical or other means. Second, the energy is deposited in a system along the tracks of charged particles, and as a result, the reactive intermediates such as ions, excited molecules, etc., are produced in a very nonhomogeneous spatial distribution. This can influence both the qualitative as well as quantitative aspects of the reaction, and the interpretation of results has required a special type of diffusion kinetics. But in addition to the inhomogeneous concentration of intermediates, there can be other extreme transient conditions existing in the particle tracks such as high local temperature and high charge that could influence markedly the course of reactions. These conditions have seldom, if ever, been considered in interpreting the chemical effects of radiation. The possibility of thermal effects in particle tracks was proposed by Dessauer forty years ago in his "point heat" theory; however, there has been little or no experimental evidence concerning this possibility. About three years ago we obtained evidence from which we postulated that thermal effects in alpha-particle tracks are a significant factor in the decomposition of nitrate crystals. We recently tested this hypothesis further by measuring the chloride yield in the decomposition of sodium chlorate by gamma rays and by alpha particles, and by determining the effect of post-irradiation annealing on these yields. We found that on annealing at 185°C the salt that had been irradiated with gamma rays at 25°C, the chloride yield was raised by about 30 percent. The yield for decomposition by alpha particles at 25°C was about 40 percent higher than for gamma rays, and there was no effect of postirradiation annealing at 185°C. The results are consistent with the previous postulate that thermal effects in alpha-particle tracks are a significant factor in the radiolysis.

Carbon Dioxide Sensitized Radiolysis of Hydrogen and Oxygen

In the radiolysis of gases, there has long been evidence for the importance of ions to stages of the process later than the initial act, and there is currently great interest in establishing the extent and manner of the participation of ions. Lind observed long ago that the rare gases sensitize some radiolytic reactions. He explained the sensitizing action by the concept of charge transfer from primary ions He^+, Ne^+, or Ar^+ to such molecules as H_2 and O_2, both of which have lower ionization potentials than any of these rare gases. The use of an inert gas of ionization potential between those of the two reactants provides an obvious further test of this concept. This has now been done for the reaction of hydrogen and oxygen to form water, with CO_2 as the component with intermediate ionization potential. The CO_2 was demonstrated to be inert by complete recovery of the amount added. Like the rare gases, CO_2 did sensitize the reaction, but not by the full amount corresponding to the ionization of the CO_2. A mechanism was developed which quantitatively explains the results. The key steps in the mechanism are reactions in which CO_2 robs H_2^+ of charge, and deactivates the excited ions O_2^{+*} and CO_2^{+*}; O_2 deactivates CO_2^{+*}, and H_2 reacts with CO_2^{+*} to form the reactive intermediate HCO_2^+. Information concerning reactions of excited ions has become available from mass spectrometric studies.

ORGANIC CHEMISTRY

Recent Studies on Molecular Rearrangements

When compound I is dissolved in cold, concentrated sulfuric acid, it rearranges to the ketone II. The first persons to carry out this reaction [D. C. Kleinfelter and P. von R. Schleyer, *J. Am. Chem. Soc.* 83, 2329 (1961)] did not start with an optically active form of I, so the question of whether the product is II*a* or II*b* was left unanswered.

The rearrangement of I to II is an example of a general reaction called the "pinacol rearrangement," and we in the organic group at ORNL have studied and clarified many reactions which are in this class. A review article has been written on the subject [C. J. Collins, "The Pinacol Rearrangement," *Quart. Rev.* 14, 357–77 (1960)].

UNCLASSIFIED
ORNL-DWG. 64-3247

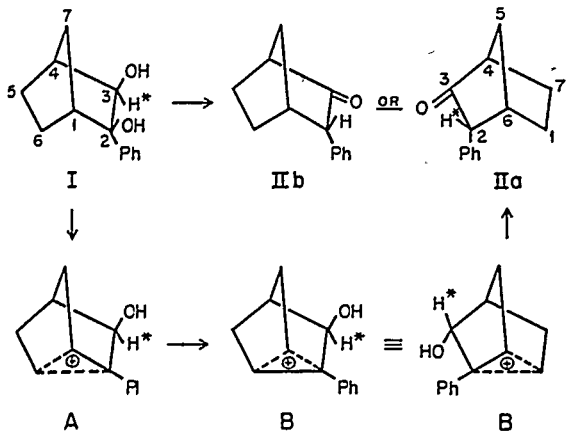

The interesting thing about the rearrangement of I is that none of the well-established reaction paths seemed beforehand to be very likely. We were unable to say with any confidence how we thought this reaction should take place, so it seemed an excellent problem for study. Richard Werth of Concordia College in Minnesota and Zafarullah K. Cheema of Knoxville College (both ORINS research participants), working together with B. M. Benjamin, used tritium and carbon-14 to trace the rearrangement. They also prepared I in optically active form and showed that optically pure II*a* and *not* II*b* was produced. Each carbon atom in the product II*a* could then be identified with a corresponding carbon atom in the starting material I, and the numbers surrounding the structures I and II*a* show this relationship. We were able then to propose a reasonable mechanism for the reaction in which I goes initially to the *bridged* carbonium ion *A*. Ion *A* then rearranges to *B*, which goes to product II*a* with an accompanying migration of the hydrogen (marked with the asterisk) on carbon No. 3. The so-called "open" or "nonbridged" carbonium ion intermediates appear to be excluded by our experiments, and this fact is of considerable significance to the current controversy over the existence or nonexistence of bridged (or "nonclassical") carbonium ions [see, for example, H. C. Brown and co-workers, *J. Am. Chem. Soc.* 86, 1246, 1247, 1248 (1964)].

Isotope Effect Studies

In a further application of the differential method [V. F. Raaen, A. K. Tsiomis, and C. J. Collins, *J. Am. Chem. Soc.* 82, 5502 (1960); V. F. Raaen *et al.*, *J. Am. Chem. Soc.* 85, 3497 (1963)] for determining very small isotope effects of carbon-14, we have measured the isotope effects exhibited by compounds substituted with deuterium. In the differential method, the product is not allowed to accumulate, but instead very small portions of it are withdrawn as formed. The method can be illustrated by an example in which the reaction studied is the formation of the 2,4-dinitrophenylhydrazone of benzaldehyde-^{14}C (the asterisk means labeling with carbon-14):

$$\mathrm{Ph\overset{*}{C}HO} + \mathrm{H_2NNHR} + \mathrm{H^+} \rightleftharpoons \mathrm{Ph\overset{*}{C}H{=}NNHR} + \mathrm{H_2O} + \mathrm{H^+}.$$

Since the reaction is quantitative, and since the product is a solid insoluble in the alcohol-water mixture used, we can collect the solid (quantitatively) on a filter. It is necessary only to add very small portions of the reagent, $\mathrm{RNHNH_2} + \mathrm{H^+}$, filter the product, and then add more reagent to the filtrate. If the aliquots of the product obtained are kept small (one percent of the total or less), then the relationship between the molar radioactivity (A_0) of starting material ($\mathrm{Ph\overset{*}{C}HO}$), and of each small aliquot (A) of product to the fraction of reaction (f) and isotope effect (k^*/k), is given by the following equation:

$$A = A_0 \frac{k^*}{k} (1 - f)^{(k^*/k) - 1} .$$

Thus, if we know A_0, A, and f, we can calculate k^*/k for the reaction.

We studied the isotope effect owing to deuterium in the α-deuterated benzaldehyde PhCDO by mixing the two species $\mathrm{Ph\overset{*}{C}HO}$ and PhCDO and repeating the process just described. The ratio of k^*/k for the first and second experiments then eliminates k^*, and provides the isotope effect due to deuterium alone. The method was also applied to the mixture PhCDO:PhCHO.

Experiments with both mixtures showed that the deuterium in PhCDO slows down the reaction with 2,4-dinitrophenylhydrazine ($\mathrm{RNHNH_2}$) about five percent.

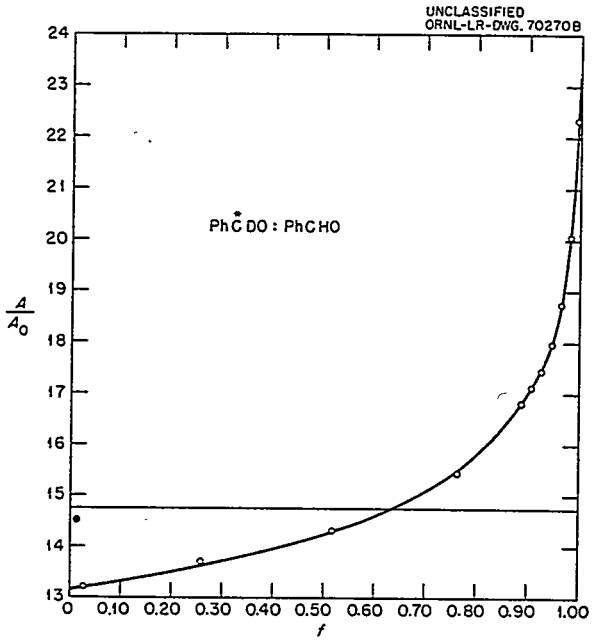

Deuterium isotope effect in the formation of the 2,4-dinitrophenylhydrazone of benzaldehyde. The first point is well above the curve. Similar behavior has been noticed in several differential experiments and demonstrates, we think, that caution must be exercised when measuring isotope effects by the low-conversion approximation, in which the isotopic content of only the first aliquot is compared with that of the reactant.

New Organic Solvents for the Extraction of Source and Fissionable Materials

Among the various types of organic compounds that have been successfully employed for the solvent extraction of materials of interest in nuclear energy programs, neutral compounds with strong polar groups have been very important. Our current interest has been devoted to amides, partly because the small amount of published work has shown them to be suitable solvents, and mainly because synthetic methods are available for the preparation of a wide variety of structures. A series of *N,N*-dialkyl amides has been prepared from 2-ethylhexanoic acid,

$$C_4H_9CH(C_2H_5)CONR_2 ,$$

where R was methyl, ethyl, *n*-propyl, *i*-propyl, *n*-butyl, and $-NR_2$ was morpholine. Tests of the extraction of uranyl and thorium nitrates from nitric acid solutions have been conducted by members of the Chemical Technology Division. Uranyl nitrate was extracted with higher distribution coefficients (20- to 2000-fold greater) than thorium nitrate. The effect of the size of the R groups was greater with thorium. A more dramatic difference was noted when the branching of the acid chain was adjacent to the carbonyl group. The *N,N*-dimethyl amide of neotridecanoic acid, a commercial mixture represented by

$$C_9H_{19}C(CH_3)_2CON(CH_3)_2 ,$$

extracted uranyl nitrate much more strongly than thorium nitrate. The results indicated that greater selectivity can be achieved by branching on the carbon atom adjacent to the carbonyl atom than by varying the size of the alkyl groups on nitrogen.

Grafting Polymers onto Cellulose Membranes

The members of ORNL who are studying the hyperfiltration of salt solutions for the Water Research Program, supported financially by OSW, have requested membranes for testing. An ion exchange membrane has been prepared by the grafting of polyacrylonitrile onto cellophane film, followed by hydrolysis to polyacrylic acid. An exchange capacity up to 3.5 milliequivalents per gram of dry film can be achieved with only a slight loss of water flow through the film. Higher exchange capacities are accompanied by weakening of the film until, at some capacity above 4 milliequivalents per gram of dry film, the conversion to the sodium form is accompanied by disintegration of the membrane. Hyperfiltration studies by J. S. Johnson (ORNL Chemistry Division) have been used to demonstrate salt rejections of about 30 percent. Other monomers will be grafted onto cellophane and other polymers in a continuation of this study.

Purification of Organic Compounds

Organic compounds of high purity are required by members of the Water Research Program for physicochemical measurements. Many of the commercially available compounds that were thought to be pure were found to have unpredictable behavior during these measurements, and some of these compounds were found to be mixtures. The monomethyl and monoethyl ethers of diethylene glycol contained ethylene glycol as a contaminant. Ethylene glycol monoacetate and glycerol diacetate are normally obtained pure by synthetic methods that involve several steps. It has been found, however, that all of the above compounds can be purified by countercurrent batch distribution between chloroform and water. Although these compounds have a high solubility in water, their distribution was controlled by controlling the ratio of chloroform to water.

SOLUTIONS OF METALS IN MOLTEN SALTS

Studies, expecially those of the alkali metals carried out by M. A. Bredig, H. R. Bronstein, and A. S. Dworkin of the Chemistry Division, had led to the discovery that many electropositive metals dissolve readily in the melts of their halides. Recent measurements by these workers of the solubility of the alkaline-earth metals calcium, strontium, and barium in their molten chlorides, bromides, and iodides and of the electrical conductance of the solutions formed showed that these metals behave quite similarly to the corresponding alkali metals lithium, sodium, and potassium. For instance, the temperature of complete miscibility of metal with salt in the liquid state was found to be as low as 910°C for barium iodide–barium metal and thus not very much higher than in the corresponding potassium system. In the calcium and strontium metal solutions, as in the sodium systems, mobile, that is, conducting, electrons are thought to be increasingly trapped in pairs with increasing metal solute (electron) concentration to form dimeric calcium(I) and strontium(I) ions, Ca_2^{2+} and Sr_2^{2+}. These are analogous in electronic structure to neutral diatomic alkali-metal molecules, and somewhat similar to the well-known mercurous ion, Hg_2^{2+}. In the barium metal solutions, as in potassium metal solutions, electric conductivity rises with increasing rate as the metal concentration increases. The trapping of the electrons is far less pronounced because the stability of diatomic alkali-metal molecules or dimeric alkaline-earth(I) ions is lower for electropositive metals with higher atomic numbers.

DEVELOPMENT OF AN ELECTROCHEMICAL pH STAT

The accurate control of acidity in aqueous solutions is of great importance in many chemical processes and researches. An apparatus has been developed which controls automatically the acidity of unbuffered solutions. This method of pH control takes advantage of favorable properties of the hydrogen gas–hydrogen ion reaction ($H_2 = 2H^+ + 2e^-$) on platinum or other inert electrodes.

An electronic potentiostat (a device for automatically controlling the potential of an electrode) is used to control precisely the potential of a large platinum electrode in a solution saturated with hydrogen gas. The potential difference between the large platinum electrode and a reference electrode provides the input voltage to the potentiostat. Any difference between this voltage and the reference voltage setting (preset) on the potentiostat is amplified and actuates a flow of current between the platinum electrode and an auxiliary polarizing electrode located in an external chamber connected to the cell by use of a salt bridge or porous plate. The passage of current through the large platinum electrode forces the hydrogen reaction to proceed, and this causes an increase or decrease of hydrogen ion concentration with time. When the solution pH approaches the value at which the reversible potential of the platinum electrode equals the potentiostat reference voltage, current flow approaches zero, and the pH is subsequently controlled (automatically) with a precision which depends on the control characteristics of the potentiostat.

This method of pH control possesses certain advantages. No complex electromechanical devices and no solution volume corrections because of the addition of reagents are necessary.

The pH may be changed easily and precisely by merely changing the potential at which the platinum electrode is maintained. Furthermore, the method is most effective in the pH region near neutrality, where precise pH control is most difficult to obtain in unbuffered solutions.

The kinetics of reactions which produce or consume hydrogen ions may be measured at constant acidity by use of the electrochemical pH stat. This capability is particularly valuable in the case of corrosion reactions, since the technique provides a continuous measurement of corrosion rate without the necessity for weight loss or electrochemical polarization measurements.

ELECTROCHEMICAL STUDY OF THE MECHANISM OF CORROSION INHIBITION ON IRON

In typical "noninhibiting" aqueous solutions, such as deoxygenated acidic sulfate, perchlorate, and chloride solutions, iron corrodes by an electrochemical mechanism which involves anodic oxidation of metallic iron to ferrous ions and simultaneous cathodic reduction of hydrogen ions to molecular hydrogen. In "inhibiting" solutions, such as those containing benzoate ions which are adsorbed on the iron surface, spontaneous corrosion is considerably retarded.

The mechanism of this inhibition, as well as of the corrosion and hydrogen evolution reactions, was established in detail at ORNL by precise electrochemical measurements on current density or reaction rate as a function of electrode potential and reactant concentrations. The adsorption of benzoate ion causes two effects: (1) it accelerates or catalyzes the rate of the hydrogen evolution reaction on the iron surface; (2) this acceleration, which by itself would tend to increase the overall corrosion rate, is compensated by a great inhibition of the anodic iron dissolution reaction, by several orders of magnitude below the rate in sulfate solution. The net effect is a substantial decrease in the spontaneous corrosion rate.

A theoretical model of the adsorption process was developed which, for the first time, explains both transient and steady-state measurements or the corrosion of iron in the presence of an adsorbec inhibitor.

THE CRYSTAL STRUCTURES OF SOME XENON FLUORIDES

The revolutionary discovery, about two years ago, that the element xenon can form chemical compounds with fluorine demolished the long-standing belief that the noble-gas elements are chemically inert. To assist in understanding the nature of these compounds, knowledge of the detailed arrangement of atoms within the molecules is necessary. H. A. Levy, P. A. Agron, and R. D. Ellison of the Chemistry Division and J. H. Burns of the Reactor Chemistry Division used the methods of x-ray and neutron diffraction to obtain such information for the two molecules xenon difluoride (XeF_2) and xenon tetrafluoride (XeF_4) as they exist in crystals of XeF_2, of XeF_4, and of $XeF_2 \cdot XeF_4$.

From such analyses the symmetry of the molecules, the lengths of bonds between atoms, and the kind of thermal motion which the molecules exhibit were determined. The molecular addition compound of xenon difluoride and xenon tetrafluoride ($XeF_2 \cdot XeF_4$), discovered by J. H. Burns, was found to consist of discrete molecules of xenon difluoride and xenon tetrafluoride packed together in the crystal. The xenon tetrafluoride molecules have the four fluorine atoms at corners of a square with the xenon atom at the center and in the plane of the square; the xenon difluoride molecules are linear. Both these configurations and the xenon-fluorine distances in each molecular species are the same as those in crystals of the individual compounds xenon tetrafluoride and xenon difluoride. Forces holding the molecules together are believed to arise from electrostatic attraction between the slightly charged xenon atoms and the oppositely charged fluorine atoms of other molecules. Thermal energy causes the molecules to move about; since the forces within each molecule are stronger than forces between molecules, they tend to vibrate as rigid bodies in the crystal.

Perspective drawing of the crystal structure of $XeF_2 \cdot XeF_4$, showing interatomic distances. This remarkable example of a true molecular crystal, in which both the XeF_2 and the XeF_4 units retain their identity, was discovered and its structure was determined at ORNL in the course of the very recent world-wide intensive study of xenon and other noble gas compounds.

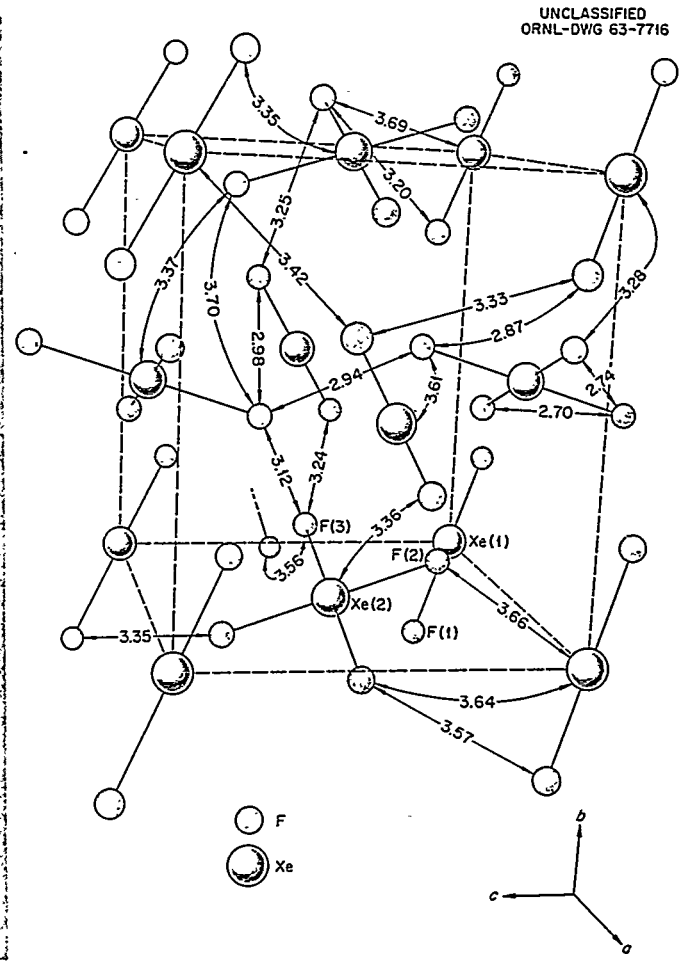

DETERMINATION OF MOLECULAR AND CRYSTAL STRUCTURE OF SUCROSE BY NEUTRON DIFFRACTION ANALYSIS

The molecular and crystal structures of sucrose were determined by G. M. Brown and H. A. Levy of the Chemistry Division from neutron diffraction data obtained with the automatic single-crystal diffractometer by using a neutron beam from the Oak Ridge Research Reactor. The structure, previously known only very roughly from older x-ray studies, is now known in complete detail, in the sense that all spatial relationships among the atoms are clarified by the precise specification of every interatomic distance. Such data are part of the fundamental information required for understanding the chemical behavior of any molecule. The data on molecular shape and dimensions for the sucrose molecule are particularly valuable because sucrose is a molecule of importance in biochemistry and commerce.

The structure study on sucrose was part of a continuing program in development and application of the method of crystal-structure determination from neutron diffraction data. The method is very similar to x-ray analysis. The significant advantage is that in neutron analysis, light atoms can be located precisely in the structure, even when much heavier atoms are present (for example, hydrogen atoms in the presence of carbon and oxygen atoms, or of even much heavier atoms). Often, as in the case of sucrose, information on hydrogen atoms is very important chemically. The structure analysis on sucrose is the largest problem

ever undertaken by the neutron method, as measured by the complexity of the subject crystal and by the number of data obtained.

MOLECULAR-BEAM STUDIES IN PHYSICAL CHEMISTRY

The use of atomic and molecular beams in the study of gas reaction kinetics permits the avoidance of the complicating phenomena that are generally associated with chemical kinetic studies. Multiple collisions and wall reactions may be eliminated, and the energies of the reacting species may be closely controlled. This fine control over the reaction parameters enables one to resolve the total chemical reaction cross section into its component differential cross sections, thus elucidating the dependence of the reaction upon the collision energy, the angular momentum, the orientation of reactants at time of collision, and the internal energy of the reactants. The molecular-beam technique is the only known technique which will yield these parameters, so necessary in the fundamental understanding of the mechanism of a chemical reaction.

Measurement of the differential elastic scattering cross section can give information about the intermolecular potential. For any intermolecular potential which has both a repulsive and attractive part, a maximum should exist in a plot of the differential cross section versus scattering angle. The position of the maximum, called the "rainbow angle," is related to the depth of the well in the potential curve. Such peaks were observed in the scattering of a velocity-selected atomic beam of potassium from xenon, and an analysis indicated a binding energy of 200 calories.

Information about the nature of these potentials can also be obtained from the total scattering cross sections. A measurement was made of the relative total scattering cross sections of potassium in molecular and atomic iodine. (The atomic iodine beam was formed by thermal dissociation of I_2 at 1000°K.) The effective size of the I_2 molecules was only 1.2 times as large as that of the iodine atoms. This result is not in accord with the assumption of a simple, mutual polarization interaction for both I_2 and I. It is, however, in accord with a long-range electronic exchange interaction with iodine atoms leading to a KI collision intermediate in either a singlet or triplet state.

With molecular-beam techniques, the consequences of single collisions of molecules in well-defined energy states with uncontaminated surfaces may be determined. Fundamental studies may thus be made in adsorption mechanisms, in energy transfer, in accommodation phenomena, and in the field of surface catalysis.

When a cold helium atomic beam was reflected from a hot platinum surface, it was found that the atoms rebounded in much the same manner as light striking a mirror surface. However, a velocity analysis of the reflected particles showed that they had picked up more energy than was possible by the single collision with so massive a particle as a platinum atom. The inference that the surface was covered by a low-atomic-weight impurity (probably carbon) was borne out by the change in behavior accompanying the admission of a trace of oxygen to the system. The reflection became truly specular, and under some conditions of incidence angle the distribution was not unlike that expected from diffraction by an atomic surface grating. The results of this type of study find application in such space technology problems as molecular drag and reentry.

RADIO-FREQUENCY AND MICROWAVE SPECTROSCOPY

We are using the electron spin resonance method to study paramagnetic centers formed in solids by irradiation with gamma rays or ultraviolet light. The solids are usually kept at a low temperature to preserve the very reactive centers, often best described as chemical free radicals. Single crystals are used to better interpret and understand the spin resonance spectra.

After irradiation with gamma rays from cobalt-60, single crystals of dimethylglyoxime exhibited two prominent, complex spectra that have been studied in detail. One of the spectra arises from a species that contains a single unpaired electron interacting strongly with a single nucleus of nitrogen. Six numerical parameters describing the magnetic

character of the unpaired electron and six additional parameters describing its hyperfine interaction with nitrogen were accurately evaluated. This free radical is probably formed by the ejection of a hydrogen atom from the otherwise diamagnetic molecule. The second spectrum was found to result from a species containing two unpaired electrons (triplet state) which interact strongly with two nuclei of nitrogen. Surprisingly, the magnetic and hyperfine parameters were essentially the same as those found for the above free radical. This strongly indicated that the species are made up of pairs of free radicals in nearby crystal lattice sites. An analysis of the strength and direction of the interaction of the pair of electrons with each other confirmed this interpretation and showed that the pairs of radicals are spaced one unit cell distance apart along a direction defined by two adjacent molecules in the crystal.

Single crystals of hydrogen peroxide are being studied after photolysis with ultraviolet light. The simple radicals OH and HO_2, each containing a single unpaired electron, were expected to form. A variety of very complex spectra are being measured, and it is now clear that many of these arise from triplet-state species (two unpaired electrons). The situation may be very much like that for dimethylglyoxime; that is, pairs of the simple radicals form triplet-state ensembles.

These studies are of fundamental interest in radiation chemistry, since many of the radicals encountered are the ones that play important roles in the chemical changes brought about by radiation. The studies also are of interest in solid-state physics.

PHYSICAL CHEMISTRY OF GASEOUS THERMODYNAMIC WORKING FLUIDS

The control of fission-gas migration in nuclear reactors is but one of many applied problems associated with the transport phenomena exhibited by gases. From a broader and more fundamental viewpoint, however, these phenomena (the transport of mass, energy, and momentum) provide an invaluable aid to an understanding of molecular collision processes. It is with this motivation that the two research programs outlined below have been initiated.

The first program concerns gaseous diffusion, that is, the process by which a nonuniform gas mixture tends toward uniformity. Unlike viscosity and thermal diffusion, the constant-temperature diffusion process is largely sensitive only to unlike-molecule collisions and thus affords a method for a study of unlike-molecule interactions which is relatively free from the additional problems introduced by the effect of collisions between molecules of the same type.

Diffusion experiments are very difficult to perform, although the procedure is deceptively simple; one merely provides a means by which two gas mixtures of differing composition can intermix, and then monitors the rate at which mixing occurs. A prototype diffusion apparatus has been designed and constructed and is being used to study the interactions among the noble gas atoms (helium, neon, argon, krypton, and xenon).

When certain molecules collide, part of the energy that is transferred from one molecule to another may alter the rate at which either of the two molecules rotates or vibrates, rather than altering their respective velocities. This type of interaction, an "inelastic collision," has little effect on gaseous diffusion, but seriously affects any transport process in which thermal energy is involved.

The second program concerns an investigation of such inelastic collisions through experimental studies of the thermal transpiration effect exhibited by gases. Briefly, the phenomenon involves the transfer of mass, in a pure gas, from a colder region in space to a warmer region, and has long been recognized as a serious source of error in pressure measurement whenever a temperature gradient is present.

Unlike the shock-tube and ultrasonic experiments currently used to investigate inelastic collision processes, studies of thermal transpiration do not require elaborate equipment; the quality of thermal transpiration data is governed almost totally by the sensitivity of the pressure-sensing devices employed. Furthermore, the experimental procedure is relatively free from complexity.

Present investigations of the transpiration effect are of a more or less exploratory nature and are being performed with the gases argon, krypton, nitrogen, and carbon dioxide.

PHYSICAL CHEMISTRY OF MOLTEN SALTS

Chemical Studies in Support of the Fluoride Volatility Process

The Fluoride Volatility Process developed at ORNL is based on the fact that uranium hexafluoride and plutonium hexafluoride are volatile at elevated temperatures, whereas the fluoride compounds of most fission products are not volatile. Consequently, the process has become one of the most promising methods for chemically repurifying nuclear reactor fuel materials. The volatile uranium or plutonium fluoride may be further decontaminated from the few volatile fission products by selective sorption on and desorption from sodium fluoride. Thus, when a used fuel element (metal cladding, unused fuel, and fission products) is converted into a mixture of fluorides and treated with fluorine, substantially only uranium and plutonium are removed from the mixture. In the first chemical step of the process, used fuel elements are converted to fluorides in a molten mixture of inorganic fluorides as a solvent by treatment with HF – a controlled corrosion reaction in which the HF corrodes the fuel element. The principal component which must be dissolved is the fuel element cladding. It is desirable to have a solvent mixture which will dissolve the largest possible amount of fuel element material; generally, raising the temperature will increase the solubility of this material. However, raising the temperature also increases the corrosion of the container vessel, and an upper temperature limit is usually set to minimize the extent of this corrosion process. Within this temperature limit, a systematic exploration of the solubility of fuel materials has been made by R. E. Thoma and B. J. Sturm of the Reactor Chemistry Division. During 1963, attention was devoted to solvents for fuel elements clad with aluminum, and it was discovered that mixtures of potassium fluoride (KF) and zirconium fluoride (ZrF_4) were particularly good solvents for aluminum-clad fuel elements. At 600°C, a solvent containing 63 mole percent KF and 37 mole percent ZrF_4 was found to dissolve up to 15 mole percent of aluminum trifluoride (AlF_3), a very satisfactory amount. Mixtures of KF and ZrF_4 were recommended for large-scale tests in the extension of the Fluoride Volatility Process to use with aluminum-clad fuel elements.

Chemical Behavior in Molten Fluoride Solutions

The chemical behavior of molten mixtures of inorganic salts has been of increasing interest to chemists in recent years as this less familiar class of liquids finds application in processes requiring high temperatures, electrically conducting media, or solvents for materials insoluble in, or decomposed by, more conventional liquids. Molten fluoride mixtures, especially those containing fluorides of lithium and beryllium, are of particular interest because they appear promising as solvents for nuclear reactor fuels. Many classical techniques for study of solutions cannot be applied to molten fluorides because the molten mixtures attack most container materials. However, a method has been developed by C. F. Baes, Jr., and co-workers of the Reactor Chemistry Division which is yielding information about the relative stability and reactivity of various metal salts dissolved in molten lithium and beryllium fluorides. Although many metal oxides are only slightly soluble in these mixtures at 500 to 700°C, the resulting small amount of dissolved oxide ion (O^{2-}) reacts readily with gaseous hydrogen fluoride (HF) to produce gaseous water (H_2O) and fluoride ion (F^-) as shown in the following equation:

$$O^{2-} + 2HF \rightleftharpoons H_2O + 2F^-.$$

In accordance with the laws of chemical equilibria the amounts (or chemical reactivity) of the oxide and fluoride present are directly related to the pressure of gaseous hydrogen fluoride and water above the molten solution.

Pressures of these gases are conveniently determined by bubbling a carrier gas (usually hydrogen) that contains hydrogen fluoride and water in known amounts through the molten-salt solution and analyzing the gas as it leaves the system. Such measurements have shown that, when low concentrations of HF and H_2O are present, the exit gas is of a composition determined by the equilibrium shown above. These measurements are yielding the solubilities of metal oxides and the chemical stability (the free energy) of added metal fluorides and are, in addition, providing a much needed method of analysis for dissolved oxide in this medium.

Complex Compounds Between Fluorides

When mixtures containing the proper quantities of two simple salts [such as potassium fluoride (KF) and aluminum fluoride (AlF_3)] are melted and then crystallized by cooling, the result is frequently a complex compound, an example of which is cryolite ($3KF \cdot AlF_3$). A large number of complex fluoride compounds have been identified in the careful, extensive studies on molten fluoride mixtures for the Molten-Salt Reactor Program. It has been discovered by R. E. Thoma of the Reactor Chemistry Division that the compositions (formulas), crystallographic form, dimensions of the crystallographic unit cell, and the indices of refraction of the complex fluorides depend primarily on the ratios of the radii of the metallic cations in the starting materials. It has been possible, therefore, to predict from the known behavior of several pairs of pure fluorides the properties of the complex compounds to be obtained from untested pairs. This predictability should prove especially valuable when applied to salts of the transuranic elements which are very difficult to handle experimentally. Such predictions are valuable not only as contributions to pure chemistry but also because they may suggest useful methods for the identification or even separation of these complex materials.

Recent experiments with sodium fluoride (NaF) and with the trifluorides (designated MF_3) of the ten heaviest rare-earth elements, samarium (Sm) through lutetium (Lu), have corroborated the predictable behavior of such pairs. Each of the ten systems shows two complex compounds: $NaF \cdot MF_3$ and $5NaF \cdot 9MF_3$. The first occurs in a hexagonal crystalline form in all systems and in an additional cubic modification in some of the systems. The compound $5NaF \cdot 9MF_3$ occurs in a tetragonal and a cubic crystalline form. The two cubic forms of the 1:1 and 5:9 compounds are mutually soluble in all proportions in the systems in which both occur. The dimensions of the crystal unit cell and the refractive indices of all compounds observed vary smoothly as the ratio of cation radii changes from Na^+/Sm^{3+} to Na^+/Lu^{3+}. From these and similar earlier studies it appears that the behavior of alkali-metal fluorides with the transuranic element trifluorides will be similar to that of alkali-metal fluorides with the trifluorides of the lighter, rather than heavier, rare earths.

HIGH-TEMPERATURE AQUEOUS SOLUTION CHEMISTRY

Electrical Conductance of Aqueous Solutions at Very High Temperatures and Pressures

The properties of water and aqueous electrolyte systems under extreme conditions of temperature and pressure, reaching far into the supercritical region, have been inferred from the results of studies by W. L. Marshall and A. S. Quist of the Reactor Chemistry Division of electrical conductance from 0 to 800°C and pressure from 1 to 4000 bars. Detailed results show that the combination of temperature and pressure (or solution density) which yields the maximum value of equivalent conductance occurs at values which are far above those conventionally used in previous studies. From measurements on dilute aqueous solutions of K_2SO_4, $KHSO_4$, and H_2SO_4, it has been possible to estimate the first and second ionization constants of sulfuric acid as a function of temperature and pressure; the degree of ionization of the HSO_4^- ion was found to decrease with increasing temperature, and above 300°C the dissociation constant became too small (less than 10^{-5}) to be evaluated by the method used. The volume change in ionization of bisulfate was calculated to be approximately –30 cubic centimeters per mole at 100 and 200°C. The first ionization constant of sulfuric acid was also found to decrease with increasing temperature; at a density of 0.8, the value was $10^{-1.6}$ at 400°C and $10^{-3.5}$ at 600°C. The values for K_2 (bisulfate ionization) obtained from conductance measurements were found to be in good agreement with the values reported by M. H. Lietzke and R. W. Stoughton of the Chemistry Division, based on Ag_2SO_4 solubility measurements.

High-Temperature Acidity Measurements: Thorium(IV) and Iron(II) Hydrolysis

Most salts, when they dissolve in water, dissociate at least partially into ions, and these ions hydrolyze (that is, react with water molecules) to some extent to produce hydrogen or hydroxyl ions in the solution. The extent of hydrolysis depends not only on the chemical constitution of the added salt but also on the quantity of salt

added and the temperature of the solution. Definition of the actual ionic species in solution – which is necessary for understanding of their behavior – frequently requires, therefore, precise determination of the acidity (hydrogen or hydroxyl ion concentration) and its change with temperature and quantity of added salt. Acidity measurements at or near room temperature have been made by many workers with glass- or hydrogen-electrode systems. In a continuing study by C. F. Baes, Jr., in the Reactor Chemistry Division, modifications of both electrode systems have been used to produce precise and accurate data at elevated temperatures.

The hydrolysis of thorium in perchlorate solution has been studied at temperatures from 0 to 95°C. While it has not yet been possible to make an unequivocal selection from several possible schemes, each of them involves the species $ThOH^{3+}$ and $Th(OH)_2^{2+}$ and a highly polymeric species containing 5 to 7 thorium atoms [for example, $Th_5(OH)_{12}^{8+}$ or $Th_6OH_{14}^{10+}$].

The hydrolysis of iron(II), of great importance in corrosion reactions, had previously been studied at room temperature; it is now being studied from 95 to 200°C, and preliminary results are consistent with a simple hydrolysis reaction:

$$Fe^{2+} + H_2O \rightleftharpoons FeOH^+ + H^+$$

with equilibrium quotients at 25, 95, 150, and 200°C estimated to be, respectively, $10^{-9.5}$, $10^{-7.5}$, $10^{-6.3}$, and $10^{-5.9}$.

High-Temperature Isopiestic Studies

Valuable information about the way water interacts with salts dissolved in it can be obtained from measurements of its vapor pressure above such solutions. Salt solutions show lower vapor pressures than does pure water, and high concentrations of salt lower the vapor pressure of water more than do lower concentrations. Moreover, one salt may interact more strongly with water than does another at the same concentration and may, thereby, depress the vapor pressure to a greater extent.

A technique that simultaneously exposes, at a uniform temperature, solutions of several different salts to the same vapor pressure of water and which determines the concentrations of the resulting solutions has been adapted by B. A. Soldano of the Reactor Chemistry Division for the study of salt-water interactions at temperatures up to 200°C. This "equal-pressure" (isopiestic) method eliminates many possible experimental errors by comparing the behavior of many salts under identical conditions. The apparatus is complex and difficult to build, but the technique is relatively simple. Open containers, each containing a known weight of a salt dissolved in some water, are placed in a large, closed metal vessel which is heated to the desired temperature. Some salt solutions lose, and others gain, water until each arrives at a concentration unique to that salt under conditions of the test. The containers are weighed inside the large metal vessel by an electrical balance which also is held within the pressure vessel; the final concentrations are computed from the weight of the solution and the original weight of the salt. The data are converted to osmotic coefficients to facilitate a direct comparison of the interactions of salts with water and to reveal the change in such interactions with temperature.

Isopiestic studies have now been extended to above 150°C for many important salts. The behavior of salt solutions at elevated temperature has been found to be decidedly different from that normally observed at room temperature. During the past year, information was obtained at 150°C for many test salts over a range of concentrations that included very dilute solutions. A quite unexpected increase in the osmotic coefficients was found at low concentrations, followed by a decrease as the concentrations were increased. The observed maximum at low concentrations should lead to, and, in fact, requires, an improvement in the theories which describe the chemical interaction between dissolved salts and water.

Phase Equilibria in High-Temperature Systems

Among the most extensive studies ever reported of solubility relations in multicomponent aqueous systems at high temperatures are those which were

made by W. L. Marshall and co-workers in the Reactor Chemistry Division for the system UO_3-CuO-NiO-SO_3-H_2O and its heavy-water analog. Both the five-component system and the underlying three- and four-component subsystems were explored from 200 to over 400°C by means of ingenious experimental arrangements permitting visual and quantitative observation of phase changes. The systematically obtained data will permit tests of theories of far more sophistication than those now available. In this respect, experiment has far outstripped theory. Nevertheless, in less complicated systems, such as solutions of $CaSO_4$ and $NiSO_4$ in various nitrate, sulfate, and chloride media, remarkable correlations, which are certain to be of theoretical interest, have been found, demonstrating at temperatures up to 200°C and higher and to ionic strengths of 6 molal, a linear relationship between the logarithm of the solubility and an empirical ionic strength function $[I^{1/2}/(1 + 1.5\, I^{1/2})]$, similar to that of the Debye-Hückel theory for the solubility of electrolytes at low temperature in media of low ionic strength.

As an extension of the solubility studies to include the effects of pressure, the boundaries of the region of liquid-liquid immiscibility found previously in uranyl sulfate–water systems have been delineated with respect to pressure, temperature, and solution composition. The results of the study have proved to be extremely stimulating; an extraordinarily good correlation was found in the relationship between the temperature and pressure at which immiscibility occurred for a given solution – the relationship was almost perfectly linear, with increasing temperature requiring a corresponding increase in pressure. Moreover, the slope of the relationship was essentially the same for solutions of widely varying concentrations of uranium, suggesting that the phenomenon was more a property of the solvent water than of the solute. Further examination revealed that the slope coefficients were indistinguishable from the partial derivatives of temperature with respect to pressure *at constant density* for pure water. Later, it was found that the partial derivative taken at a constant value of DT (the product of dielectric constant and temperature) gave an even better correspondence with the observed results. The exploitation of these correlations promises to lead to much better theories of the solubility of electrolytes in water at high temperatures.

ISOTOPE CHEMISTRY

Studies were made of the chemistry and molecular spectroscopy of isotopic molecules to obtain information needed for an understanding of isotopic fractionation in physical and chemical processes. When appropriate, the data resulting from these researches are used to develop methods of concentrating needed isotopes. Isotope separation factors for the system LiCl(aq) versus LiR, where R represents Amberlite IR-120 and Zeo Karb ion exchange resins, were determined as a function of aqueous electrolyte concentration. In the Zeo Karb system, the fractionation factors varied from 1.0008 to 1.002 as the eluant HCl concentration was changed from 5 *N* to 0.1 *N*. The fractionation factor in the Amberlite IR-120 system increased from 1.001 for 5 *N* HCl to 1.003 for 0.1 *N* HCl eluant. These data refute recent literature assertions of abnormally large fractionation factors in such systems. Nitrogen isotope effects in the thermal decomposition of α,α'-azobis-(isobutyronitrile) and the various methyl-substituted benzene diazonium fluoborates were measured. Differences in reaction rates of 4 to 5 percent were found at 40°C between the nitrogen-14 and nitrogen-15 species studied. The fluorine-19 nuclear magnetic resonance spectra of several of the new xenon fluorides were observed and measured. Chemical shifts were determined for liquid XeF_2, XeF_4, $XeOF_4$, and XeF_6; ^{19}F-^{129}Xe spin-spin coupling constants were obtained for XeF_4 and $XeOF_4$. The spectra of XeF_4 and $XeOF_4$ indicate the magnetic equivalence of the four fluorine atoms, in agreement with the square planar structure reported for XeF_4 and the fourfold symmetry axis shown by the Raman and infrared spectra of $XeOF_4$. Raman and infrared spectra of ClO_2F were also obtained. All fundamental frequencies of the molecule were observed in both spectra. Valence force constants were calculated which closely reproduced the observed frequencies, as well as the isotopic shifts observed when the molecule was labeled with chlorine-37 and oxygen-18. The thermodynamic effects of mixing light and heavy water were studied. New isotopic equilibrium constants for the vapor and liquid phase reactions were computed from recent experimental data. Excess thermodynamic functions of mixing were derived for the H_2O-D_2O system, permitting the computation of a heat of mixing which was in

agreement with that observed experimentally. The BF_3 complexes of ethyl ether, ethyl sulfide, and triethylamine were examined. Isotopic equilibrium constants for the exchange of boron between these complexes and gaseous BF_3 were measured at several temperatures for each system; related thermodynamic parameters were also derived. The ethyl sulfide system is a potentially interesting method for separating boron-10 and boron-11; its separation factor is the largest recorded for this type of chemical exchange reaction. The feasibility of fractionating isotopes of beryllium and potassium by means of the chemical exchange reactions

$$^{1}M_{(Hg)} + {}^{2}M^{+}_{(aq)} = {}^{2}M_{(Hg)} + {}^{1}M^{+}_{(aq)},$$

where ^{1}M and ^{2}M represent different isotopes of the same element, was examined. The first prerequisite, adequate solubility of the metal in mercury, was satisfied for potassium but not for beryllium. A fractionation factor $(^{39}K/^{41}K)Hg/(^{39}K/^{41}K)aq$ of 1.0006 ± 0.0004 (95 percent confidence interval) was measured for the potassium reaction. The small value of this factor precludes the use of this reaction as an effective means of separating potassium isotopes. However, substantial separation of sodium, rubidium, and cesium from potassium did occur in this system. Thus, at 25°C, these factors were cesium/potassium, 3.0; rubidium/potassium, 1.19; sodium/potassium, 1.9; with potassium concentrating in the aqueous phase of each system.

OXYGEN ISOTOPE ENRICHMENT

The separated isotopes of oxygen are important to biological, chemical, and physical research. Oxygen-17 is of special importance since it can be detected by nuclear magnetic resonance techniques. A facility to provide research quantities of water enriched to 50 percent in oxygen-17 and 99 percent in oxygen-18 has been constructed at ORNL. Isotope enrichment is effected, first, by distilling water, then thermally diffusing the partially enriched oxygen derived from this water. The isotope facility must be operated without interruption for two to three years before the desired concentrations of oxygen-17 and oxygen-18 can be achieved. Satisfactory progress toward this goal was achieved during 1963. The Water Distillation Cascade performed well, with the exception of two minor disturbances near midyear. At the close of the year the oxygen-17 concentration was 1.0 percent, and the oxygen-18 was 78 percent. The Thermal Diffusion Cascade was activated near the end of the year; after 13 weeks of operation the oxygen-17 and oxygen-18 concentrations were 2 and 99.5 percent respectively.

TARGET PREPARATION

More than 1000 targets were prepared during 1963, and they were custom fabricated to specifications of research scientists. Most targets were of the thin film type having thicknesses as low as 0.1 microinch (one ten millionth of an inch)

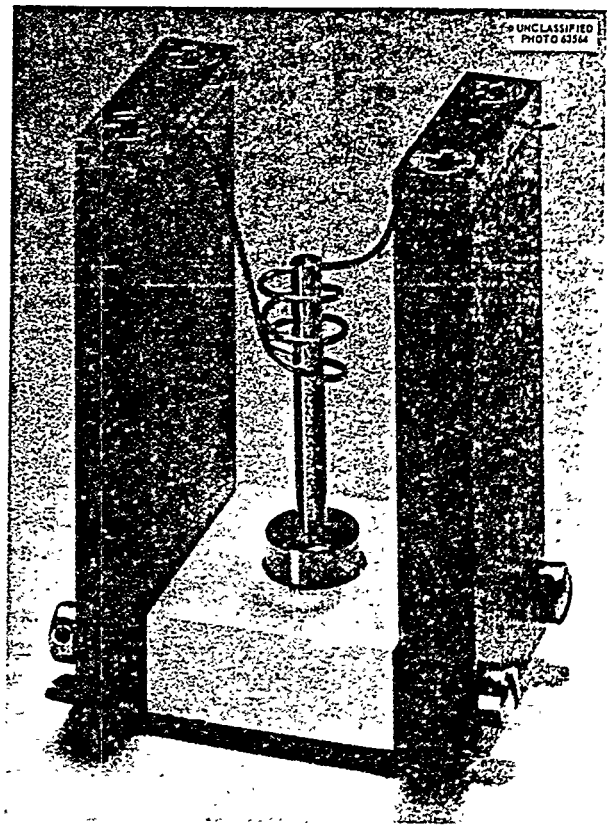

Water-cooled copper electrodes support a helical tungsten filament used to emit electrons which bombard the annular tungsten crucible. With electron bombardment power of approximately 40 watts, crucible temperatures above 2200°C can be reached. Evaporants are collimated from the howitzer-type crucible.

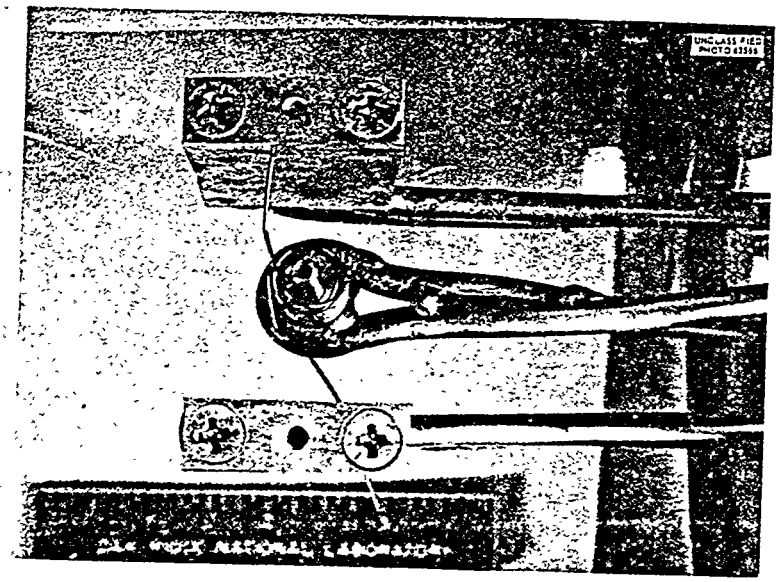

Top view of electron bombarded howitzer type evaporation crucible. Inside diameter of crucibles can be varied from 1/16 inch to 1/2 inch. Collimation of evaporant allows 10 to more than 90 percent efficiency of vapor condensation, depending upon substrate distance from the crucible. Crucible temperatures above 3000°C can be easily obtained.

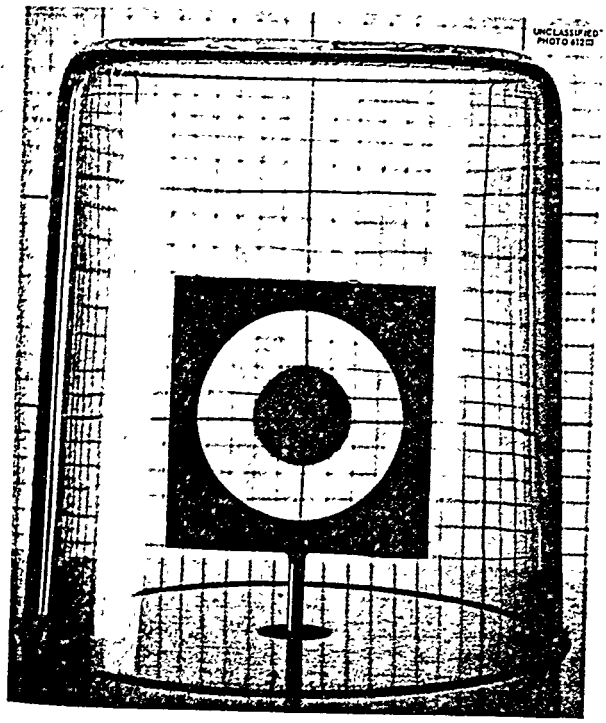

A standard tandem Van de Graaff target prepared by vacuum evaporation and condensation of selenium-87 onto a Formvar film. The area of the target spot (center) is 1 square centimeter and contains 100 micrograms of the isotope. At this thickness, 0.000008 inch (2000 angstroms), the red, high-temperature form of the condensed film is transparent.

and containing as little as 5 micrograms (5 millionths of a gram) of isotopically enriched element.

Improvements in evaporation-condensation techniques have resulted in a hundredfold conservation of valuable enriched isotopic material, with a simultaneous material cost reduction. Work to develop vaporization heat systems capable of high-temperature operation (more than 2000°C) and simultaneous vapor collimation is continuing.

Study of film formation using radioactive materials has made possible the fabrication of targets and very thin sources of beta- and gamma-emitting elements as well as alpha-emitting isotopes.

Development of electron-bombardment vapor sources capable of attaining temperatures above 3000°C has allowed the reduction of oxides of rare earths to their respective metals in quantities of less than 50 milligrams. For the first time this has provided rare-earth metal isotopes in a form suitable for rolling into foils approximately 1 milligram per square centimeter thick. Extension of this technique to the condensation of metal vapors into single-crystal form has been studied with some success. A single crystal of magnesium-24 showing well-defined hexagonal crystal faces was grown in this manner.

TRANSURANIUM PROCESSING PLANT

Construction of the Transuranium Processing Plant (TRU), a facility designed for the chemical processing and recovery of large amounts of the

very heavy man-made elements for research purposes, was started on July 1. The plant site is adjacent to the High Flux Isotope Reactor (HFIR), in which californium and berkelium will be produced by bombardment of several hundred grams of the lighter actinide elements with intense neutron fluxes. These starting materials (plutonium-242, americium-243, and curium-244) themselves were produced by a long-term irradiation of 10 kilograms of plutonium-239, the normally available isotope, in AEC production reactors at Savannah River. During the past year, the recovery and decontamination of these elements were completed, and they were shipped to ORNL for further processing and fabrication into target rods for irradiation in the HFIR.

Construction of the TRU has progressed to the point where all structural steel for roof and wall supports is in place, and the massive concrete shielding walls (4½ feet thick) for the nine processing cells are being poured. The facility will be completed in the spring of 1965. Approximately a year later, after installation and testing of the processing equipment, full-scale separations of the heavy elements will be in progress. Design of this equipment has been under way for over a year and is now about 50 percent complete. Equipment procurement has started.

Development and testing of the chemical processes to be used in the TRU were continued during 1963. A significant achievement was the discovery that the addition of small amounts of methanol to process solutions greatly suppressed the detrimental effects of the intense alpha radiation associated with the actinide elements. Formation of hydrogen and oxygen by the radiolysis of water and the destruction of free acid greatly complicated many steps in the process. The free acid, in particular, must be controlled very closely in the Tramex process, in which the actinide elements are separated from the chemically similar rare-earth fission products; the addition of methanol solves this problem. A development facility designed for testing the TRU process flowsheets at full radioactivity levels and for the production of curium-242 for isotopic power sources was completed, and initial operations have begun.

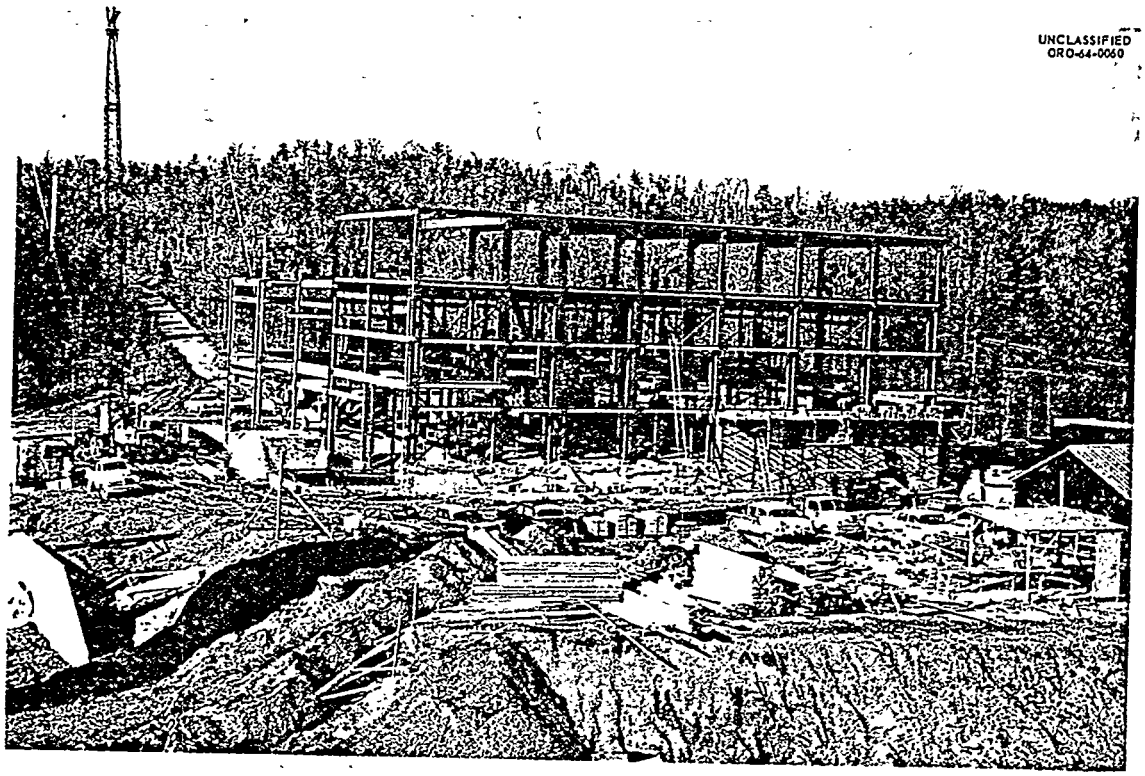

General view of Transuranium Processing Plant (January 15, 1964).

Metallurgy and Materials

PREPARATION OF PURE MATERIALS

Purification of Beryllium by Solvent Extraction and Preparation of Pure Beryllium Hydroxide

A process for purifying beryllium by the solvent extraction of beryllium acetylacetonate (BeX_2) in the presence of ethylene diamine tetraacetic acid (EDTA), followed by back extraction of the beryllium into nitric acid and precipitation of beryllium hydroxide with ammonia, was developed in 1960 in the Reactor Chemistry Division by R. E. Moore and demonstrated on a 100-gram scale. Research on the chemistry of the process and the production of kilogram quantities of purified beryllium hydroxide were undertaken by C. F. Baes, Jr., and C. E. L. Bamberger (IAEA Research Fellow from Argentina), and this work has now been concluded.

Quantitative expressions were developed for the variation of the important extraction system parameters with solution composition at 25°C; the kinetics of the process were studied, and the reaction $BeX^+ + H^+ \rightarrow Be^{2+} + HX$ was shown to be the rate-controlling step in the hydrolysis of BeX_2; a quantitative treatment was developed for the decontamination of beryllium from other metallic impurities which form stable species with complexing agents such as EDTA; the efficacy of the process was demonstrated by the purification of beryllium which had been deliberately contaminated with 1000 parts per million each of soluble salts of Na^+, Mg^{2+}, B(III), Cu^{2+}, Al^{3+}, Fe^{3+}, and Cr^{3+}.

Four batches of beryllium hydroxide product, each equivalent to 500 grams of BeO, were produced, in 85 percent yield; the total content of all metallic impurities present in measurable amounts was less than 5 parts per million. The purified beryllium hydroxide prepared in this program is available to other research workers whose needs for such pure material are consistent with its value. It is obvious that much larger amounts could be made by the relatively simple process which has been demonstrated if a material of high purity is needed.

RESEARCH AND DEVELOPMENT ON PURE MATERIALS

Information for Materials Research

Some three years ago a research and development program devoted to the preparation of high purity and perfection research specimens for solid state research was initiated at ORNL. The materials chosen for attention were either those materials of specific interest to research programs being conducted at ORNL or those better specimens of which would contribute to important progress in some area of solid state research. If it is to be successful, such a program involves much more than the growth of single crystals; purification of starting materials, zone refining, choice of the appropriate method of growth, development of analytical techniques to detect minute quantities of impurity, and the characterization of the specimens by physical measurements are all important elements of the program. The preparation and evaluation of a given material, therefore, involves considerable effort and specialized equipment

so that as a rule a single research group can include no more than a few materials in its purview. A little reflection suggests that the obvious way of extending the effectiveness of any research materials program manyfold is through a comprehensive program of information exchange.

Detailed information concerning the availability of research quality materials has always been difficult to obtain. Open literature publications seldom indicate the source and purity of starting materials, the method of crystal growth, and assay of the end product. Moreover, it is often difficult to find who has experience in preparation of any but the more common or "fashionable" materials. The Research Materials Information Center was therefore established as a part of the Pure Materials Program at ORNL to collect and provide information on the purification, production, characterization, and availability of research quality materials to both producers and users. A companion listing is also made of those materials that are not currently available but are desired by various investigators.

Pertinent information is solicited from all research groups known to be interested in solid state or materials science. Already the Center has received more than 1500 data sheets on a wide variety of research materials which have been submitted by some 600 individuals representing more than 100 research organizations. In addition to voluntarily contributed information, the published literature since 1957 is being gleaned for information on crystal growth techniques, analytical methods, and physical evaluation techniques, as well as for information on the availability of the more exotic materials. To aid in retrieval, the information is coded and placed upon film which can be searched automatically.

The Center is happy to answer inquiries from any interested research group or scientist. If the desired information is not currently available, the request is placed on file to be answered as soon as the matching information is obtained. Numerous requests for information have already been fulfilled and the number of inquiries is increasing daily.

REACTIONS AT METAL SURFACES

Mechanism of Metal Oxidation

A major limitation in the use of metals and alloys as structural materials results from the corrosion that occurs when metals are exposed to air and other media. Corrosion frequently involves a chemical reaction between oxygen and the metal to form a thin oxide film on the surface of the metal. Such films often constitute a barrier that protects the metal from further attack. In some instances (for example, on aluminum), the film may be only 20 angstroms thick yet provide almost complete protection from air. The scale on iron, on the other hand, is much less protective. Many of the special metals, such as tantalum, niobium, and zirconium, which are so important in nuclear reactors, rocket motors, and other applications where strength at high temperatures is required, form oxide films that offer almost no protection. The Reactions at Metal Surfaces Group of the Metals and Ceramics Division is performing research to discover those factors that are responsible for such a variation in the protectiveness of oxide films on metals.

These investigators have studied the influence of surface impurities on the oxidation characteristics of copper to correlate oxidation rate with the state of crystalline imperfection, or lattice disregistry, of the oxide. They conclude that in general an increase in lattice disregistry in the oxide should lead to an increase in the oxidation rate, and the degree of lattice disregistry in the oxide has been identified as an important factor in determining the overall oxidation rate of a metal. By x-ray diffraction, they have investigated the thin oxide films on several crystallographic planes of copper single crystals. This research indicated that the lattice disregistry in the oxide varied with the orientation of the substrate and suggested that the marked oxidation rate anisotropy exhibited by copper may be related to a comparable anisotropy of the degree of lattice disregistry in the oxide.

This group has studied the effect of anodically deposited oxide films on the reaction of niobium

and tantalum with gaseous oxygen at 500°C. The anodic film decreased the initial rate of oxygen uptake only slightly, particularly in the case of tantalum. For both metals, the thickness of the surface oxide remained virtually unchanged during reaction with oxygen, indicating that the oxygen consumed dissolved directly in the metal. This discovery has enabled a more detailed study of the process by which oxide platelets precipitate in these metals. In both metals, the oxide platelets formed were considerably larger and better defined than those obtained during oxidation without a prior anodic oxide film. Platelet formation could be induced in niobium under conditions of temperature and oxygen pressure at which platelets do not usually form. On tantalum, the anodic films themselves appeared to be particularly inert at temperatures from 400 to 500°C. They were amorphous and could be neither crystallized nor dissolved in the metal by annealing in vacuum for several hundred hours.

DEFORMATION OF CRYSTALLINE SOLIDS

Fundamentals of Metal Deformation

The most important single property resulting in the wide usefulness of metals is the capacity to undergo extensive plastic deformation. This capacity is essential for fabrication and often necessary in the ultimate use. The Deformation of Crystalline Solids Group of the Metals and Ceramics Division are furthering the understanding of deformation with fundamental measurements of the changes that occur during this process. Recent advances concern changes in internal energy, strength, and atomic arrangements.

By a combination of several advanced measurement techniques, including a very sensitive calorimetric method, the energy stored by single crystals of copper was measured. This measurement, combined with previous measurements of the greater effect in polycrystalline material, has confirmed the major role of dislocations in energy storage during deformation. The magnitude of the stress required to cause plastic deformation in tantalum and in alloys of copper and silver with aluminum was found to be that required for rapid multiplication of dislocations, as revealed by the dependence of this stress on temperature and strain rate. The effect of the same variables on the stress-induced ordering of carbon atoms during creep (deformation under continuous stress) of an iron alloy gave further clues to the motion of dislocations.

Deformation of Refractory Metals

The fabrication capability of metals depends on their ductility, or ability to deform plastically under applied stress without fracturing. The response of crystalline materials to an applied stress is determined by the behavior of defects called dislocations and the interaction of these dislocations with other imperfections in the crystal. By direct observation of these defects, using transmission electron microscopy, the Electron Microscopy and Structure of Metals Groups of the Metals and Ceramics Division have correlated the deformation behavior of the refractory body-centered cubic metals – niobium, tantalum, tungsten, and molybdenum – with the arrangement of the dislocations into regular patterns. These patterns, in turn, explain the influence of temperature, strain rate, and impurities on the ease of deformation. In these metals, ductility results from the movements of many dislocations. This research showed that the grain boundaries are the primary sources of dislocations. When large numbers of impurity atoms are present, they collect at these boundaries; one result is that the boundaries no longer act as dislocation sources. It is this lack of sources that causes brittleness in tungsten and molybdenum and not the presence of a brittle layer at the boundary, as thought by many metallurgists. These studies suggest ways to improve the low-temperature ductility of this important class of metals.

STRUCTURE OF METALS

Grain Growth During Recrystallization of Aluminum

When a metal has been deformed, the resulting strains can be relieved during heating by recrystallization. The Structure of Metals Group of the Metals and Ceramics Division has observed an unusual type of growth of recrystallized grains (separate crystals) during the early stages of recrystallization in high-purity aluminum rods that had been extruded at 77°K. During the course of annealing specimens at a constant temperature of 65, 100, or 187°C, the growth rate of certain grains did not remain constant with time, but decreased drastically from an initial very rapid rate. The initial growth rates of these grains were much higher than expected from the energy available and the impurity level.

An x-ray orientation analysis revealed these grains to be members of a component of the recrystallization fiber texture of these rods that may be described as a scattered <114> to <012> orientation in the standard stereographic triangle. These grains were further characterized by their orientation relationship with the matrix into which they were growing; the relationship was always near one of the coincident-site relationships.

Neither a decrease in the driving force for movement of grain boundaries due to annealing out of stored energy nor an increase in the grain boundary impurity concentration due to the sweeping up of impurities can adequately account for the growth behavior of these grains. Excess vacancies (crystalline lattice points not occupied by atoms), which are produced and frozen in the lattice during deformation, appear responsible. These observations indicate that such point defects, which can be introduced during deformation or irradiation, may exert an important influence on the subsequent behavior of the material.

Structure of Molten Salts

Molten salts have many unique and useful properties as engineering materials. They are, for example, major components of nuclear reactors and fuel cells that are currently under development. Nevertheless, molten-salt technology is beset by a lack of fundamental understanding, particularly of the chemical properties of these materials. We have long recognized that the chemical properties of molten salts are vitally influenced by the clustering of ions into complexes, but concrete information on these complexes has been very difficult to obtain.

In the past few years, a group under G. P. Smith of the Metals and Ceramics Division has had considerable success in pinpointing details of the structure of molten salt complexes by using optical spectroscopy. In recent studies of complexes centered on nickel ions in a large number of molten salts, this team has learned much about their configurations and the forces that hold them together. In a number of molten salts, nickel complexes had simple geometric shapes. For example, the nickel complex formed in a molten mixture of lithium fluoride, sodium fluoride, and potassium fluoride was an octahedron of six fluoride ions surrounding a central nickel ion. In molten cesium chloride and other chloride, bromide, and iodide salts with large positive ions, nickel complexes consisted of tetrahedra of four halide ions centered around a nickel ion. In one medium, a molten mixture of lithium and potassium chlorides, two different shapes of nickel complexes were found to exist in an equilibrium that was shifted by changing the temperature or the ratio of lithium ions to potassium ions. In molten nitrate and sulfate salts, three nitrate or sulfate ions clustered about a nickel ion. In each instance, two oxygen atoms from each nitrate or sulfate ion were in contact with the nickel ion to form a distorted octahedron of six oxygen atoms. The amount of distortion depended on the nature of the positive ions present.

FUNDAMENTAL RESEARCH IN X-RAY DIFFRACTION

Structure of Irradiated Beryllium Oxide

In x-ray diffraction, the locations and arrangements of atoms in crystalline materials are determined from the deflections of x rays by these materials. The X-Ray Diffraction Group of the Metals and Ceramics Division is using this method to determine atom locations in crystalline solids

of unknown structure and to study the effects of such external conditions as temperature and radiation on solids of known structure. H. L. Yakel has recently made a major contribution to the understanding of the structure changes that occur in beryllium oxide due to irradiation.

Knowledge of how materials are damaged by radiation is important both to the development of practical reactor materials and to the understanding of the fundamental processes involved. Beryllium oxide has favorable nuclear properties and exhibits a variety of damage effects. Single crystals of beryllium oxide, grown at high temperature from molten mixtures of metal oxides, have been irradiated at various temperatures to fast-neutron doses of over 10^{21} neutrons per square centimeter. At 100°C and below, the irradiation debris is distributed in agglomerates of 10 to 100 defects each, which do not affect the scattering of x rays by the crystal lattice. At 650°C, the agglomerates are much larger, and the crystal fractures. Above 1000°C, there is much less damage, as though it has been annealed out, but there still remains sufficient damage to cause appreciable swelling.

PHYSICAL PROPERTIES STUDIES

Fundamental Properties of Metals and Alloys

The metals titanium, zirconium, hafnium, niobium, tantalum, molybdenum, and tungsten form alloys that are important for use in nuclear reactors, in space rockets, in superconducting magnets, and in very corrosion-resistant materials. A theory from which one may make predictions about many properties of these materials from only a few measurements has not been developed; such a theory can only be developed when certain electronic properties have been carefully measured. J. O. Betterton and co-workers in the Metals and Ceramics Division have recently measured several of these.

This group has cooled solid solutions of titanium, zirconium, and hafnium to temperatures near absolute zero and determined the density of states (the number of electronic states per unit energy interval) and the Debye temperatures. Also, they determined the temperatures at which superconductivity develops in the titanium-zirconium alloys. The superconductivity of the 50 atomic percent alloy persisted to higher temperatures than that of either pure metal, because the density of states is greatest at this composition. The relationship between this temperature limit and the density of states may be of use in predicting new superconductors with high transition temperatures.

These same properties were determined for scandium and its alloys with zirconium. Superconductivity could not be observed in these materials, although the experiments were carried down to 1.1°K. The alloys are generally understood in terms of the number of electrons that they contain outside the closed shells. The number of these electrons in zirconium (four) should be reduced by additions of scandium, which has three outer electrons. The low-temperature properties of the scandium-zirconium alloys confirmed this prediction by showing an effect on the density of states opposite to the effect observed previously when elements with more than four outer electrons per atom were added to zirconium.

The Theory of Alloying Group has also measured the electrical resistances of single crystals of very-high-purity tungsten and beryllium at a temperature near absolute zero in a high magnetic field. They showed that tungsten has equal numbers of electrons and holes (a hole is a group of electrons that acts as if it has a positive electrical charge). In this interpretation of the data, the maximum energy surface of the electrons in tungsten separated into small closed surfaces when plotted against electron momentum, in agreement with theoretical calculations and with the small value measured for the specific heat of the electrons of tungsten near absolute zero. The beryllium single crystal showed results that indicate the energy surface of the electrons in beryllium is continuous along the c axis. The shape of these energy-momentum surfaces is useful for confirmation of theory that will enable prediction and understanding of important high-temperature properties.

The Mössbauer effect was used to investigate the structure of grain boundaries in nickel and the precipitation of cobalt in aluminum. Preliminary results showed a decrease of the effective Debye temperature in nickel from 450°K for the lattice

to about 300°K for atoms located at grain boundaries. In aluminum a highly asymmetric phase formed when specimens of high-purity aluminum to which approximately 0.01 percent cobalt had been added were annealed between 300 and 400°C. Also, an intermediate state of precipitation of as-yet-unknown nature was found. Mössbauer measurements of localized magnetic moments in superconductors are planned.

Thermal Conductivity of Uranium Dioxide and Iron

The rate of heat transport frequently limits the performance of nuclear reactors. To gain a better understanding of heat-transport mechanisms, the Physical Properties Group of the Metals and Ceramics Division is developing techniques for measuring the related physical properties with improved precision and accuracy. Using special care with the control and measurement of temperature, they have developed an improved, steady-state, absolute radial-heat-flow apparatus that yielded results with a probable accuracy of ±1.5 percent and a reproducibility of ±0.1 percent. With this apparatus, more knowledge has been obtained on the thermal conductivity of uranium dioxide, a widely used nuclear fuel, and Armco iron, a widely used standard for thermal-conductivity measurements.

The thermal conductivity of uranium dioxide was measured from −57 to 1100°C. The variation with temperature – including a maximum near room temperature – could be related to the atomic vibration motion, as is typical for nonmetallic

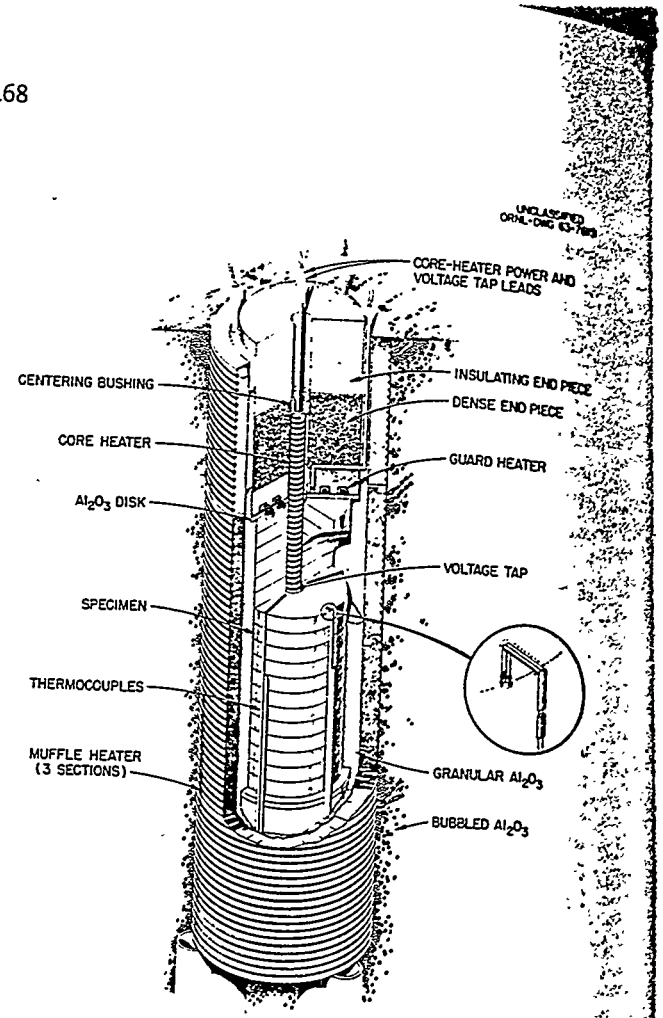

Radial heat flow apparatus for measurement of thermal conductivity. By extremely careful measurement of temperatures and equally careful control of temperature gradients to ensure that heat flows through the specimen only in the radial direction, heat conduction has been measured with improved accuracy. This has led to the discovery of previously unobserved features in the thermal conductivities of uranium dioxide and iron.

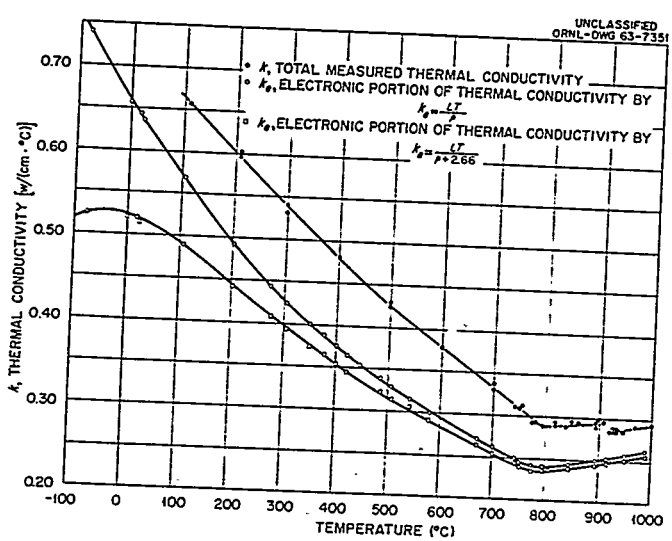

Thermal conductivity of Armco iron from 100 to 1000°C. The upper set of points shows the experimental measurements and their representation by four straight lines. The lower curves show the contribution of electronic motion to heat conduction, as calculated from the electrical resistivity by two methods. The main features of the temperature dependence are seen to be due to the electronic contribution. However, the previously unmeasured abrupt change at 912°C, the allotropic transformation temperature, results from a change in the atomic vibrations.

crystalline materials. The absolute value of the thermal conductivity depended on the impurity content, but the temperature dependence did not.

The thermal conductivity of Armco iron was measured between 100 and 1000°C. The temperature dependence of the thermal conductivity may be described to ±1.5 percent by four linear equations, with slope changes at 410 and 780°C and a discontinuity at 912°C. While most of the thermal conductivity is attributed to electronic motion, as is usual for a metal, there is an unusually large contribution of atomic lattice vibrations, which dominates the discontinuity at the allotropic transformation temperature.

CRYSTAL PHYSICS

Growth and Study of High-Temperature Crystals

Material technology of tomorrow depends on improved understanding of presently known materials and insight into new materials. The Crystal Physics Group of the Metals and Ceramics Division is studying single-crystal growth processes of high-temperature inorganic compounds and investigating select physical properties of grown crystals. They have synthesized more than 20 compounds in single-crystal form within the last year. Some of these crystals have been used in neutron-irradiation, magnetic, and optical investigations. These studies should lead to increased understanding of the character of radiation damage and magneto-optical effects in select crystalline materials.

Members of this group are growing crystals by several methods: from molten-salt solvents, from supercritical aqueous systems, by a method of material transport, by traveling-solvent techniques, and by the general flame fusion method. Single crystals of beryllium oxide and thorium dioxide, both stable at very high temperatures and useful in nuclear technology, were successfully synthesized, with high purity and quality. Also thorium dioxide crystals are being grown as a host lattice for rare-earth ions. The electronic character of the rare-earth ions in these crystals is being measured by electron spin resonance by the Solid State Division and by optical absorption methods with the cooperation of the Analytical Chemistry Division.

This group has synthesized a family of new rare-earth germanomolybdate crystals, which have the formula R_2GeMoO_8, where R represents a rare earth, and a tetragonal crystal structure like that of scheelite ($CaWO_4$). These crystals may prove useful in magneto-optical devices, and the group is investigating their magneto-optical properties. These crystals transmit most of the visible light, are strongly paramagnetic, and have a large magnetic anisotropy (that is, the crystals have preferred crystalline alignment in a magnetic field). The rare-earth-doped thorium dioxide or the rare-earth compounds may contribute to the very important technology of light amplification by stimulated emission of radiation (laser action).

FUNDAMENTAL INVESTIGATION OF RADIATION DAMAGE IN SOLIDS

Interactions Between Color Centers in Alkali Halides

After some 30 years of intensive study of color centers in alkali halides, it is perhaps surprising that any significant experiments relative to this topic remain to be done. Yet in the past two years effort in this area of research has intensified and has been yielding very important results that have caused a major modification of accepted ideas concerning lattice defects in alkali halides. One aspect of this rapid progress relates to a composite defect called the *M* center, a color center responsible for an optical absorption band at 8000 angstroms in KCl crystals. Only recently has the identity of this center been established: It is comprised of two adjacent *F* centers, that is, two nearest neighbor halide-ion vacancies, each occupied by an electron.

Once the identification of the *M* center has been established, the mechanism of its creation by radiochemical and photochemical means may be profitably investigated. Experiments of this nature at ORNL have been quite fruitful, since they have led to an understanding of the mechanism for *F*- to *M*-center interconversion. The experimental observations involve the relationship between the concentrations of *F* centers and *M* centers in KCl irradiated with cobalt-60 gamma rays or Mev electrons. First it was observed that the *M*-center concentration is always proportional to the square of the *F*-center concentration for the rather wide range of exposures employed. Also, the proportionality constant was observed to vary

from one "pure" crystal to another in a way which suggested that the relationship is sensitive to the concentration of certain trace impurities; the *M*-center concentration relative to that of *F* centers was invariably smaller in those crystals known to contain calcium or strontium impurity. In addition, the proportionality constant was extremely sensitive to the intensity of radiation employed in the coloration process, the relative *M*-center concentration decreasing with increasing ionizing intensity. Finally, during a single coloration run, the *M*-center–*F*-center relationship could be readily cycled from a condition (proportionality constant) characteristic for one intensity of the incident radiation to that for another. This last observation indicates that in a radiation field a "radiation" equilibrium exists between *F* centers and *M* centers.

The main questions posed by these observations are: (1) How do the *F* centers migrate and get together to form *M* centers under the influence of the radiation field? (2) How do *M* centers break up to form *F* centers once again? The following course of events has been found consistent with all experimental observations: The ionizing radiation creates electrons and holes as well as color centers. *F* centers may capture an extra electron to form an *F′* center, which is postulated to be much more mobile than either *F* centers or halide-ion vacancies. *F′* centers, whose lifetime is only $\sim 10^{-2}$ seconds at room temperature, interact with *F* centers to form *M* centers. On the other hand, capture of a hole by an *M* center releases 4 to 5 electron volts of energy at the site; this should be enough energy to separate the composite center into two halide-ion vacancies which, upon electron capture, become *F* centers once again. From this mechanism the origin of the sensitivity of the *F*- to *M*-center relationship to radiation intensity is immediately apparent: The steady-state concentrations of electrons, holes, and *F′* centers, which determine the relative concentrations of the end products of the reaction, are markedly dependent upon ionization intensity. Also, since certain impurities may act as efficient electron-hole recombination centers or traps for electrons or holes, it is easily seen from this model how trace impurity and, therefore, specimen origin play a role in establishing the "radiation equilibrium" point.

The Theory of Atom Ejection Patterns

One of the most intriguing phenomena which occur when a metal crystal is irradiated with energetic ions is the ejection of metal atoms from the crystal, not in all directions, but only near a very small number of crystallographic directions. These directions are those along which fairly closely packed rows of atoms occur in the crystal. As an aid in understanding the experimental ejection patterns (as they are called), studies have been conducted of a very simple model using a program written for the CDC 1604A computer (a similar code is also available for the IBM 7090 computer). The crystal is regarded as constructed of impenetrable spheres, arranged correctly in space, and with a surface of specified crystallographic orientation. At a specified depth below this surface, a lattice site is designated as the source point: The atom on this site is started moving in a randomly chosen direction with a specified energy. It and its progeny, the lattice atoms with which it collides, are followed, as long as they have sufficient kinetic energy and are moving in the general direction of the crystal surface, until they are ejected from the crystal. The entire calculation is repeated for a large number of different starting directions of the source particle and, from the results, a theoretical ejection pattern is constructed. The effects on this pattern can then be studied of changes in the crystal geometry (type of surface, type of crystal), the size of the atomic spheres, and the depth of the source point. The model in effect involves the playing (numerically) of a game of three-dimensional billiards with somewhat specialized rules.

Calculations have been made to date for close-packed crystals of the cubic (for example, copper) and hexagonal (for example, zinc) systems and the results have been compared with experimental ejection patterns obtained by the 1 to 5 kev Ar^+ ion irradiation of Al, Cu, and Au and of Mg, Zn, and Cd. The close-packed cubic calculations and experiments show the presence of both $\langle 110 \rangle$ and $\langle 100 \rangle$ collision sequences; the hexagonal crystals show both $\langle 20\bar{2}3 \rangle$ and $\langle 10\bar{1}0 \rangle$ sequences. Furthermore, the calculations indicate that only very short rows of atoms (2 to 6 atoms long) are sufficient to give ejection pattern spots of angular character-

istics similar to those observed experimentally. The differences among Al, Cu, and Au may be interpreted as indicating that Au atoms fill their lattice more fully than do those of Al and Cu.

The calculations with this simple model are sufficiently encouraging to suggest that a full scale study of sputtering (ion bombardment) by computer methods would be worthwhile. A computer program for this purpose is now being designed.

The Pseudo-Potential and Liquid Metals

Very often in physics one knows the correct equations to solve in order to calculate macroscopic physical quantities, but is frustrated by mathematical difficulties. An important example of this kind is the way in which a conduction electron scatters against an ion in a solid or liquid. Here we have a Schrödinger equation appropriate to a *strong* Hartree field, to be solved subject to certain exclusion principle requirements on the solution. Each of these matters presents serious difficulties, and the two together have represented an insuperable obstacle. Now, however, beginning with the work of Kleinman and Phillips (1959), it is becoming apparent that the composite problem is simpler than that of its two parts. The two difficulties cancel each other out to leave a problem appropriate to a weak pseudo-potential without any stringent conditions on the solutions. We "play off" one difficulty against the other.

At the present time, we are using the technique to calculate the electrical resistivity of liquid alkalis both as liquids and as highly compressed vapors. The results for the liquids are encouragingly in agreement with experiment. This gives us confidence in predicting vapor resistivities (not experimentally known) which are needed in appraising the value of such vapors in magnetohydrodynamic power generator design.

Theoretical Studies of the Electronic Structure of Lattice Defects in Ionic Crystals

Although an enormous amount of experimental work has been done on the properties (especially optical) of lattice defects in ionic crystals, relatively few detailed theoretical calculations of their electronic structure have been made. As a complement to the experimental work on these defects which is being carried out at ORNL, an intensive program of theoretical calculations was started during 1963.

One of the simplest defects which can occur in ionic crystals is the F center, which consists of an electron trapped at a negative ion vacancy. This defect gives rise to one very intense absorption band (the F band) in the visible region and, it is now believed, a number of much weaker bands (K, L_1, L_2, L_3) at higher energies. Also, the F band has rather interesting luminescent properties which are not yet fully understood.

The M center is another very common defect in ionic crystals which, it has been fairly well established, is composed of two F centers bound together at nearest neighbor halide sites in much the same way that the hydrogen molecule is made up of two hydrogen atoms. In addition to the M center, there are the R centers, which are believed to consist of larger aggregates of F centers. There are many other defects in ionic crystals, but we have devoted our attention primarily to the F and M centers.

Thus far, the theoretical program at ORNL has yielded results which compare reasonably well with experimental data on the electronic structure of the M center in LiCl and LiF. A calculation of the higher excited states of the F center in LiCl has established that the K and L bands mentioned above may, indeed, be attributed to transitions of the F center electron to these states, but much more work is needed in this area. At present, a computer program is being written which, it is hoped, will enable the calculation of the structure of a number of lattice defects in ionic crystals to be treated in a quite general way.

Diffusionless Self-Anneal in Vacancy-Interstitial Clusters

In displaced atom cascades produced in solids by energetic radiation, the defect densities (vacancies and interstitials) can be so high that annihilation of pairs takes place by purely static and attractive forces of short range, without diffusive motion. Recent work has indicated that this effect may drastically reduce the number of

defects from that predicted by the usual methods. The percentage of all defects removed by this mechanism has been calculated by Monte Carlo methods as a function of the initial defect density for the case of random distributions. The results are such that for currently accepted values for defect densities and for the range of the attractive forces it is reasonable to conclude that the static self-annealing may account for some of the discrepancy between the calculated and observed rates of damage to crystals.

It has been shown that the calculation can also be done analytically. Further, the analytic method allows one to take into account the important possibility of correlation among the defects with respect to their positions in the initial distribution.

Nonlinear Ultrasonic Effects in Metals

Whereas the linear component of the binding forces in solids has been investigated by ultrasonic techniques for some time, it has been found at the Oak Ridge National Laboratory that the nonlinear component of these binding forces as well can be studied by new developments in these techniques. If a pulsed ultrasonic stress wave of a given frequency and sufficiently large amplitude is generated at one end of a metal sample, then, on progressing through the metal, it generates harmonics as it progresses. The amplitude of the harmonics at any distance is determined by the nonlinear nature of the forces within the solid, the amplitude of the stress wave, and the attenuation coefficient of the medium. Attempts are now being made to determine the absolute values of the harmonic amplitudes, as well as the initial stress wave amplitudes, and the attenuation coefficient of the medium. If these measurements can be made to sufficient accuracy, then a new method is available for determining the third order elastic constants, which are measures of the anharmonicity of the forces within a material.

Preliminary experiments on polycrystalline aluminum and copper single crystals have demonstrated that indeed in these two metals, and presumably others, a new wave is generated within the material whose frequency is twice that of the applied wave, and whose amplitude is proportional to the square of the amplitude of the applied signal. As indicated above, this basic result gives information about the magnitude of the third-order elastic constants of the materials. It may be anticipated that the effects of dislocations and radiation-produced defects on the harmonic wave production and propagation may also be studied.

Chemical Reactivity of Metal Surfaces

Single crystals of copper are used to study the effects of crystallographic orientation and defect structure on the reactivity of the metal surface. Since dissolution processes depend, in general, on the rate of movement of steps over the surface as well as the rate of nucleation of steps, electrochemical techniques are employed to study these phenomena. The points where dislocations intersect the surface not only are energetically more favorable as sources for formation of steps, but in some cases the enhanced reactivity is such that etch pits are formed. The rates of increase of depth of etch pits and the lateral motion of the ledges (bunches of atomic steps) forming their sides are being studied as a function of orientation, rate of dissolution, and solution composition. A necessary, but not sufficient, condition for pit development is a reduction in the rate of movement of steps on the surface at any given total dissolution rate. Often this can be accomplished by adding specific reagents to the different systems. An understanding of these phenomena is being gained by measuring such electrochemical parameters as current and potential relationships for crystals of various orientations as a function of solution composition. These data, coupled with electron and optical microscopic observations of surfaces, indicate the relative energies necessary for step motion and nucleation, and a reasonable comparison of the variations of these values with crystal orientation.

Anomalous X-Ray Transmission in Copper Crystals

As a part of the program for investigating imperfections in copper crystals the anomalous transmission of x rays through nearly perfect crystals is being studied. For crystals of low dislocation density appreciable x-ray transmission can be obtained through crystals about 1 millimeter thick, and the transmitted beam can be used to make an x-ray picture, topograph, at unit magnification of a crystal. The strain in the lattice associated

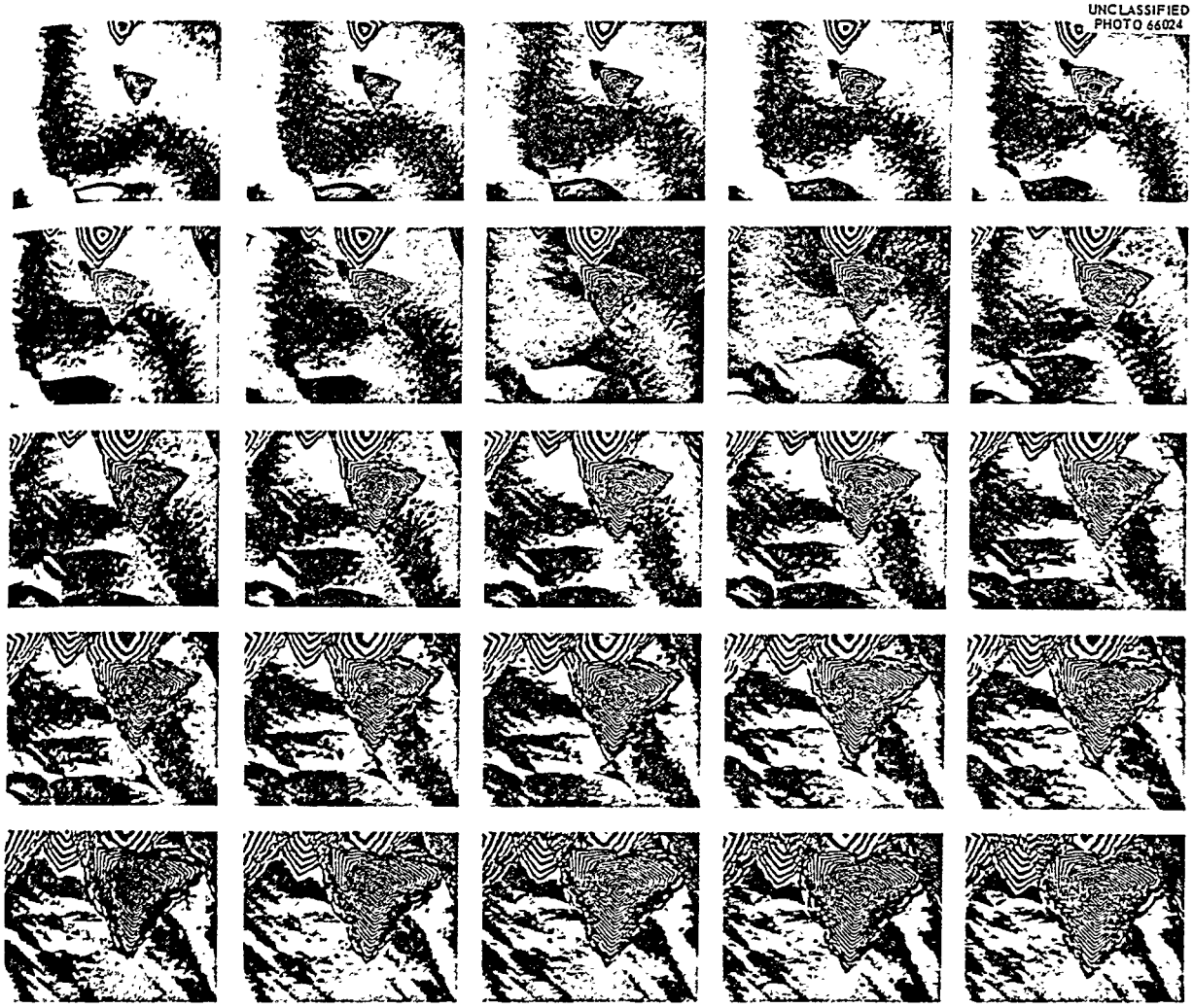

Time-lapse interferrometric photomicrographs of an etch pit being formed at a dislocation site during the electrolytic dissolution of the (111) surface of a copper crystal. The study of the development of etch pit profiles yields information on the anisotropy of reaction rate and on the role of defects in the dissolution of surfaces. The etching solution used was a mixture of HCl and HBr. Current density 10 milliamperes per centimeter, time interval between frames 10 seconds, depth interval between contours 0.27 micron.

with a dislocation line scatters the transmitted beam in its vicinity, and consequently the dislocation line can be seen as a line of decreased intensity on the topograph. By this method dislocations can be investigated in bulk crystals which are nearly perfect, as opposed to the thin imperfect crystals used in electron microscopy. The observation of the anomalous transmission through copper crystals of such thickness is further evidence of their perfection.

By comparison of a series of x-ray topographs from the several close-packed planes of a copper crystal it is possible to determine the types of the dislocations and their spacial arrangement in the crystal. The sources of gliding dislocations and their arrangement on the glide planes are

being investigated under microstrain conditions. There is a correlation between the dislocations observed on the x-ray topographs and the etch pits which are formed at the points of intersection of the dislocations with the crystal surface.

Nearly perfect copper crystals being extremely soft are easily deformed plastically, and therefore it was very difficult to maintain such crystals in near perfect condition. However, by irradiating the crystals with fast neutrons the dislocations were prevented from moving easily, and it was possible to handle the crystals without plastic deformation. Apparently the point defects introduced by irradiating with 10^{17} neutrons per square centimeter did not decrease the intensity of the anomalous transmitted x-ray beam.

Phonon Scattering by the *F*-Center Electron

Previous calculations to determine the effect of *F* center on thermal conductivity have ignored the interaction between the *F* electron and the lattice vibrations. This effect has now been considered in detail with a calculation, using conventional perturbation theory, of the scattering of phonons by the electron bound to the *F* center. The process is analogous to the scattering of light from an atom, in which the electron makes virtual transitions to an excited state. It has been found that transitions to a level lying above the first excited state are the most important and that the scattering rate initially follows a Rayleigh law with the intensity proportional to ω^4, where ω is the phonon frequency. However, as ω becomes larger than about half the Debye frequency the scattering becomes weaker. Using the results of this calculation, it has been possible to account for most of the experimentally observed effect of *F* centers on the thermal conductivity.

Electron Microscope Studies of Fission Fragment Damage in Molybdenum Trioxide

Electron microscope studies of thin films and foils permit the direct observation of the damage induced in the materials by irradiation with energetic particles. Particular emphasis has been directed toward the study of fission damage in solids in order to relate the observable damage with specific interactions between the fragments and the solid. Transmission electron micrographs of thin crystals of molybdenum trioxide (MoO_3), irradiated with fission fragments, have shown tracks about 150 angstroms wide of light contrast, frequently with dark margins. A small fraction of the crystals were oriented such that fringe patterns of 6.93 angstroms spacing were observed, which relate directly to the (020) planes in the crystals and from which information about the state of the lattice may be inferred. An example of the fission fragment track structures observed under these conditions is shown in the accompanying figure. In most cases, the fringes are not continuous through the tracks, indicating local disruption of the crystal structure. Displacement of the fringes in the vicinity of the tracks indicates the presence of internal stresses due to reduced volume of the disturbed region and indicates that the dark margins are most likely due to the effect of these strain fields on diffraction contrast and not to displaced material. These observations suggest that the tracks represent modification and loss of material in the track volume from thermal effects associated with the fission spike.

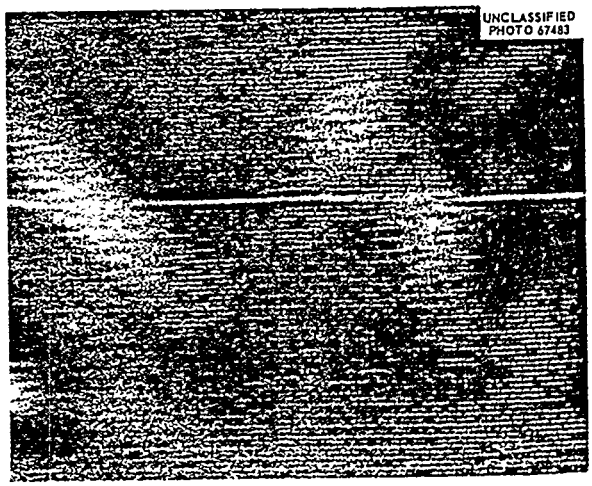

Transmission electron micrograph of fission fragment tracks in MoO_3. The regular fringe pattern present here arises from the (020) planes of 6.93 angstrom spacing in the crystal and their absence in the track regions indicates disruption of the original crystalline structure. 1,500,000X. Reduced 37%.

Electron Spin Resonance of Defects in Diamagnetic Insulating Materials

The investigation of the structure of glasses by measuring the electron spin resonance of intrinsic paramagnetic states has been extended to GeO_2 glass and powdered crystals. Many differences were found between the centers in the glass and those in the crystalline material, and one of the intrinsic paramagnetic states of this glass has certain similarities to one observed in SiO_2 glass. However, a greater variety of intrinsic paramagnetic states has been observed in the GeO_2 glass than was found in the SiO_2 glass. Similarities in the temperature dependence of the spin-lattice relaxation time of a particular center in the GeO_2 glass and a similar center in the SiO_2 glass have been interpreted in terms of a defect vibration mode. The excess strain generated at the center of this mode, which may have been observed in the temperature dependence of the specific heat of the SiO_2 glass, dominates the temperature dependence down to $\sim 1°K$ in both glasses. Paralleling the study of the glasses, investigations of the defects of single crystal quartz have continued with the observation of intrinsic defects with a spin state of $S = 1$. Such states are relatively stable at room temperature although an irradiation at 78°K was required for their production. A paramagnetic center, which has been identified as atomic hydrogen, has also been found in quartz, and in contrast with the hyperfine interaction term found for atomic hydrogen in silica glass, the hyperfine term of atomic hydrogen in quartz is greater than that for the free atom. Although the electronic wave function of free atomic hydrogen is spherically symmetric, perturbation of this spherical symmetry would be expected in a crystal, and the observed spectra exhibit such perturbations.

Resistive Transitions and Critical Fields in Pb-Tl Superconducting Alloys

Considerable developmental effort has been concerned with the use of high field superconductors in solenoidal magnets for various purposes, but many features of these alloy superconductors are not understood. In order to clarify some of the existing problems, different types of investigations have been performed on identical alloys of the lead-thallium system. These alloys, containing up to 50 percent thallium, have been examined in both cold-worked and fully annealed conditions. Magnetization curves yielded constant values of H_{c2} for alloys of each composition and these values correlated well with the measured normal residual resistivity in the type of analysis made from the GLAG theory. Studies of critical currents were also made and the resistive transitions above H_{c2} with current parallel to the field gave constant values of H_{c3}, the upper nucleation field, in annealed wire specimens. The ratios of H_{c3}/H_{c2} agree well with those predicted in the recent theory for superconducting-phase nucleation fields.

Controlled Thermonuclear Research

DCX-1

In the activities centered around DCX-1, 1963 has been unusually revealing and has given us an opportunity for further development of our knowledge of the basic processes that cause the spreading of the plasma – knowledge that is required if we are to develop means to prevent it. The subject has now become refined and detailed.

Trapping by Lorentz dissociation of H_2^+ has been made to work successfully, and it turns out to be a rather beautiful technique, yielding much more trapping for an input beam of a few tenths of a milliampere than has been obtained with gas dissociation at 10 milliamperes. In contrast with injection of neutral atoms the small, controlled beam presents no disposal problem.

The increased number of trapped particles has brought us to the unpleasant realization that already at a density of 10^8 fast protons trapped per cubic centimeter, we are up against a limitation caused by the plasma spreading. When you trap more particles, they simply occupy more volume; the density does not increase. We have reached 10^8 particles per cubic centimeter many times in the past using gas dissociation; it has been the Lorentz dissociation, enabling us to attempt to go beyond this, that has shown that plasma spread is stopping us much sooner than we had hoped. Furthermore, the spreading that was observed a long time ago at densities of 10^9 in DCX-1 when the carbon arc was used appears now to be not necessarily attributable to the arc, except insofar as the arc accelerated the trapping rate.

We can now see that at containment times longer than about 10 seconds, there is appreciable particle loss by some mechanism other than charge exchange.

Electron-cyclotron heating at modest microwave power levels (up to 20 watts) had some beneficial effects. The effects of central-zone heating (26.6 kMc) and end-zone heating (35 kMc) were investigated, and operation with long plasma containment times (5 to 20 seconds) was emphasized. The results with end-zone heating were not very interesting; again only minor changes in plasma properties were observed. Central-zone heating consistently produced a suppression of the radio-frequency signals that can be associated with longitudinal currents, a suppression of the burstlike ejections of electrons out of the mirrors, and a significant reduction in plasma potential. The effects on the spatial distribution of the trapped fast protons were less pronounced and not entirely consistent. On some occasions the addition of the central-zone heating resulted in a reduction of the axial extent of the plasma and in increases in the central proton density of about 10 percent while the total number of trapped protons remained the same. At other times this heating appeared to leave the spatial distribution unchanged, but to reduce the total number of trapped protons by about 30 percent. The specific operating conditions that determine which of these modes is obtained are not yet known.

Measurements of the azimuthal distribution of slow plasma currents out of the mirrors have

shown the first low-frequency rotational phenomenon to be found in the DCX-1. There is an intermittent slight modulation of the electron component of this current sometimes at 2 to 4 kilocycles, sometimes at 8 to 12 kilocycles, and at other times at both frequencies. The disturbance appears to be rotating in the direction of ion rotation in the field at the lower frequency. There is also evidence for a modulation of plasma potential at these same frequencies.

As a function of operating pressure, three characteristic radio-frequency modes are defined: high-pressure, intermediate or flare, and the low-pressure, or burst. In the high-pressure mode, median-plane magnetic probes show only B_z signals that are appropriate for the motion of proton clusters. In the intermediate and low-pressure modes, B_θ signals are also observed, and these are found to be correlated with the pulse-like ejections of electrons out of the mirrors and with sudden increases in the plasma potential.

DCX-2

The application of improved diagnostic methods to DCX-2 has shown that our earlier appraisal of its performance was much too pessimistic; the trapped plasma in DCX-2 is more dense than had previously been thought, and there is little loss other than by charge exchange. Typical figures, using a lithium arc as dissociator, are: 2×10^{15} particles trapped; peak density of fast particles, 2×10^{10} per cubic centimeter; input beam, 30 milliamperes, which is 30 percent dissociated in the arc; base pressure, 10^{-7} torr, seriously modified by arc and plasma pumping. The decay times are about 14 milliseconds, a provisional figure because the shape of the decay curve is not yet understood.

The bursts of escaping ions that had been seen on the gridded probes, and which were partly the cause of our earlier evaluation, are presumably still there; but as a loss mechanism they are now known to be minor in comparison with charge exchange. A reconciliation still has to be made with the shape of the decay curve, but the picture given by the energy-sensitive detectors is so complete and coherent that it is hard to see how the peak particle density of 2×10^{10} fast protons per cubic centimeter can be wrong – this with an input H_2^+ beam of about 38 milliamperes that is about 30 percent dissociated on a lithium arc.

One of the most interesting of the observations on DCX-2 has been the extent of the energy spread that takes place in the trapped-proton population. This is measured by observation with collimated solid-state detectors of the energies of the emergent charge-exchanged neutrals. A substantial correction is required to take into account the variation of the charge-exchange cross section with energy; but when this is applied, it shows that the protons, although trapped at 300 kev, have a mean energy of about 600 kev and some have energies of over 1 Mev. Apparently the energy spreads both up and down, and because of the larger cross section, the protons that lose energy are rapidly charge exchanged, so that in the equilibrium state their number is depleted.

There is some interest in comparing the peak density of 2×10^{10} in DCX-2 with old results in DCX-1. In the past, when the carbon arc was used in DCX-1, mean densities in the range 10^9 to 10^{10} per cubic centimeter were repeatedly reported, with H_2^+ injection currents of about 5 milliamperes and containment times of a few milliseconds. Thus, the DCX-2 densities with the lithium arc are somewhat higher, although per milliampere of injected beam they are no greater than those of DCX-1 with the carbon arc. This probably means only that DCX-2 has not yet reached its full potentialities.

The major results in DCX-2 during this reporting period have been obtained with axial lithium and hydrogen arcs. These arcs are run along flux lines passing through the central volume 1 inch south of the machine axis. The injected molecular ions, therefore, pass through the arc in each revolution as they spiral down the machine. The arc electrodes are located at the ends of the machine beyond the mirrors and the intermediate differential pumping region.

With gas breakup, the pressure in the plasma region is typically about 10^{-6} millimeter of mercury with beam injected, but it has been as low as 4×10^{-7}. With a hydrogen arc running, the pressure has been 4×10^{-6} or greater. Increased pumping is required in the cathode region and is being added. A lithium arc reduces the pressure, not only when the arc is running by direct plasma

pumping, but also when the arc is off after extensive running. The base pressure with the lithium arc running and the beam present is 1.5×10^{-7} millimeter of mercury.

Improved measurements of the injected beam have been carried out in an attempt to establish a complete account of the total accelerator current. It appears that a maximum current of only ~40 milliamperes of H_2^+ injected current is reached even when the accelerator current is increased to more than 100 milliamperes, for reasons that still are not clearly understood. Minor difficulties associated with intermittent turn-to-turn shorts or grounds in the coil system continue to plague operations. However, improved monitoring of critical coil parameters has permitted relatively rapid diagnosis and repair of these difficulties. Significant improvement of the drift in the field has also been accomplished by reducing the regulator amplifier drifts.

No rotational instabilities such as are seen in other machines have yet occurred in DCX-2 – even at the highest density obtained ($\sim 10^{10}$ hot ions per cubic centimeter). As a consequence of this absence of any source of plasma loss except charge exchange, we have no present intention of adding Ioffe bars or other minimum *B* arrangement to DCX-2. Some engineering studies are, however, being carried out to permit such additions with reasonable speed should higher ion density produce some form of instability that minimum *B* could be expected to cure. Principal efforts are now directed toward lowering the pressure of residual gas in the liner and improving the operating condition with both the hydrogen and the lithium arc.

ELECTRON-CYCLOTRON HEATING

In the electron-cyclotron heating studies, a major advance has been a tenfold scale-up in both volume and power. This was accomplished for economy in an existing vacuum-magnetic apparatus called EPA.

The plasma is created in a 3:1 magnetic mirror field by a 10.6 kMc microwave power source capable of delivering 50 kilowatts continuous wave. Preliminary results show that the plasma volume is ~40 liters and contains several hundred joules of stored energy with 25 kilowatts continuous wave microwave power.

The main answers sought by the experiment have already been obtained; (1) for the same microwave power input per unit volume one obtains the same energy density as was obtained in the smaller Physics Test Facility apparatus; and (2) the larger plasma is more stable than the smaller one, in the sense that the proper combination of operating parameters is far less tricky to attain.

Measurements have been made of the bremsstrahlung from the electron-cyclotron plasma in the EPA facility operated with 25 kilowatts of 10.6-kMc microwave power. A 3- by 3-inch NaI(Tl) crystal mounted on a multiplier phototube viewed ~40 cubic centimeters of plasma through a ¼-inch-diameter pinhole. The fractional solid angle subtended by the crystal was $\sim 6.5 \times 10^{-7}$. From a comparison of the observed spectrum to the theory developed by Heitler (*The Quantum Theory of Radiation*, 3d ed., p. 252, Clarendon Press, Oxford, England, 1960), a plasma "temperature" of ~120 kev was determined. By measuring the counting rate of photons above 120 kilo-electron volts, a plasma density of $\sim 5 \times 10^{11}$ electrons per cubic centimeter was inferred. These numbers give an energy density of $\sim 5 \times 10^{16}$ electron volts per cubic centimeter, or $\sim 8 \times 10^{4}$ ergs per cubic centimeter.

This measurement checks well with a measurement of the energy density computed from the voltage induced in an external coil when the klystron power is turned off. The voltage induced in this coil is related simply to the total magnetic moment of the plasma. The energy density is computed with a plasma radius and length estimated from Hall-probe measurements and pinhole-camera x-ray photographs. It is found to correspond to a steady-state beta of 0.3, which is about the same as is inferred from the bremsstrahlung measurement. This accomplishment of a stable, steady-state, high-beta plasma has increased our determination to try to heat the ions. Plasma decay times are consistent with these density and temperature figures on the basis of electron-electron collisions. The energy stored in the plasma is some hundreds of joules.

An odd observation on EPA concerns the x-ray bursts that occur when the gas feed is reduced below the rate required for stability. The bursts are rather uniform in size, small bursts not being seen. In this mode of operation, the x-ray emission

from EPA can be quite dangerous despite the lead shield.

Meanwhile, a few experiments have been continued on the smaller hot-electron plasma in the Physics Test Facility. Measurements of density by means of microwave interferometry have disagreed with everything else; it is now found that this is true for 8-millimeter microwaves as well as 4-millimeter microwaves, the interferometer yielding density values three to ten times lower than the other measurements. Another experiment involved the dropping of a ball through the plasma while simultaneously observing x rays axially and in the midplane, and $d\phi/dt$ in a surrounding coil. The result confirmed the fact that high-energy electrons occupy space around the plasma, but showed that these electrons do not hold the main energy content of the plasma.

PLASMA PHYSICS

Some of the experiments that were done in the wide field of general plasma physics during 1963 concerned the discovery of moving striations in the positive column of rare-gas discharge and their identification with ion sound-wave phenomena, the measurement of ion sound wave velocity by time-of-flight, and the improvement and reconciliation of various diagnostic methods. The effects of multipole fields were observed in small experiments, and weak Ioffe fields were found to have a quieting effect upon the plasma that was used in the experiment. One field of unusual interest was that of beam-plasma interactions. These can lead to some surprising phenomena; for example, a beam of 7-kev electrons interacting with its self-generated plasma in a mirrored configuration can, under some conditions, cause the emission of x rays up to 1 Mev in energy and, under other conditions, can lead to a heating of the ions to some hundreds of electron volts. The latter observations are of course being subjected to further experimentation and scrutiny.

VACUUM ARC RESEARCH

The magnetically constrained, high-density deuterium arc plasma has been shown previously to be highly ionized and relatively quiescent. It appeared to be a good plasma for the study of plasma diffusion across a magnetic field in the regime where only charged-particle collisions were important. However, Langmuir probe measurements of the region outside the main arc plasma indicate that the particle transport across the magnetic field is dominated by flutes generated by the main arc plasma. The flutes, with a cross-sectional area of about 0.2 square centimeter, apparently extend the full length of the arc through a 2:1 magnetic mirror. The flutes have both radial and azimuthal velocities of 1 to 5 $\times$ 10^5 centimeters per second across the magnetic field which are dependent on the magnetic field strength, the

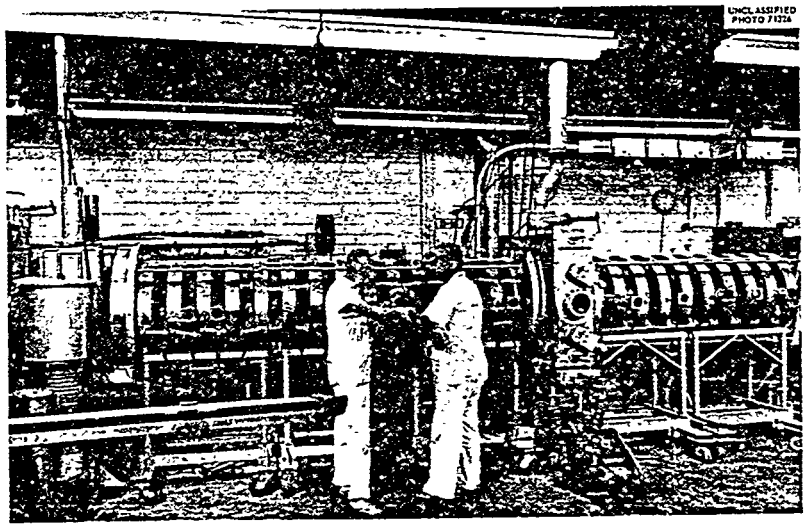

The Long Solenoid Facility, as used for studies of the properties of extended vacuum arcs. Arcs as long as 20 feet can be maintained continuously in magnetic fields up to 13 kilogauss in strength. Hydrogen, helium, argon, and other gases and the vapors of lithium and carbon have been introduced at the electrodes to maintain the arcs.

arc current, and the radius at which the measurement is made. These flutes apparently solve a long-standing mystery as to the mechanism of the escape of deuterium from the arc; but, more importantly, their presence in such a convenient apparatus as the Gas Arc Facility gives us a means of study that may be most instructive inasmuch as there is a good body of theory available for comparison and guidance. If the flutes can be controlled, hope might be revived in the deuterium arc as a rather ideal dissociator or ionizer for use in high-energy injection.

In the Long Solenoid, techniques have been worked out for the running of controllable lithium arcs at various currents, and these techniques have been transferred to DCX-2. In the carbon arc work, a mechanism has been suggested that may help to explain the high ion temperatures (5×10^6 degrees) that are observed near the cathode of an 8-foot-long arc. The suggested mechanism involves collisions between metastable carbon ions, with the energy of excitation being transferred into kinetic energy of repulsion.

CROSS-SECTION MEASUREMENTS

During 1963, major emphasis has been placed on modifications of existing apparatus to facilitate measurements of atomic collision cross sections. The successful operation of the 600-kev accelerator has been plagued for the past four years with two problems: breakdown of the auxiliary power insulating transformer stack, and voltage regulation. The first problem has been solved by replacing the transformer with a generator driven with a Fiberglas rod. A fast voltage regulator utilizing a derivative amplifier and filter circuit has been fabricated and installed. For output voltages of 300 kev the short-time variation in voltage is now less than 500 volts, and the voltage drift is within this value for periods of several hours.

The fabrication and initial vacuum tests of the cross-beam apparatus have been completed. After bakeout at 120°C, the pressure was 10^{-8} torr without titanium pumping. The addition of titanium pumping on liquid-nitrogen-cooled surfaces lowered the pressure to 7×10^{-10} torr. Minor design changes are now being made to improve the efficiency of the titanium pumping.

Throughout the history of atomic collision cross-section measurements, a need has existed for a low-current detector and energy analyzer of neutral particles in the kilo-electron-volt range. Common scintillators and solid-state detectors provide a suitable detector for protons or neutral hydrogen atoms above 20 kev. A proportional counter has been designed and fabricated to

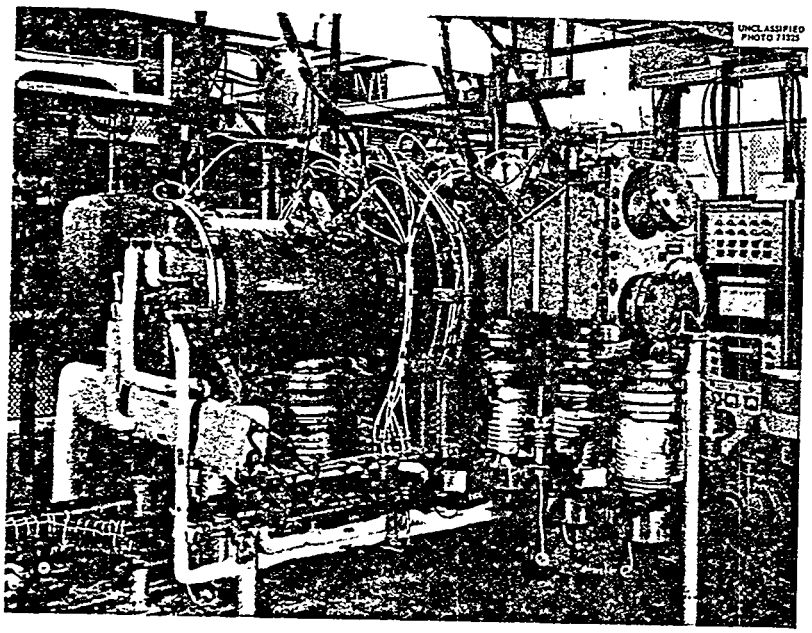

Apparatus for measurement of atomic collision cross sections by the method of crossed beams. A beam of H_2^+ ions, for example, is made to enter the vacuum tank from the region in the background of the picture and intersects an electron beam running axially in the cylindrical tank. Instruments in the two ports of the divergent chamber near the right can then be used to measure the relative numbers of charged and neutral particles that result from the collisional dissociation of the H_2^+ ions.

provide for detection of hydrogen particles down to 2 kev. The entrance of the counter consists of a 0.001- by 1.5-inch slit covered with a thin film of Formvar. The slit is scanned laterally over the spatial extent of the beam. The counter is filled with approximately 1 torr of methane. Preliminary results with high-energy alpha particles indicate good energy resolution, and tests are proceeding in determining the energy resolution and minimum energy for protons.

A complete revision has been made of ORNL-3113, *Atomic and Molecular Collision Cross Sections of Interest in Controlled Thermonuclear Research.* The collection now includes 135 graphs of evaluated data, along with a bibliography of 1800 references. These references have been collected and filed for further evaluation.

PRODUCTION, ACCELERATION, AND INJECTION OF IONIC AND ATOMIC BEAMS

The 600-kilovolt high-intensity beam test stand has delivered up to 95 milliamperes of H_2^+ ion current through a 4-centimeter aperture located 350 centimeters from the ion source. The previously observed current limitation of 60 milliamperes proved to be a decreased relative production of H_2^+ ions in the duoplasmatron ion source. This limitation was removed by small changes in the geometry of the source. The DCX-2 injector system, which has several operating requirements not included in the 600-kilovolt test stand, is apparently limited to an injected H_2^+ current of only 40 milliamperes. Since the calorimetric beam accountability is only 80 percent of the drain on the supply, it is not certain that the injected current is really this low. Successive modifications in the epoxy "skirts" have continued to improve the voltage holding capacity of the 600-kilovolt accelerating column on the atmospheric side.

A hollow-cathode arc ion source has been satisfactorily operated at 30 kilovolts in an assembly which will permit comparison of neutral beam production from either a gas cell or another hollow-cathode discharge. A total hydrogen ion beam of 35 milliamperes has been attained with a divergence angle of 10 degrees.

VACUUM

Mass spectra of two medium-carbon-number hydrocarbons have been obtained with a time-of-flight spectrometer. The absence of metastable mass peaks (due to dissociation) was noted, as was also an enhancement of primary peaks relative to peaks due to fragmentation of primary species. The spectra of mechanical pump oils have been obtained; they normally show peaks past mass number 350, with large amounts of methane and other low-carbon-number hydrocarbons.

The ultrahigh-vacuum test facility instrumentation was improved by the incorporation of higher-speed recording equipment for vacuum gages and more stable ion gage controls. Because of the limited compression ratio of a diffusion pump for methane (reportedly $\approx 10^6$) and since methane appears to be the predominant gas during operation of large systems in the 10^{-10}-torr range, an interstage diffusion pump has been added in series with the existing pumps and has been operated.

Tentative procedures have been developed for the testing of block-type vacuum valves for helium leak and permeability rates and for conductance.

MAGNETICS AND SUPERCONDUCTIVITY

Theoretical and experimental work seems to demonstrate the merits of so-called "absolute *B* minimum field configurations" for plasma containment. Various analytical solutions have been presented recently; however, very few numerical data of the field quantities concerned have been published to date. We studied, in detail, the following special cases: the magnetic field resulting from the superposition of a quadrupole field ("Ioffe bars") and the regular magnetic field of DCX-2; three cases of field configurations produced by an axisymmetric coil arrangement suggested by J. Andreoletti; and finally, we made a numerical analysis of a field configuration due to two infinitely long current loops as described by D. A. Baker. Only the Ioffe-bar arrangement produces a relatively large increase of the magnitude of *B* around the field axis in the zone of interest.

During several years, an appreciable number of magnet coils have been built in this division for

producing a great variety of magnetic field shapes. The standard design of such magnet coils consists of "pancakes" of hollow, water-cooled copper conductors. Since the rated currents of the available direct-current generators are large (5000 to 8600 amperes), the cross sections of the copper conductors must also be large, and therefore the surface of coils made up of such pancakes consists of cylindrical parts with radii and axial lengths varying in relatively large steps. For special purposes, much smoother surfaces are very desirable. A new method is described which permits the building of magnet coils with considerably improved surfaces without disadvantages with respect to simplicity and reliability of the design.

During the last report period, the new magnet laboratory went into full operation. This laboratory serves for developmental work on conventional and superconducting magnet coils and consists presently of one magnet coil for 60 and another for 90 kilogauss (3 and 6 megawatts direct current, respectively), both with a working diameter of $6\frac{1}{2}$ inches. Furthermore, a 50-kilogauss superconducting magnet coil is available. Necessary regulated current sources and ample instrumentation for experiments with high-field and soft superconducting materials are provided. This magnet laboratory, which is one of the largest of its kind, could be built with relatively low costs, since the large direct-current power supplies of the Thermonuclear Division were available.

An extensive systematic study was made on models of high-field superconductors proposed by H. London, by C. P. Bean, and by Y. B. Kim *et al.* Sets of equations for tube magnetization and magnetic moment curves have been derived which are more comprehensive than those previously published. Furthermore, a measurement method for simultaneous investigations on tube magnetization and magnetic moment of high-field superconductors is described. Finally, magnetic moment measurements of bundles of niobium-zirconium wires are reported which gave well-reproducible results for complete magnetization cycles. These results are compared with calculated curves based on the model of Kim *et al.*, and the connection with the flux-creep theory applied to a comparable case is discussed.

PLASMA THEORY AND COMPUTATION

The correspondence between hot-electron and hot-ion plasmas generated in our experiments and the predictions of stability theory has been under continuous review. Stability of hot-electron plasmas generated by cyclotron heating is attributed to conductivity to end walls by cold plasma, and possibly to other stabilizing effects of the low-energy component of the plasma continually replenished by ionization of the large neutral gas background necessary for stable operation. In the DCX experiments, enhanced energy and spatial diffusion (in DCX-1) are attributed to charge bunching, for example, by ion-electron microinstabilities as suggested by Harris. The development of Harris's theory is reviewed. It is argued that flutes and other macroinstabilities are ruled out by finite orbit effects.

In another section, the values of density and magnetic field such that a two-temperature ion distribution is stable against the Harris instability are mapped for various ratios of temperature parallel and perpendicular to the magnetic field.

A previously developed technique for obtaining exact upper bounds on growth rates of instabilities has been applied to configurations confined in mirror machines. The fastest growth is that of Harris's electrostatic streaming instabilities.

The same technique is used in obtaining bounds on growth rates which are then employed in setting a lower bound on the diffusion time across a magnetic field. It is found that, for practical purposes, confinement of quite dense plasmas, if they are several (for example, 10) ion gyro-radii across, is not limited by cross-field diffusion, even if microinstabilities are present. The implication is that closed containers designed for macrostability, such as the toroidal multipole, should be stable in practice.

Effects on hot-electron plasmas of energy loss by radiation following collisional excitation of impurities have been calculated. Qualitative agreement is obtained with experiments in which xenon was introduced into the Physics Test Facility hot-electron plasma.

A new approach to stabilization of bounded plasmas by electron streams has been undertaken.

Shortcomings of an infinite plasma theory applied to this problem necessitated the new approach — that of considering the system as a finite, bounded plasma. Results for various boundary conditions are being investigated.

In electron-electron and electron-ion collisions, the presence of a strong magnetic field theoretically is shown to impede the transfer of energy from the direction parallel to the field to the perpendicular directions.

Preliminary phenomenological fits to data for energy diffusion in DCX-2 by microinstabilities give diffusion times a factor 10^7 to 10^8 shorter than Coulomb diffusion, but $\sim 10^4$ longer than the microinstability growth time.

A study of H_2^+ and H^+ orbits in a four-pole infinite Ioffe-bar field added to the standard DCX-2 field has begun. Particles initially near a bar are found to be lost in a few microseconds.

CHEMICAL STUDIES OF HIGH-VACUUM TECHNOLOGY FOR THERMONUCLEAR FUSION EXPERIMENTS

In the experimental program to develop controlled thermonuclear fusion, extremely low pressures must be maintained in large systems. Heavy gas molecules, including hydrocarbons such as those produced by decomposition of vacuum-pump oils, are extremely undesirable, because in collisions with the hot ions such molecules absorb energy and cool the plasma. However, the walls of the test chamber may be cooled without cooling the magnetically confined plasma. Condensation (or adsorption) of heavy gas molecules on the cooled walls is, therefore, under study by R. A. Strehlow and D. M. Richardson of the Reactor Chemistry Division with the aim of developing a technique for attaining low pressures.

The vacuum chamber being used is of a volume (15 cubic feet) sufficient to permit safe extrapolation of the results to large thermonuclear assemblies. The inner surface is covered with vapor-deposited molybdenum (a metal which may ultimately serve as a liner for a practical thermonuclear machine) and is cooled to about −281°F by liquid nitrogen; the surface temperature can be controlled or quickly changed by altering the pressure at which the liquid nitrogen boils.

Adsorption and desorption of hydrogen and several contaminant gases have been measured under conditions in which the molecules cover less than one one-thousandth of the molybdenum surface. From these data the energy of adsorption of a molecule of the test gas is obtained; the transient pressure drop which should follow a sudden decrease in liner temperature can be calculated from the energy of adsorption. It appears that one can, by quickly lowering the temperature, effectively lower the abundance of heavy molecules in the apparatus before the startup of a fusion experiment. Moreover, if the liner has been kept cold for long periods and has effectively "scavenged" the heavy molecules (which constantly leak in at slow rates) and then is warmed suddenly, much of the gas is released; in this case the pressure rises to a value such that the desorbed gas can be effectively removed with conventional high-vacuum pumps. Thus, a cycle of alternate heating and cooling may be employed to make the liner an effective "pump" for those gas species which are most undesirable.

Reactor and Hot-Cell Operations

REACTOR OPERATIONS

The ORR achieved the highest efficiency of operating time in its history when the reactor operated 89 percent of the time for the January–March quarter of 1964.

ACL

On July 1, 1963, one fuel plate of a 19-plate element in core position D-1 of the ORR was melted because a neoprene gasket accidentally blocked the cooling water flow through the fuel element. No serious contamination resulted from this incident, there was no overexposure of personnel, and the reactor was back in operation less than two days after the accident. Because of this melting, modifications were made in the water system, in procedures, and in some equipment to prevent such an accident from recurring, to detect boiling before fuel melts, and to limit the severity of the accident if it should recur.

The beryllium-cadmium shim rods and beryllium-reflector core pieces in the ORR were found to be bowing due to fast-neutron damage. Some of this beryllium was removed from the reactor as unusable, and measurements showed bowing of as much as 50 mils in one piece approximately 30 inches long. New beryllium is being prepared to replace the damaged pieces.

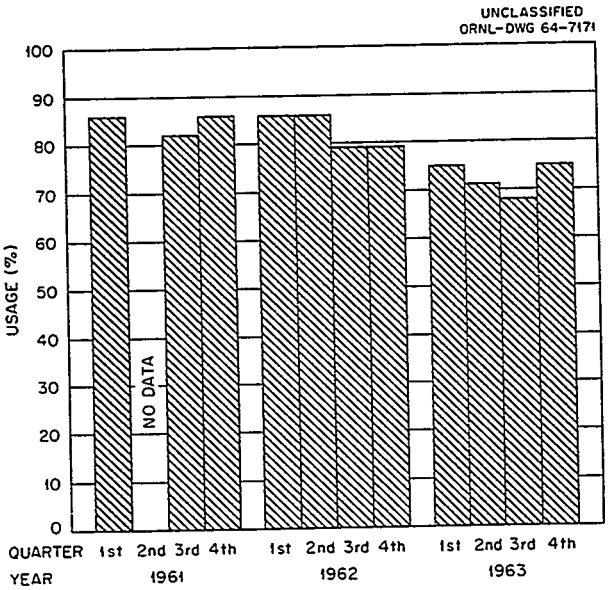

LITR usage of experimental facilities (1961–1963).

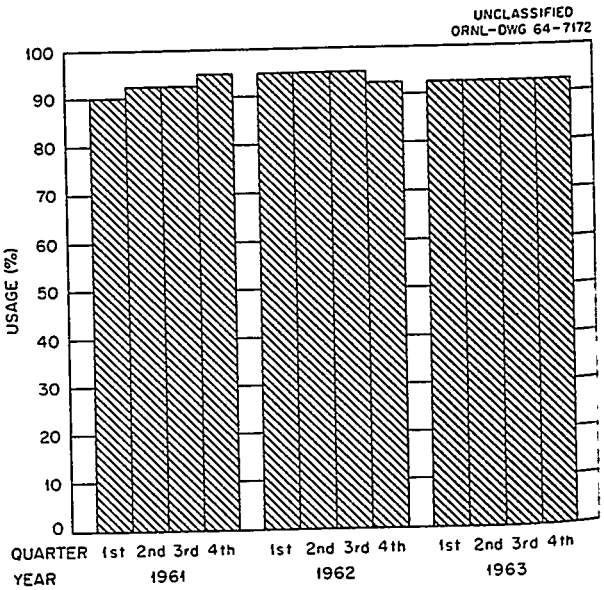

ORR usage of experimental facilities (1961–1963).

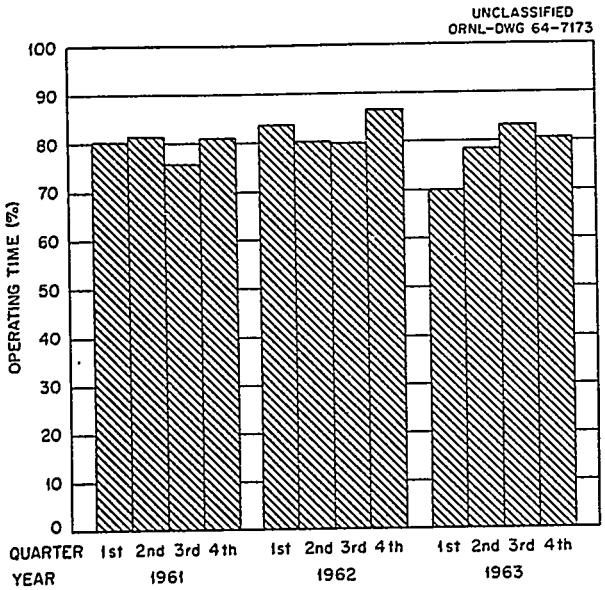

ORR operating time.

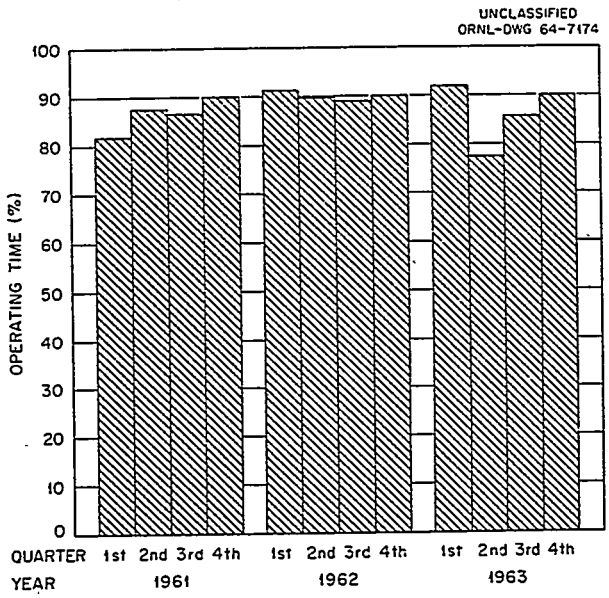

LITR operating time.

On November 4, 1963, after 20 years of operation, the ORNL Graphite Reactor was shut down permanently. Provisions have been made to maintain a negative pressure in the reactor to prevent the escape of radioactive particles from fuel elements which might oxidize.

The remote control desk for the LITR, formerly at the Graphite Reactor, was moved to the ORR control room. Operation of the LITR and ORR from a common point has been very successful; a significantly smaller number of personnel are required.

The experiment facilities in the ORR were in great demand. Experiment groups were assisted in designing experiment rigs, fuel test loops, and irradiation capsules. Approximately 126 reviews of experiments were conducted to ensure that reliable components, proved circuits, and other standards necessary for safe reliable operation were used. Containment to prevent release of radioactive contamination and proved operation and maintenance procedures have helped reduce spurious shutdowns and accidental release of radioactivity to a very low amount.

The purpose of the reviews was to confirm that repeat-type experiments or tests met already approved specifications, to evaluate changes in experiment conditions, and to approve new experiments.

RADIOACTIVE WASTE DISPOSAL

The release of radioactivity into the environment continued its downward trend. The reduction was brought about by improvements in waste handling practices and the early detection of accidental releases made possible by intensive monitoring of the waste disposal system streams. A comparison of activity discharged in liquid waste to the Clinch River during the last four years, measured by the Health Physics Division, is shown in the table.

The total release of iodine-131, the only contaminant released to the atmosphere in any significant quantity, was 54 curies in 1963 as compared to 121 curies in 1962. The release of particulate iodine-131 was 0.4 curie in 1963 and 1.8 curies in 1962.

Activity Released in Liquid Waste to Clinch River

Year	Strontium-90 (curies)	Ruthenium-106 (curies)	Total Activity (curies)	Average Concentration in River (% MPC)[a]
1960	27	1890	2187	24
1961	22	2035	2228	18
1962	9	1383	1436	7
1963	8	430	469	5

[a]The MPC (maximum permissible concentration) in the Clinch River is the weighted average of the MPC values of individual radioisotopes as recommended for populations in the neighborhood of a controlled area by national and international committees on radiation protection.

HOT-CELL OPERATIONS

Operations in the hot cells were normal. Forty-three capsules fueled with UO_2, BeO-UO_2, coated UC_2 particles, or graphite balls with (Th-U)C_2 particles were disassembled and examined in detail. Examinations included dimensional analysis, gamma scanning, sampling of the fission gas and fuels for chemical analysis, density check, metallography, and other. Additional experiments disassembled and examined include four UO_2 meltdown (in-pile) experiments, two SM-1 (APPR) reactor fuel elements from Fort Belvoir, three Army PM-1 experimental fuel bundles, and an irradiated lithium hydride test. Three BeO experiments (about 180 BeO pellets each) from the ETR and two MSRE experiments (six capsules each) from the MTR were examined in detail. A tensile machine was installed, and about 220 irradiated specimens were tested. Cut-up equipment for large experiments was installed, and several experiments from ORR-GCR Loop 2 were disassembled.

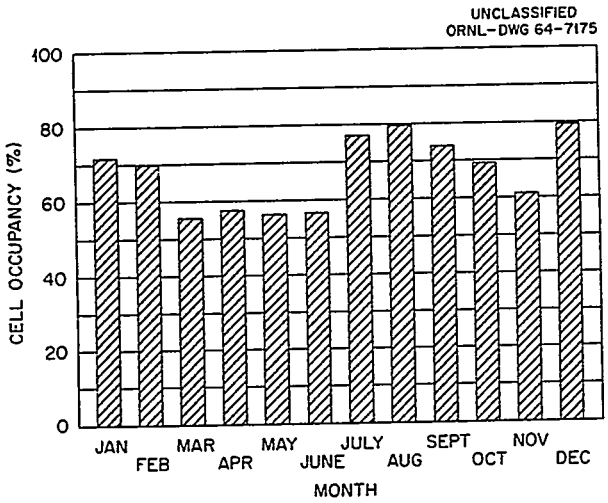

Cell occupancy for Buildings 3025, 3026D, and ORR hot cells.

Installation of equipment in the High-Radiation-Level Examination Laboratory (HRLEL) was started in April. The H. K. Ferguson Company installed a radioactive liquid waste catch tank, and 35 master-slave manipulators and three GM manipulators with companion cranes were installed by ORNL. A cutoff saw, a mounting press, a rough grinder, polishers, an etching sink, and dryers were installed for preparation of metallography specimens; installation of the metallographs, the x-ray diffraction equipment, and the gamma scanner was begun. Other equipment installed included a stage and two stereomicroscopes, milling machine, TV camera, and about 80 percent of the in-cell work tables.

The radiation monitoring system with centralized panel was completed, the cell mockup was moved to the HRLEL, and the technique of changing an alpha seal window was successfully demonstrated. Installation and testing of other equipment is proceeding; it is anticipated the HRLEL can begin hot operation during the first half of 1964.

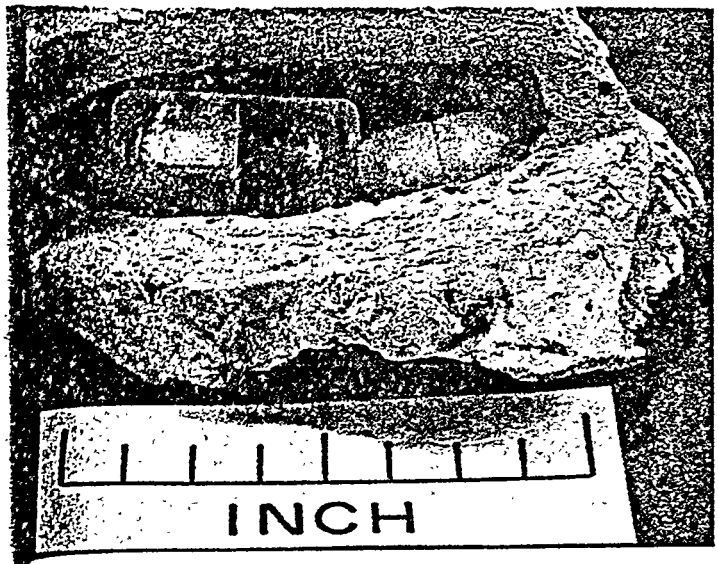

Biology and Medicine

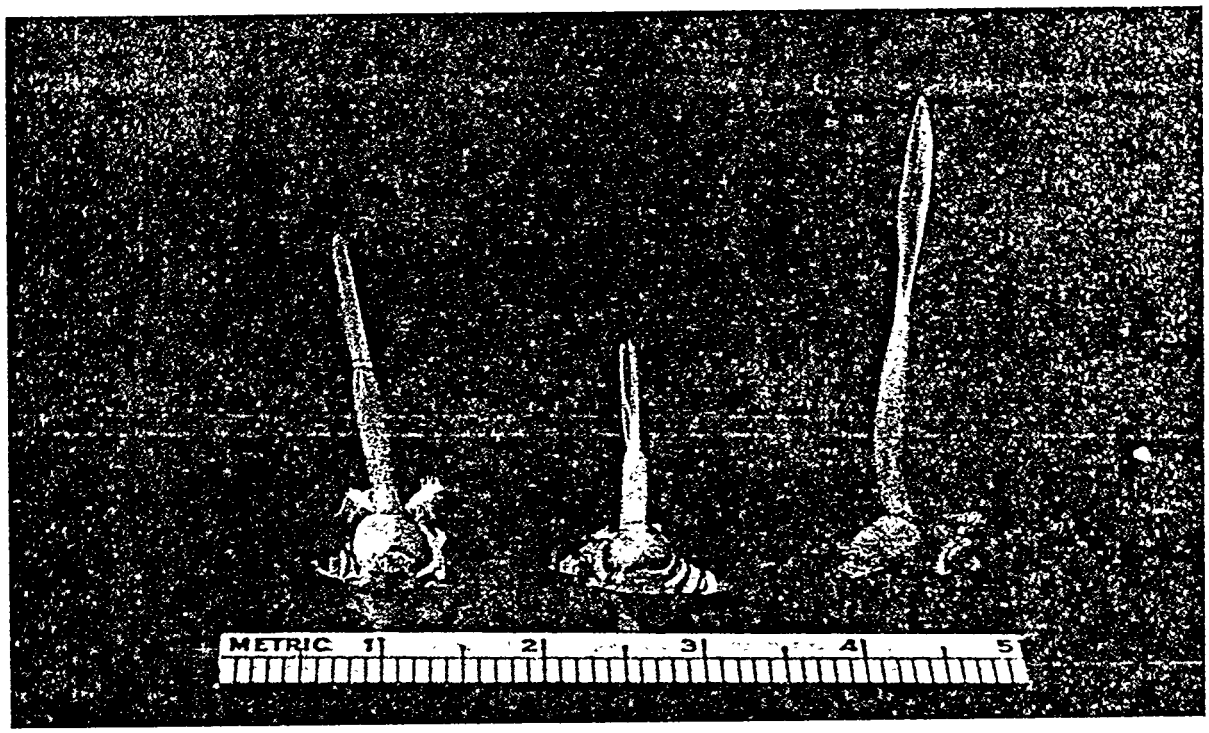

a long period of time present a major problem in the logistics of collecting and analyzing data. Already, information from the breeding studies carried out in the pilot program is available for examination at regular intervals, so that more precise estimates may be made of the specific needs for the different phases of the long-range experiment. It is likely that the data from this experiment will be collected automatically by means of some data collection system.

A retrospective and a prospective study, in cooperation with the Mammalian Recovery Section of the Biology Division, are under way in an attempt to understand the factors responsible for spontaneous circumvention of secondary diseases or spontaneous cures which favor survival of irradiated mice treated with foreign bone marrow. The retrospective study involves summary analyses of all bone-marrow experiments carried out in a single laboratory of the Biology Division since 1955. It is hoped that some influential factor in spontaneous recovery from secondary disease will be found in the results of such analyses. The prospective study involves the use of experiments specifically designed to determine the possible interaction of variables that have been known, or suspected, in the past to have an influence on mortality from secondary disease.

Retrospective studies are being made, in conjunction with the Health Division, of death rates and of vital information collected in the course of dispensary visits and regular health examinations of employees at the local AEC installations during the past 10 or 12 years. Health records are maintained at present in 80-column Hollerith cards. It has been proposed that these data be transferred to magnetic tape for processing by high-speed computers. In such processing, more complete studies of both past and current information will be feasible.

A sampling plan was devised to calculate the amount of radioactivity in the top 2 feet of the soil of the bed of White Oak Lake, which has long been used as a settling basin for low-level radioactive discharges. The sampling plan was stratified, with optimum allocation of sampling units to strata in the lake bed. From 250 soil cores allocated proportionally to the area of the strata and to the variability within the strata, the total amount of radioactivity was estimated to within about 10 percent.

A computer program was written to solve a problem in the estimation of physical parameters of a highly nonlinear function which describes the internal friction spectrum of niobium-zirconium wires. The solution to this problem had been very elusive for several years. However, by combining several statistical and computing techniques into a single package, a program has been developed which will solve problems of this nature routinely.

During the past year the Statistics Group has been called on several times by the Division of Biology and Medicine of the Atomic Energy Commission to evaluate proposals for funds for experiments in biology. Members of this group have also been asked to review and comment on statistical techniques employed in scientific studies dealing with the effects of radiation on humans. In all cases where such requests were made, an evaluation of the particular experiment or document was presented without delay to the Division of Biology and Medicine.

Also, consultation services were provided to members of the staffs of the Oak Ridge Institute of Nuclear Studies, the University of Tennessee, both at Memphis and at Knoxville, Vanderbilt University, and the UT-AEC Agricultural Research Laboratory. In general, the policy of the Statistics Group has been to provide statistical assistance and consultation to everyone who seeks it. It is the feeling of the Group that the education of investigators in the areas of the physical and biological sciences to statistical methods will serve to minimize the cost of experimentation and maximize the yield from these experiments.

Radiation Effects

IDENTIFICATION AND ISOLATION OF BONE-MARROW STEM CELLS

The long-standing question as to whether or not different types of blood cells have a common precursor has been partially resolved at ORNL by the transplantation of subpopulations of marrow separated into discrete cell types by passage through glass-wool filters.

This work, performed with mice, has shown that of the various types of cells in the bone marrow, only the small, round lymphocyte-like cells can repopulate the depleted blood-forming tissues of an irradiated recipient. These cells thus appear to be capable of sustained proliferation and of forming daughter cells that mature into different hematologic types (i.e., granulocytes, erythrocytes, platelets, etc.).

The marrow "lymphocyte" differs in this respect from the morphologically similar lymphocyte of lymphoid tissues, although its precise relationship to the latter remains to be determined.

Bone-marrow cell in metaphase. Arrow indicates morphologically abnormal marker chromosome. Marker chromosomes are studied at ORNL because they are thought to occur in leukemic cells only.

A SPECIFIC CHROMOSOMAL ABNORMALITY IN MICE WITH MYELOID LEUKEMIA

At ORNL, bone-marrow cells of a particular strain, RF, of mice with passaged, radiation-induced myeloid leukemia have been found to contain both an extra and a marker chromosome. The marker is an intermediate-size chromosome which appears to have a region of secondary constriction about one-third of the distance from its distal end. The proportion of cells containing the abnormality varies with the stage of the disease, being highest in mice with the most extensive dissemination of

leukemic cells. For this reason and because the abnormality has not been seen except in mice with the leukemia, the chromosomal changes are thought to occur in the leukemic cells alone.

The significance of the cytogenetic abnormality in relation to the cause of the leukemia remains to be determined. Its constancy, however, in mice with disease, whether the leukemia was induced by inoculation of cell-free ultracentrifugates or by leukemic cells, implies that the change is not merely a reflection of the nonspecific aneuploidization commonly associated with malignant growth. Moreover, its presence in leukemias induced by cell-free inocula indicates that it may result from the direct action of the leukemia virus on a specific region of the chromosome. Although it has been observed consistently in the mice of two separate passage lines, each of which came from a different radiation-induced primary leukemia, its presence in mice developing the disease spontaneously or as a result of irradiation is yet to be determined.

It is noteworthy that the only other instances in which specific chromosomal aberrations have been consistently associated with primary neoplasia involve abnormalities of chromosome 21 in human leukemia; that is, the Philadelphia chromosome in persons with chronic myelogenous leukemia and triplication of the same chromosome in individuals with Down's disease, which predisposes to leukemia of various types. Investigation of the chromosomal abnormality in mouse leukemia, therefore, may help to elucidate the significance of karyotype changes in neoplasia generally and provide insight into the mechanism of carcinogenesis.

Radiation Genetics

EFFECTS OF RADIATION ON PLANTS AND SEEDS

It has long been known that low doses of ionizing radiation can kill cells and organisms that have been irradiated. These low doses of radiation are not enough to inactivate cellular biochemical processes per se, and it has been found that the primary biological effect of radiation is on the nucleus of the cell. It is the nucleus that contains the genetic apparatus (genes and chromosomes) and is considered to be the governor of all the reactions that go on in the cytoplasm. If the nucleus is damaged, then the rest of the cell will not function properly. In an attempt to get a fundamental understanding of the interaction of radiation with the genetic material and also of how the genetic material is organized and functions, experiments have been carried out at ORNL on the radiation genetics of various plant materials. The plants used have been selected because they are easy to handle, because they have large, easily seen chromosomes, and because at the nuclear level one can generalize from one biological organism to another (i.e., results obtained on plant nuclei are essentially true for all cell nuclei).

Studies on the kinetic relations as to how a certain type of mutagenic event, called a two-break intergenic mutation, increases with increasing doses of ionizing radiation have led to the realization that the genetic material is organized within the nucleus in a certain specific fashion. For instance, the chromosomes do not wander about vigorously within the nucleoplasm but are relatively fixed in such a way that one chromosome rarely approaches another. Within a given nucleus there are very few places where the chromosome strands come close to one another. Since this is true, it is only a very small proportion of the chromosome breaks induced by radiation that can rejoin to form intergenic mutations such as chromosome translocations.

The knowledge that there are a limited number of places for the formation of such genetic damage has given insights that help explain many of the hitherto puzzling aspects of radiation on chromosomal material. For instance, it had been noted that as the chromosomes proceed from one portion to another of the cell division cycle, the apparent sensitivity of the chromosomes to radiation changes. It is now possible to explain most of these changes, not in terms of a change in the actual sensitivity of the molecular entity called the chromosome itself, but by a change in the spatial relations of chromosomes within the nucleus. Thus broken ends that differ in their propinquity differ in their ability to rejoin to form intergenic mutations rather than undergoing the type of repair known as restitution.

Similarly we have been able to characterize the distribution of two-break chromosome exchanges among the cells only if we take into account the limited number of sites for exchange formation.

It has long been thought that x radiation and far-red radiation were cooperative in their action in that when both types of radiation were given to a cell, more chromosomal mutations were produced than the sum of those produced by each of the radiations individually. It has now been found that far-red radiation delays the cell division cycle, so

that at any given time after giving this radiation a different group of cells can be found in metaphase where the chromosomes can be scored. Since the number of sites for exchange differs in the various portions of the cell cycle, different numbers of exchanges can be produced by a given number of nuclear breaks. The far-red x-ray synergism seems to be resolved simply as being caused by the phenomenon of nuclear selection, that is, after a dose of x rays plus far red, cells from a more sensitive stage to the radiation are found at metaphase and are compared to cells that were in a less sensitive stage if only x rays had been given.

In another area of fundamental radiobiology of the nucleus, radiation was used to determine exactly when in the cell cycle the chromosome duplicated. The chromosome doubles just before cell division, so that each daughter cell can contain the same genetic material as the mother cell. If the chromosome is irradiated before it duplicates, then so-called chromosome aberrations result. These affect both the daughter chromatids that are present after duplication. In other words, a break is produced and then the chromosome duplicates and, in effect, the break itself is duplicated. If, however, the radiation is not given until after the two daughter chromatids are produced by replication, then the break will be in only one of the two chromatids giving rise to chromatid aberrations. In studies in which it was possible to pinpoint the time of replication of the deoxyribonucleic acid (DNA) by the administration of radioactive thymidine that becomes incorporated into the new DNA, it was found that the chromosome reacts to radiation as though double (i.e., gives chromatid aberrations either before the DNA begins to duplicate or at the very beginning of the duplication process before much DNA has been made). This has been interpreted to indicate either that the chromosome is already two-stranded before the DNA has replicated, or that the protein part of the chromosome duplicates before the DNA does. Such studies are important because they give clues as to the possible organization of the chemical components that form the chromosome.

STUDIES ON THE NATURE OF INITIALLY REPARABLE PREMUTATIONAL LESIONS

There is good evidence that the amount of mutation produced by a given dose of ionizing radiation, even radiations of high linear energy transfer (LET), can be diminished considerably by treatment during a limited period after irradiation. Work at ORNL with the protozoan *Paramecium* has provided much, but not all, of this evidence and has traced the effect to enzymatic repair of premutational chromosomal lesions during the period between irradiation and the next chromosomal duplication.

Recent work at ORNL with *Paramecium* has been concentrated on finding out more about the initial, reparable lesions. Among other things, it has been shown, by studying the distribution of mutations among the products of division of the irradiated cell, that the lesions not only cause the newly synthesized chromosomal strands to be mutant but also are themselves converted to an irreparable form by the duplication process. This establishes beyond further doubt that repair of the lesions is limited to the period between irradiation and duplication. There is no question that the cell can repair a large part of the radiation-induced chromosomal lesions, but the repair process ordinarily is slow and the time available for it is limited. It is possible, experimentally, to increase the amount of repair by increasing the time or accelerating repair.

GENETIC ANALYSIS OF RADIATION BEHAVIOR IN *ESCHERICHIA COLI*

The linkage map of *Escherichia coli* K-12 contains several genes that influence the sensitivity of the organism to both ionizing and nonionizing radiation. Recent experiments at ORNL have been directed toward the mapping of one of these genes and a study of its influence on sensitivity to ionizing radiation. Mating experiments have established that the gene is located between the loci controlling ability to utilize lactose and galactose. It is closely linked but separable from the gene controlling sensitivity to the bacteriophage T6. A strain (AB1899) containing a mutant allele at this locus fails to show the changes in radiation sensitivity during the early stages of the cultural cycle that are typically observed for *E. coli*. It also fails to show the increase in radiation resistance observed for many *E. coli* strains when grown in glucose-containing complete media.

The unusual radiation behavior of strain AB1899 seems to be a reflection of a more basic alteration caused by mutation at this locus. Phase-microscope studies have allowed us to observe that cells of this organism continue to grow for some time after exposure to ionizing radiation but fail to form the cross walls that are an essential step in the division cycle of *E. coli*. They therefore form long, nonseptate filaments. These filaments eventually stop growing and never develop into a macroscopically visible colony when plated on nutrient agar. If, however, the filaments are plated on nutrient agar containing pantoyl lactone, a large fraction of these regain the capacity for cell division and produce macroscopically visible colonies of normal length cells. This agent has previously been shown by other investigators to induce normal division in a filament-forming species of *Erwinia*.

The data suggest that the mutation present in AB1899 has enhanced the radiation sensitivity of the cross-wall-forming mechanisms. Other aspects of cell growth appear to be relatively normal when compared to the parent culture AB1157. We intend to investigate in greater detail the function of this mutation, since it is involved in a basic aspect of cell division in *E. coli* and has important consequences for ionizing radiation sensitivity.

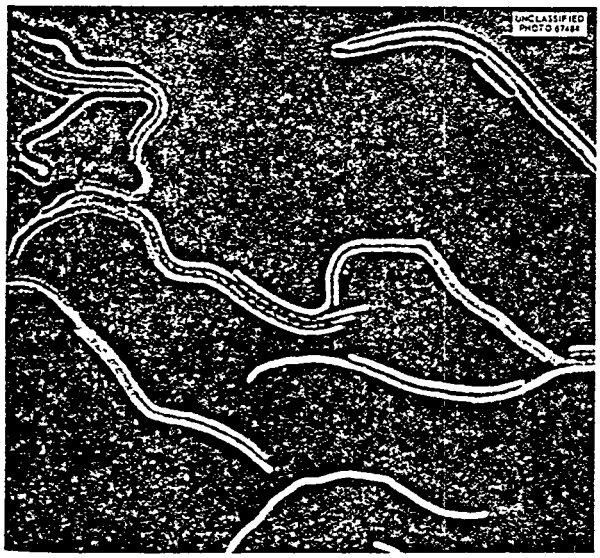

Radiation-induced filaments in *Escherichia coli* K-12. Phase-microscope studies have allowed us to observe that these cells continue to grow for some time after exposure to ionizing radiation but fail to form cross walls.

MAMMALIAN GENETICS

Radiation Mutagenesis in Mice

In 1947, the year the Atomic Energy Commission was founded, estimates of the genetic hazards of radiation in man still had to be based on quantitative values for mutation rates obtained in the fruit fly, *Drosophila*, and on a set of principles of radiation genetics established from experimental work on *Drosophila* and other organisms. Good pioneer work had been done on the induction by radiation of inherited chromosomal aberrations in mice and guinea pigs, but there was virtually no information on radiation-induced gene mutation in any mammal.

Recognizing the importance of obtaining such information, the AEC, in that same year, started a research program in mammalian genetics at ORNL. This was several years before the general public became concerned over the genetic effects of fallout. The program at Oak Ridge was, and still is, modest in terms of the number of senior scientific personnel engaged on it, but it has provided facilities for genetic tests on large numbers of mice. The results from this experimental work have necessitated substantial changes in our evaluation of the expected genetic risks of radiation in man. These changes are perhaps greater than anybody had anticipated.

In the first place, the experiments yielded markedly higher radiation-induced frequencies than those found in *Drosophila*, indicating that the hazard in man may be larger than had been assumed. Of greater basic importance than this are the more recent findings, from this research program, that some of the principles of radiation genetics that were believed to be quite general are, in fact, valid only under some conditions, or only in certain cells, and are not applicable to the germ-cell stages important in human hazards. A third contribution from the study of radiation genetics in mice is the information obtained on problems which, for one reason or another, were not explored in other organisms. Examples of

Drs. W. L. and L. B. Russell examining mutant mice in one of the animal rooms of the Mammalian Genetics Section of the Biology Division.

these three aspects of this work on mice are reviewed here, with special emphasis on the results of recent and current experiments.

The mutagenic effects of radiation vary markedly according to the stage the cell is in at the time of exposure. The differences are much more complex than mere quantitative changes in mutation rate. Understanding of the experimental results and their application to human hazards, therefore, requires some knowledge of the cell stages involved and the nature of their differential responses.

Let us consider the male first. In the mature testis, certain cells, called spermatogonia, continue throughout the reproductive life span to bud off, by division, cells which go through further divisions and through successive stages known as spermatocytes, spermatids, and spermatozoa. The production of a mature spermatozoon from a spermatogonial cell takes about five weeks in the mouse and almost twice as long in man. The spermatozoa do not persist for long in the body. It is clear that if a man is exposed to continuous irradiation for a long time – ten years, for example – prior to fertile mating, then the spermatozoon involved in that fertilization will have had a history of ten years of irradiation, *but* most of that dose of radiation will have been received when the cell was a spermatogonium. Only a small part of the total dose will have been received while the cell was going through the short-duration postspermatogonial stages of spermatocyte, spermatid, and spermatozoon. Therefore, provided the postspermatogonial stages are not vastly more radiosensitive than the spermatogonial, the important thing to know, for such conditions of irradiation, is the mutational response of spermatogonia.

Now, suppose a man is exposed to a single dose of radiation in a short time, say the few seconds of an accident or the few hours or days of exposure to immediate fallout from a nuclear detonation. If he should have a fertile mating shortly afterwards, then the spermatozoon used in that mating would have received all of its radiation dose in one or more of the postspermatogonial stages. However, the chance of a fertile mating within this short interval of time is small even if individuals fail to follow the recommendation to refrain from procreation for a few weeks after exposure to large doses of radiation. After these few weeks, the spermatozoa used in future fertilizations will have received *all* of that particular dose of radiation

when they were spermatogonia. Thus, again, the spermatogonial stage is the important one.

Accordingly, when work on the radiation induction of mutations in male mice was started, experiments on the spermatogonial stage were given priority over those on postspermatogonial stages. This was in contrast to experiments on *Drosophila*, which had concentrated heavily on the mutational effects of spermatozoal irradiation. Since the reproductive life span of male mice is scarcely affected even by near-lethal doses of irradiation, the collection of data on genetic effects of spermatogonial irradiation presents no special difficulties. After irradiation of the animals, one simply waits the length of time necessary for the maturation and disappearance from the animal of all cells irradiated in postspermatogonial stages. From then on, the spermatozoa used in all subsequent matings will be cells that were irradiated as spermatogonia.

Since there was almost no information on radiation-induced gene mutation in mammals when the Oak Ridge investigations on the mouse were started, the mere measurement of mutation rate was itself of considerable interest. The first experiment showed an x-ray-induced mutation rate much higher than that for *Drosophila*. After additional confirmatory experiments in the mouse and the collection of parallel data from irradiation of *Drosophila* spermatogonia, it appears that the induced mutation rate per gene locus in the mouse is about fifteen times the *Drosophila* rate. On the assumption that the response in man may resemble that of the mouse more closely than that of *Drosophila*, estimates of induced human mutation rates, and the consequent genetic hazards, are now taken to be greater than had been heretofore calculated on the basis of *Drosophila* results.

Another investigation, which yielded results that have been confirmed in all later experiments, deals with a problem that had not been directly explored in other organisms. This is the question of whether the probability of gene mutation in the offspring of an irradiated male might decrease as the time interval between irradiation and mating increased. Are offspring conceived 18 months, for instance, after irradiation of the male as likely to bear a mutation as those conceived 3 months after irradiation? Here there is no change in the cell stage irradiated. All the cells used in such matings would have been spermatogonia at the time of irradiation. But it was conceivable that, with time, the proportion of mutant spermatogonia might tend to decrease if they were less viable than the nonmutant cells, or if their rate of cell division were impaired.

Any hopes along this line have, however, been dashed by the experimental results. There is no evidence – in what are now rather extensive data on mouse spermatogonia – of any significant change in mutation frequency with time, even up to the end of the reproductive life, which in the experiments on mice is about 2 years after irradiation. Thus, although some reduction in the risk of transmission of genetic damage by an individual exposed to acute irradiation can be achieved by postponement of procreation for the few weeks necessary for the individual to pass beyond the phase in which the spermatozoa come from cells irradiated in the somewhat more sensitive postspermatogonial stages, nothing is gained by any further delay.

Most of the radiation-induced mutations have a serious effect on the individual. In fact, about three-quarters of the mutations induced in spermatogonia turn out, on testing, to be lethal when inherited from both parents. Many of these have clear-cut deleterious effects even when they are inherited from only one parent.

One of the most unexpected findings from the genetic work on mice at Oak Ridge has been the series of results obtained on the effect of radiation dose rate. It had long been believed, primarily on the basis of excellent experiments on *Drosophila*, that, so far as gene mutations are concerned, mutation frequency is independent of dose rate and depends only on the total dose of radiation. In other words, it had been clearly demonstrated that a given dose of radiation would produce the same number of mutations regardless of whether it was delivered in a few seconds or minutes, or spread out over hours, days, or weeks. However, the first experiments made to test this principle on mouse spermatogonia produced results in direct conflict with it. Radiation doses delivered at 0.009 roentgen per minute produced only from one-third to one-quarter as many mutations as did the same doses delivered at 90 roentgens per minute. The difference was highly significant statistically and it held up under repeated tests. For a while, there was a possibility, although not a likely one, that the effect was due to radiation quality rather than dose rate. It had been more convenient to do the acute (90 roentgens per minute) experiments with 250 kilovolts peak x rays and the chronic (0.009

roentgen per minute) ones with cesium-137 gamma rays. Thus it was conceivable that the difference in mutation frequencies could be attributed to a difference in effectiveness of x rays and gamma rays, although other work on mutation had never led to any expectation of such a marked contrast in effect between these two sources of radiation. An experiment with acute gamma irradiation of mouse spermatogonia soon settled this point. The mutation frequency obtained was in close agreement with that from acute x irradiation. More recently, information was collected from an experiment in which x irradiation was given at a reduced dose rate, and this shows a low mutation frequency. Thus, the effect of dose rate on mutation frequency in mouse spermatogonia has now been established by experiments using only gamma rays and by experiments using only x rays.

Having determined that the effect was really due to radiation dose rate, it was clear that this phenomenon, regardless of its biological explanation, was of vital importance in the estimation of genetic hazards in man. It was also clear that an explanation of the biological mechanism responsible for the dose-rate effect might yield important insights into the nature of the mutation process itself, and would, in any case, provide some of the additional data needed for a well-informed application of the finding to the problems of human hazards. The important question arises: Is this a new intracellular phenomenon? Before such an interpretation could be accepted, the

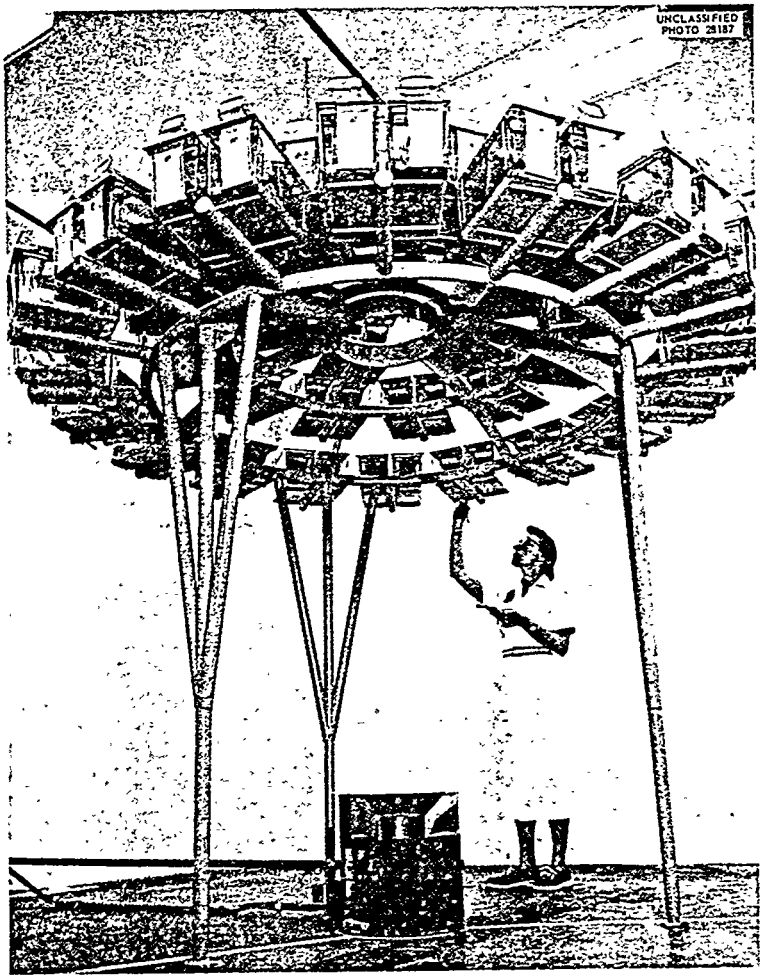

Facility for long-term low-dose-rate irradiation of mice used for mutation-rate studies by the Mammalian Genetics Section of the Biology Division, Oak Ridge National Laboratory. Cages are arranged at equal distances from the ^{137}Cs gamma-ray source located in a lead pot on the floor. By means of the rod, shown in the lower left of the picture, the source can be rotated to an opening in the top of the lead pot.

possibility had to be considered that the pattern of cell damage, cell killing, or selective elimination after chronic irradiation might differ from that after acute irradiation, and that this could result in a different mutation frequency in the surviving cells.

The simplest way to answer this question was to test for a dose-rate effect in females. In females, the germ cells pass through all the oogonial divisions, and reach an oocyte stage, in the embryo. By about three days after birth, in the mouse, the oocytes have gone into an arrested state, called dictyate, which they maintain until a few hours before ovulation. Thus, in irradiated adult females, the population of germ cells that will be used in the postirradiation matings does not go through any cell divisions, not even during a long-continued period of chronic irradiation. Furthermore, the oocytes that are destined to give rise to the first postirradiation litters are not easily killed by radiation, and so one does not have to worry about the possibility of selective elimination of mutant cells in this material. The results of the mutation experiments on females showed not only a dose-rate effect, but a considerably larger one than had been found in males. Furthermore, the effect was found even when the data were restricted to the first litter after irradiation, that is, to the portion of the oocyte population in which cell destruction is negligible. It was concluded, therefore, that the dose-rate effect is not a secondary result of a disruption of the germ-cell population, but on the contrary, it is due to an intracellular mechanism closely connected with the mutation process itself. This view is upheld by all later work, including recent experiments on spermatogonia in which the range in dose rates was too narrow to produce any significant difference in the extent of cell destruction, but which, nevertheless, still gave a marked difference in mutation frequencies.

That the dose-rate effect is an intracellular phenomenon is of far more significance than if it had turned out to be due to cell selection or some similar secondary consequence of a cell-population change. It can be used for further exploration into the nature of the mutation process. Already it indicates that, at low dose rates, some repair or prevention of the genetic damage is occurring. Since mutant genes are quite stable, it seems unlikely that repair could take place after the mutation is actually completed. Therefore, prevention of the final step, perhaps through repair of premutational damage, is suggested as a probable mechanism, and this view is greatly strengthened by the results of recent work on microorganisms. At high dose rates, it is supposed, on this hypothesis, that the repair process is saturated, or even itself damaged by the radiation. In any case, it seems highly likely that at least those mutations which are preventable by lowering the dose rate are ones that are not produced immediately by the initial radiation damage. These comprise at least two-thirds of the mutations induced in spermatogonia and almost all of the mutations in oocytes. With this much, and perhaps more, of the mutation frequency being a result of additional chemical steps following the primary action of radiation within the cell, it can be supposed that, through an influence on these processes, sizable changes in the radiation-induced mutation frequency may be possible with a variety of factors. It can also be supposed that naturally occurring biological variables may influence these processes. If so, there may well turn out to be a greater complexity in the mutational response to radiation than was anticipated when the interaction between radiation and the gene material was thought to be more direct.

Recent experiments have increased our knowledge of the dose-rate effect. In spermatogonia, a reduction of dose rate from 0.009 roentgen per minute to 0.001 roentgen per minute produced no further decrease in mutation frequency. Thus, there is no evidence in males for a threshold dose rate – that is, a dose rate below which no mutation occurs. Exploration with intermediate dose rates indicates that, in males, most of the effect of lowering the dose rate below 90 roentgens per minute has occurred when the rate of 0.8 roentgen per minute has been reached. The results from females present a quite different picture. The mutation frequency at 90 roentgens per minute is higher in oocytes than in spermatogonia, but, at 0.009 roentgen per minute, oocytes have a much lower mutation frequency than do spermatogonia – so low, in fact, that the present values, even for a total dose of 400 roentgens, are not, statistically, significantly above the spontaneous mutation frequency. Thus the dose-rate effect is much greater in females. Another point of difference is that, at 0.8 roentgen per minute, the oocytes have an intermediate mutation frequency, whereas in

spermatogonia the frequency was not significantly different from that at lower dose rates. These results are summarized below:

Mutation Frequencies in Mice at Various Radiation Dose Rates

Dose Rate (r/min)	Mutation Frequency	
	Spermatogonia	Oocytes
90	High	Very high
9	Intermediate	
0.8	Low	Intermediate
0.009	Low	Very low
0.001	Low	

These recent findings provide examples of some of the complexities that can be expected to turn up now that it is realized that the mutation process is not generally as simple and direct as it appeared to be from experiments on *Drosophila* spermatozoa. Other complexities appearing in current experiments are being actively explored.

There has long been an urgent need for data on the induction of gene mutations by neutrons in mammals. The inadequate estimates of genetic hazards of neutron irradiation in man were based on theory or speculative extrapolation from limited information. Now, however, extensive genetic data are being collected from mice exposed to various doses of fission neutrons at various dose rates. This important project was made possible by collaboration between the Health Physics Division and the Mammalian Genetics Section of the Biology Division. The new Health Physics Research Reactor provides an excellent facility for these long-needed experiments, and some of its first operational time was made available to the Mammalian Genetics Section. As far as genetic hazards are concerned, the most important of the results that have already emerged from this study is the finding that, for gene mutation induction, the biological effectiveness of neutron irradiation relative to gamma is unexpectedly high for acute irradiation and even higher for chronic exposures. Considerable revision of the estimates of the genetic risk from neutron irradiation will, therefore, be necessary.

Mouse Cytogenetics

Mutations and chromosomal aberrations recovered in the course of mutation-rate experiments, as well as genetic changes occurring spontaneously in the large mouse colony at Oak Ridge, provide excellent material for explorations in the basic genetics and cytogenetics of mammals. Tissue culture methods and other cytological analyses are used in conjunction with some of these studies.

Our recent knowledge that sex in mammals is determined by the presence or absence of a Y chromosome is based largely on results of combined genetic and cytological experiments of the Mammalian Genetics Section of the Biology Division. These results supported and strengthened the purely cytological evidence collected on human cases at about the same time. In the mouse, genes located on the X chromosome can be used as markers to provide quick recognition of the exceptional individuals with abnormal sex-chromosome constitutions. Such methods have been developed at Oak Ridge to study the stage in germ-cell and embryonic development when sex-chromosome aberrations are most likely to occur spontaneously, and the factors that may affect their frequency. In addition, the abnormal sex-chromosome types have been used as tools for studying radiation-induced chromosome aberrations. In this manner, different stages in the development and union of the germ cells have been compared for radiation sensitivity. One stage found to be exceedingly vulnerable is the stage shortly following the entry of the sperm into the oocyte.

Further Oak Ridge work on the sex chromosomes has played a major part in the development of the theory that in mammals, including humans, only one of the two X's of a normal female is genetically active. More recently, results of experiments using translocations between the X chromosome and one of the autosomes have led to a modification of this theory. It now appears that, while one X is active, not the entire second X is inactive; furthermore, the inactivity seems to spread from some center along a gradient.

In addition to the sex-chromosome work, numerous experiments are being carried out on autosomes.

In these, the nature of the genetic changes induced by radiation and those occurring spontaneously is being analyzed as finely as present genetic and cytological methods permit. For example, among mutations analyzed, some involve small chromosomal deletions – that is, damages more extensive than those affecting single gene loci. These were found much more frequently after irradiation of oocytes and spermatozoa than after irradiation of spermatogonia. No spontaneous occurrences have yet been observed. In other experiments, changes within loci are being analyzed. Studies of these types contribute to our knowledge of both the genetic material and the radiation effect.

Radiation-Induced Death in Different Mammalian Germ-Cell Stages

The histological and cytological response of the testis and ovary to radiation is being studied in conjunction with the mouse genetic experiments at Oak Ridge in order to assess the importance of cell selection and disturbances in the dynamics of gametogenesis in the effect of dose rate on mutation frequency in spermatogonia and oocytes, and of dose fractionation in spermatogonia. These experiments also have yielded information on the process of normal gametogenesis and on the effect of irradiation on fertility.

It is clear that spermatogenesis is basically the same in all animals, but the time required for production of spermatozoa from the stem cell (spermatogonium) varies widely between species. As a result, basic radiation response of the testis is the same in all male animals, but the time at which specific effects are observed after irradiation varies. Thus, in the male, extrapolation of results from one species to another is relatively straightforward.

A quite different situation obtains in females, however. While formation of the definitive oocytes usually occurs *in utero* or in early postnatal life, and the same general sequence of cell stages occurs, certain of these stages are greatly modified. This applies especially to the nuclear stage at which oocyte development is arrested. [Oocytes develop to a specific stage, and then remain quiescent (arrested) until growth of the follicle begins prior to ovulation.] This arrest always occurs in the diplotene stage, but the cytological appearance can vary greatly, as between guinea pig and mouse. This difference in nuclear structure is associated with differences in radiation response. In the guinea pig, 30 percent of the early, arrested, oocytes of the adult female survive 200 roentgens, while in the mouse, only 0.1 percent of the early oocytes survive 50 roentgens. This oocyte loss leads to permanent sterility in the female mouse after about four litters, but on the basis of histological observations, fertility of female guinea pigs should be almost normal after doses of several hundred roentgens. This is now being investigated with a dose of 300 roentgens. Examination of the ovaries of humans, goats, and dogs also revealed characteristic nuclear cytology for each species, though the differences are small in some cases. Thus, in the adult female, both fertility and frequency of genetic damage may vary widely between species.

No differences in spermatogonial killing at dose rates of 90, 9, and 0.8 roentgen per minute, for total doses ranging from 5 to 600 roentgens, have been observed. The genetic studies, however, showed an effect on mutation frequency in spermatogonia over this range of dose rates. Thus, cell selection appears to be an unlikely explanation of the dose-rate effect on mutation frequency in spermatogonia.

Intensive study of spermatogonia surviving 500 and 1000 roentgens given in single doses as compared with 1000 roentgens given in two fractions 24 hours apart is in progress in an attempt to evaluate the relationship of cell survival, synchronization of cell stages, and disturbances of cell division to the effect of total dose and dose fractionation on mutation frequency.

Molecular- and Cellular-Level Studies

MOLECULAR CHANGES THAT LEAD TO RECOVERY FROM RADIATION DAMAGE

Recent work in the Biology Division has led to the identification of a change in molecular structure that is responsible for a large fraction of the killing effects of ultraviolet radiation. Some of the molecular changes that take place as cells recover from the effects of radiation have also been identified. Thus for ultraviolet irradiation it is possible to describe radiation injury and recovery at the molecular level, and it is hoped that these investigations may be extended to the effects of ionizing radiations.

Deoxyribonucleic acid (DNA) is the repository for cellular information. Any changes that radiation induces in such molecules will have profound effects on the ability of cells to survive or to mutate. Several physicochemical techniques have been used to show that the most important structural change produced by ultraviolet irradiation of DNA or of DNA in cells is the linking of two components of the DNA chain. These linked components are adjacent thymine residues, and the linkage is usually described as a thymine dimer. It has been shown that thymine dimers inhibit DNA synthesis. Inhibited cells are unable to multiply because they cannot make more DNA and hence they cannot duplicate the information they contain and pass it on to their daughter cells. From biochemical studies it is indicated that the inhibition of DNA synthesis arises from the changed structure of DNA in the neighborhood of a thymine dimer. The dimer blocks further synthesis, and in the few cases in which synthesis seems to take place around such blocks, one observes that the information content (as measured by the sequence of the DNA components) has been changed. DNA that is synthesized around such blocks is a mutant DNA.

Many, but not all, strains of bacteria can recover from the effects of radiation. The blocks produced by thymine dimers in their DNA are either circumvented or removed. It has been shown that the major step in the resumption of DNA synthesis and therefore in the recovery of cells from the effects of ultraviolet radiation is the removal of thymine dimers from the irradiated cellular DNA. Those cells that can remove the dimers can recover from radiation effects; cells that cannot remove them die. A knowledge of the metabolic activities that enhance cellular recovery of dimer removal will obviously be of great use in studies of resistance to radiation.

It has been known for some time that radiation resistance probably depends more on so-called recovery mechanisms than on differences in the initial changes produced by radiation. The work described briefly above is the first indication of the existence of specific molecular repair mechanisms. The surprising conclusion is that regions of DNA molecules that are "wrong" are bodily removed from the DNA. Such a mechanism not only will lead to recovery of cells from radiation but also might be thought to represent a general type of mechanism that would enable cells to correct any mistakes that had been made during the synthesis of their most important component, DNA.

R. B. Setlow of the Biology Division (Biophysics Group) of ORNL is shown adjusting a device used to irradiate DNA with ultraviolet light. This instrument has led to the identification of a molecular change that leads to the death of cells.

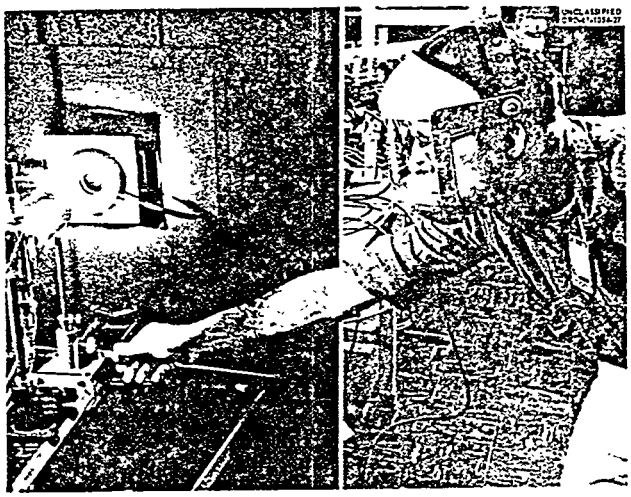

STUDYING PLANT DEVELOPMENT USING IRRADIATION TO PREVENT CELL DIVISION

The growth and development of a higher organism is closely associated with the increase in cell number brought about by cell division. A typical effect of ionizing radiation is a reduction in the frequency of cell division. In addition to cell division, other developmental processes appear to be injured. However, work at ORNL has shown that dry cereal grains are exceptional in that the injury they suffer after enormous exposures (from 500,000 to 1,000,000 roentgens) of gamma irradiation is subsequently expressed as inhibition of cell division with very little injury otherwise. The only gross abnormalities in such seedlings are those which would be expected from the absence of cell division alone. Absence of cell division in seedlings grown from the irradiated grains is shown by absence during growth of the typical nuclear configurations (mitotic figures) which normally precede nuclear and cell division and also by constancy of cell numbers. The irradiation also prevents the formation in the nucleus of additional genetic material (deoxyribonucleic acid) without preventing the formation of another type of substance (ribonucleic acid) that migrates from the nucleus into the cytoplasm (i.e., that part of the cell outside the nucleus). Those structures (e.g., roots and leaves) that normally grow with cell divisions grow much less after the irradiation than do unirradiated controls. Those few structures that have already attained their final cell number in the mature grain and thus grow without cell division in unirradiated controls grow to the same final size, irrespective of irradiation. This finding indicates that when the irradiation decreases growth and arrests development in this system, it does so largely by preventing cell division. Net protein synthesis, that is, increase in total amount of protein, and the formation of functional enzymes (protein molecules which facilitate biochemical reactions) and enzyme complexes also occur in the seedlings growing without cell division from the heavily irradiated grains.

Many aspects of development that are normally accompanied by cell divisions occur in apparently normal fashion despite absence of cell division. Other aspects of development, on the other hand, appear to have been prevented by the prevention of cell division. Detailed developmental studies of such seedlings growing without cell division thus indicate the roles of cell division in various specific aspects of development. One general conclusion from this work concerns the inadequacy of the "cell theory of development," according to which the growth and form of an organism is biologically determined by the extents and directions of formation of its cellular building blocks. A

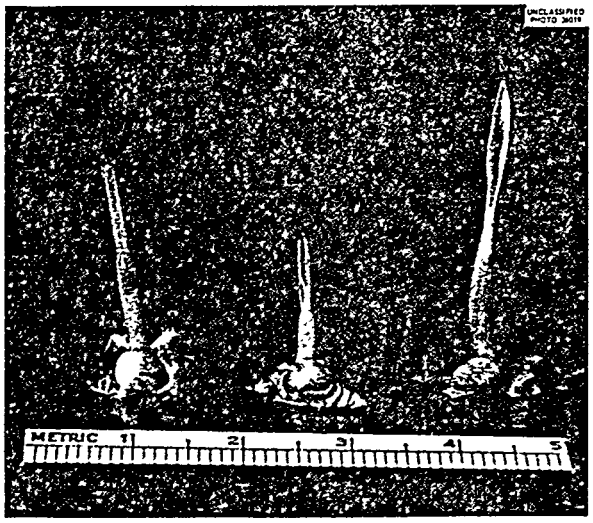

Growth of wheat seedlings, on each of three different chemical media, without cell division after gamma irradiation (800,000 roentgens) was given to the dry, intact grains. These 9-day-old seedlings are nearing their final size. The number of cells in each has not increased from the number in the embryo within the mature grain. Normal, unirradiated seedlings of comparable size have undergone about a tenfold increase in cell number during their germination. This picture illustrates the normal responses of the seedlings, growing without cell division after irradiation, to certain chemical treatments. Compare the water-control seedling (left) with the seedlings treated with a growth-reducing chemical, (2-chloroethyl) trimethylammonium chloride (center), and a growth-promoting chemical, gibberellic acid (right).

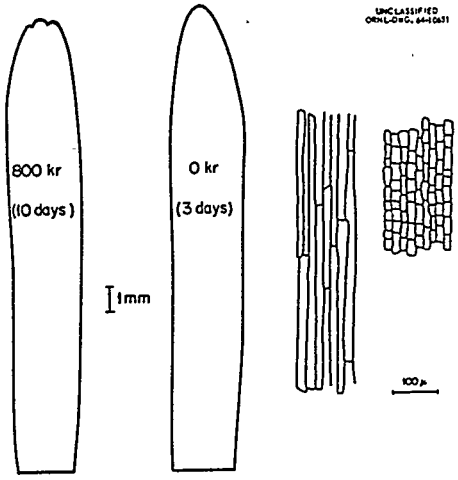

Illustration of similar shapes of leaves of the same size after germination and growth without vs with cell division. The tracing of the leaf on the left represents a ten-day-old seedling that grew to 25 times its original length without cell division after the dry grain was exposed to 800,000 roentgens of gamma irradiation. At the same magnification is the leaf tracing at left center, representing a three-day-old unirradiated control. At right center are represented the sizes and shapes of cells of the leaf that grew without cell division. At the extreme right are shown sizes and shapes of cells of the leaf that grew normally with cell divisions. The cells are at the same magnification, which is greater than the magnification of the leaves. This figure illustrates that the specific size and shape of an organ is not biologically determined by means of the number, sizes, shapes, and arrangement of its constituent cells.

given size and form of a wheat leaf is not biologically determined by means of the number, sizes, and arrangement of its constituent cells.

LOCALIZATION AND PROGRESSIVE APPEARANCE OF LENS ANTIGENS IN TRANSFORMATION OF THE IRIS INTO THE LENS

When the lens in the adult newt is completely removed, the cell population at the dorsal rim of the iris transforms into a new lens. Autoradiographic study indicates that an enhancement of protein synthesis occurs in the lens regenerate beginning from the seventh day after lens removal. A study of appearance and localization of lens-specific antigens during lens regeneration was carried out at ORNL by use of the immunofluorescent technique, immunoelectrophoresis, and an agar diffusion technique.

The antilens serum was prepared by injecting rabbits with adult *Triturus viridescens* lens homogenate in 0.15 *M* sodium chloride. The serum from normal healthy rabbits was used as the control. The gamma-globulin fractions from each serum were conjugated with fluorescein isothiocyanate. Normal lens, normal iris, lensless eyeball, the regenerating lens of various stages, blood serum, and liver of *T. viridescens* were used as sources for antigens.

The fluorescent antibody did not stain any tissues other than the lens and the surface of corneal epithelium. Further, on immunoelectrophoresis and the agar diffusion test, the extracts of normal lensless eyeball, iris, liver, and blood serum did not produce precipitin bands.

The present experiments demonstrate that lens-specific antigens appear in the cytoplasm of primary lens fiber cells between the lens placode stage and the earliest lens vesicle stage. The time of first appearance of lens antigens approximately coincides with that determined by other investigators with the precipitin technique. Our results suggest that the appearance of lens-specific antigens is correlated with morphogenetic events occurring in the ectoderm cells reacting to the lens-inducing influence of the optic cup but not with inducing activities of the optic cup.

PHOTOSYNTHESIS

The process by which higher plants convert energy of visible light into chemical oxidation and reduction potential is now believed to involve two photoreactions which are linked by enzymes. This initial process of photosynthesis produces adenosine triphosphate and reduced pyridine nucleotide, these two high-energy compounds being utilized to provide energy for reduction of carbon dioxide to sugars in enzymatic dark reactions of the Calvin cycle. Earlier work from ORNL has shown that the initial steps of photosynthesis include purely electronic processes as well as enzymatic reactions and that energy-conversion processes within the photosynthetic apparatus may be studied by means of the delayed-light emission of living plants.

The photosynthetic delayed light is emitted from the singlet-state transition of functionally active chlorophyll. It is a complex phenomenon which is intimately associated with enzymatic reactions and has decay characteristics of untrapping of electrons in a semiconducting crystal. The presence of two photosynthetic pigment systems can be deduced from the different decay curves produced on excitation of the different pigment systems. Emission in the millisecond time range seems to measure enzymatic utilization of high-energy electrons from a chlorophyll system during the forward reaction of photosynthesis. ORNL is now stressing experiments at the fast times in an attempt to clarify the physical processes involved in photosynthetic quantum conversion.

We have continued the development of apparatus to measure delayed light at very short times after illumination and have now reached 5×10^{-5} second, which is 20 times as fast as any previously published value. The intensity of the delayed light at 5×10^{-5} second is approximately 1 percent of the fluorescent intensity. Extrapolation of the decay curve to even shorter times suggests that a large fraction of the in vivo fluorescence of green plants may actually be delayed light.

HORMONAL CONTROL

Three systems in which steroid hormones play a regulatory role in protein biosynthesis are currently being studied at ORNL.

Changes in the metabolism of ribonucleic acid (RNA) that accompany induction of hepatic enzymes of hydrocortisone in vivo have been analyzed by pulse-labeling techniques. We found a marked increase in the rate of synthesis of nuclear RNA, which begins shortly after hormone administration and which precedes the increased enzyme synthesis that results in induction. Synthesis of cytoplasmic RNA was unchanged. Characterization of the hormonally stimulated RNA revealed little detectable difference from that synthesized in the absence of hormone with regard to such criteria as size distribution (sucrose gradient analyses) or base composition. Analyses for messenger activity in vitro, defined here as capacity to stimulate amino acid incorporation in a fully supplemented system from rat liver, indicated a small (5 to 10 percent) increase due to hormone treatment. Assays of RNA polymerase activity in vitro, carried out on crude preparations from liver nuclei, indicated no change in specific or total activity of this enzyme.

Estrogen effects on protein synthesis in the rat uterus have been studied with a ribosomal-supernatant amino-acid-incorporating system prepared from this tissue. Shortly after ovariectomy, the capacity of ribosomes for leucine–carbon-14

incorporation is impaired, but this capacity is restored to the normal level within a few days after surgery. Ribosomes prepared from ovariectomized animals, while equivalent to normal with respect to leucine incorporation, are much more responsive to added messenger (poly uridine) than are ribosomes from normal animals or estrogen-treated castrates. These results are interpreted as indicating that the diminished population of ribosomes in the castrate uterus carry out a synthesis that is essentially independent of renewal of messenger RNA (i.e., utilizing stable templates).

Androgen effects on RNA synthesis in the seminal vesicle of the rat are being investigated. Techniques developed during our study of corticosteroid effects in liver are being modified as required by the particular characteristics of this gland and its mode of response to steroid administration.

Terrestrial and Fresh-Water Ecology

RADIATION ECOLOGY

Glass-Rod Dosimetry in Environmental Studies

Evaluation of the long-term effects of ionizing radiation on natural populations of plants and animals is one objective of ecological research at ORNL. This radiation may result from radioactive materials introduced in the air, water, or soil; or it may result from a catastrophe such as a nuclear accident or war.

Regardless of the source or mode of radiation it is exceedingly important to obtain accurate measurements of radiation dose when evaluating the ecological effects of ionizing radiation. Miniature (1 × 6 millimeters) solid-state dosimeters – such as silver-activated metaphosphate glass rods – are relatively new devices which already are proving useful in environmental radiation studies. Not only are they suitable for measuring radiation dose in air, but they can be used for the measurement of absorbed dose in such media as tissue, soil, and water. Moreover, their small size makes possible measurements within any plant or animal which is large enough to contain them without impairment of its biological processes. Another use of these devices is to measure movement of radionuclides in organisms.

In new dosimetry studies at ORNL, miniature metaphosphate glass rods are being used to estimate absorbed dose in air and in plants and soil of the radioactive White Oak Lake bed. They are also being used to measure movement of cesium-137 in trees and to measure the dose being delivered to mud-dauber wasp eggs and larvae from the radioactive mud used in the construction of the nest.

On White Oak Lake bed the combined beta and gamma doses in the top inch of mineral soil determined from rods buried at that depth ranged from 20 to 25 rads per day, compared with air doses of

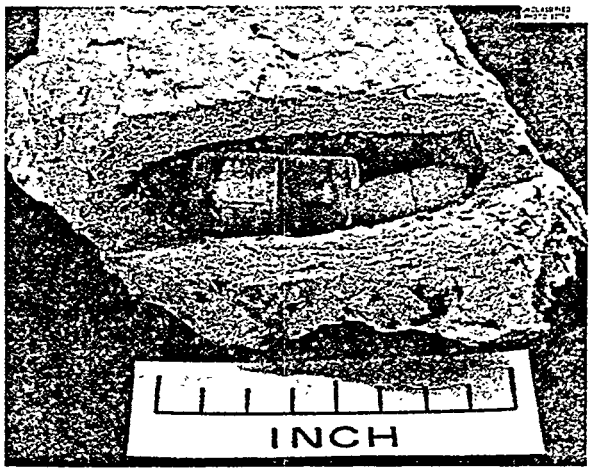

Shielded miniature glass-rod dosimeters placed within a mud-dauber wasp nest constructed of radioactive mud. These dosimeters are being used to measure the beta and gamma dose to wasp egg and to the larva which live in the nest.. The left rod is shielded in 2-millimeter-thick Lucite, which blocks the entry of beta rays. The right shield (Nylon) allows entry of both types of ionizing radiation. By subtracting the dose on the left rod from the dose on the right rod, one obtains the beta dose.

6.2 rads per day at ground level and 2.8 rads per day at 5 feet above the ground. (A rad is a measure of the energy imparted to any *specified* material by ionizing radiation. It corresponds to an energy absorption of 100 ergs per gram of material irradiated.) The dose to root systems of plants was 3 to 7 times as high as the dose to shoot components. Soil-inhabiting animals at this depth (1 inch) are receiving about 5 times as much radiation as those animals living above the ground.

Biological Half-Life of Strontium in White Crappie

Another objective of ecological research at ORNL is the development of quantitative information on biological accumulation and movement of fission products and other radioisotopes in plants and animals. An important aspect of this investigation is associated with the problems encountered with fresh-water organisms – notably fish – which can accumulate radionuclides directly from their environment, in contrast to terrestrial organisms which derive their nutrient elements primarily by way of a more elaborate food chain.

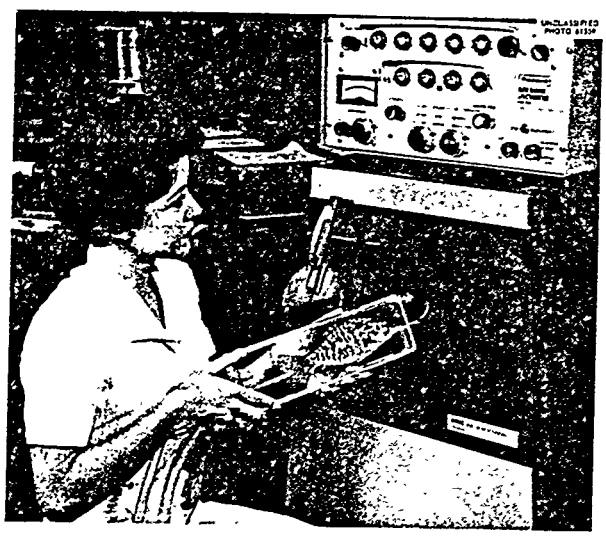

Whole-body counting of fish. At ORNL, ecologists have fashioned a device which enables them to measure uptake and elimination of radionuclides by small and medium-sized fish. Fresh spring water is pumped continuously through the chamber which contains the live fish. At the same time, the entire device is inserted in the detector. By this means it is possible to measure the short turnover times of certain isotopes. Such studies are being used to aid in determining the extent of radionuclide uptake by fish in their native stream environments.

The rate of turnover of strontium-90 by fish is an important factor in determining the extent to which radioactive strontium will be accumulated in the fish's body. One method by which the rate of uptake can be determined is to measure the time it takes for an organism to eliminate one-half of the radionuclide burden in its body (biological half-life). The shorter the half-life the more rapid the rate of uptake and, therefore, the greater the turnover.

The biological half-life of strontium in white crappie has been determined by tagging fish with strontium-85 and then counting the same fish at 1-minute intervals in a small-animal whole-body counter. The radioactive half-life of strontium-85 is sufficiently long that no correction for it need be made in determining the biological half-life. In experiments conducted at ORNL, it was found that the biological half-life of strontium in the flesh of individual fish ranged from 12 to 48 minutes.

Measurement of the turnover of strontium in flesh was complicated by the rapid deposition and high concentration of strontium in fish bone, which literally masked the strontium in soft tissues. This difficulty was circumvented by constructing a fish-holding assembly, which was inserted in the detector chamber of the counter. Water was pumped through the assembly during the experiments to remove excreted strontium-85 and to provide a supply of oxygenated water.

These results indicate that crappie flesh will reflect quickly the strontium-90 concentration in the water; consequently, sampling the water may serve better to indicate environmental contamination than the sampling of fish flesh. On the other hand, sampling of fish bone provides a sensitive indicator, because of the concentration of strontium in bone. Furthermore, these results suggest that the distribution of strontium and strontium-90 should be compared in bone only and not in flesh.

Biological Movement of Strontium-90 by Emergent Aquatic Insects

The transport of strontium-90 from the Clinch River below ORNL by emerging aquatic midges (Chironomidae) was compared with the accrual of strontium-90 to the river from weapons test fallout. The purpose of this study was to test the idea that insects in large numbers may be significant movers of radioactivity from one place to another. In their larval form, Chironomidae live in the mud of ponds and streams. Since these insects, as adults, emerge in numbers approaching millions, they were felt to be a good test organism, especially because in this location (Clinch River) the larval development occurs in river-bottom sediments which contain radioactive wastes.

Emerging adults were caught in insect light-traps operated on the river bank at dusk. Adults in one large, composite sample contained 8.76 times as much strontium-90 (3.5 micromicrocuries per gram of insect dry weight) as did an equal quantity of river-bottom sediment from the same location. Studies elsewhere have shown that the mass of such insects emerging can approach 10 grams per square meter of water per year. On the basis of the above radionuclide concentrations, this emergent insect mass would transport 35 micromicrocuries of strontium-90 per square meter per year from the river bottom (river bottom sediment = 30.7 micromicrocuries per gram).

The average increment of strontium-90 from fallout in the United States between 1959 and 1960 was 4.2 millicuries per square mile or 1620 micromicrocuries per square meter. On the basis of these figures, it appears that fallout entering the river directly would add 45 times as much strontium-90 as that removed by emerging midges.

Transport of Radioactive Mud by Mud-Dauber Wasps

Radioactive mud nests of the yellow-legged mud-dauber wasp were found in electronic gear, instrument panels, cabinets, field equipment, and buildings near the pits for liquid radioactive chemical waste as well as in the vicinity of White Oak Lake bed at ORNL. Ecological factors involved in this situation have been assessed. The flight range of the wasp from its contaminated mud source was from 6 to 650 feet. Eighty-nine percent of 112 nests from four different locations near the waste pits were radioactive, delivering a dose rate to the eggs of approximately 1 rad per hour from mixed gamma and beta radiation. One female wasp constructs the equivalent (at least) of a mud nest weighing about 60 grams (2 ounces). The maximum gamma activity of the first 50 radioactive mud nests assayed was 361 microcuries per gram; the radioactive isotopes involved were cesium-137, ruthenium-106, cobalt-60, and zinc-65.

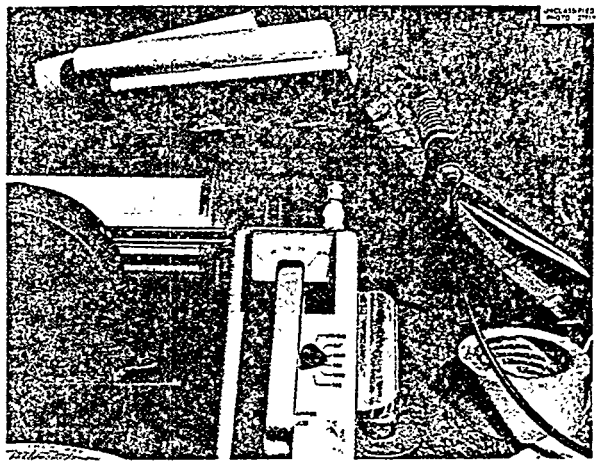

Interior of the cabinet of a field monitor station showing a freshly made radioactive mud nest of the yellow-legged mud-dauber wasp. The Geiger tube of a radiation survey meter has been placed beside the nest. The meter shows an air dose rate of 43,000 counts per minute, or about 14 milliroentgens per hour.

The study revealed that this phenomenon is a localized human health hazard. It is not a general health hazard at ORNL because the flight range of the wasp is relatively short, and the total contamination is small. Mud-dauber wasps are ubiquitous, and this problem can arise at any place where they gain access to radioactive mud.

The pipe-organ mud nest wasp, related to the yellow-legged mud wasp, has built numerous non-radioactive nests (100 percent of 150 were non-radioactive) at some of the same locations as the radioactive nests of the latter species. If both species use the same — and they are apparently the same — kinds of mud for nest construction, then it may be that the pipe-organ wasp discriminates against muds containing some or

all of the above radioisotopes, or perhaps against ionizing radiation from them.

X-ray diffraction studies of the clays in the nests of both kinds of wasps show no significant differences. Further chemical, physical, and organoleptic ("feel," workability, etc.) tests are in progress to account for this fundamental difference. If discrimination against radiation can be demonstrated for the pipe-organ wasp, it will be a unique case among the insects and would be worth investigating among other kinds of insects.

EVALUATION OF FISSION PRODUCT DISTRIBUTION AND MOVEMENT IN WHITE OAK DRAINAGE SYSTEM

Accumulation and Movement of Radionuclides in White Oak Creek Basin

For the past 20 years radioactive materials have been discharged into surface streams, soils, and the atmosphere at ORNL. A major fraction of the activity has remained at the disposal sites; some has moved from one part of the disposal complex to another; and, finally, modest quantities of fission products have moved from the environment of the Laboratory into the Clinch and Tennessee Rivers. The White Oak Creek drainage basin includes all ORNL facilities that contribute significant quantities of radioactive waste to the environment. The fate of the radioactive materials, after release to the environment, is of vital concern, since the overall usefulness of this environment for planned discharge, as well as an assessment of the hazards to man resulting from accidental releases of radioactive wastes, depends on the distribution, retention, and rates of movement of radionuclides in and through the system.

One of the contamination sites of present concern within the ORNL area is the bed of former White Oak Lake. This 44-acre impoundage formerly served as a final detention basin for low-level radioactive wastes discharged from the Laboratory. The temporary holdup, provided by the impoundage, afforded some dilution and a period for the decay of short-lived radionuclides before release to the Clinch River. It also allowed the deposition and accumulation of large quantities of contaminated sediments. When the lake was drained, about 1,000,000 cubic feet of contaminated lacustrine materials was left behind. To determine the quantity and distribution of the various radionuclides presently in the lake bed, a series of 250 core samples were taken within the area and radiochemically analyzed. Ruthenium-106 (1038 curies) and cesium-137 (704 curies) account for more than 90 percent of the total activity present, while cobalt-60 (152 curies), the rare earths, exclusive of yttrium-90 (17 curies), and strontium-90–yttrium-90 (15 curies) make up the remainder. More than half of the activity was found in the 0- to 6-inch layer of soil, while less than 5 percent of that detected was associated with the 18- to 24-inch layer of soil.

Cesium-137 is one of the more hazardous fission products, and the amount of it in the lake bed is relatively large. It is of interest to understand more fully the relation of this material to the lake sediment. Physical analysis of the sediment indicates a composition of approximately 5 percent sand, 60 percent silt, and 35 percent clay. More than 80 percent of the cesium was found to be associated with the clay fraction of the sediment which, by x-ray diffraction techniques, was found to be predominately illite. To determine the degree of fixation of cesium on the illitic clay, samples of the lake sediment were leached with salts, acids, and bases, as well as with tap water and distilled water. Significant quantities of cesium were removed only when strong acids were used as the leaching agents. Tests on selected clays, including illite, have shown that this clay mineral has a high affinity for cesium at levels of the same order of magnitude as that sorbed on lake bed soil and that desorption is only accomplished after destruction of the lattice structure. It is thus concluded that most of the cesium sorbed on the lake bed soil occupies sites on the illitic fraction of the clay and is not in exchangeable form; therefore it would be extremely difficult to remove by percolating ground water or surface water. This conclusion is highly significant in forecasting the extent to which this long-lived radionuclide, once released to soils and sediments, will remain relatively immobile.

Radiological Physics, Health Physics, and Radiation Instrumentation

HEALTH PHYSICS RESEARCH REACTOR STUDIES

The ORNL Health Physics Research Reactor (HPRR) became operational at the Dosimetry Applications Research Facility on May 31, 1963. This bare metal, unshielded reactor is a highly versatile source of fast neutrons for health physics and radiobiological research. The radiation field intensity can be varied by a factor of 10^{12}. This wide range in dose rate is useful for studying the effects of dose rate variation on physical, chemical, or biological systems. In order to make similar studies in other neutron-source facilities, it is necessary either to move the experiment or to add or take away shielding material. Such practice introduces changes in the radiation field characteristics (changes both the neutron and gamma-ray energy spectrum and changes the ratio of neutron dose to gamma-ray exposure). Because the reactor core is small (8 inches in diameter by 9 inches high), the neutron leakage is large (1.3 neutrons per fission), thereby yielding a ratio of neutron dose to gamma-ray exposure of 10:1 at a distance of 3 meters from the core. Of the experiments for which the HPRR has been used, about 40 percent have been for radiation dosimetry research, 40 percent for radiobiological research, and 20 percent for miscellaneous research problems.

RADIATION PHYSICS AND DOSIMETRY

Interaction of Low-Energy Electrons

When radiation strikes matter, low-energy electrons are released which then interact with atoms and molecules of the medium. The interaction which takes place and the immediate biological effects are not understood, although details of some of the processes which occur have been revealed by recent studies of electron motion in water vapor mixed with other gases.

Electron-attachment coefficients and drift velocities have been measured in mixtures of water vapor with nitrogen, with methane, and with carbon dioxide. Electron capture takes place only in the water–carbon dioxide mixture, probably because of the formation of small quantities of carbonic acid, and even in this case the attachment coefficient is quite small. Thus, low-energy (less than 1 electron volt) electrons in general do not form stable negative ions with water. Electron drift velocities are very sensitive to the addition of small quantities of water vapor in all the mixtures. When certain other polar molecules (acetone, heavy water, methyl alcohol, dimethyl ether, hydrogen sulfide, toluene, and nitrous oxide) were mixed with ethylene, it was found that the decreases in drift velocity correlated well with the magnitude of the electrical dipole

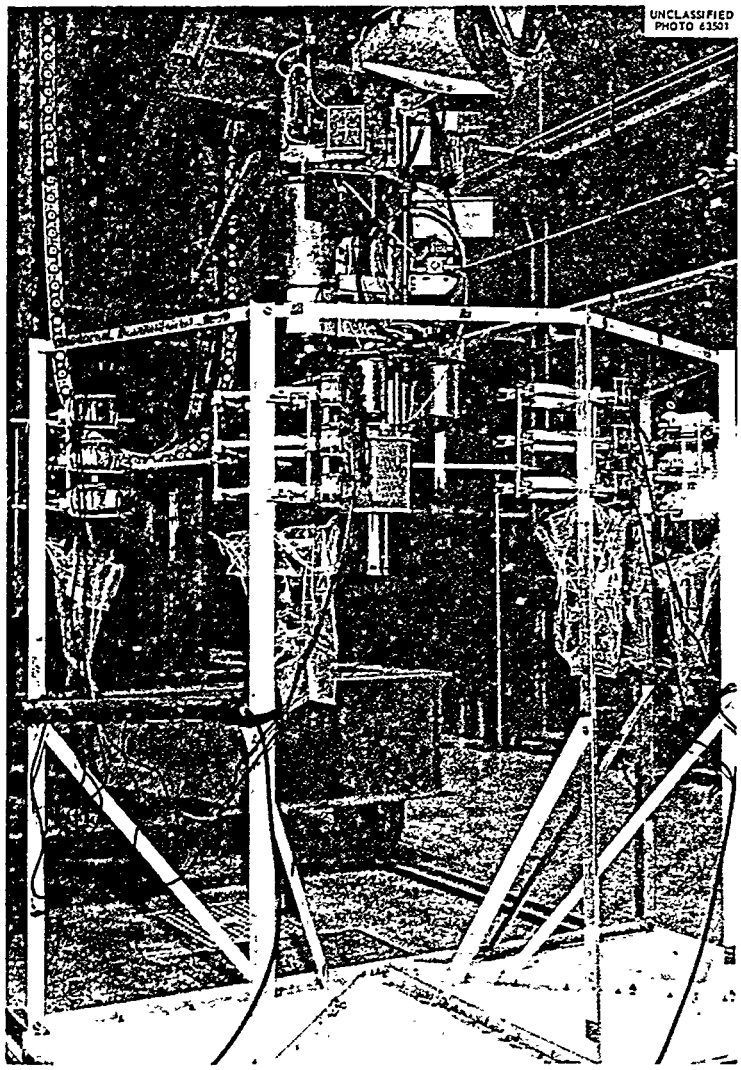

The HPRR is located at the center of an array of Sprague-Dawley rats. This experiment (performed by a member of the staff of the University of Pittsburgh) is part of an investigation to develop a biological dosimetry system through studies of the relative biological effectiveness of fast neutrons compared to gamma rays for certain changes in the hemapoietic system. Approximately 40 percent of the HPRR schedule is devoted to similar radiobiological studies of this type. The reactor core is suspended beneath the support structure which houses the mechanical and electronic components. The assembled reactor is seen suspended from the remotely controlled positioning device.

moments. The drift-velocity data were analyzed to obtain the cross sections for momentum transfer. These cross sections are in fair agreement with theory, except for water, heavy water, and hydrogen sulfide, where the experimental values are twice as large as predicted by theory. This discrepancy may be due to molecular rotational enhancement of the momentum-transfer cross section or it may be due to the temporary formation of negative ions, an effect which would decrease the observed drift velocity.

Electron Spectra in Irradiated Matter

Success has been achieved in a long attempt to measure the complete spectrum of electrons generated by ionizing radiation in matter. Since damage to biological systems is thought to be proportional to the number of electrons at each energy, the development of a spectrographic technique to determine this number represents an important fundamental advance. An analogy may be made to the first measurement of the neutron

flux in a nuclear reactor and its subsequent importance to an understanding of reactor operation. The technique employed in the electron flux studies utilizes the "Keplertron," a spherical, electrostatic-energy analyzer developed in the Health Physics Division. The spectra of primary events, such as beta-ray emission and generation of Compton electrons from x- and gamma-ray bombardment, may be seen as well as the secondary electron spectra resulting from the slowing down of those primary electrons. For example, for a source of beta rays from copper-64 slowing down in copper, the electron flux is found to decrease with decreasing energy from 40 kilo-electron volts (kev) (the upper limit of energy capability of the Keplertron) to a broad minimum of about 8 kev and is thought to represent the contribution from the primary beta rays. Below this energy, the flux is attributed to secondary electrons and rises rapidly to achieve a maximum at 3.3 electron volts (ev), below which it declines. The unprecedented energy span of the Keplertron (1 ev to 40 kev) coupled with the large range of intensities which may be studied (six orders of magnitude) permit a detailed study of radiation-induced electron flux in matter, hitherto considered impossible.

Studies of Plasma Effects in Solids

The transmission of high-energy electrons through thin films has revealed the existence of an interaction between the incident electron and many electrons interacting collectively, the motion of the latter being determined by the electrostatic forces between them. This "plasma" of electrons is thought to exist in many materials, including all metals, and including organic materials such as graphite, carotenoid molecules, and molecules containing benzene rings. The universality of these collective or plasma processes has made it quite important to study as many aspects of these processes as possible. Most recent studies have been concerned with the decay of the plasma to its unexcited state with the emission of light. The light has been identified in electron-irradiated silver films by its color, its direction of emission, and its dependence on film thickness and electron energy. In separate experiments the reflectivity of the films for ultraviolet and visible light has shown a minimum at the plasma wavelength (color) which identifies the electron motion as a "sloshing" of electrons back and forth from one face of the film to the other. It is thought that the confining effect of the film surfaces may be duplicated in a similar fashion in graphite, molecules containing benzene rings, and the carotenoid molecules, except that the individual molecules themselves provide the boundaries which confine the electronic motion. In graphite and in molecules containing benzene rings, the motion is in a doughnut-shaped region above and below the hexagonal atomic array; in the carotenoids, it is in a tube oriented along the length of these long-chain molecules. Optical studies are under way to check the validity of these models.

Energy-Loss Processes from Low-Energy Heavy Particles

A new technique has been developed to permit study of the energy losses experienced by heavy particles of energies as low as 1 kilovolt as they pass through matter. Such particles are typical of those occurring as recoil ions in materials exposed to neutron irradiation from reactors or as recoil ions following the emission of an alpha particle from a radionuclide. The technique consists of vacuum evaporation of a thin layer of silicon monoxide (50 to 100 atoms thick) onto a solid. Then a thin film of the material to be studied is evaporated onto the silicon monoxide. The latter provides electrical insulation between the solid and the film, so that the final stopping place of an incident charged particle may be determined by measuring the currents to the solid and the film. Any charged particle which may be generated in an ion source may be used with films as thin as 50 atoms. Information is obtained also on the charge state of the ion as it leaves the thin film, that is, whether or not it has captured an electron. Such a process is common for a charged particle at such a low energy that its velocity is equivalent to that of an electron with an energy of 0.5 electron volt. Thickness of the insulating layer is measured by determining its radioactivity after neutron irradiation in a reactor. For the thin film, thickness is

determined by interferometry, that is, the interference of the light rays reflected from the front and back faces.

Calculation of Radiation Dose from Protons of Energy up to 400 Mev

The Monte Carlo technique has been used with a digital computer to obtain estimates of dose in a homogeneous tissue slab irradiated by a broad beam of perpendicularly incident monoenergetic protons and also for portons incident from all directions on a homogeneous parallelepiped of tissue. Incident proton energies as high as 400 million electron volts (Mev) were considered. These radiation situations are similar to those which, as a result of a solar flare, may be encountered by the astronauts on their way to the moon. The dose is found to be essentially uniform throughout the slab when the proton energy is above 200 Mev, so that most protons which enter the body emerge from the other side. At all proton energies the ratio of rem dose to rad dose is generally about 1.4 if rem dose estimates are based on values of relative biological effectiveness (RBE) in current use for long-term occupational exposure to ionizing radiation.

[A rad is a measure of the energy imparted to any *specified* material by ionizing radiation per unit mass of irradiated material. The rem is the unit of biological dose. Biological dose is the sum of the dose in rads due to the various particles, each contribution being weighted by a factor (RBE factor) which takes account of its effectiveness in producing biological damage.]

The contributions to dose from various ranges of linear energy transfer values which arise have been calculated also. The nuclear interactions considered are cascade and evaporation phenomena. The effect of the presence of pions is assumed to be negligible at incident proton energies not exceeding 400 Mev. An analysis of nuclear interactions has been made from the standpoint of dose assessment. From the results of the detailed Monte Carlo calculations, a simplified model has been derived which permits a rapid and accurate estimation of proton dose. A method of handling relative biological effectiveness in a flexible manner is given also.

Cross Sections for Emission of Light from Electron-Irradiated Metals

When sensitive optical instruments are used, virtually all materials are found to give off light when irradiated by nuclear radiation. Metals are of particular interest, because the large body of knowledge concerning their electronic energy levels renders possible a quantitative interpretation of the emission data. If one omits from consideration the light of one wavelength, such as arises from electron plasma decay, the remaining emitted light may be considered to arise from two fundamental processes. Both processes emit light that is continuous in wavelength (white light). The most important contribution is called transition radiation and occurs when a high-energy particle enters the solid from a vacuum. The second occurs for media independent of boundaries and is due to deflection of the high-energy particle by the nuclei it passes. The deflection of the particle causes it to radiate light called bremsstrahlung, from the German meaning "braking radiation." The two radiations may be distinguished by their different polarizations, and many optical spectra (measurements of color) have been taken on various foils of copper, germanium, silver, tin, antimony, gold, and aluminum. The light has an inverse intensity dependence on wavelength and has, for the transition radiation, an intensity of about 10 electron volts per incident electron per steradian per centimeter of wavelength at a wavelength of 2500 angstroms (in ultraviolet). In simpler terms this means that one light ray or photon is emitted for each 1000 high-energy electrons which strike a foil. The intensity of bremsstrahlung is about one-tenth this value. All observations are in excellent accord with theoretical expectations. Although this means of light production is not practical for ordinary illumination, it is an excellent source of light for experiments requiring polarized light in the far ultraviolet and is very useful in investigating the electronic properties of solids.

ESTIMATION OF INTERNAL DOSE

Work with radioactive materials involves the possibility that some of the material may be deposited in the bodies of workers or, when it is

dispersed to the environment, of various population groups. For example, military uses have produced low levels of fallout material over the entire earth, and atomic power plants or laboratories generally release some radioactive materials to the environment. The most efficient application of atomic energy requires accurate estimates of maximum permissible concentrations (MPC) of radionuclides in air, in water, and in food that will limit exposure of employees and of the population to acceptable levels. The Internal Dose Estimation Section of the Health Physics Division is primarily concerned with this problem.

In order to estimate these permissible levels in air or water, the metabolic pattern of the element in the human body must be known. The metabolic pattern of the element may be studied by several methods:

1. Because the body does not distinguish between the stable and radioactive forms of an element, data on the distribution of stable elements in the body may be used to predict the chronic distribution of the radioactive forms. For this reason the Internal Dose Estimation Section has obtained samples of various tissues of grossly normal individuals that come to autopsy, from which the distribution of various inorganic elements has been determined.

2. Known quantities of radionuclides may be administered to animals; these animals may be sacrificed at different time intervals and the distribution of the radionuclide in the various tissues determined.

3. In humans, the metabolic pattern of the radionuclide may be studied by sensitive whole-body counters or by analysis of excreta or by both in: (*a*) volunteer patients who have an incurable disease; (*b*) persons who voluntarily ingest or take a tracer amount of a radionuclide; and (*c*) persons who have been exposed accidentally to a radionuclide.

Data obtained from each of these sources are compared and incorporated into mathematical models from which MPC and body-burden values are obtained. The Internal Dose Estimation Section has estimated MPC and body burden values which are applicable to radiation workers and to the population at large for approximately 250 radionuclides. These estimates are the bases for most of the recommendations by the International Commission on Radiological Protection (ICRP) and the National Committee on Radiation Protection (NCRP) which largely serve as norms for the control of exposure to radioactive materials.

For example, all of these methods were employed to establish the MPC for strontium-90. Every tissue in the human body contains some stable strontium, but 95 to 98 percent is found in the bone. By comparison of stable strontium in average American diets and levels of strontium found in human bone, it is possible to arrive at an MPC in an average sense, that is, for normal adults consuming an average diet. The data on stable strontium in bone used here were obtained by the Internal Dose Estimation Section as mentioned above under 1. A few persons voluntarily ingested or took strontium intravenously, and the amount excreted was measured. The excretion following an oral dose essentially parallels the excretion following intravenous injection; this suggests that the metabolic pattern is the same, except that only about 30 percent of the oral dose is absorbed into blood. Various animals have been given radioactive strontium and sacrificed at various times so that the metabolic pattern could be followed.

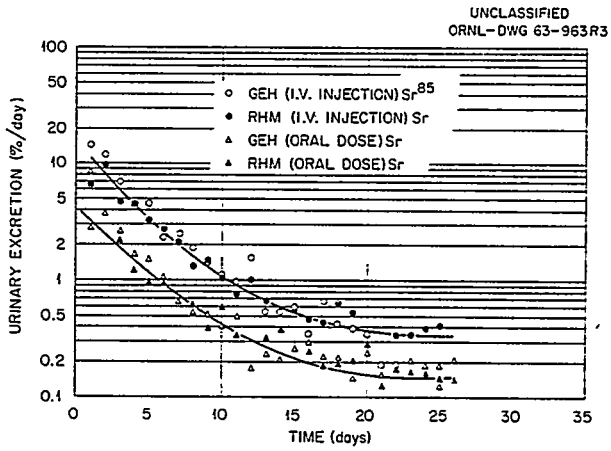

Urinary excretion of strontium following oral or intravenous administration to the same individual. The fact that the curves remain essentially parallel suggests that strontium taken orally is metabolized in much the same fashion as strontium taken by intravenous injection, except that only about 30 percent of the oral dose appears to be absorbed in the blood.

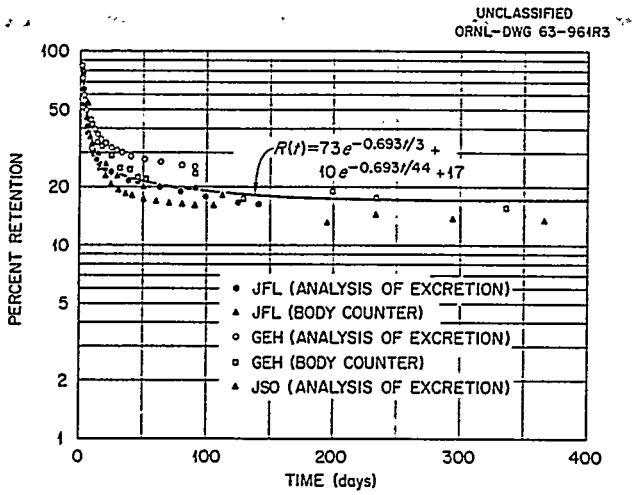

Retention of strontium following intravenous administration. The graph indicates the percent of dose of strontium remaining in the body during the first year following administration to adults by intravenous injection. In some cases the estimate of retention is based on direct measurement of strontium-85 using a body counter, and in other cases the estimate is based on analysis of excreta. The use of both methods of estimation has increased the spread of estimates, but all the data indicate a trend which can be represented by a constant (17 percent) plus two exponential terms.

Data from all of these separate studies have been evaluated and interpreted to obtain MPC values which would adequately limit exposure of employees to strontium-90. These new values have recently been recommended by the ICRP as suitable bases for control of occupational exposure to strontium-90. The data and interpretations offered above illustrate the methods by which acceptable levels of exposure are determined for the hundreds of radionuclides in use and for a wide variety of exposure situations.

BASIC INSTRUMENTATION

Lithium-Drifted Germanium Detectors

The development of gamma-ray detectors using lithium-drifted germanium has extended the usefulness of semiconductor radiation detectors into the million electron volt (Mev) energy range. Excellent energy spectra with high resolution [6.5 kilo-electron volts (kev), full width at half maximum (fwhm)] were obtained for a gamma-ray energy of 1.33 Mev from cobalt-60. It appears feasible that such detectors may be used at gamma-ray energies as high as 7 Mev. For gamma energies in this range, germanium, because of its higher atomic number, may be from 2 to 40 times as effective as silicon.

Although germanium detectors require cooling, both in use and for prolonged storage, this disadvantage is largely offset by the convenience of dealing with gamma rays rather than charged particles. A gamma ray may pass through a considerable thickness of material without energy degradation; thus, the radioactive source need not be infinitely thin and, more important, the detector does not require a thin window. Advantage was taken of this by hermetically sealing the germanium in an evacuated aluminum container by a cold-welding process. Thus, the detector can be cooled repeatedly without condensation of moisture on the germanium surface. Nonetheless, gamma energies as low as 20 kev can easily be detected through the wall (one millimeter) of such a container.

Charge-Sensitive Preamplifier

With the achievement of improved energy resolution of semiconductor radiation detectors, the quality and performance of the associated electronic instrumentation must also be improved; otherwise, the electronics will limit the usefulness of the detectors. A charge-sensitive preamplifier using a field-effect transistor in the input stage was developed at ORNL for use with semiconductor radiation detectors. The resolution (i.e., the spread in the energy spectrum due to amplifier noise) obtained with this preamplifier when the field-effect transistor was cooled was comparable to the resolution of the best vacuum tube preamplifier and about 6 times as good as that of the best bipolar transistor preamplifier. With a detector capacitance of 10 picofarads the resolution was 3.8 kev fwhm at room temperature (25°C), 2.7 kev fwhm at a temperature of −78°C, and 2.0 kev fwhm at the optimum temperature (−150°C). With further studies to optimize the

field-effect transistor preamplifier, better resolution may be achieved. Better resolution combined with less sensitivity to vibration, greater reliability, less power consumption, and smaller size makes the transistor preamplifier preferable to a vacuum tube preamplifier.

Instrumentation for Photosynthesis Studies

Photosynthesis is the process by which plants convert light energy to chemical energy and store it as sugars, carbohydrates, etc. The means by which plants absorb light and convert the energy are not completely understood.

When a plant is illuminated, it emits light, called fluorescence. When the illumination is stopped, the plant continues to emit a much dimer light, called delayed light. These emissions represent energy which plants do not use for photosynthesis. It is believed that a better understanding of them and the conditions that affect their production will clarify the initial energy-handling mechanisms in photosynthesis.

Groups in the Biology Division and the Instrumentation and Controls Division, working in collaboration, developed two rotating-sector shutters and a "one shot" CO_2 operated shutter. With these devices and sensitive photomultiplier and current measuring techniques, several new measurements were made: (1) the time course (decay) of the delayed light from 50 microseconds to one millisecond after illumination; (2) the spectrum of the delayed light at one millisecond; (3) the ratio of the intensity of delayed light to fluorescence; and (4) the effects of poisons, which are known to inhibit photosynthesis, on the intensity and decay of the light.

The measurements of the ratio of delayed light intensity to fluorescence intensity at short times, when extrapolated, suggest the interesting possibility that a large fraction of the in vivo fluorescence of green plants as ordinarily observed may be delayed light.

The preliminary results on the emission spectrum of the delayed light indicate that the light comes from the bulk of the chlorophyll rather than from a special component of the chlorophyll.

The effects of poisons on the light emitted at one millisecond imply that the light comes from chlorophyll which is closely linked to an enzyme step.

Nuclear Energy Civil Effects

ICHIBAN DOSIMETRY PROGRAM

The Ichiban Dosimetry Program is a collaborative program between ORNL and the Atomic Bomb Casualty Commission, aimed at assigning values of radiation dose to the survivors of Hiroshima and Nagasaki. One of the important phases is the determination of shielding factors for Japanese dwellings. Extensive neutron and gamma-ray data were accumulated during weapons tests and during use of the ORNL Health Physics Research Reactor (then temporarily installed at the Nevada Test Site) in projects conducted at the Nevada Test Site. During 1963 these data were correlated with the physical parameters associated with numerous arrays of typical Japanese dwellings, and simple empirical formulas were developed for application to the individual cases in Japan.

In order to determine these formulas, a method had to be used which would choose variables relative to their importance, predict within a reasonable degree of accuracy the measured dose, and be based on the large body of existing measured data. The statistical data analysis of "multiple regression and correlation" was used to obtain the best fit of a set of observations of dose in the presence of numerous independent and dependent variables by an equation of the form

$$y = b_0 + b_1X_1 + b_2X_2 + \ldots + b_nX_n, \qquad (1)$$

where y is the dependent variable, the X's are independent variables, and the b's are the coefficients to be determined. A multiple regression solution of this equation gives the least-squares best value of the coefficients for a particular sample of observations.

In the final analysis, equations (2) through (4) were found to predict the first collision tissue dose at a point in a dwelling relative to the dose at the same slant range in air with a probable error of not over 6 percent:

$$D = D_{\text{air}}\,(a_0 + a_1e^{-g_1} + a_2e^{-g_2} + a_3e^{-g_3} + a_4g_4 + a_5g_5 + a_6g_6)\,, \qquad (2)$$

$$D = D_{\text{air}}\,(a_0' + a_1'e^{-g_1'} + a_2'e^{-g_2'} + a_3'g_3' + a_4'g_4' + a_5'g_5' + a_6'g_6')\,, \qquad (3)$$

$$D = D_{\text{air}}\,(a_0'' + a_1''e^{-g_1''} + a_2''e^{-g_2''} + a_3''e^{-g_3''} + a_4''g_4'' + a_5''g_5'' + a_6''g_6'' + a_7''g_7'' + a_8''g_8'' + a_9''g_9'')\,. \qquad (4)$$

In equation (2), D is the gamma-ray exposure in a dwelling at a point not directly behind a window; in equation (3), D is the gamma-ray exposure in a dwelling at a point behind a window with no bulk shielding between the window and the point of explosion; and in equation (4), D is the neutron dose at any point in a dwelling. In these equations, D is the first collision tissue dose at the

point in question, D_{air} is the first collision tissue dose in air outside the dwelling at the same slant range, and the g's include parameters such as slant penetration into the dwelling, horizontal distance from an opening in the dwelling, height above the floor, number of internal wall structures attenuating direct radiation, and number of internal wall structures which attenuate scattered radiation.

Isotope Development

Nuclear Analysis Research and Development

DETERMINATION OF THE ORIGIN OF OPIUM

The feasibility of using neutron activation analysis to determine the origin of opium has been studied. A plant's ability to reflect the mineral composition of the soil where it grows is the characteristic that is utilized.

Samples of opium (of authenticated origin) furnished by the United Nations were irradiated in the ORR for 10^{17} neutrons per square centimeter. After irradiation the decay of the gamma-ray spectrum of each sample was obtained. Over 100 opium samples were processed in this manner.

Computer programs were written to plot each gamma-ray spectrum and to compare the spectra with each other. Computer analysis of these spectra indicated that only three matched with any degree of probability. Among these 100 samples were samples taken from the same location over a period of several years. There were no matches among these samples, indicating that probably the uptake of trace minerals depends markedly on climatic conditions from year to year. However, samples taken from the same location during one growing season match rather well.

Activation analysis alone is not sufficient for determining the "exact" origin of opium; but in conjunction with other analytical methods, infrared spectrometry, absorption spectrophotometry, alkaloids content, etc., a degree of confidence may be realized.

NEUTRON ACTIVATION ANALYSIS OF WOOL

An animal nutrition experiment was carried out to study the soil-plant-animal relationship on two New Zealand soils, Hastings and Napier, not only as a study in its own right but also in hopes it might provide background information for other biological studies. Ten pairs of twin male lambs were selected at birth for this study. At weaning, the pairs of lambs were split and raised as wethers on each of the soils in New Zealand. Some of the wethers were killed at 15 months, the rest were killed at 28 months of age, and a range of soft tissue samples were taken for analysis. The wool samples were analyzed by neutron activation analysis here, while the other tissues were analyzed by conventional wet analysis in New Zealand. Because of the debris in the wool samples, they were cleaned with a nonionic detergent before irradiation and analysis. Ten elements (Mn, Zn, Cu, Al, S, Se, Mo, W, V, and Al) were measured quantitatively, and the presence of small amounts of four others (Ag, Hg, Sb, and Cr) was noted. In five of the elements (Mn, Zn, Cu, Se, and W) the concentration appeared to reflect variations in the soil and plants on which the twin wethers were raised. These differences in wool trace elements were larger than the differences in the soft tissues of the same wethers. It is suggested that wool offers some possibility in following animal nutrition without killing the animal.

NEUTRON ACTIVATION ANALYSIS STUDIES ON HAIR

Neutron activation analysis has been used to study the effectiveness of the method used to clean hair prior to trace element analysis. In methods reported in the literature, organic agents that removed primarily the sebaceous material from hair were used. To evaluate the effectiveness of these

agents to clean the inorganic matter, including perspiration residues, from the hair, the hair was neutron irradiated and then washed in the agent. The amount of the material removed from the hair varied with each organic agent used to wash the hair. Because of these nonreproducible results, other cleaning agents were tried, including shampoos and a non-ionic detergent. Removal of inorganic contamination was much greater and more consistent with these agents; sodium, for example, was completely removed. Activation analysis data are now being collected for trace elements present in a number of washed hair samples. The trace elements found in hair are Zn, Cu, Hg, Au, As, Sb, Se, Mn, Al, Mo, I, W, and V, with occasionally a small amount of Br and Cl that is not removed by washing. This information is being used to evaluate the feasibility of hair analysis as an investigative method in forensic science.

GUIDE TO ACTIVATION ANALYSIS

Members of the Nuclear-Radiochemical Analyses Group have written a book entitled *Guide to Activation Analysis*. It is expected to be published by early fall 1964. The book presents background information useful to persons engaged in activation analysis.

Applications of Radioisotopes in Analytical Chemistry

RADIOISOTOPE STUDIES OF DETERMINATIONS OF THE ALKALINE-EARTH ELEMENTS

The gamma-active tracers calcium-47, strontium-85, and barium-133 were used in a study of methods of separating and determining alkaline-earth elements. Tracer methodology was emphasized, rather than development of specific analytical methods. Studies included solubility and coprecipitation of barium oxalate, preliminary testing of separation methods, and analysis of reagents, mineral samples, and tap and river water.

Familiar advantages of the gamma-tracer approach include speed and use of nonquantitative methods. Preparation of samples is simple and gamma counting is precise. Two or three tracers were used in simultaneous isotope-dilution analyses, and the activities were distinguished by gamma spectrometry. A reference portion of the tracer(s) was counted at any time and in any desired configuration, eliminating the need for decay and "geometry" corrections.

EXTRACTION AND DETERMINATION OF CESIUM AND RUBIDIUM WITH 4-*sec*-BUTYL-2(α-METHYLBENZYL)PHENOL (BAMBP)

A method has been developed for the rapid separation of cesium and rubidium from essentially all other elements. The separation is achieved by selectively extracting cesium and rubidium from basic tartrate media with 1 *M* solutions of 4-*sec*-butyl-2(α-methylbenzyl)phenol (BAMBP) dissolved in cyclohexane. Measurement can be made directly on the organic solution or in 1 *M* HCl after back extraction of cesium and rubidium. Flame photometry is recommended as a general method of determination. For radiochemical applications, gamma spectrometric measurement of cesium-134, cesium-137, and rubidium-86 in the organic extract should

be used. The method has been applied to silicates and carbonate ores as well as to solutions of fission products and is adaptable for generalized application in the analysis of these two elements.

LIQUID SCINTILLATION COUNTING OF CARBON-14 USING A "BALANCED QUENCHING" TECHNIQUE

A new method was developed for liquid scintillation counting of carbon-14 at a constant, known efficiency in quenched samples. This technique eliminates the manipulation and calculation problem of other methods of yield correction and avoids the radiochemical contamination inherent in the internal standard method. Once initial counting conditions have been established for a given sample type, count rate can be read directly from the instrument at a predetermined counting efficiency. This "balanced quenching" technique is insensitive to differences in activity levels from sample to sample and small shifts in instrument operating parameters. The method does not require the use of counting instruments with dual scalers or coincidence circuitry, but backgrounds are reduced significantly with coincidence operation. The method is ideally suited for routine counting of similar types of samples in any activity range.

WEAR RATES IN AUTOMOTIVE ENGINES BY LIQUID SCINTILLATION COUNTING OF IRON-55

A new radiotracer technique for determining wear rates of selected automotive engine parts was demonstrated for piston rings. The technique uses iron-55 instead of iron-59 as the radiotracer. A liquid scintillation method for counting iron-55 is necessary since it decays by electron capture and emits only the manganese characteristic x ray of 5.9 kiloelectron volts. A simple method for extracting the wear particles from the engine oil and getting the iron into the liquid scintillation mixture was developed. Counting yields of 8 to 9 percent are obtained by the method.

The advantages of this technique are longer radiotracer half-life (2.6 years as compared to 45 days), less radiation hazard, ease of calibration for the determination of absolute wear rates, and the use of the radiotracer that is produced in the greatest abundance. This technique will allow wear studies on larger engine parts and probably can be used outside of controlled laboratories because of the greatly reduced radiation hazard. The minimum detectable wear for the conditions of this study is 35 micrograms.

A NEW LIQUID SCINTILLATOR FOR NEUTRON DETECTION

A liquid scintillator system was developed for the detection of neutrons. The method employs the $^{6}Li(n,\alpha)^{3}H$ reaction. The resulting tritons and alpha particles interact with the scintillator to produce light photons, which are detected in the usual manner. Lithium-6 salicylate is used as the active component of the scintillating solution and is unusual in that it serves not only as a target for the $^{6}Li(n,\alpha)^{3}H$ reaction but is also used as the solution fluor.

SELECTIVE DETERMINATION OF MERCURY BY ISOTOPE EXCHANGE

A procedure was developed for the determination of mercury in an acid aqueous phase by interchange with mercuric di-*n*-butyl phosphorothioate in an organic phase. The D_{Hg} is measured by means of mercury-203, which is either added as a tracer to the aqueous phase or incorporated as a label in the mercuric di-*n*-butyl phosphorothioate. A simple proportional relationship exists between D_{Hg} and the concentration of mercury in the aqueous phase. Only Pd^{2+}, Au^{+}, and Cu^{+} are known to give serious interference. Mercury was determined over a range of 10^{-7} to 10^{-2} gram. The application of isotope exchange reactions to analytical chemistry is potentially a method of great industrial importance. It can improve both selectivity and sensitivity and is simple in regard to both apparatus and procedure.

Analysis of Gamma-Ray Nuclides by Electronic Spectrum Resolution

ELECTRONIC RESOLUTION OF GAMMA-RAY SPECTRA

Collection of gamma-ray spectral data in a standard-response-function "library" is under way, and the library contains responses for 42 radionuclides. Three standardized source mounts, each counted twice, are used in compiling the response for each radionuclide. A "pooling" program for the IBM 7090 is utilized to check for nonstatistical counting behavior and to correct for gain-shift effects. The resultant response functions are stored in digital format at the IBM 7090 facility for subsequent recall or for use in a spectrum resolution program. This program consists in least-squares fitting of an experimental spectrum with spectra from the library.

Recall of response functions from the library may be made in punched-paper tape or in graphical formats. Punched-paper tape spectra have found considerable use in both qualitative and quantitative analytical gamma-ray spectrometry, particularly in analytical gamma-ray spectrometry for short-lived nuclides when standards are not readily available. Further work in this project will be concerned with testing the reliability of the library for direct analyzer usage as well as computer spectra resolution.

GAMMA-RAY BRANCHING DETERMINATIONS

Absolute disintegration-rate determinations by means of gamma-ray spectrometry techniques have an important place in radiochemical and nuclear analyses. A prerequisite for the gamma-ray spectrometry method is a knowledge of the gamma-ray branching for one or more prominent transitions in the decay of a radionuclide. Nuclear data tabulations frequently omit this information or present it in an ambiguous manner. A program for the determination of these parameters for several commonly encountered nuclides is under way. Gamma-ray branchings have been determined for ^{99}Mo, ^{99m}Tc, ^{116}In, ^{38}Cl, ^{82}Br, ^{140}La, and ^{128}I. In many cases, previous literature values have been corrected; in others, confirmation of existing values has been obtained.

Experimental techniques necessary for the absolute measurements have resulted in new half-life determinations for some of the nuclides. In the case of ^{99}Mo-^{99m}Tc, a rapid solvent extraction separation scheme for these nuclides has been perfected.

Additional nuclides will be studied in this program to improve the literature compilations of nuclear data and to facilitate absolute gamma spectrometry determinations.

Isotopic Power and Heat Sources Development Curium Program

The long-term goal of the curium program is to develop technology and processing capacity for curium-242 and curium-244 heat sources which will be used in isotopic power systems. Short-term goals are the completion of processing facilities for purification of curium and fabrication of encapsulated sources, development of purification and source fabrication processes, development of

source and capsule materials compatible with the utilization environment, and demonstration of prototype power-conversion units using curium-242.

The curium program is an integral part of the AEC-wide program to provide isotopic power systems for aerospace and terrestrial use. Heat from radioisotopes is converted to electrical energy by thermoelectric or thermionic devices for powering satellite instrument systems, weather station transmitters, signal buoys, and other uses.

The installation of equipment for the separation of curium-242 from fission products formed during the neutron irradiation of americium-241 and for preparing encapsulated heat sources is 90 percent complete. Removal of fission product gamma activities, essential to the use of the alpha-emitting curium isotopes in aerospace, was demonstrated by using milligram quantities of curium-242 in an aqueous concentration equivalent to full-scale conditions. We found that the acid value in the feed solution, a sensitive control point, was destroyed rapidly by radiolysis. The discovery that methanol represses the radiolytic attack represents a significant advance in the processing of solutions containing high concentrations of alpha emitters. We also demonstrated steps in the fabrication of a curium-242 heat source by using milligram quantities of curium-242 and americium-241. Special attention is being given to the development and characterization of high-melting-point curium source forms.

Radioisotope Production and Separations Technology Development

The objectives of the radioisotope development program are the development of useful radioisotope preparations, the means to produce them, their characterization (to permit an evaluation of the operational and safety aspects of their use), the promulgation of their use by the training of scientists and cooperative demonstration programs with industrial participation, and the dissemination of information on radioisotope production and utilization.

FISSION PRODUCTS DEVELOPMENT

The objectives of the fission products development program are to develop or improve separation processes for the fission elements, to develop processes and procedures for the conversion of fission products into useful compounds and source forms, and to determine the physical and chemical properties of radioactive sources of radiation or heat prepared from fission products.

In line with the current interest in the development of applications of fission products as sources of heat, emphasis was placed on the development and characterization of isotopic power source forms. Cesium-137 glasses of the silicate, borosilicate, and aluminosilicate types containing 40 to 50 weight percent of fission product cesium were prepared, and their melting point ranges, volatility, and solubility were determined. A major improvement in the technique of preparing cesium-137 source forms was made by the development of the cesium tetraoxalate precipitation process to replace the former cesium chloroplatinate metathesis process.

An important contribution to the nuclear data of cesium-137 was the determination of its half-life by three independent methods using the fission product cesium recovered from a 9.5-year-old gamma source. We found the average value of the half-life to be 29.8 years by measuring the isotopic ratio of cesium-137 to cesium-135, the quantity of

barium-137 produced by the decay of cesium-137, and the specific activity of the cesium.

The development of high-melting-point cerium-144 compounds is being emphasized. We developed an improved process for obtaining cerium-144 of high purity (greater than 99 percent) in which Ce^{3+} is electrolytically oxidized to Ce^{4+} and extracted into D2EHPA in a recirculating differential solvent extraction system. Very pure CeO_2 produced by our processes does not have good sintering properties; we successfully solved this problem by adding small controlled quantities of sintering aids. Other properties of fission products determined were the solubility of $^{90}SrTiO_3$ powder and pellets in HCl and seawater, the thermal power of promethium-147 (0.414 ± 0.012 watt/kilocurie), and the radiation spectra from sources of promethium-147.

Technetium-99 metal was deposited from ammonium oxalate solution to form a thin, uniform source on metal backing. The potential utilization of the weak beta emission from technetium-99 in this form as a treatment for certain eye disorders is being explored in cooperation with physicians of the Oak Ridge Institute of Nuclear Studies.

Our studies in the field of mechanical forming of sources included pellet fabrication techniques by hydraulic pressing, isostatic compression, and explosive compaction. The invention of an air-pulsed mixer-settler by R. E. McHenry provides a valuable remotely operated tool for solvent extraction in that all moving parts are located external to the radioactive region of a hot cell. A wide-range calorimeter was developed for determining the heat released by radioactive materials. Special equipment for attaining high temperatures, determining melting points, testing compatibility of materials, and measuring gas evolution from a radioactive material was designed. Remote welding techniques for the joining of refractory metals used as encapsulating materials for isotopic power fuels were perfected.

The stockpiling of strontium-90 and cesium-137 continued in the Fission Products Development Laboratory for use in the development and demonstration of fission product utilization techniques; the processing of 650,000 curies of cesium-137 and 547,000 curies of strontium-90 was completed. The largest source prepared at the Fission Products Development Laboratory was one containing 215,000 curies of cesium-137 for use in the demonstration of a food irradiator at Brookhaven National Laboratory.

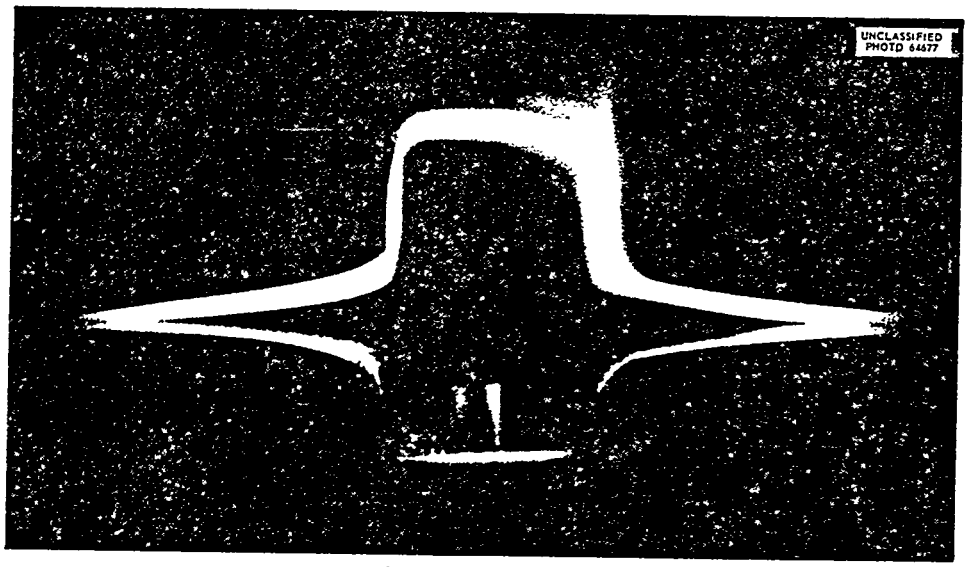

A strip heater furnace in operation. A $\frac{1}{16}$-inch-diameter actinide oxide pellet is being heated by two electrically heated tungsten strips. The pellet is resting on an MgO plate in contact with the lower strip. The temperature of the pellet was measured as 1520°C with an optical pyrometer.

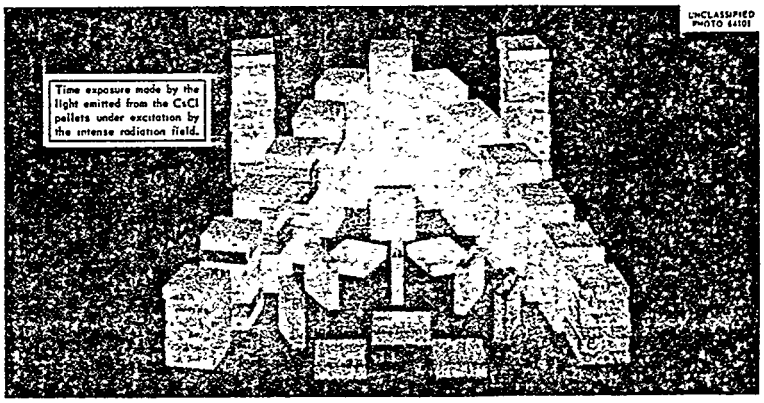

Rectangular blocks of $^{137}CsCl$. These blocks contain 70,000 curies of cesium-137 and were included in the 215,000-curie food sterilization source prepared for Brookhaven National Laboratory by the Isotopes Development Center of ORNL. Each block contains 15 grams (400 curies) of $^{137}CsCl$ compressed to a density of 3.2 grams per cubic centimeter.

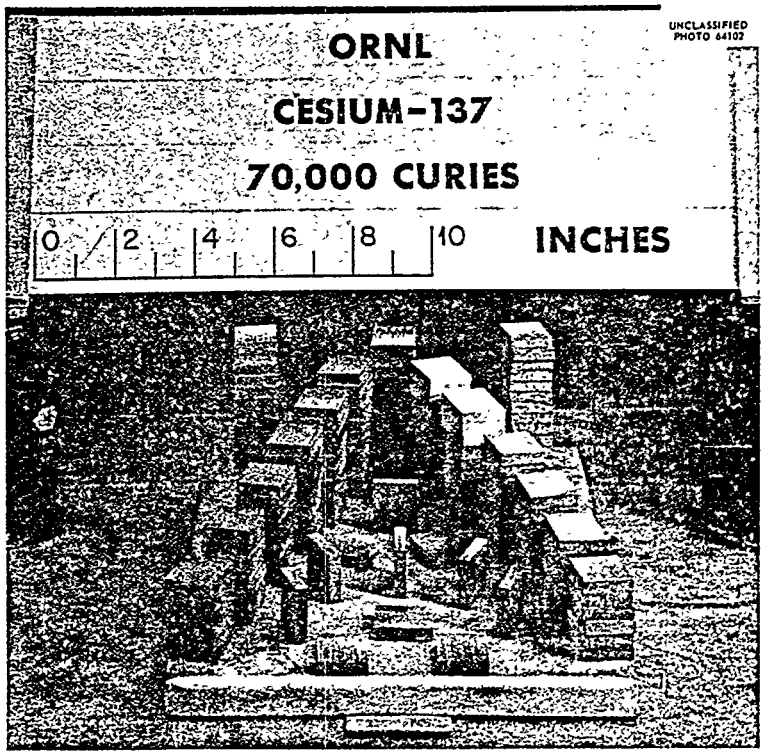

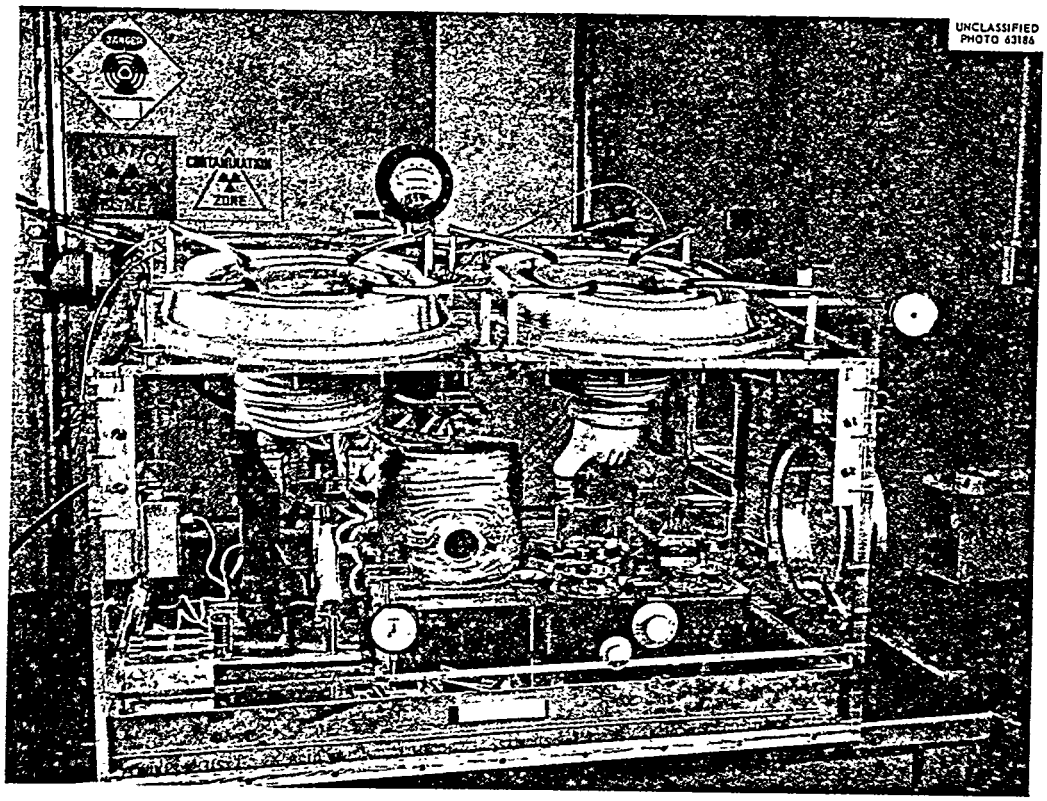

A plastic confinement box for extra-hazardous materials which is operated in a conventional hot cell. This box contains equipment for weighing, pellet formation, and sintering operations. Air inlets and exits are protected by absolute filters.

NEUTRON PRODUCTS DEVELOPMENT

Radioisotopes produced by neutron interaction with target materials were the first furnished under the ORNL radioisotope program and still constitute the mainstay of the program to the great majority of users in the fields of medicine, industry, and agriculture. The objectives of the neutron products development program are to provide new and useful radioisotope preparations; to develop improved processing techniques for those radioisotopes now prepared; and to determine reactor production parameters and pertinent physical, chemical, and nuclear data of radioisotope products.

Iodine-125, because of its half-life (57.4 days) and gamma energy (0.035 Mev), is an excellent isotope for certain diagnostic and treatment applications. Results of our program to determine the optimum production conditions of iodine-125 were as follows:

1. The thermal neutron cross section of xenon-124 in the $^{124}Xe(n,\gamma)^{125}Xe \xrightarrow{\beta} {}^{125}I$ reaction was determined to be 94 barns, and the resonance integral in the epithermal neutron region is about 1300 barns.
2. Design studies on expected production rates for batch and continuous and discontinuous loops were made.
3. Large-scale irradiation tests of a batch process in the Low Intensity Test Reactor (LITR) were initiated.

We proved, using solvent extraction and paper chromatography, that the polyphosphate content of the ORNL $^{32}PO_4^{3-}$ product does not exceed 0.5 percent of the total activity.

The high-energy neutron fluxes in the LITR and ORR pneumatic tubes, hydraulic tubes, isotope production stringers, and partial fuel elements were determined by iron-54 and cobalt-59 monitors. An intensive program of investigation of *n,p* and *n,α* reactions in partial fuel elements was instituted.

CYCLOTRON PRODUCTS DEVELOPMENT

The objectives of the cyclotron development program are to improve the operating efficiency of the cyclotron, to determine production data for cyclotron irradiations, and to develop new cyclotron-produced radioisotope preparations.

A "generator" for strontium-87*m*, produced by the decay of yttrium-87 retained on an ion exchange column, was developed. Iron-55 production parameters by the $^{55}Mn(p,n)^{55}Fe$ reaction were determined.

The penetration depths of 23-Mev protons into iron, nickel, copper, and rhodium were determined by exposing foils of these materials to the proton beam at a 6-degree incident angle. We found that more than 95 percent of the activity is produced in the outer 2.5 to 6.0 mils of the foils, dependent upon the nuclear reaction in the material.

We also studied the technology of producing beryllium-7, cobalt-56, and silver-105.

An improved proton ion source unit design now allows much longer operating periods (approximately 140 hours versus approximately 40 hours formerly) before replacement is necessary.

ADVANCED TECHNOLOGY

Advanced planning for future avenues of radioisotope development activities, advanced study projects, and cooperative demonstration programs with industrial participants constitutes the advanced technology program.

Planning was completed for a cobalt-60-fueled, hydrogen-propelled thruster demonstration. The "Thrustor," developed by Marquardt Corporation, will convert gamma rays emitted by cobalt-60 into heat by absorbing them in tungsten plates. The heat will be transferred from the tungsten plates to a stream of hydrogen in order to supply thrust to a space vehicle.

Also in the planning stage is the demonstration of a strontium-90-powered thermoelectric converter developed by RCA. Preliminary tests leading to the fabrication of 3.5-inch-diameter $^{90}SrTiO_3$ pellets, the largest yet attempted, are under way.

The preliminary study of an experimental thermal diffusion system for enriching krypton-85 from its 5 percent concentration in fission krypton to 45 percent was completed. The system will consist of six Calrod-heated column assemblies containing 36 tubes each and has a designed capacity for 3000 curies of 45 percent krypton-85. Operating parameters of the system will be studied.

A relatively inexpensive, high-intensity neutron source was developed by combining americium-241 and beryllium and irradiating the mixture with neutrons to form 162.5-day curium-242. The high-specific-activity alpha emitter curium-242 yields approximately 2×10^6 neutrons per second for each original milligram of americium-241 irradiated for eight weeks in a flux of 2×10^{14} neutrons cm^{-2} sec^{-1}.

SAFETY TESTING

The safety testing program is concerned with determining the ability of radiation sources and of shipping casks to contain radioactive material under conditions encountered during normal operation and in conceivable accidents. The objectives of the source testing program are to develop methods of classifying sources in a few groups according to their ability to withstand mechanical and environmental stresses, a system of rating sources with respect to their use environment and reliability index, and simple quality control tests which will enable manufacturers to ensure the integrity of sources. This program is related to other AEC testing programs and is specifically oriented toward assisting licensing, regulatory, and licensee surveillance groups.

A total of 308 radiation sources were subjected to tests to enable us to develop the classification schemes. In general, these tests showed that the great majority of source designs can provide containment of the radioactive material under conditions of normal use and accidental exposure to greater than normal stresses. Using the results of the test program thus far, we have written the first draft of a sealed-source classification

system and have submitted it to the AEC for review.

The durability of an encapsulated $^{137}CsCl$ source was proved by our examination of the first cesium-137 teletherapy source made at ORNL. This source was fabricated in 1954 and had been in use at the Oak Ridge Institute of Nuclear Studies hospital since then. The pellets had retained their original shape, and the stainless steel capsule showed no evidence of corrosion or radiation damage.

ISOTOPES INFORMATION AND QUARTERLY REVIEW

The objectives of the isotopes information program are to collect, store, and disseminate information on radioisotope utilization and processing. These objectives are attained by establishing an isotope information storage center for efficient retrieval and transmittal of information in answer to direct inquiries, publication of a quarterly technical progress review, and training of visiting scientists in Isotope Development Center activities. Brochures and bibliographies dealing with specific areas of the isotopes programs as well as critical state-of-the-art reviews will eventually be a major contribution of the Information Center.

The first quarterly technical progress review, *Isotopes and Radiation Technology*, was published, and the mats for the second and third issues were submitted to the AEC for review prior to publication. An accession system, indexed by the Termatrex method, was instituted for the storage and retrieval of isotope information.

Electromagnetic Stable Isotope Separations

The electromagentic isotope-separations program at Oak Ridge National Laboratory provides more than 250 high-purity, highly enriched isotopes for use in a wide variety of research and technical applications. More than 17,000 grams of separated material was collected during the year in 28 of the calutrons allocated for this program. For the majority of elements, this output represents the total quantity of stable nuclides to be made available for worldwide use; and these materials are essential for nuclear research and high-energy programs. In addition, specific isotopes have application in medical and biological research (for example, calcium-46 under neutron bombardment produces calcium-47, which is supplied to a program for diagnosis and treatment of cancer).

Continuing improvements in equipment and processes enable this program to meet increasing demands for larger quantities of separated material at higher isotopic purities and reduce funded costs from approximately $25 per calutron hour in 1959 to about $10 per calutron hour in 1963.

Two 255-degree inhomogeneous field separators (20 inch radius) were fabricated and recently incorporated into the facility. Assays of collected material from these instruments show substantial increases in isotopic purity over the best samples previously received from conventional beta calutrons (24 inch radius). Two outstanding examples are:

Isotope	Isotopic Purity of Best Calutron Sample (Percent)	Isotopic Purity of 255 Degrees Sample (Percent)	Percentage of Increase
Lanthanum-138	7.03	13.5	92
Tantalum-180	0.30	0.44	47

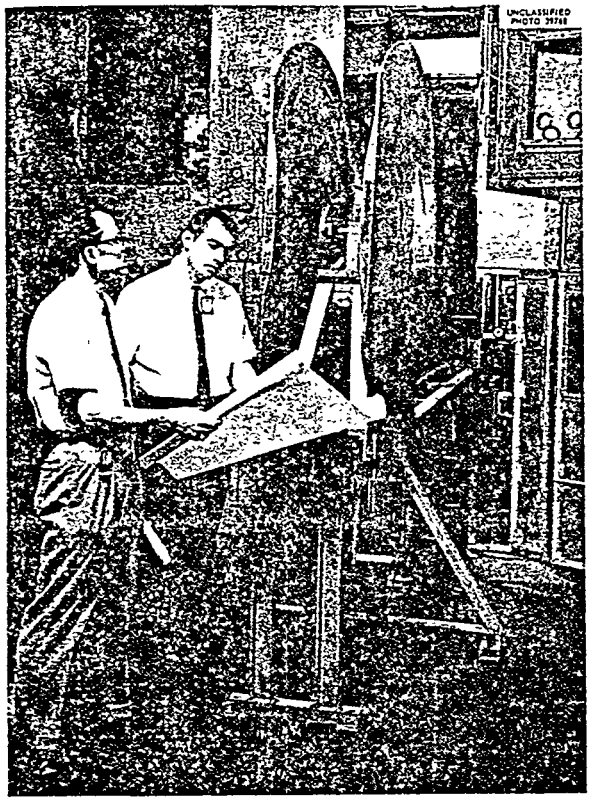

Installation of specially machined shims in calutron tank at ORNL to provide magnetic field for 255-degree inhomogeneous field isotope separator. Field intensities produced by the initial set of shims showed a maximum effective deviation of only 0.4 percent from the field theoretically required for optimum focal point.

Calcium-48 fluoride crystal containing approximately 10 grams of 96.3 percent calcium-48 (natural abundance 0.185 percent) electromagnetically separated at ORNL and valued at approximately $250,000. Crystal was prepared for use in double beta decay studies conducted at Brookhaven National Laboratory.

Additional efforts on equipment improvement are being directed toward finalization of design criteria for a sector-type isotope separator. Such an instrument is required for processing small samples of rare and/or expensive materials to achieve very high isotopic enrichments. Ultimately this type of separator could be applied in processing the heavier transuranic elements. In connection with this study, two types of miniature ion sources were designed and are ready for use.

In addition to the separation of isotopes, the calutron is being used in preparing specific isotopic targets and in studying sputtering and saturation values. These studies have increased basic knowledge pertaining to ion impact phenomena, and the information has dictated receiver designs which resulted in greater retention of separated isotopes.

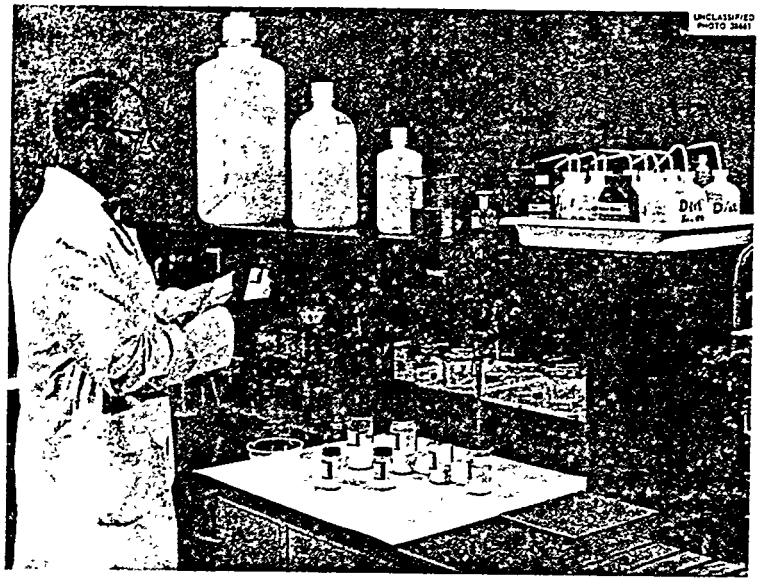

Labeled bottles contain more than 676 grams of highly enriched neodymium isotopes valued at $800,000 which were separated at ORNL using the electromagnetic process. Material was recovered and refined from collector pockets representing more than 16,000 hours of calutron processing, and isotopic purities range from 74.9 percent for neodymium-145 (natural abundance 8.3 percent) to 96 percent for neodymium-142 (natural abundance 27.13 percent).

SPECIAL SEPARATIONS

Electromagnetic processing of plutonium for one year in the new containment facility at ORNL provided more than 240 grams of enriched plutonium isotopes for use in planned research projects. Program emphasis was placed on separation of high-purity plutonium-241 and the following tabulation summarizes the year's collection:

Isotope	Estimated Weight (g)[a]	Approximate Purity (%)
Plutonium-242	16	90
Plutonium-241	32	95
Plutonium-240	126	98
Plutonium-239	71	95

[a]Based on monitored ion current.

In order to provide 1 to 2 grams of 99.9 percent plutonium-242, a second-pass separation is scheduled using 15 grams of plutonium-242 from the initial separation as feed material.

At present ORNL has the only functioning plutonium separation facility outside of Russia. Modifications of equipment and processes have increased the annual separation rate by a factor of 20, with greater isotopic purities being achieved.

This doubly contained plant is also scheduled for use in separating uranium, thorium, and other mildly alpha-active materials. Uranium separations are to provide 50 to 60 grams of uranium-233 with a uranium-232 content of about 10 parts per billion for use in measuring the ratio of neutron capture to fission cross section over a wide energy range. Uranium-238 containing 1 to 20 parts per million of all other isotopes will be made available for use in fission chambers and for nuclear studies.

Education and Training

subjects as quantum mechanics, neutron physics, subcritical assemblies, reactors, and plasma physics. Twenty participants completed the program and received certificates of completion.

Under a formal program which has recently been arranged, nuclear engineering students from the University of Tennessee will use ORSORT and other ORNL facilities to conduct some experiments as a part of their regular, required laboratory work. A total of twenty-one undergraduate students conducted five experiments at ORNL. The five experiments were: minimum criticality mass, importance function, pulsed neutrons (determination of diffusion coefficient), scattering of neutrons, and epithermal control. The University of Tennessee has requested that the program be conducted on a continuing basis.

Under the Nuclear Technology Training Program for University Faculty Members, ORNL accepts faculty members for one-year training programs at the Reactor School. Participants of the program have selected courses in the standard ORSORT curriculum and utilize the same facilities as does the ORSORT faculty. One faculty member from the University of Massachusetts completed this program in 1963, and one faculty member from the University of Idaho entered the program in September 1963.

Since ORSORT has well established programs in Operations Supervision and Hazards Evaluation, ORNL is frequently requested to conduct shorter training programs to help alleviate shortages of qualified reactor personnel that exist when new AEC programs are implemented. Such programs have included the three-month program for Reactor Operations Supervision Training for USS Savannah Personnel and the four-month program for Reactor Safeguard Specialists. The Division of Nuclear Education and Training has speculated that in the future ORSORT may be asked by the Department of Defense to conduct courses in Civil Defense related to nuclear energy.

In October 1962, ORNL was informed of plans for transfer of the program and budget responsibility for ORSORT at AEC Headquarters level from the Division of International Affairs (DIA) to the Division of Nuclear Education and Training (DNET). This transfer became effective July 1, 1963. In this connection, a detailed survey of ORSORT programs was made available for a management decision on the future role of ORSORT programs.

Recent discussions with DIA and DNET concerning the survey indicate there is a need for continuation of ORSORT programs for at least five years. DNET estimates that there is almost an emergency requirement for training several hundred managers, supervisors, and hazards evaluators for domestic and foreign research, test, and power reactors. On the domestic side, there are approximately twelve large (100–5000 kw) university reactors coming into being within the next five years, with little trained personnel available. Overseas, there are approximately 27 research reactors, in place or under construction, which are only partially manned. Most of these prospective trainees want the practical training afforded through ORSORT – not necessarily the academic credit offered by a university. ORSORT training facilities are also urgently needed by the Division of Personnel for the upgrading of young AEC technical recruits and other AEC personnel.

In recent discussions concerning the future of ORSORT programs, DNET's ORSORT Steering Committee commented as follows:

"The two programs at ORSORT were established primarily for the training of foreign nationals, but in recent years the demand for this training by domestic students has grown to such a degree that attendance by U.S. citizens is greater than that of foreign students. This change from a program basically international in character to one primarily devoted to the training of domestic students has prompted the proposed shift of responsibility for these courses from the Division of International Affairs to the Division of Nuclear Education and Training. Thus, it is anticipated that the two courses will continue to function, but as a domestic program under which qualified foreign students will continue to be accepted."

No changes in the scope of the ORNL programs are anticipated. In view of this, there would appear to be a continuing need for the ORNL programs in meeting our commitment to foreign countries and national needs resulting primarily from AEC grants toward research- and training-reactor projects.

ORNL-3650
UC-2 – General, Miscellaneous, and Progress Reports
TID-4500 (37th ed.)

INTERNAL DISTRIBUTION

1. E. A. Bagley
2. P. S. Baker
3. L. H. Barker
4. C. F. Barnett
5. S. E. Beall
6. D. S. Billington
7. R. E. Blanco
8. E. P. Blizard
9. A. L. Boch
10. E. G. Bohlmann
11. C. J. Borkowski
12. G. E. Boyd
13. M. A. Bredig
14. J. C. Bresee
15. R. B. Briggs
16. K. B. Brown
17. F. R. Bruce
18. C. E. Burchsted
19. G. C. Cain
20. A. D. Callihan
21. S. F. Carson
22. T. F. Connolly
23. L. T. Corbin
24. W. B. Cottrell
25. D. D. Cowen
26. J. A. Cox
27. J. H. Crawford
28. F. L. Culler
29. J. E. Cunningham
30. A. C. Downing
31. D. E. Ferguson
32. J. L. Fowler
33. A. P. Fraas
34. J. H Frye, Jr.
35. J. H. Gillette
36. H. E. Goeller
37. A. T. Gresky
38. W. R. Grimes
39. C. S. Harrill
40. J. A. Harvey
41. A. Hollaender
42. A. S. Householder
43. F. T. Howard
44. R. W. Johnson
45. W. H. Jordan
46. C. P. Keim
47. M. T. Kelley
48. B. H. Ketelle
49. E. Lamb
50. J. A. Lane
51. C. E. Larson
52. T. A. Lincoln
53. R. S. Livingston
54. L. O. Love
55. R. N. Lyon
56. H. F. McDuffie
57. F. K. McGowan
58. R. A. McNees
59. H. G. MacPherson
60. F. C. Maienschein
61. A. J. Miller
62. E. C. Miller
63. K. Z. Morgan
64. M. L. Nelson
65–66. R. B. Parker
67. S. K. Penny
68. M. E. Ramsey
69. L. P. Riordan
70. A. F. Rupp
71. H. E. Seagren
72. E. D. Shipley
73. A. H. Snell
74. W. S. Snyder
75. E. G. Struxness
76. C. D. Susano
77. E. H. Taylor
78. F. C. VonderLage
79. G. M. Watson
80. Katharine Way
81. A. M. Weinberg
82. J. C. White
83. E. O. Wollan
84. R. G. Wymer
85. Gale Young
86. A. Zucker
87–89. Central Research Library
90. Reactor Division Library
91. Biology Library
92–93. ORNL – Y-12 Technical Library, Document Reference Section
94. ORNL Patent Office
95. Laboratory Records, ORNL R.C.
96–170. Laboratory Records Department

Printed in USA. Price $6.00. Available from the Clearinghouse for Federal Scientific and Technical Information, National Bureau of Standards, U.S. Department of Commerce, Springfield, Virginia

LEGAL NOTICE

This report was prepared as an account of Government sponsored work. Neither the United States, nor the Commission, nor any person acting on behalf of the Commission:

A. Makes any warranty or representation, expressed or implied, with respect to the accuracy, completeness, or usefulness of the information contained in this report, or that the use of any information, apparatus, method, or process disclosed in this report may not infringe privately owned rights; or

B. Assumes any liabilities with respect to the use of, or for damages resulting from the use of any information, apparatus, method, or process disclosed in this report.

As used in the above, "person acting on behalf of the Commission" includes any employee or contractor of the Commission, or employee of such contractor, to the extent that such employee or contractor of the Commission, or employee of such contractor prepares, disseminates, or provides access to, any information pursuant to his employment or contract with the Commission, or his employment with such contractor.